Reduction of Bridge Pier Scour Through the Use of a Novel Collar Design

Christopher Valela

Thesis submitted in partial fulfillment of the requirements for the degree of

Doctorate in Philosophy Civil Engineering

Academic advisors: Prof. Ioan Nistor and Prof. Colin D. Rennie

University of Ottawa
Ottawa, Ontario, Canada

Abstract

Bridge piers within moving water are exposed to an additional failure mechanism known as scour. Upon the scour depth reaching the foundation of the pier, the structural integrity of the pier, and consequently the bridge, can be jeopardized. Bridge pier scour is the result of a three-dimensional flow separation consisting primarily of the horseshoe vortex, flow acceleration along the sides of the pier, and wake vortices. There are numerous factors that can affect bridge pier scour, of which many of them have been studied extensively. However, there are still some factors where the knowledge base is limited: one example is the presence of an ice cover around bridge piers. In order to reduce the risk of failure induced by scour, regardless of the cause, a preferred option is to use scour countermeasures. However, an ideal countermeasure does not exist. Therefore, the purpose of this research is to design and test an improved bridge pier scour countermeasure, while also better understanding the effects an ice cover has on scour.

Achieving a new countermeasure design consisted of a hybrid approach that combined both numerical and experimental modelling. The numerical model was used in an iterative manner to expedite the design process, as well as to reduce experimental costs. Upon testing and improving the initial collar design numerically, physical models were constructed for the purpose of testing experimentally. Experimental tests were performed at a 1:30 scale in the presence of a sand bed. The same experimental setup was used to investigate bridge pier scour under an ice cover, except a rigid structure was constructed to replicate an ice cover. The artificial ice cover possessed either a smooth or a rough underside and was installed in such a way to replicate a floating or fixed (pressurized) ice cover.

The purpose of the new countermeasure design was to improve on the flat plate collar by guiding the horseshoe vortex in a novel manner. By doing so, the quantity of erosive forces contacting the bed was greatly reduced. In order to reach a final design, a series of prototype designs were tested, and are outlined in this thesis, as they provide valuable insight into the scour problem. The final countermeasure design resembles a contoured collar but is made of riprap, where it was found to reduce the scour depth and volume by 81.0% and 92.3%, respectively, while using 18% less riprap than the conventional flat riprap countermeasure. Upon investigating scour in the presence of an ice cover, it was found that the quantity of scour increases as the ice cover becomes rougher and as the flow becomes more pressurized beneath. Specifically, the scour depth under the rough ice cover and the most pressurized condition increased by 412%.

It was demonstrated that implementing any device which increases the width of the pier has inherent limitations for reducing scour. Instead, having a depression around the pier, especially made of riprap, such that it is flush with the bed and can help guide the horseshoe vortex, was found to greatly reduce scouring. Furthermore, it was observed that the presence of any ice cover on the surface of the water generates greater pier scour, therefore necessitating that ice cover always be taken into consideration when designing bridges in cold climates.

Acknowledgements

I would like to graciously thank my supervisors, Professor Ioan Nistor and Professor Colin Rennie, for everything they have done. They sparked my interest to pursue graduate studies and have truly made my PhD an excellent experience. They provided me with countless opportunities, both locally and internationally, which allowed me to grow and develop. Through their endless encouragement, guidance, and support, they made me a better researcher and I would not be where I am today if it had not been for them.

I would like to thank the large group of people that assisted, in some capacity, to my thesis. Professor Colin Whittaker for collaborating on live-bed scour research and for so generously providing me with the facilities to perform such tests. Professor Javier L. Lara, Professor Maria Maza, and Gabriel Barajas for their continued support regarding numerical modelling and for hosting me in Spain. Professor Jacob Stolle for his academic mentoring and day-to-day assistance. Furthermore, I would like to thank the following students who assisted in my research: Dario Sirianni, from the University of Ottawa, Canada; Anthony Brévot and Quentin Giraud, from the University of Grenoble, France; Ryan Gallie, from the University of Auckland, New Zealand; and Fabrice Bailly, from the University of Strasbourg, France.

I would also like to thank my family (Mother, Father, and Brother) and girlfriend (Ashley) for always being there. Their support and encouragement have been endless throughout this enduring journey for which I am very grateful for.

Lastly, I would like to acknowledge the Alexander Graham Bell Canada Graduate Doctoral Scholarship (CGS D) provided by the Natural Sciences and Engineering Research Council of Canada (NSERC), and the National Research Council (NRC) of Canada for their financial support throughout my graduate studies. Furthermore, I would like to acknowledge the financial support provided by my supervisors through their research funds, particularly the NSERC Discovery Grants of Profs. Nistor and Rennie.

Table of Contents

List of Figures

List of Tables

List of Acronyms

3-D	Three Dimensional
ADCP	Acoustic Doppler Current Profiler
ADV	Acoustic Doppler Velocimeter
CFD	Computational Fluid Dynamics
CNC	Computer Numerical Control
CPN1	Collar Prototype No. 1
CPN2	Collar Prototype No. 2
CPN3	Collar Prototype No. 3
DDES	Delayed Detached Eddy Simulation
DES	Detached Eddy Simulation
FHWA	Federal Highway Administration (U.S.)
FR	Flat Riprap
FPC	Flat Plate Collar
FVM	Finite Volume Method
HEC-18	Hydraulic Engineering Circular No. 18
HEC-23	Hydraulic Engineering Circular No. 23
LES	Large Eddy Simulation
MAE	Mean Absolute Error
MR	Mounded Riprap
NBI	National Bridge Inventory (U.S.)
NBIS	National Bridge Inspection Standards (U.S.)
P	Photograph
PISO	Pressure Implicit Split-Operator
PLA	Polylactic Acid
POA	Plan of Action
RANS	Reynolds-Averaged Navier-Stokes
RCPN3	Riprap version of Collar Prototype No. 3
RMSE	Root Mean Square Error
SP	Scour Plot
SST	Shear Stress Transport
TLS	Terrestrial Laser Scanner
URS	Ultrasonic Ranging System

List of Symbols

C_s	Roughness constant (-)
D	Pier diameter (m)
d_{50}	Median grain diameter (m)
d_i	Scour depth caused by the ice cover only ($d_s - d_p$) (m)
d_p	Scour depth caused by the pier only ($d_s - d_i$) (m)
d_s	Maximum scour depth (m)
E	Model constant (-)
E'	Rough wall function constant (-)
Fr	Froude number (-)
g	Gravitational constant (m/s^2)
h	Height of vertical ring on hooked-collar (m)
k_s	Sand-grain roughness height (m)
p	Pressure (Pa)
Q	Flow rate (m^3/s)
Re	Reynolds number (-)
s_i	Ice cover submergence (m)
t	Test duration (h)
u	Velocity (m/s)
u_*	Shear (friction) velocity (m/s)
u_{avg}	Depth-averaged velocity (m/s)
u_{cr}	Depth-averaged critical velocity (m/s)
u_i	Fluid velocity components with respect to the Cartesian coordinates (u_1, u_2, u_3) (m/s)
u_{in}	Inlet velocity (m/s)
V_s	Scour volume (m^3)
x_i	Cartesian position vector with respect to the reference frame (x_1, x_2, x_3) (m)
y	Flow depth (m)
y_s	Specified depth within the flow (m)
y_i	Flow depth under ice (m)
y+	Wall distance (-)
κ	von Karman constant (-)
λ_L	Geometric scaling ratio (-)
λ_t	Temporal scaling ratio (-)
λ_u	Velocity scaling ratio (-)
ρ	Fluid density (kg/m^3)
ν	Kinematic viscosity (m^2/s)
ν_t	Turbulent viscosity (m^2/s)

Chapter 1. Introduction

1.1 Background

Designing and building bridges has always been a complex process especially when spanning over water. A large majority of bridges in the U.S., approximately 83% of the 583,000 bridges recorded in the U.S. National Bridge Inventory (NBI) in 2007, are constructed over water (Lagasse et al., 2007). In many situations it is unavoidable to place piers within the water, due to the distances that are being spanned, which subjects the bridge to a major failure mechanism known as scour. Scour is the erosion of bed material from around the base of bridge piers, as shown in Fig. 1-1, and is caused by the movement of water around the piers (Arneson et al., 2012). This is problematic because the foundations can become undermined jeopardizing the structural integrity of the bridge. Not only does this pose a large concern for infrastructure, but also public safety, as scour has led to 60% of bridge failures in the U.S. (Lagasse et al., 2007). A specific example was in 1994 in Georgia, U.S., where tropical storm Alberto made land fall and over 500 bridges were damaged specifically because of scour. Of the 500 bridges mentioned, 31 were deemed unsafe and required rebuilding, as scour reached depths between 4 to 6 m (Arneson et al., 2012). It is evident that scour is a widespread problem and it has proven, through many incidents, to cause a large quantity of damage.

Fig. 1-1. Bridge pier scour at the Agassiz Bridge in the Fraser River, B.C. from Valela et al. (2018).

Many existing bridges in the U.S. were not built to withstand the scour they are currently experiencing, as the full scour potential may not have been apparent at the time of construction. Some reasons for the differences between the predicted and actual scour depths can include

changes in flood magnitudes and frequencies, evolving channel geometries, or additional factors such as the presence of an ice cover (Arneson et al., 2012; Lagasse et al., 2007). An ice cover on the surface of the water around bridge piers acts as an upper boundary to the flow, which ultimately changes the velocity profile beneath. When the surface of a river is open, the velocity profile resembles a logarithmic shape, but when there is an additional boundary on the surface, the velocity profile resembles a parabolic shape like that of a pipe flow. By changing the shape of the velocity profile, the location of the maximum velocity shifts downwards closer to the bed, causing an increase in bed shear stress. This increase in bed shear stress has been found to generate greater scour, but the current knowledge pertaining to ice covers and bridge pier scour is limited (Beltaos, 1983; Wu et al., 2016; Zabilansky et al., 2006).

The U.S. Federal Highway Administration (FHWA) requires that owners of new and existing bridges maintain a bridge inspection program, outlined in the National Bridge Inspection Standards (NBIS), which consists of pier scour evaluations and underwater inspections. One key aspect of the program is to identify vulnerable bridges which are predicted to fail from scour if a given flood event were to occur. These bridges are labelled as *scour-critical*. In 2011, the FHWA had indicated that over 23,000 bridges in the U.S. were classified as scour-critical (Arneson et al., 2012).

Once a bridge has been identified as scour-critical, it is required that a Plan of Action (POA) be developed. A POA, which is outlined in the NBIS, consists of site-specific actions for the purpose of improving public safety and minimizing the likelihood of bridge failure. The POA usually consists of, at a minimum, monitoring programs to track and alert bridge owners of any scour progression. Often, it is warranted that additional actions be taken, which will bring the bridge to a non-scour-critical state. These additional actions consist of installing certain types of accepted scour countermeasures, but in the extreme cases when scour has developed beyond the capabilities of countermeasures, then a replacement or substantial rehabilitation of the bridge is necessary (Arneson et al., 2012; Lagasse et al., 2009).

Scour countermeasures are defined by the Hydraulic Engineering Circular No. 23 (HEC-23) as methods designed to prevent, delay, or reduce the severity of scour (Lagasse et al., 2009). There are numerous countermeasures used today, but each one is unique in that they have their own advantages and disadvantages. Currently, there is not one ideal countermeasure that eliminates scour in all conditions while is also appealing in terms of cost, maintenance, and installation. This makes choosing a countermeasure challenging, as an expert in the field is needed and likely a compromise needs to be made. Therefore, the need for further research into scour countermeasures is crucial, because countermeasures are a primary solution to the widespread scour problem that ultimately jeopardizes the safety of the public.

1.2 Objectives

The intent of this thesis is to develop an improved method of reducing scour around the base of bridge piers, through a new scour countermeasure, and to understand better the influence an ice cover around bridge piers has on scour. Therefore, the primary objectives are to:

1) Design a novel bridge pier scour countermeasure, which achieves greater scour reduction, when compared to existing countermeasures.
2) Utilize a numerical model, specifically the open-source Computational Fluid Dynamics (CFD) toolbox OpenFOAM, to aid in the iterative design process required to reach a better performing scour countermeasure.
3) Evaluate the new scour countermeasure performance through a comprehensive experimental program while also testing existing countermeasures for comparison purposes.
4) Examine the effect an ice cover, of different physical characteristics, has on the resulting bridge pier scour below, by means of an experimental investigation.

1.3 Scope

The objective of this thesis is to study bridge pier scour, through developing an improved solution to reduce scour and investigating the influence ice covers have on scour. To accomplish these objectives, both numerical and experimental methods were employed. Due to inherent time and resource constraints associated with both methods, this thesis possesses a number of limitations:

- Only circular bridge piers with a constant diameter were investigated in this study, due to a time limitation. However, other shapes and sizes of bridge piers, such as elongated, are commonly used in the field. The final scour countermeasure design was created in such a way where it can be adapted to accommodate different piers, but such work was not completed in this thesis.
- Despite piers frequently being designed and constructed in groups, only a single bridge pier was studied in this thesis. The scour behaviour changes when there is more than one pier in a close proximity, thus extending beyond the desired scope of this study.
- The final scour countermeasure was designed in such a way to accommodate flows from all directions, but due to a limitation in laboratory capabilities and time, only unidirectional flows were tested.
- Prototype scale or real-life tests were not performed. Obtaining permission to test a prototype countermeasure design on a scour-critical bridge was not possible. Meanwhile, collecting measurements of a pier experiencing scour while in the presence of an ice cover is very dangerous. Therefore, only numerical and experimental investigations possessing a model scale of 1:30 were executed.

- The ice cover tests were performed using artificial ice as opposed to real ice, due to the associated difficulties in generating real ice. Furthermore, maintaining real ice throughout the duration of each test would require a refrigerated facility which was not feasible.
- The best performing scour countermeasure, that was designed and presented in this thesis, was not tested under ice covered conditions. This is because the ice cover tests were completed prior to the development of such countermeasure.
- All ice covers were completely horizontal and maintained a constant depth beneath. Including nonuniformities in the ice covers such as a toe, heel, or ridges, that would cause localized depth reductions, was beyond the scope of this thesis.
- Only clear-water and transition-flow conditions were studied. Live-bed experiments were planned to occur at a facility equipped with a sediment recirculation flume, but due to Covid-19, they were unable to be completed.
- The numerical model simulations were completed with a rigid bed, as opposed to a more realistic mobile sediment bed. This is due to a constraint of the OpenFOAM toolbox, such that sediment transport capabilities were not available at the time of these tests.

The different possible conditions under which bridge pier scour can be examined are endless. For that reason, the scope of this thesis was chosen such that a new countermeasure would be designed and validated, and information would be generated for scour under an ice cover, for some of the most applicable worst-case conditions. Further research can be performed to broaden the findings beyond the benchmark data provided.

1.4 Contributions and Novelty of the Study

The contributions to the research knowledge base and the novelty of this thesis lie in three different areas: the scour countermeasure designs, the hybrid approach taken to develop the new countermeasure designs, and the data obtained pertaining to bridge pier scour in the presence of an ice cover.

The countermeasures presented in this study are novel in that each design is unique and never before tested. The countermeasures were designed with the intention of containing the horseshoe vortex within a three-dimensional (3-D) cavity structure. By doing so, the horseshoe vortex is safely guided around and away from the pier so that the harmful vortex forces are unable to contact the riverbed. This approach of addressing the horseshoe vortex is different than that of any other countermeasure because rather than attempting to diminish such vortex, it is permitted to occur quasi-naturally in a desired manner. Through the process of progressively developing and improving on each countermeasure presented in this thesis, the design was fine-tuned such that a countermeasure that outperforms existing methods was created.

The approach used to arrive at an improved scour countermeasure was hybrid in nature, which is less common in the field of Civil Engineering. For this thesis, hybrid refers to the use of both numerical and experimental methods in an iterative manner. First, the OpenFOAM CFD toolbox was used to save experimental time and costs, as well as to provide detailed flow field

information. Upon reaching a satisfactory design, a physical model was constructed and tested experimentally. By repeating this hybrid approach iteratively, a better countermeasure was achieved while saving time and money.

The Hydraulic Engineering Circular No. 18 (HEC-18) currently identifies that an ice formation or jam on the surface of a river is a factor that affects local scour around bridge piers (Arneson et al., 2012). However, the HEC-18 pier scour equation does not take into consideration the presence of ice covers, rather it states that scour data from nearby bridges should be obtained to estimate the expected scour at the bridge in question. The available scour data in the presence of ice covers is limited, therefore this thesis provides experimental data and prediction equations pertaining to the quantity of scour that occurs as a result of different common ice cover conditions. Specifically, smooth and rough ice covers that are either fixed to the bank forming a pressurized condition or floating on the surface, were examined. Hains and Zabilansky (2004) attempted to perform a similar study with floating and pressurized ice covers however, live-bed conditions were reached during some of the tests causing such scour data to be unusable and the final results to be incomplete. By providing extensive pier scour data in the presence of different ice covers, the intention is to grow the knowledge base so that engineers can better predict bridge pier scour in cold climates and improve public safety.

1.5 Publications

1.5.1 Journal Articles

1) **Valela, C.**, Whittaker, C. N., Rennie, C. D., Nistor, I., and Melville, B. W. (n.d.). "Novel Riprap Structure for Improved Bridge Pier Scour Protection." *Journal of Hydraulic Engineering*. [In review].
    - The author (Christopher Valela) was responsible for creating the new riprap placement design. Furthermore, the author planned and performed the experimental program which occurred in Ottawa, Canada and Auckland, New Zealand. The author wrote the paper. The manuscript can be found in Chapter 5.
2) **Valela, C.**, Sirianni, D. A. B., Nistor, I, Rennie, C. D., and Almansour, H. (2021). "Bridge Pier Scour under Ice Cover." *Water*, 13(536), 1-17. https://doi.org/10.3390/w13040536
    - The author was responsible for generating an experimental program, building the testing apparatus, executing the experiments, and writing the paper. The manuscript can be found in Chapter 6.
3) Sirianni, D. A. B., **Valela, C.**, Rennie, C. D., Nistor, I., and Almansour, H. (n.d.). "Effects of Developing Ice Covers on Local Bridge Pier Scour." *Journal of Hydraulic Research*. [In review].
    - The author assisted with the planning and execution of the experiments as well as with the editing of the manuscript. The manuscript is not included within this thesis.

4) **Valela, C.**, Rennie, C. D., and Nistor, I. (2021). "Improved Bridge Pier Collar for Reducing Scour." *International Journal of Sediment Research*. DOI:10.1016/j.ijsrc.2021.04.004.
    - The author was responsible for producing the countermeasure design changes. In addition, the author planned and performed the numerical and experimental tests to evaluate and compare the countermeasure's performance. The author wrote the paper. The manuscript can be found in Chapter 4.
5) **Valela, C.**, Nistor, I., Rennie, C. D., Lara, J. L., and Maza, M. (2021). "Hybrid Modelling for Design of a Novel Bridge Pier Collar for Reducing Scour." *Journal of Hydraulic Engineering*, 147(5), 04021012. DOI:10.1061/(ASCE)HY.1943-7900.0001875.
    - The author was responsible for developing, iterating, and testing the new countermeasure design. This included generating and running the numerical model, as well as planning and executing the experimental tests. The author wrote the paper. The manuscript can be found in Chapter 3.

1.5.2 Conference Proceedings

1) **Valela, C.**, Rennie, C. D., and Nistor, I. (2019). "A Novel Collar Design to Mitigate Bridge Pier Scour." *38th IAHR World Congress*, Panama City, Panama, 4391–4400. DOI:10.3850/38WC092019-0671.
    - The author was responsible for the countermeasure re-design, in addition to the numerical and experimental testing of the new countermeasure. The author wrote the paper. The manuscript can be found in Chapter 4.
2) **Valela, C.**, Nistor, I., and Rennie, C. D. (2018). "Reduction of Bridge Pier Scour Through the use of a Novel Collar Design." *6th International Disaster Mitigation Specialty Conference 2018*, Canadian Society for Civil Engineering, Fredericton, Canada, 235–244.
    - The author was responsible for creating the countermeasure design as well as performing the numerical simulations. The author wrote the paper. The manuscript can be found in Appendix A.

1.6 Outline of the Thesis

To accomplish the objectives stated in Section 1.2, the thesis consists of a series of studies examining bridge pier scour with a focus on two primary areas: designing an improved scour countermeasure and investigating scour in the presence of an ice cover. To organize the research and present the findings in a logical manner, the thesis was divided into the following chapters:

- Chapter 2.0 consists of a comprehensive literature review pertaining to bridge pier scour and the various scour countermeasures that are practised in the field. The advantages and limitations of each countermeasure are discussed and noted for the purpose of assisting with creating a new scour countermeasure design. Furthermore, a literature review

regarding the current state of knowledge about bridge pier scour in the presence of ice covers is included.

- Chapter 3.0 introduces a new pier scour countermeasure, referred to as Collar Prototype No. 1 (CPN1), which takes the shape of a pier collar. This new collar design contains and guides the horseshoe vortex for the first time, so that the harmful erosive forces are unable to contact the riverbed and scour is reduced. This design was achieved using a hybrid approach that incorporates numerical modelling and experimental testing. The performance of CPN1 was compared experimentally to that of a Flat Plate Collar (FPC) and a pier without any scour countermeasure.
- Chapter 4.0 attempts to improve on the design of CPN1, as to reduce collar undermining and increase overall scour reduction. This was accomplished through the design iterations of Collar Prototype No. 2 (CPN2) and Collar Prototype No. 3 (CPN3). CPN2 possessed a more streamlined shape but was found to perform poorer than CPN1. Upon altering the collar design to reside below the bed, CPN3 eliminated collar undermining while slightly improving scour reduction. An extensive experimental program was undertaken to validate the design of CPN3 and prove its advancement over the FPC.
- Chapter 5.0 describes a new shape of riprap placement, which achieves substantial pier scour reduction, while using less stone material than the conventional Flat Riprap (FR) countermeasure. The countermeasure design utilized the shape of CPN3, but the material consists of riprap so that it possesses a rough surface and remains flexible. Both RCPN3 and the FR countermeasure were tested experimentally under clear-water and transition-flow conditions.
- Chapter 6.0 examines bridge pier scour when ice is present on the surface of the water. The aim of this study was to collect scour data under a variety of ice cover conditions for the purpose increasing the knowledge base on the topic. With this data, basic equations were generated which can be used to help predict the scour depth of bridge piers located in cold climates.
- Chapter 7.0 summarizes the thesis through identifying the general findings of each study. In addition, future work is outlined which can be done to overcome some of the limitations presented in this thesis.
- The appendices consist of additional information which does not directly contribute to achieving the objectives specified in Section 1.2.

Chapter 2. Literature Review

2.1 Scour Process

The presence of a pier within water, where the water possesses some nonzero flow velocity, induces a blockage on the passing flow. This blockage generates a pressure field on the upstream face of the pier which causes the approach flow to separate around the pier (Ettema, Nakato, et al., 2006). Upon separating, the pressure field causes a portion of the approach flow to be drawn downwards immediately in front of the pier. This portion of the flow continues down to the riverbed where it is redirected in the upstream direction. It travels upstream for a very short distance until it is redirected by the passing flow back downstream. This motion forms a continuous 360-degree flow path which causes such flow to circulate many times as it propagates around the front and down the sides of the pier until it dissipates into the passing flow. This overall behaviour is more formally known as the *horseshoe vortex* (Ettema, Nakato, et al., 2006). Since such vortex resides directly on the riverbed and is very powerful because of the downward flow, it removes a large quantity of sediment from around the front and sides of the pier and transports it downstream. For that reason, the horseshoe vortex is known as one of the largest sources of pier scour (Chiew, 1992).

The remainder of the flow that is not drawn down to the riverbed but is still influenced by the presence of the pier, in addition to the horseshoe vortex, experiences an increase in velocity as it passes the sides of the pier (Ettema et al., 2017). This occurs because in order for the flow to bypass the pier it must travel a farther distance, therefore resulting in a flow contraction and ultimately an increase in velocity. This increased velocity induces a higher shear stress on the bed on either side of the pier, which directly leads to scouring in such locations (Arneson et al., 2012).

The third and final substantial source of scour is caused by the flow passing the sides of the pier, such that the shear layers next to the pier create vortices which possess an axis in the vertical direction (Ettema, Nakato, et al., 2006). These vortices, which are Reynolds number dependant, are generated along the sides of the pier and are shed off of both downstream edges, one at a time, in an oscillatory pattern. Once they are shed, they can form a trail of vortices that travel downstream losing energy as they progress further away from the pier. Due to the vertical orientation of the vortices, the revolving flow of each vortex creates a low-pressure region in the center which draws sediment off of the riverbed and up into the vortex. These vortices are referred to as *wake vortices* and can assist, to a smaller degree, in scour that occurs along the sides and rear of the pier (Ettema, Nakato, et al., 2006; Marris, 1964; Stevens et al., 1991).

The three scour sources mentioned above are illustrated in Fig. 2-1. It can be seen that the horseshoe vortex occurs largely upstream of the pier, the accelerated velocity occurs mainly along the sides of the pier, and the wake vortices occur primarily behind the pier, implying that

the combination of the three can lead to bed erosion on all sides of the pier (Ettema et al., 2017). Therefore, whenever a pier is present within moving water, it is likely that some form of scour will occur.

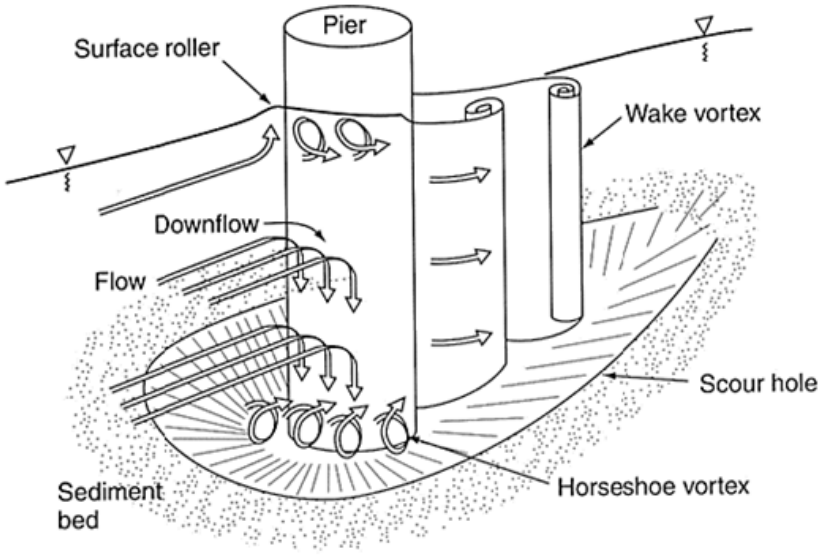

Fig. 2-1. Flow behaviour around a bridge pier from Abdalla (2016).

Through the scouring processes mentioned above, the sediment that is removed from around the pier must be relocated elsewhere. Specifically, the sediment is transported a short distance downstream and is deposited when the flow no longer possesses enough energy to keep the sediment suspended (Ettema, Nakato, et al., 2006). The flow increases in velocity near the pier, due to the pier induced flow behaviours mentioned earlier, and then returns to the mean velocity downstream, hence why sediment is removed from around the pier but then deposited a short distance downstream. It is understood that scouring is a problem, but sediment deposition can also pose problems because it can, for example, greatly reduce the water depth (Ettema, Nakato, et al., 2006). This is concerning when boat traffic is active in the region because running aground becomes a possibility requiring dredging to mitigate the issue. As a result, neither scour nor the associated sediment deposition is desirable and a solution to this complex problem is highly warranted.

2.2 Clear-Water and Live-Bed Scour

There are two primary conditions under which scour can occur and understanding the difference between them is important as they can impact the resulting scour depth. The first condition is when scouring exists only locally around the pier, while the rest of the bed remains stable. This means that the flow velocity upstream of the pier is below the threshold of sediment mobilization. Scour equilibrium around the pier is simply reached when the passing flow can no

longer remove any more sediment from within the scour hole. This condition is referred to as *clear-water scour* (Ettema, Nakato, et al., 2006).

The second condition is when sediment transport is present upstream, implying that the flow velocity is above the threshold for sediment mobilization. This can result in bed material being deposited into the local scour hole around the pier, therefore reducing the overall scour depth. In order for equilibrium to be reached, the quantity of sediment being deposited into the scour hole must equal the quantity that is being removed, however these quantities are prone to fluctuations due to the passing of bedforms. This condition is referred to as *live-bed scour* (Ettema, Nakato, et al., 2006).

Since the scour hole is not replenished under clear-water conditions, often 10% greater equilibrium scour depths can be experienced under such conditions despite possessing a lower velocity (Arneson et al., 2012; Raudkivi, 1986). However, the cyclic nature of the passing bedforms under live-bed conditions can induce greater instantaneous scour depths. Therefore, both conditions can possess concerning quantities of scour but in different regards. Furthermore, many rivers can experience both conditions, such that normally they possess clear-water conditions, but during flooding, the flow velocity increases inducing live-bed conditions (Hong et al., 2017; Lu et al., 2008).

2.3 Ice Cover

Bridge pier scour is influenced by a number of parameters, of which extensive research has been done to better understand the effects of each. However, there still exists some parameters where there is a limited knowledge base. One example is the presence of an ice cover around bridge piers. In colder regions such as Canada, ice tends to reside on the surface of water creating an added wetted boundary. This has been found to greatly alter the flow behaviour beneath the ice, as shown by Wu et al. (2016) in Fig. 2-2a (u = velocity, u_{avg} = depth-averaged flow velocity, y = flow depth, and y_s = specified depth within the flow,) (Ettema et al., 2011; Shen & Wang, 1995; Sui et al., 2010). As a result, such changes in the flow, specifically pertaining to the velocity, can affect the quantity of sediment transport and therefore deform the riverbed differently (Sui et al., 2000, 2010).

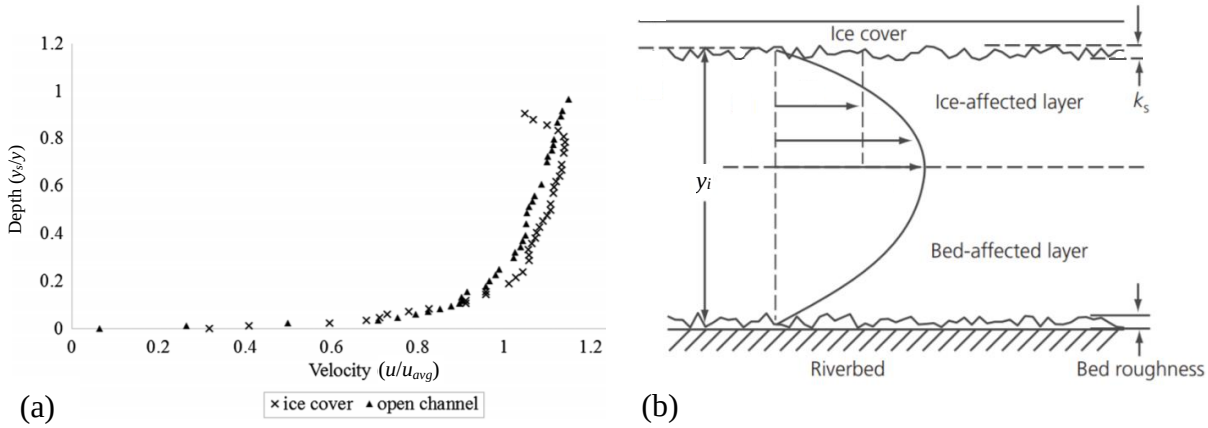

Fig. 2-2. Velocity profiles beneath an ice cover: (a) a comparison of a velocity profile in an open channel versus under an ice cover (Wu et al., 2016), and (b) the effects of riverbed and ice cover roughness on the velocity profile (Li, 2012).

The lack of a solidified understanding of pier scour under an ice cover may stem partly from the substantial variation in ice properties, which can change in both time and space (Li, 2012). Ice covers around a pier can form and grow through different methods which greatly impacts its properties. When the ice cover is generated thermally, due to cold temperatures and mild flow conditions, the ice thickens and creates a relatively smooth surface contacting the water (Zabilansky et al., 2006). Whereas, when the ice cover forms from mechanical means, such as shoving during freeze-up or break-up periods, the ice cover tends to consist of many broken fragments that conglomerate into a rough surface (Beltaos, 1983; Zare et al., 2016).

Measuring the roughness of an ice cover is challenging to perform in the field due to the unsafe conditions, causing there to be a limited amount of available data (Wuebben, 1988). An attempt to obtain field roughness values of an ice jam was performed by Beltaos (2001) using a remote technique. This consisted of deploying a floating sensor beneath an ice jam. The sensor recorded the elevation of the ice jam underside as it was carried with the flow for multiple kilometers. A total of 20 data sets were collected from various locations and the roughness values varied from 0.24m-1.15m (with one data point omitted due to an extremely large value), therefore averaging 0.79m (Beltaos, 2001). In addition, Zare et al. (2016) attempted to quantify the Manning's roughness values under an ice cover. This was accomplished using a bottom-mounted Acoustic Doppler Current Profiler (ADCP) that measured velocity profiles over multiple months. By fitting the time-averaged velocity profiles to the log-law, Zare et al. (2016) estimated the Manning's roughness of the bottom of the ice cover to vary from almost zero to as large as 0.08. Therefore, the roughness of the underside of an ice cover can range from being smooth to very rough.

The method of ice cover formation is important as it affects the roughness of the underside of the ice contacting the passing flow. Since the ice cover acts as a surface boundary to the flow, the roughness of the underside is critical in shaping the velocity profile of the flow beneath. Fig. 2-2b, from Li (2012), displays a velocity profile beneath an ice cover possessing the same roughness as the bed. The velocity profile behaves similar to that of a pipe flow, where the velocity decreases at the top and bottom boundaries while reaching a maximum in the middle of the flow depth (Li, 2012; Wu et al., 2016). Meanwhile, if one boundary is rougher than the other, the location of the maximum velocity shifts towards the opposite boundary, as it imposes less resistance on the flow (Beltaos, 1983; Zabilansky et al., 2006). Regardless of the roughness, the presence of an ice cover causes the location of the maximum velocity to move closer to the bed, resulting in an increase in near bed velocity (Wu et al., 2016). Consequently, this can generate greater bed shear stress (Li, 2012).

Wu et al. (2016) further explored this topic and are amongst the first pioneers to collect bridge pier scour data in the presence of an ice cover. Experimental tests were performed with and without an ice cover, where the ice cover was modelled using a large sheet of Styrofoam resting on the water surface. The resulting equilibrium scour patterns from Wu et al. (2016) can be seen in Fig. 2-3 (d_s = maximum scour depth and D = pier diameter), such that it is evident that an ice cover increases the quantity of scour that is experienced around bridge piers (Wu et al., 2016). Specifically, scour is increased in both depth and width when an ice cover is present. The data provided by Wu et al. (2016) forms a sound knowledge base, however in order to accurately predict scour in the presence of an ice cover, more data under different conditions are required.

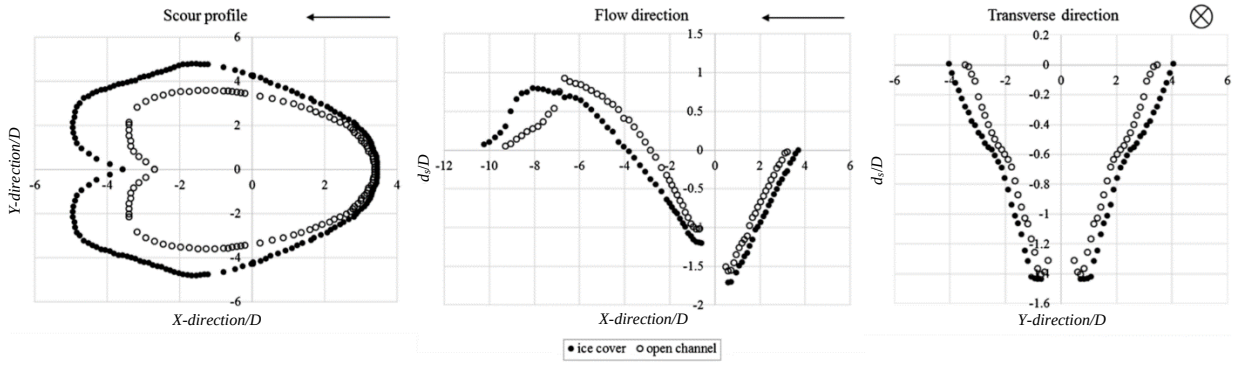

(a) (b) (c)

Fig. 2-3. Bridge pier scour comparison from different perspectives (Wu et al., 2016).

In addition to varying ice cover roughnesses, another factor which can affect the quantity of scour is whether or not the ice cover is attached to the banks. When the ice cover is unattached to the banks, such that it is floating on the surface of the water, it can change elevation to accommodate variations in water levels. Whereas, when the ice cover is attached to the banks, it can not adjust to increases in the water level, which can result in pressurized flow conditions beneath the ice cover (Zabilansky et al., 2006). Frequently, when an ice cover is attached to the

banks, it can thicken from mechanical processes, as pieces of floating ice collect in front and underneath the ice cover (Ambtman & Hicks, 2012). This can accelerate the rise in water level upstream while reducing the cross-sectional area beneath the ice cover for water to pass through. When the ice cover is attached to the banks, an increase in flow rate or reduction in cross-sectional area beneath the ice cover can cause an increase in flow velocity under the ice cover. Such increase in velocity can ultimately generate greater pier scour (Ambtman et al., 2011; Zabilansky, 2002).

Based on the current research, when designing bridge piers for colder climates, ice covers need to be taken into consideration. This is because ice covers have been shown to alter the flow behaviour, which can consequently induce larger scour depths around piers. However, the HEC-18 design guidelines currently do not outline a procedure for estimating scour under an ice cover, but it states that ice effects need to be taken into consideration. HEC-18 simply suggests investigating the scour experienced at nearby bridges to obtain a scour estimate (Arneson et al., 2012). This confirms that the concept of bridge pier scour, provoked by the presence of an ice cover, is something that requires further research as it has been indicated to be problematic but very little literature exists on the topic in order to address it.

2.4 Countermeasures

Scouring is a problem that is not always foreseeable at the design stage, but something that can emerge later on. Due to the potential devastation and public safety concerns associated with scour, a retrofit solution is something that is essential. HEC-23 refers to such solutions as countermeasures. They define a countermeasure as something used to "…monitor, control, inhibit, change, delay, or minimize stream instability and bridge scour problems" (Lagasse et al., 2009). Countermeasures are extremely beneficial as they can be installed to solve an existing scour problem or to prevent future scour problems. Since scour has been an ongoing problem for many years, there are a number of countermeasures used today. Each one has its own benefits but also downfalls, which makes it challenging as an engineer to select the most correct one for the given situation. HEC-23 categorizes the countermeasures into four groups consisting of: hydraulic countermeasures, structural countermeasures, biotechnical countermeasures, and monitoring (Lagasse et al., 2009). The following sections discuss these groups in more detail providing examples of specific countermeasures and highlighting the pros and cons of each.

2.4.1 Hydraulic Countermeasures

Hydraulic countermeasures are the first group and they aim to alter the flow path by means of river training structures or riverbed armouring (Lagasse et al., 2009). By doing so, the structure of the bridge is not altered but instead everything around it is. The benefit to this approach is that it can be cost effective, less harmful to the bridge, and potentially easier to install. Both of these subgroups, river training structures and armoring, are explained further below.

2.4.1.1 River Training Structures

River training structures are used to change the flow behaviour upstream or around the bridge pier for the purpose of minimizing the potential scour caused by the passing flow. They can be built of different materials such as wood, metal, or concrete just to name a few, but what is more important is how they are oriented in the flow. Specifically, they can be constructed perpendicular to the flow, parallel to the flow, or dispersed across the river, each providing different benefits (Lagasse et al., 2009).

2.4.1.1.1 Perpendicular

One of the most common river training structures are groins; which are orientated perpendicular to the flow. Groins are structures made usually of rock that protrude out of the riverbank at some angle for the purpose of reducing erosion along a riverbank or for redirecting the passing flow. They reduce riverbank erosion by pushing the fast-moving flow away from the bank therefore decreasing the shear stress that the riverbank is exposed to (Melville et al., 2008). Often, multiple groins are installed, a short distance apart form one another, along a riverbank which creates pools of slow-moving water between such groins. This promotes sediment deposition and helps to stabilize the corresponding riverbank (Jamieson et al., 2013). However, groins can also be used to redirect the passing flow which is more useful for bridge applications (Melville et al., 2008). If a bridge is located near a meander in a river, one or multiple groins can be installed to redirect a large quantity of the fast-moving flow away from the pier in a harmless direction. The angle in which the groin is installed at determines the direction of the passing flowing. Specifically, if the groin is pointed in the upstream direction, the flow is shifted away from the bank, but if the groin is pointed in the downstream direction, the flow is drawn towards the riverbank. The reason for this is because of the location of the scour hole that forms around the groin itself, as it has the ability to influence the passing flow (Ettema, Nakato, et al., 2006). When groins are designed and installed correctly, they can serve to greatly reduce scour around bridge piers but the number of situations where they are useful is limited.

2.4.1.1.2 Parallel

The next type of river training structure is orientated parallel to the flow and is referred to as guidebanks. Guidebanks are rigid structures mounted to the banks of rivers and used primarily to reduce erosion of such banks. However, they can also be installed along the sections of a river which vary in width to alleviate contractions, as localized narrowing of the riverbanks can cause an increase in the flow velocity. This is done by installing the guidebanks either parallel to one another or angled outwards in the downstream direction (Melville et al., 2008). By maintaining a constant or increasing width, the flow velocity does not increase, and its behaviour becomes more predictable. This is beneficial when piers are present because guidebanks can be constructed along such sections, as this will help to maintain a constant flow velocity and reduce turbulence around the piers. Therefore, guidebanks are not a direct solution for pier scour but under certain conditions such as river narrowing, they can help reduce scour (Melville et al., 2008). Similar to groins, the number of instances where guidebanks are applicable is limited so they are not a common choice for reducing scour.

2.4.1.1.3 Area Covering

The last type of river training structure is not located along the banks like the others mentioned, but rather spread across the upstream flow. This type is referred to as an area covering treatment where two popular forms exist, sacrificial piles and vanes (Lagasse et al., 2009). Sacrificial piles are simply piles made commonly of steel or wood which are anchored into the riverbed upstream of the bridge pier to deflect the high velocity flow. By deflecting the high velocity flow, a lower velocity wake region is created behind the piles which reduces scouring around the pier. The effectiveness of the sacrificial piles is dependent on a series of factors consisting of the number of piles, pile diameter, pile height, and pile orientation to only name a few. It was found that the best orientation is in the shape of a triangle pointing in the upstream direction, as seen in Fig. 2-4 (Melville & Hadfield, 1999). Further studies have been performed on sacrificial piles as a scour countermeasure and it was found that the maximum possible scour reduction from sacrificial piles is 56% (Melville & Hadfield, 1999). This is a respectable amount, however as soon as the angle of approach begins to increase, the scour reduction drops significantly. Therefore, Melville and Hadfield (1999) suggest that sacrificial piles should not be used as a scour countermeasure unless the flow approaches head-on.

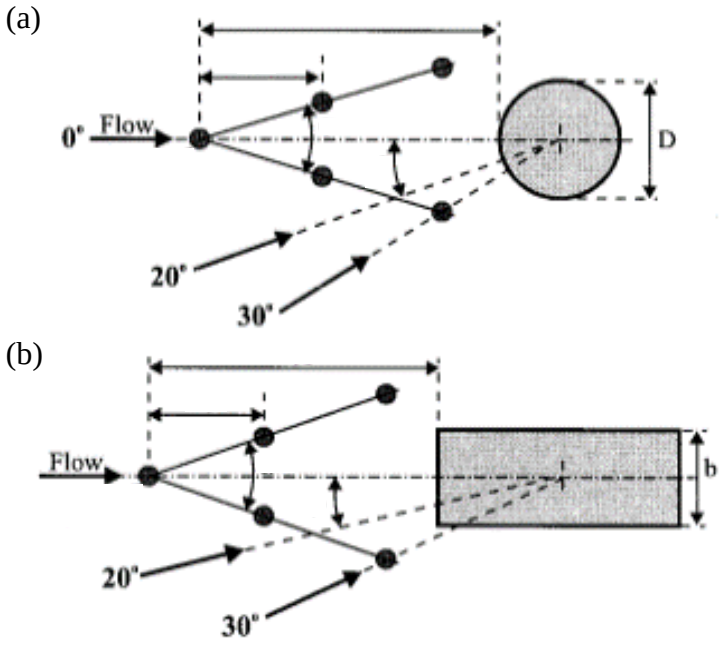

Fig. 2-4. Sacrificial pile orientation: (a) for a cylindrical pier, and (b) for a rectangular pier (Melville & Hadfield, 1999).

The second form of area covering treatment is vanes. They are similar to sacrificial piles because they are rigid and installed upstream of the pier within the flow, but they possess a different shape. The shape is more rectangular as opposed to cylindrical. Due to this rectangular shape, they are able to direct the passing flow instead of only blocking it. For that reason, vanes are commonly angled inwards, as shown in Fig. 2-5, because the goal is to direct the passing flow towards the pier so that secondary vortices can be created. These vortices are used to

interfere with the horseshoe vortex while also promoting sediment deposition in front of the pier (Ghorbani & Kells, 2008; Melville et al., 2008). By doing so, the scour depth around the pier can be reduced. However, a similar problem to that experienced with sacrificial piles is possible such that if the passing flow changes approach angles, the effectiveness can be greatly reduced. In addition, vanes are more prone to collecting debris which can damage the vanes or create damming within the river, therefore generating additional problems. The effectiveness of vanes is dependent on a number of factors such as vane height, angle, length, spacing, flow depth, and flow velocity to name a few. Ghorbani and Kells (2008) found the performance of vanes to vary greatly, from increasing scour by large amounts to decreasing scour by large amounts, depending on the aforementioned factors. Therefore, if the vanes are installed correctly, they can be very effective, but if any of the influencing factors change, their effectiveness can greatly decrease.

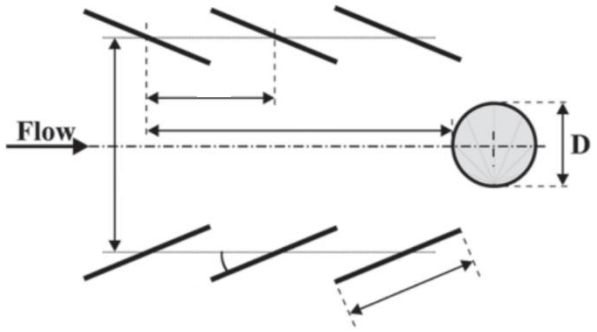

Fig. 2-5. Orientation of vanes upstream of cylindrical pier (Melville et al., 2008).

Three different types of river training structures were introduced, consisting of perpendicular, parallel, and area covering treatments. Each one has potential to reduce scour under very specific conditions but not one performs exceptionally well under all conditions. For that reason, river training structures are not the best choice as a scour countermeasure.

2.4.1.2 Armouring

Armouring methods as a scour countermeasure are much more common than river training structures. Armouring works by providing a protective layer over the riverbed so that the erodible material beneath can resist greater forces induced by the passing flow (Lagasse et al., 2009). In general, armouring can be used to protect large areas and riverbanks, or it can be used to protect against localized scour such as around bridge piers, with the latter being the focus of this research. Armouring countermeasures usually do not greatly alter the flow behaviour, nor do they vary in function, but they do vary largely in material and assembly. Furthermore, armouring countermeasures can be categorized into two groups, depending if they are flexible or not, where each group possesses positive and negative characteristics (Lagasse et al., 2009). Various forms of both flexible and nonflexible countermeasures are introduced in this section and discussed in further detail.

2.4.1.2.1 Riprap

One of the most common forms of scour prevention is riprap. Riprap has been used for many years and is still to this day a favoured pier scour countermeasure due to its proven performance and universal acceptance (Chiew, 1995). Riprap consists of stones that are larger in size than the riverbed material and are placed on top of the riverbed in the scour prone locations, specifically where the horseshoe vortex and accelerated flow contact the riverbed. Due to the larger mass associated with the riprap stones, greater shear stresses from the passing flow are required to dislodge the stones, thus reducing scour (Lauchlan & Melville, 2001). One of the largest benefits of riprap is its easy installation, such that large rocks are simply placed around the base of the bridge pier. Riprap is classified as a flexible countermeasure and that is because the stones are not attached to one another and can conform to changes in the riverbed. This is advantageous because the stones can shift to fill in scour holes or deformations that form during high flow events, ultimately reducing further scouring, whereas nonflexible countermeasures are unable to do so (Lagasse et al., 2009).

Riprap is a flexible countermeasure that is prone to three failure methods in clear-water conditions. The first failure method is due to shear, which occurs when the stones are simply too small and do not possess enough mass to overcome the shear stress induced by the passing flow. The level of protection that is supplied by riprap depends greatly on the size and angularity of the stones, so for that reason, it is very important that the stones are designed and chosen correctly otherwise the effectiveness will decrease as the stones become ejected (Chiew, 1995; Lagasse et al., 2009). The second failure method is due to winnowing, which is the erosion of finer riverbed material from beneath the coarse riprap layer. This problem, which is especially common in the presence of the down flow on the upstream face of a pier, is dependent on the magnitude of the flow and the difference in size between the bed material and the riprap stones. If winnowing continues to occur, scour holes can form around the pier as the riprap is providing little to no protection (Chiew, 1995). The last failure method is due to edge failure, which is the process of scouring around the edge stones of the riprap layer. This can cause some of the edge stones to become dislodged and carried downstream, therefore exposing and ultimately eroding the finer material beneath the riprap layer. In time, this can lead to the inner stones becoming dislodged, causing the entire riprap layer to fail (Chiew, 1995).

Meanwhile, in live-bed conditions, riprap can experience an additional failure method. This failure method is an embedment failure where the riprap layer subsides into the finer material of the riverbed. This is a common failure method because it is caused by the riprap stones falling into the trough of a passing bedform. Once the crest of the following bedform arrives, the fallen stones become buried beneath the scour hole. This type of failure method can occur for thin layers of riprap or when winnowing is experienced (Chiew & Lim, 2000).

Overall, riprap is a great scour countermeasure if it is designed and installed correctly, as it can be used under a wide range of conditions unlike many other countermeasures, but it is

prone to a series of possible failure mechanisms which can jeopardize the level of provided scour protection.

In order to help reduce the possibility of the aforementioned riprap failure methods, a series of guidelines have been created. When implementing riprap as a scour countermeasure, the design process can be divided into: (1) stone selection, and (2) riprap installation. Some of the key components of each will be briefly outlined, but for more details, refer to HEC-23 (Lagasse et al., 2009).

When selecting the stones that will be used in a riprap countermeasure, a number of factors need to be taken into consideration. First, the stones need to be large enough such that they can withstand the expected velocity in the vicinity of the pier including any velocity increase induced by the bridge constriction. There are various methods that can be used to determine the minimum riprap size such as the Isbash or Shields stability criteria to name a few (Froehlich, 2013; Lagasse et al., 2009; Tabarestani & Zarrati, 2013). Riprap is more stable when the stones are not uniformly graded, therefore gradation guidelines exist for the optimal combination of sizes. Next, the shape of the stones need to meet a specified criteria. Specifically, the stones should not be thin, nor should be they long and skinny. To ensure the stones are the correct shape, the length of the major, intermediate, and minor axes are measured, and the ratio of the major axis versus the minor axis is recommended to be less than 3.0 (Lagasse et al., 2009). In addition, the stones should possess a subangular to angular surface to promote interlocking and stability. Lastly, the stones must surpass a minimum density such that a specific gravity of 2.5 or greater is generally required (Lagasse et al., 2009).

In addition to stone selection, the installation of the riprap plays an important role in its performance. Prior to installing the riprap, one option is to install a filter layer beneath the stones which is generally recommended, however there is some debate as to whether or not it affects the performance of the riprap (Lagasse et al., 2009; Parker et al., 1998). The purpose of the filter layer is to: (1) prevent large amounts of native bed material from migrating into the voids of the riprap, (2) permit the dissipation of hydrostatic pressure under the riprap, and (3) evenly distribute the weight of the armour layer to allow for a more uniform settlement. Filter layers can be a granular material, a geotextile material, or both depending on the characteristics of the bed material (Lagasse et al., 2009).

When installing riprap, whether or not a filter layer is included, results from Lagasse et al. (2007) indicate that the best performance occurred when the riprap extended a minimum of 2D outwards from all sides of the pier. Furthermore, such results were achieved when the riprap was installed in a flat pre-excavated hole around the pier with the top surface of the riprap flush with the bed (Lagasse et al., 2007; Lauchlan & Melville, 2001). Frequently riprap is placed on top of the bed forming a mound, due to ease of installation, lower cost, and inspection purposes (Lagasse et al., 2009). However, any test executed by Lagasse et al. (2007) with mounded riprap performed poorer than riprap installed flush with the bed. Therefore, riprap should always be

embedded with the top surface flush with the surrounding bed. In regards to the depth of riprap, often the minimum thickness recommendation is 2-3 times the median riprap stone size, but Lagasse et al. (2007) suggest 3 times the median riprap stone size as performance improved with increased riprap thickness (Lagasse et al., 2009; Lauchlan & Melville, 2001). Fig. 2-6 shows the aforementioned configuration of riprap around a bridge pier, where if installed as specified, can help reduce the chances of riprap failure.

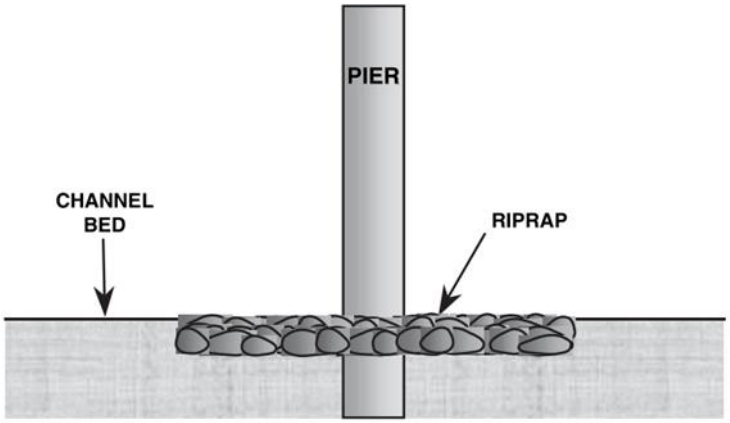

Fig. 2-6. Riprap configuration (Lagasse et al., 2007).

2.4.1.2.2 Partially Grouted Riprap

Partially grouted riprap is the same as standard riprap except a portion of the voids between the stones are filled with grout. First, the stones are chosen and installed, then the grout, often made of a cement base, is pumped into the cracks filling only approximately 50% of the voids, as seen in Fig. 2-7. By filling only a portion of the space between the stones, the countermeasure possesses greater stability in resisting shear forces but is also still flexible. The grout acts like a glue as it helps to hold the stones together, allowing for smaller stones to be used, however it is not strong enough to hold them together permanently (Lagasse et al., 2007). Therefore, if scouring were to occur beneath the riprap layer, the partially grouted riprap would theoretically break apart under its own weight and fill the scour holes. This approach takes the already successful riprap and improves it because it can withstand greater forces while using smaller stones, which makes installation easier and more cost effective. In addition, the smaller rocks do not protrude out of the riverbed as far implying they have less of an impact on the passing flow. This is beneficial because the more the armour layer protrudes into the passing flow, the more scour is likely to occur around the armour layer, hence why it is suggested to embed the armour layer into the riverbed (Lagasse et al., 2007). Tests were performed comparing standard riprap to partially grouted riprap and it was found, upon reaching a flow velocity of 2m/s, that the standard riprap was beginning to displace whereas the partially grouted riprap remained untouched (Lagasse et al., 2007). This proves that partially grouted riprap is more effective at reducing scour than standard riprap.

Fig. 2-7. Partially grouted riprap with pencil for size reference (Lagasse et al., 2009).

A few concerns exist with partially grouted riprap and they pertain to its installation. The first concern is ensuring exactly 50% of the voids have been filled while on the jobsite. Procedures have been developed to assist with this but it is not always known the exact quantity of the voids that have been filled, implying that the system could be more flexible or rigid than desired (Lagasse et al., 2009). The second issue is that grouting is not always possible due to the site location and equipment and grout availability, so this method is limited to certain locations (Lagasse et al., 2009). Therefore, if partially grouting is an option and done correctly, partially grouted riprap has the potential to be a better scour countermeasure than standard riprap in certain situations.

2.4.1.2.3 Cable-Tied Blocks

Cable-tied blocks, also known as articulating concrete blocks, are large concrete units held together by cables or geotextile fabric for the purpose of creating a large mat (Melville et al., 2006). The mat is positioned around the base of bridge piers and on top of the riverbed to act as a protective layer. An example of a cable-tied block system can be seen in Fig. 2-8. The purpose of connecting the blocks is so that they can act together as a system rather than individual blocks. This increases their stability allowing for greater forces to be resisted. Also, smaller blocks can be used, that would otherwise be dislodged by the passing flow, because the applied force is shared amongst the neighbouring blocks. Therefore, the chances of individual ejection, like with riprap, are reduced by connecting the blocks (Melville et al., 2006).

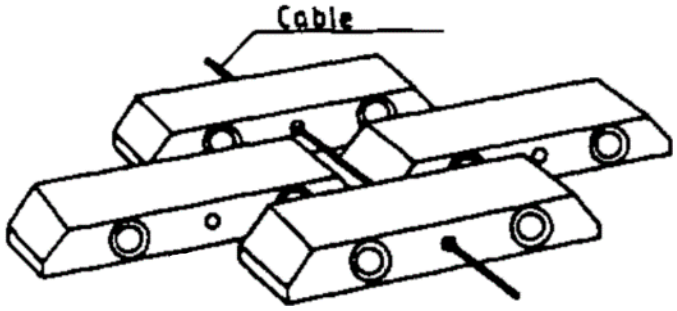

Fig. 2-8. Cable-tied blocks as a protective mat (Ettema, Nakato, et al., 2006).

There are three failure methods which can occur because of the system behaving like a mat. The first is when the leading edge of the mat overturns and rolls up, and this is initiated by the passing flow inducing turbulence on the mat. Once the edges of the mat begin to vibrate, slack forms within the mat allowing the edges lift. The passing flow then overturns the edge blocks and the mat rolls up like a carpet. As soon as the mat begins to roll up, the system has failed, and the scour protection is lost. To avoid this problem, the edges of the mat can be anchored into the riverbed so that they won't vibrate and become susceptible to overturning (Melville et al., 2006). The second failure method is when the front of the mat is anchored and the rest lifts off of the riverbed, which is caused by high velocity flow passing over the mat. When the mat is not embedded into the riverbed, the passing flow must travel up and over the mat causing a constriction of the streamlines. This constriction forces the flow to increase in velocity, consequently causing a reduction in pressure. This drop in pressure over the mat induces an uplift force which causes the mat to lift off of the riverbed, therefore lessening the scour protection provided. One method of reducing this problem is to embed the cable-tied block mat into the riverbed so that there is little to no flow acceleration over the mat (Melville et al., 2006). The last failure method for cable-tied blocks is when scouring occurs between the mat and the pier, within the critical region, therefore putting the pier at an increased risk of failure. This happens when a gap is present between the mat and the pier, such that the downflow can penetrate between the two and create a scour hole. To avoid this problem, it is best to tie the mat to the pier, so it does not drift away, and then to physically seal the gap to disallow any water passage (Lagasse et al., 2007).

There is an additional complication associated with cable-tied blocks, regardless of the failure method, which pertains to the ejection of blocks from within the mat itself. Lost blocks are much more difficult to repair after the system has been installed, since a new block must be reconnected under water at the base of the pier. Therefore, maintenance and even original installation can be more challenging and costly when compared to other methods. However, if cable-tied blocks are installed correctly such that the failure methods mentioned above are addressed, then this countermeasure is a viable solution (Lagasse et al., 2007).

2.4.1.2.4 Grout-Filled Containers

Grout-filled containers can come in two different forms, grout-filled mattresses or grout-filled bags. The two behave differently so grout-filled mattresses will be discussed first. Grout-filled mattresses are large bags made of synthetic fabric that are divided into a number of compartments which are connected by small passages (Lagasse et al., 2007). To install such system, the empty mattress is laid in the final location around the bridge pier and grout is pumped in. Due to the small passages, the grout travels into all of the cavities and then hardens in place, forming a large grid of connected blocks. These blocks are able to move within the mattress deeming this a flexible countermeasure (Lagasse et al., 2007). Grout-filled containers are very similar to cable-tied blocks in how they perform and their failure methods. Specifically, rolling up of the mattress, lifting of the mattress caused by the passing flow, and scour between the mattress and the pier, are all possible failure methods. Therefore, the solutions mentioned above for cable-tied blocks to avoid such failure methods, also apply to grout-filled mattresses (Lagasse et al., 2007).

The longevity of grout-filled mattresses, as well as cable-tied blocks, has had limited testing for pier applications, but it is suspected that wear and tear from the movement of the individual components is possible for both. Specifically, the cables could break for cable-tied blocks, and the mattress could rip open for grout-filled mattresses (Lagasse et al., 2007). The main difference that exists between cable-tied blocks and grout-filled mattresses is how they are installed, such that cable-tied blocks are laid down like a mat whereas grout-filled mattresses are filled in place. Therefore, one would be primarily chosen over the other based on specific site installation requirements.

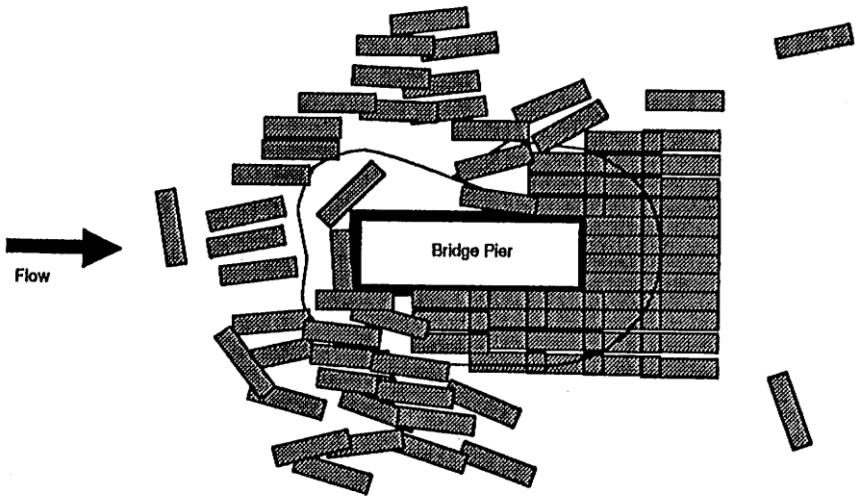

Fig. 2-9. Grout-filled bags failure method (Parker et al., 1998).

The second type of grout-filled container is different because it consists of individual bags filled with grout which are not connected, known as grout-filled bags (Parker et al., 1998).

To install grout-filled bags, first, a series of empty fabric bags are placed around the base of a bridge pier in some specified orientation, then they are individually filled with grout. This type of scour prevention system is prone to various failure methods. The first failure method is simply undersized bags which cannot withstand the passing flow. This is a frequent problem because the bags are commonly rounded and smooth, unlike riprap which is angular, so the bags do not interlock together requiring larger sized bags to withstand the same flow velocity (Parker et al., 1998). The second failure method is scouring around the grout-filled bags, since they are larger in size to accommodate the lack of interlocking, they are also more prone to scouring unless they are embedded into the riverbed (Parker et al., 1998). The last failure method is from bag movement, as seen in Fig. 2-9, such that as soon as the bags lose their original orientation, the scour protection decreases. The best approach to avoid a majority of these failure methods is to stitch the bags together onto a layer of geotextile. By doing so, the bags will hold their orientation for longer and have more stability, but this also makes the system prone to mat related failure methods, as mentioned for cable-tied blocks. Based on the number and severity of failure methods associated with grout-filled bags, they are not recommended as an ideal pier scour countermeasure (Parker et al., 1998).

2.4.1.2.5 Gabions

The last type of armouring countermeasure that will be discussed is gabions. Gabions are large wire mesh containers that are filled with stones, wired closed, and placed around the pier on the riverbed, as seen in Fig. 2-10. The benefit of gabions is that they can be filled on site with any type of stone, specifically stones that are smaller in size, as the same quantity of scour protection is still provided because the stones are contained together (Yoon & Kim, 2001). The wire mesh allows the containers to deform and adapt to moderate changes in the riverbed, for example in the case of undermining, deeming this a flexible countermeasure (Lagasse et al., 2007).

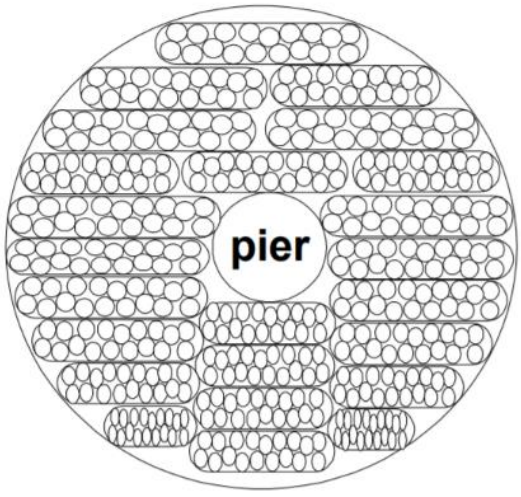

Fig. 2-10. Gabion sac placement around pier (Yoon & Kim, 2001).

Gabions are similar to grout-filled containers because they can come in the form of mattresses or individual sacs. To create a gabion mattress, numerous individual sacs are simply wired together generating a large mat like some of the other countermeasures (Lagasse et al., 2007). However, gabions are not susceptible to all of the same failure methods as grout-filled containers and that's largely because uplift is much less likely to occur. The reason for that is because gabions are composed of loose stones which possess voids, therefore reducing the uplift force that is generated across the mattress (Lagasse et al., 2007). It is important nonetheless, to address the gap between the pier and the mattress, as well as to orient the individual sacs in a specific pattern, otherwise failure is much more likely to occur. One failure method that is specific to only gabions is deterioration of the mesh. Since the mesh containers are flexible to some degree, this induces wear on the mesh causing them to eventually break, therefore releasing the stones that are within. Once the stones have spilled out of the gabion containers, there is no added benefit of the gabion, and the stones will be washed downstream because they are usually smaller than the necessary riprap size (Lagasse et al., 2007).

It has been found through experimental testing that housing stones within a gabion container improves their stability (Yoon & Kim, 2001). However, gabion mattresses and sacs are similar to grout-filled mattresses and bags, such that it is difficult to determine which system is better. Gabion systems are not prone to uplifting but they are susceptible to mesh deterioration. Neither approach is ideal but in order to validate which is the better pier scour countermeasure out of the two, further testing is required.

To conclude this section, hydraulic countermeasures are a common approach, as they alter the approaching flow behaviour or armour the riverbed around the piers, for the purpose of addressing the harmful scour problem. Various examples of hydraulic countermeasures were discussed, with one of the most popular being standard riprap. However, sometimes it is not practical to use hydraulic countermeasures because of various reasons, such as resource limitations or environmental restrictions. Therefore, other forms of scour countermeasures which address the scour problem differently, are required. The second major group of countermeasures focus on altering the structural components of the bridge to reduce scour and are referred to as structural countermeasures. They will be discussed in more detail in the next section.

2.4.2 Structural Countermeasures

Structural countermeasures, which are an alternative to hydraulic countermeasures, are used to alter the bridge piers in some way to help reduce scour. Structural countermeasures can be divided into two categorizes depending on which part of the pier is being altered. Foundation strengthening pertains to the portion of the pier below the riverbed, whereas pier geometry modifications pertain to the portion of the pier above the riverbed (Lagasse et al., 2009).

2.4.2.1 Foundation Strengthening

Foundation strengthening is amongst one of the most thorough and resource intensive forms of mitigating scour related failures, as it consists of adding onto to the existing pier

foundation. The purpose of adding onto a pier foundation, either through increasing the reinforcement or extending the size of the foundation, is to improve the pier's stability so that failure can be avoided if the riverbed lowers due to scouring (Lagasse et al., 2009). The most common forms of foundation strengthening consist of adding concrete to enlarge the footing, filling the scour induced voids under the footing, or installing piles beneath the footing, each of which will be discussed in more detail below (Agrawal et al., 2005).

2.4.2.1.1 Extended Footings

An extended footing refers to increasing the size of the existing footing in the horizontal direction only. This countermeasure is recommended for concrete spread footings as the purpose is to increase the area in which the weight of the bridge is distributed to the riverbed, and to act as an apron around the pier to protect from the horseshoe vortex (Agrawal et al., 2005). If the intention is to shield the riverbed from the horseshoe vortex, then the elevation of the top of the footing is critical. Specifically, it was found that if the top of the spread footing is positioned at or below the riverbed height, then scour can be reduced, but if the top of the spread footing protrudes out of the riverbed, then scour can be increased (Jones et al., 1992). There are various methods of increasing the size of a pier's footing but most use concrete and require some form of containment so that the concrete sets in the desired location. One issue with extended footings is that they are only suitable for low scour regions because the footings still have the potential to become undermined since their depth into the riverbed is not increased (Agrawal et al., 2005). This solution is questionable for engineers because extending footings horizontally is an extensive procedure and does not guarantee undermining will be prevented. Therefore, this is not a preferred countermeasure for scour prevention.

2.4.2.1.2 Underpinning

During high flow events, scour is often very common such that extreme scour depths can be reached. In some cases, the foundations of piers can become undermined, therefore jeopardizing the stability of the piers. Underpinning is a technique which uses aggregate or concrete to fill such voids under the footing for the purpose of bringing the pier's stability back to a safe position (Agrawal et al., 2005). When doing so, underpinning acts as more of a repair than a countermeasure because one is assuming greater scour depths will not be reached, suggesting that the scour hole was caused by an event which is unlikely to occur again. However, this method can also be used as a scour countermeasure by increasing the depth of the footing so that in the future greater scour depths can be overcome. This is done by excavating beneath the footing and physically extending the bottom of the footing deeper into the riverbed. The problem with extending the footing in the vertical direction is that the installation becomes more extensive because the bridge often needs to be closed to traffic to avoid any added weight (Agrawal et al., 2005). By doing so, the scope of the project increases drastically and so does the cost.

If only the scour voids under and around a pier's footing are being filled and the depth of the footing is not increased, then this method is moderately easy to execute. But, if greater scour

protection is desired such that the depth of the footing is increased, then installation of this method is more costly, labour intensive, and intrusive to the surrounding environment (Agrawal et al., 2005).

2.4.2.1.3 Pile-Underpinning

Another method, which increases the stability of bridge piers, and also strengthens the foundations, is pile-underpinning. During scour, material becomes eroded from around and beneath a pier's footing, which causes the footing to lack a solid base to rest on. The purpose of piles is to extend far beneath this erosion depth, to levels that are more stable, so that scour will not affect the stability of the pier. By doing so, the weight of the bridge is transferred deeper into the riverbed to depths that can safely withstand such forces, therefore bypassing the scour region (Ettema, Nakato, et al., 2006).

Underpinning a footing using piles consists of driving piles below the pier footing into the riverbed. Once the piles are in place, they are cut off below the bottom of the footing, a pile cap which is usually made of concrete is poured on top of the piles, and then the existing footing is positioned directly on top of the pile cap to rest. This transfers the weight of the bridge from the existing footing, to the pile cap, and then through the piles into the riverbed (Lagasse et al., 2009). Another method of accomplishing pile-underpinning is with minipiles, which are driven through the existing footing and extend out the bottom, as seen in Fig. 2-11. Instead of digging a large hole under the footing and pouring a pile cap, with minipiles, the existing foundation acts as the pile cap. There are some benefits to this method, such that installation can be easier, and the machinery used to install minipiles is smaller and more site accessible. In addition, minipiles can often be installed with traffic on the bridge, unlike underpinning with standard piles which requires the bridge to be closed (Agrawal et al., 2005).

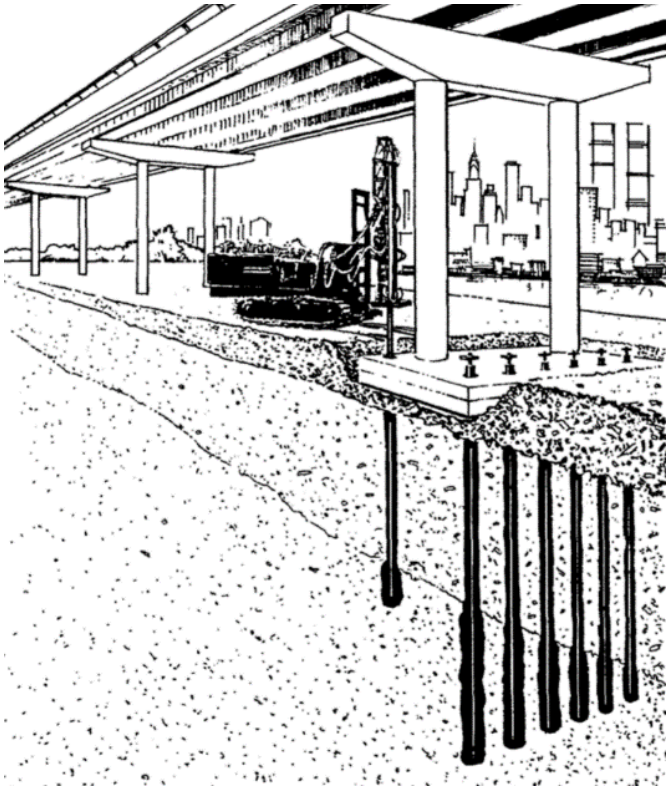

Fig. 2-11. Foundation underpinning using minipiles (Agrawal et al., 2005).

A case study was performed in New Jersey where four highway bridges had experienced large quantities of scour. Underpinning with minipiles was chosen to mitigate the problem because the piers were poorly accessible such that standard piles could not be installed (Larsson & Jog, 2014). The goal was to reduce the quantity of foundation settlement and in order to do so, over 400 minipiles were installed, each possessing a length of 6.1m. It was found through preloading the minipiles, that only 6 mm of settlement was expected over their lifespan. This is on par with standard piles suggesting that minipiles are a good alternative to standard piles (Larsson & Jog, 2014).

Pile-underpinning, whether it is done with standard piles or minipiles, is costly, labour intensive, and intrusive to install, resulting in pile-underpinning often only being used in extreme scour situations (Agrawal et al., 2005). Minipiles show promising results because they can perform as well as standard piles, they do not interfere with traffic on the bridge, and they can be installed in more difficult locations (Larsson & Jog, 2014). However, sometimes the original footings must be expanded in order to accommodate the large number of minipiles that need to be installed, which adds to the cost and labour efforts associated with minipile installation. Therefore, an engineer may choose minipiles over standard piles if traffic cannot be interrupted or if the equipment for standard piles can not access the pier location (Larsson & Jog, 2014).

Of the structural countermeasures discussed, they are all extensive to install and intrusive to the surrounding environment, when compared to some of the other countermeasures available.

Therefore, foundation strengthening countermeasures are a last resort option and the specific type should be chosen on a case-by-case basis, as there is not one that is ideal for all situations.

2.4.2.2 Pier Geometry Modifications

Pier geometry modifications address the portion of the pier that is above the riverbed, as the aim is to alter the behaviour of the passing flow. Through changing various components, such as the shape, texture, and overall geometry of the pier, the severity of the horseshoe vortex, the accelerated velocity along the sides of the pier, and the wake vortices can be reduced. This is beneficial because such flow behaviours directly affect the scour depth that forms around the base of piers. The most common geometry modifications will be introduced below.

2.4.2.2.1 Pier Shape

The shape of a pier can be altered in many ways. First to be discussed is the effect of changing the shape in plan view while maintaining a constant shape in profile view. A study was performed by Vijayasree et al. (2019) which compared five different shaped piers consisting of: rectangular (*P1*), oblong (*P2*), trapezoidal-nosed (*P3*), triangular-nosed (*P4*), and lenticular (*P5*). The flow velocity and direction was constant for all tests. The scour depth at the nose of the pier, as well as the overall maximum scour depth, was recorded which can be seen in Fig. 2-12. It was found for *P1* and *P2*, that the deepest scour was recorded at the nose of the pier and that is due to the horseshoe vortex, whereas for *P3*, *P4*, and *P5*, the horseshoe vortex was less significant because of the sharper leading edge of the pier (Vijayasree et al., 2019). By making the leading edge come to a point, it reduces the pressure gradient that forms in front of the pier and consequently reduces the severity of the horseshoe vortex. For *P3*, *P4*, and *P5*, the deepest scour holes were located on the sides of the pier because of the accelerated bypassing flow. Naturally, *P1* produced the largest scour depth, but by rounding the nose (*P2*), the scour depth was reduced by 30% (Vijayasree et al., 2019). *P3* and *P4* have interesting results such that when they are compared, *P4* has less scour at the nose because of the sharp leading edge, but it has more scour along the sides of the pier. Ultimately, *P5* reduced scour the most because of its sharp nose and mildly sloped sides, to the point where a scour reduction of 68% was achieved when compared to a rectangular pier (*P1*) (Vijayasree et al., 2019). This study proves that by changing the shape of the pier in plan view, it can have a very large impact on the scour that forms around the base of the pier.

Shape of pier	Frontal Area of piers (10^{-4} m^2)	Length AD (m)	Width EH (m)	Scour depth at nose (10^{-2}m)	Max. scour depth (10^{-2}m)	Location of max. scour (10^{-2}m)	Changes in scour w.r.t P1 (%)	Time taken for equilibrium (min)	Volume of scour geometry (10^{-4}m^3)	Blockage area (10^{-4}m^2)	Distance AB (m)
P1	99	0.50	0.29	6.8	6.8	(−7.5,0)	100	≈240	113.82	45	0.1235
P2	77.76	0.48	0.27	4.7	4.7	(−7.5,0)	71.21	148	72.76	43.07	0.105
P3	68.64	0.24	0.20	2.4	2.65	(−6.0, ±1.5)	40.15	70	48.99	38.7	0.045
P4	58.64	0.34	0.22	1.85	3.55	(−4.5, ±1.5)	53.79	89	67.43	36	0.048
P5	56.1	0.23	0.17	0.7	2.2	(−1.5, ±1.33)	33.33	60	44.59	27.68	0.025

Note: AD = Total length of scour hole; EH = Total width of scour hole and AB = Distance between leading edge of pier and u/s edge of scour hole.

Fig. 2-12. Effect of altering the pier shape on the scour depth (Vijayasree et al., 2019).

Despite the benefits associated with streamlining the pier, there is one large issue which arises and that pertains to the angle of the pier with respect to the passing flow. If the pier is positioned parallel to the passing flow, then the scour reduction values associated with the pier shape modifications mentioned earlier are valid. But, if the pier is not parallel to the flow, such that there is a skew angle, then the quantity of scour reduction decreases (Melville, 2008). This is because the frontal width of the pier increases as the skew angle increases, which causes the pressure gradient on the upstream face of the pier to grow, generating a more powerful horseshoe vortex. According to Melville (2008), increasing the skew angle to 30^o causes the depth of scour around the pier to triple. This would however not be a problem if the pier were circular. Therefore, it is recommended if the flow is likely to change direction, even by a few degrees, to use circular piers rather than streamlined piers (Melville et al., 2008).

Increasing the bridge pier width, according to Melville (2008), has proven in certain situations to increase the down flow on the upstream face of the pier, leading to a more intense horseshoe vortex. But, increasing the pier width can also have a positive effect on scour such that it can increase the size of the wake vortices. When the size of the wake vortices increase, their vorticity decreases, implying that the quantity of sediment being ejected and transported downstream from behind the pier is reduced. This is beneficial, however, the resulting increase in scour at the nose of the pier outweighs the scour reduction at the rear, making such increase in pier width ineffective (Ettema et al., 1998).

In addition to the pier width, the streamwise length of the pier has been found to also affect the depth of scour. Specifically, when the streamwise pier length divided by the pier width (pier aspect ratio) equals 0.25, the depth of scour is at a maximum. But, when the pier aspect ratio increases or decreases from that value, the depth of scour reduces (Ettema et al., 1998). The smallest scour depth, as a result of changing the pier length, occurs when the aspect ratio is above 4, such that a scour reduction of 20% can be achieved (Ettema et al., 1998). Meanwhile, a reduction in scour can also be achieved when the pier aspect ratio is below 0.25, but only by 8%. The reason the length of the pier influences the corresponding scour depth is because of the interaction between the vortices that form on the front corners of the pier and the vortices that

form on the rear corners of the pier. Depending on the length of the pier, the vortices can either be far enough away from each other that they do not interact or close enough that they merge (Ettema et al., 1998). Therefore, a longer pier is more beneficial for reducing scour.

The last component pertaining to the pier's shape, which can influence the scour depth, is the angle of the pier in profile view. It was found that creating a slope on the downstream face of the pier has negligible effects on the scour depth, but a slope on the upstream face of the pier has noticeable effects. Specifically, if the upstream slope is such that the top of the pier is further downstream than the bottom of the pier (upwards slope), scour can be reduced. However, if the slope is in the opposite direction (downwards slope), then scour can be promoted. This behaviour occurs because of the slope's ability to either increase or decrease the down flow along the upstream face of the pier, which ultimately impacts the strength of the horseshoe vortex (Melville, 2008). By adding a 2-15^{o} slope to the upstream face of a bridge pier in the upwards direction, scour can be reduced by almost 30% (Bozkus & Yildiz, 2004). Thus, sloping the upstream face is an effective way to help reduce scour, especially when designing a new pier.

2.4.2.2.2 Pier Texture

Another method, which is a simple concept but has shown to reduce scour, is altering the texture of the pier. Piers are often made with a smooth surface as that is common practise, but Gris (2010) has proven that increased surface texture can influence the passing flow in a positive way. Gris (2010) patented the idea of installing a sheath over the existing pier which possesses the desired texture, as seen in Fig. 2-13. By doing so, the pier remains untouched and its structural integrity is not harmed. The sheath consists of two different textures: one on the upstream face, and one on the sides. The upstream face uses directional grooves which are angled upwards and they help to reduce the downward flow in front of the pier. Meanwhile, the sides of the pier use a nondirectional pattern of rugosity which gives the pier an increased roughness (Gris, 2010). The purpose of the side roughness is to act like a golf ball, where the boundary layer changes from laminar to turbulent, causing the flow to remain attached to the pier for longer. This reduces the wake that occurs downstream of the pier and therefore decreases the severity of the wake vortices. Through experimentation, it was found that the addition of only the surface texture mentioned above, and not the streamlined shape shown in Fig. 2-13, reduced scour by approximately 30% (Gris, 2010). This simple addition of texture to the surface, specifically by means of a sheath, is low cost, easy to install, minimally intrusive, and potentially maintenance free, making it extremely desirable especially for new bridge piers. The problem is that surface texture only reduces scour by 30%, so it might be the most optimal when paired with another countermeasure.

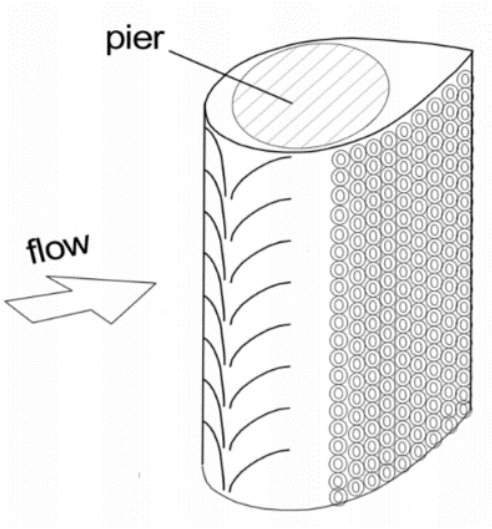

Fig. 2-13. Pier sheath designed to reduce scour (Gris, 2010).

2.4.2.2.3 Pier Slot

An alternative countermeasure, which alters the pier's geometry by removing instead of adding material, consists of incorporating a relatively large slot through the pier. The purpose of having a slot that continues through the pier in the streamwise direction is to divert or reduce the down flow on the upstream face of the pier. The width, height, and vertical location of such slot in the pier greatly impacts the resulting scour reduction (Chiew, 1992). A study was performed by Chiew (1992), where the effect of two different slot locations, in addition to various slot sizes, were examined (Fig. 2-14). When the slot was located near the bed, flow passed through the slot at an accelerated velocity, similar to a jet, which deflected a portion of the down flow in front of the pier, away from the bed. This resulted in a maximum scour reduction of 20%, and that was only possible when the slot width was 25% of the pier diameter (D) and the slot height was at least $2D$ (Chiew, 1992). When the slot was located near the water surface, the function of the slot changed such that it aided in reducing the water height, which therefore reduced the down flow in front of the pier. With a slot width measuring $0.25D$, the maximum scour reduction was 20%, but when the slot width increased to $0.5D$, the maximum scour reduction was 30% (Chiew, 1992). In order to achieve such scour reduction values with a slot near the surface, the slot must extend the entire height of the pier.

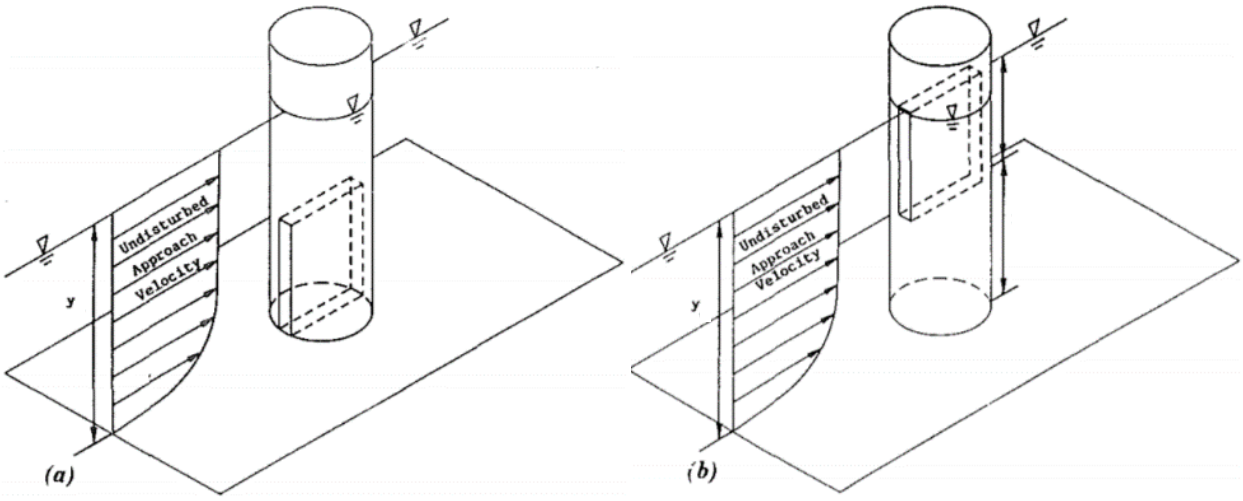

Fig. 2-14. Illustration of two different pier slot locations: (a) at the bed, and (b) at the water surface (Chiew, 1992).

By using slots, it is possible to reduce the maximum scour depth by as much as 30%, however it is not often practical to use slots because very large holes need to be cut into the pier. This is costly, difficult to install, and reduces the structural integrity of the pier. In addition, the slot is prone to debris jamming and upon this occurring, flow cannot pass through the slot rendering the countermeasure useless (Chiew, 1992). Therefore, pier slots are not recommended as an ideal pier scour countermeasure.

2.4.2.2.4 Collar

The last countermeasure, which lies within the pier geometry modifications grouping, is collars. A collar is simply a flat horizontal disk that is mounted around a bridge pier to impede the downward flow along the front face of the pier (Chiew, 1992). The shape of the collar is usually circular, varying in diameter often between 2-4*D*, while possessing the smallest possible thickness. The two largest factors that dictate a collar's performance is its diameter and location on the pier. Chiew (1992) studied these two factors in detail and the results can be seen in Fig. 2-15 ($(d_s)_o$ = maximum scour depth without a countermeasure). According to the results, by installing a collar that has a diameter of 2*D* and is located below the riverbed at a depth of 0.2*y* (*y* = flow depth), scour can be reduced by over 50%. But, as the collar moves higher up the pier, the scour reduction decreases to the point where the collar becomes ineffective above the riverbed at a height of 0.1*y* (Chiew, 1992). Therefore, the best collar placement is at or below the riverbed. In addition, Chiew (1992) discovered that as the collar diameter increases, so does the quantity of scour reduction. It is in the engineer's best interest however, to keep the collar as small as possible, this way it is less intrusive to the surrounding environment, easier to fabricate, requires less material, and is less expensive.

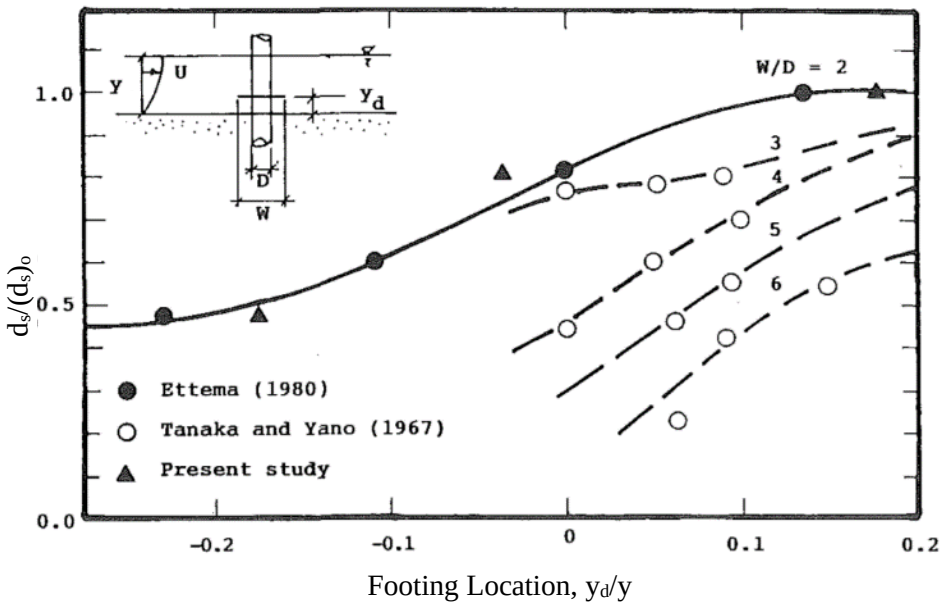

Fig. 2-15. Scour reduction as a result of collar location and size (Chiew, 1992).

One problem associated with collars is the potential for undermining to occur beneath the collar itself. This is most common within live-bed conditions where passing bed forms, which possess a trough, can expose the edges of the collar to the passing flow. As a result, scour can occur under the collar eventually exposing the pier itself, therefore rendering the collar ineffective (Chiew, 1992). However, if erosion beneath the collar could be addressed to the point where it is less of a concern, then collars have the potential to be an excellent countermeasure as they have proven to reduce scour by over 50%.

Due to the potential shown by collars, this is an active area of research. Chen et al. (2018) introduced a new type of collar, a hooked-collar, that possesses a reduced width when compared to conventional Flat Plate Collars (FPCs). The hooked-collar is similar to FPCs but has a smaller outer diameter with a vertical ring ($h = 0.25D$) mounted to the perimeter, as shown in Fig. 2-16. The added vertical ring works to deflect the downwards flow on the front face of the pier causing a reduction in the horseshoe vortex strength, while also allowing for a reduced collar diameter. There is currently a patent pending for this design, as result of Chen et al. (2018), entitled *Hooked-Collar for Piers and Bridge Including the Same*.

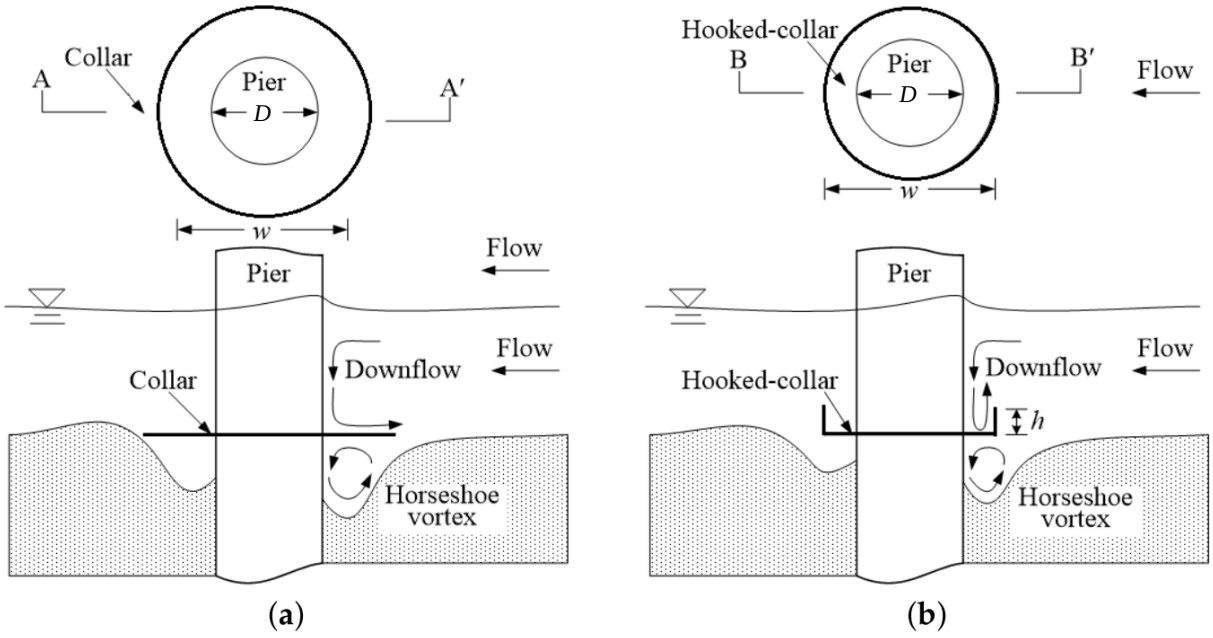

Fig. 2-16. Flow behaviour around a circular pier possessing: (a) an FPC, and (b) the new hooked-collar (Chen et al., 2018).

The hooked-collar was tested at different elevations on the pier which included below the bed, at the initial bed elevation, and above the bed, in addition to incorporating multiple hooked-collars on the pier. When the hooked-collar was positioned at 0.25*D* below the bed, a scour reduction of only 24% was achieved. When the hooked-collar was positioned at the initial bed elevation, the scour reduction improved reaching a value of 42%. However, the greatest scour reduction was achieved when one hooked-collar was positioned at the initial bed elevation and a second hooked-collar was positioned 0.25*D* above the bed, as scour was reduced by 50% (Chen et al., 2018). From this study, it can be noted that a collar positioned below the bed is not the most beneficial and the addition of a second collar provides only little scour reduction gains. The primary benefit of the hooked-collar is that it possesses a reduced width in comparison to the FPC since there is no improvement of scour reduction.

Another collar design variation was recently introduced by Applied University Research (AUR), Inc, and referred to as scAUR (Simpson, 2013). This new collar design resembles a skirt that wraps around the base of the bridge pier eliminating the 90º angle between the pier and the bed, as shown in Fig. 2-17. ScAUR is made of prefabricated stainless-steel sections, or poured in place concrete, and is designed to prevent the formation of the horseshoe vortex and other scour causing vortices while protecting the base of the pier. This design is currently patent pending and has been commercialized by AUR, Inc.

Fig. 2-17. Prototype scale example of the scAUR countermeasure (AUR Inc, 2020).

AUR, Inc, claims that scAUR completely eliminates scour, however the available data to confirm this is limited (AUR Inc, 2020; Simpson, 2013). Any laboratory tests validating the design was performed on a gravel bed where scour was minimal without any countermeasure. Due to the lack of supporting data, further testing is required to determine the performance of scAUR and its associated limitations. One can speculate that the rigid nature of the bottom of the device that rests on the riverbed would be prone to the same undermining concerns that the traditional FPC experiences.

Lately, bridge pier collars have generated increased attention in the research field by means of new designs and continued research. However, despite the recent progression, there is still not one collar design that has proven to eliminate undermining while greatly reducing scour. Therefore, there is still room for improvement regarding bridge pier collar design.

In conclusion, structural countermeasures are an approach which alter only the pier itself in an attempt to reduce scour or increase the pier's stability. They can be installed on the portion of the pier that is either above or below the riverbed, however there is not one countermeasure that greatly reduces scour, is minimally intrusive to install, and works under all conditions. Some countermeasures such as pier streamlining or collars show positive results and are less intrusive to install, however there are specific conditions in which they become ineffective. Therefore, an ideal structural countermeasure does not exist and choosing the proper one is case dependent, requiring the engineer to have a vast understanding of the pros and cons of each.

2.4.3 Biotechnical Countermeasures

Biotechnical countermeasures refer to the use of vegetation, in some form, to aid in scour reduction. They are becoming more popular due to their aesthetics, ease of installation, environmentally friendly characteristics, and low cost, however their primary use is for riverbank stabilization implying that little information is available on pier scour reduction (Lagasse et al., 2009). Some common examples of biotechnical countermeasures consist of vegetated geosynthetic products, woody mats, vegetated riprap, root wads, and live staking, such that they

are used to armour riverbeds and banks. They generally work through a two-fold technique where: 1) the roots of the vegetation are used to stabilize the soil, and 2) the exposed foliage is used to provide flow resistance which extracts energy from the passing flow (Lagasse et al., 2009). By stabilizing the soil and slowing the flow velocity, biotechnical countermeasures can provide effective erosion resistance especially because they are usually flexible and can adapt to changes in the riverbed. However, in order for living solutions to be effective, the location must be conducive to vegetation growth. Due to the lack of knowledge, trust, and growth requirements associated with biotechnical countermeasures, HEC-23 states that they should not be considered as the sole countermeasure when the safety of a bridge or highway structure is at stake (Lagasse et al., 2009). For that reason, biotechnical countermeasures are not yet used on their own for pier applications but can compliment other countermeasures if the location is conducive to vegetation growth.

2.4.4 Monitoring

The last countermeasure group is monitoring. Monitoring is different than all of the other countermeasures such that it is more of a reactive approach. The reason for that is because monitoring does not physically provide any alterations to the pier site to reduce scour, rather it notifies the necessary people that scour is occurring. Upon being notified that scour is occurring or has occurred, measures can be taken to stop and reduce further scour prior to failure (Lagasse et al., 2009). Monitoring is very useful because it eliminates the unknown factor when dealing with pier scour, as it is difficult in many situations to predict the exact scour depth that may occur. Monitoring becomes even more effective when coupled with other countermeasures because it can provide performance information on the other countermeasure as well as alert if failure is predicted to happen.

There are three types of monitoring techniques, consisting of fixed instrumentation, portable instrumentation, and visual inspection (Lagasse et al., 2009). Fixed instrumentation refers to monitoring devices that are mounted onto the bridge in a specific location. Fig. 2-18 displays an example of a fixed instrument, however more advanced instruments exist to measure scour which utilize sonar technology, for example, instead of mechanical systems. The benefit of fixed instrumentation is that it can be used to indicate when certain scour depths have been reached in real time, and in some cases, even capture a timeline of the scour process (Conaway, 2006). The downfall to fixed instrumentation is that installing a monitor on each pier is not always practical, so only a select few piers are usually chosen and monitored (Lagasse et al., 2009).

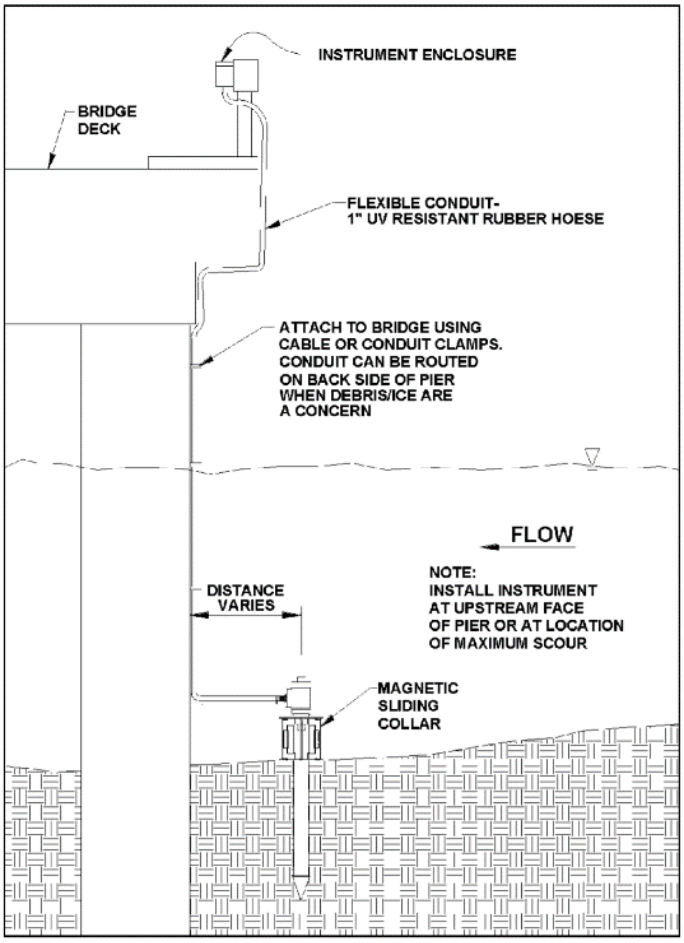

Fig. 2-18. Fixed instrument monitor on bridge (Lagasse et al., 2009).

Portable instrumentation pertains to monitoring devices that are not fixed to the bridge, rather they can be used on multiple piers of a single bridge and then transported to other bridges. By doing so, this is a much more cost-effective way to monitor the scour of numerous piers as compared to fixed instrumentation which is limited to a select few piers. The frequency of data collection depends on the risk level of the scour, such that for higher risk piers, personnel will collect data more regularly, and vice versa. However, the problem with portable instruments is that it is not possible to have a continuous watch over a specific bridge, rather data is only collected when an individual physically does so (Lagasse et al., 2009).

Lastly, visual inspection pertains to monitoring the bridge through standard methods without sophisticated instrumentation. This consists of visiting the bridge on a regular basis, as well as before and after high flow events, and recording the riverbed height around the piers. One way of accurately inspecting and measuring the scour around each pier is by performing underwater inspections, but that can be costly and pose a safety risk to the diver depending on the pier location (Lagasse et al., 2009).

Of the three bridge pier scour monitoring methods mentioned above, the best type depends on a number of case specific factors such as public safety, desired frequency of data collection, and the condition of the bridge, just to name a few. Monitoring is a very valuable resource which should be used more frequently, as it can help to identify the early stages of scour, prior to failure occurring. However, the downfall limiting its use is that monitoring on its own can not reduce scour, and for that reason it is often paired with other scour countermeasures (Lagasse et al., 2009).

2.4.5 Countermeasure Performance Evaluation

One of the most common methods of evaluating countermeasures is through measuring the resulting maximum scour depth and comparing it to that of a pier without any countermeasure. This approach, amongst others, will be used in this thesis to quantify the performance of each countermeasure. There are two methods that can used to determine scour depth in lieu of conducting prototype-scale tests: (1) experimental modelling (scaled-down), and (2) numerical modelling. Both of these methods will be briefly discussed.

2.4.5.1 Experimental Modelling

Performing tests at prototype-scale is the most accurate method of determining a countermeasure's scour depth, as there are no scaling effects or modelling inaccuracies, however this is often not feasible for many reasons. Therefore, it is more practical to perform scaled-down experimental tests at model-scale. Traditionally, experimental modelling was typically the only method of predicting scour, especially when analysing a countermeasure or complex pier geometry. Experimental modelling consists of installing a sand bed in the bottom of a flume, mounting a model pier such that it protrudes out of the sand, and flowing water down the flume (Chang et al., 2004; Dargahi, 1990; Das et al., 2013; Ettema et al., 1998; Jones et al., 1992; Raudkivi & Ettema, 1983). Then, if countermeasures are being tested, scaled models are constructed and installed in the flume (Ghorbani & Kells, 2008; Gris, 2010; Kumar et al., 1999; Lauchlan & Melville, 2001; Zarrati et al., 2004). The desired data depicts the type of instruments used to collect the data, such that for temporal scour data, maximum scour depth only, or the full bathymetry, different instruments exist (Gaudio et al., 2012; Hong et al., 2017; Zarrati et al., 2006).

2.4.5.2 Numerical Modelling

With the advancements in technology, numerical modelling has developed and become more capable and accurate. Instead of experimental modelling being the only option to determine scour depths, Computational Fluid Dynamics (CFD) simulations have also become an option. Numerical models are appealing to researchers and engineers alike because of their relatively low cost, potential time saving, high level of detail, and lack of required experimental resources. Various numerical models are available, such as FLOW-3D, Ansys Fluent, TELEMAC, and OpenFOAM to name a few, however they vary in functionality, cost, and model flexibility.

The first functionality difference amongst models pertains to whether they are hydrostatic or nonhydrostatic models. What this means is that for hydrostatic models, the vertical momentum equation of the governing Navier Stokes equations is reduced to that of a shallow water assumption, as it can save computational costs. Whereas, for nonhydrostatic models, the full vertical momentum equation of the Navier Stokes equations is employed, allowing for a more accurate depiction of flow in the vertical direction (Lai, 2018; Marshall et al., 1997; Parsapour-Moghaddam & Rennie, 2017). For the purpose of this study, where downwards flow is present in front of the pier which generates the horseshoe vortex, a nonhydrostatic model is essential.

The next functionality difference between models pertains to if they have sediment transport capabilities, or not. For studying bridge pier scour and countermeasure design, it is ideal to employ a model that possesses sediment transport capabilities, however that was not always possible. At the time when this thesis was commenced, not all CFD models had publicly available sediment transport capabilities, such as OpenFOAM. CFD models with sediment transport capabilities has become an active area of research, as researchers have been working to develop solutions that achieve accurate morphodynamic results while maintaining reasonable computational costs (Shim et al., 2016). For example, Shim et al. (2016) introduced a Discrete Element Method (DEM) coupled with OpenFOAM to simulate sediment transport. However, there showed to be large deviations in particle velocities when comparing numerical to experimental results. The author concluded that further research is needed for successful sediment transport models in OpenFOAM (Shim et al., 2016).

The models that did possess sediment transport capabilities at the time this thesis commenced were still in their infancy stages as the results were not yet reliable. A study performed by Chen et al. (2018) looked at evaluating the performance of a new hooked-collar to reduce bridge pier scour, using both numerical and experimental methods. The numerical model they employed was FLOW-3D equipped with sediment transport capabilities. When comparing the scour depths achieved from the numerical and experimental models, a maximum error of 54.55% was experienced for a single hooked-collar positioned at the initial bed elevation (Chen et al., 2018). This is a large inaccuracy which makes studying scour and evaluating countermeasures with the given model extremely difficult.

Since the beginning of this thesis, sediment transport models have shown great improvement such that Ghaderi and Abbasi (2019) achieved a maximum scour error between FLOW-3D and experimental data of only 6.38%. The recent advancements in sediment transport modelling are promising for the research and engineering community, as it will greatly aid in scour countermeasure design (Lai, 2018).

One objective of this thesis was to utilize a numerical model that was open-source, implying that it was available at no cost. Of the models mentioned, only TELEMAC and OpenFOAM are open-source, as the others are commercial products that require subscriptions. In

addition to cost, open-source software packages are frequently more flexible, such that the user has the ability to alter the model to a greater degree to achieve better results. When comparing TELEMAC and OpenFOAM from a hydrodynamic point of view, OpenFOAM is more appealing due to its impressive performance and breadth of published literature (Maza et al., 2015; Ramos et al., 2014; Tafarojnoruz & Lauria, 2020). Whereas, the available literature describing and validating TELEMAC is limited.

In conclusion, a combination of both experimental and numerical models will be employed in this thesis to predict and better understand scour. By using experimental modelling to obtain morphodynamic data and numerical modelling to obtain hydrodynamic data, the strengths of each model are utilized and the most accurate results will be achieved. Specifically, the OpenFOAM CFD toolbox without sediment transport capabilities was the best choice at the time when this thesis was commenced, as it showed to yield accurate results, possessed a large quantity of published literature, and was free to use.

2.5 Research Needs

Bridge pier scour is an issue that has been studied for many years but is still the leading cause of bridge failures (Lagasse et al., 2007). This implies that, despite the progress made thus far to better understand scour, there are still some significant areas in which a deeper understanding is required. Based on the literature review performed above, there are two primary areas where research is either lacking or could be further advanced, and those pertain to: (1) bridge pier scour countermeasures, and (2) bridge pier scour in the presence of an ice cover. Both of these areas are summarized below:

- The primary purpose of a scour countermeasure is to reduce scour, but not many accomplish that well. Based on the literature review, a majority of countermeasures reduce scour by less than 50% or their performance is simply unknown. In addition, many countermeasures are not: effective in all conditions, economical, low maintenance, or relatively easy to install. Therefore, there is a need to continue the development of pier scour countermeasures, as there is room for improvement.
- Recently, researchers such as Wu et al. (2016) have discovered that an ice cover around bridge piers can influence the flow behaviour beneath, and ultimately increase scour. These findings are not only valuable, but also critical for ensuring public safety in ice prone regions. However, the current knowledge base pertaining to scour in the presence of ice covers is very limited, such that the HEC-18 scour equation does not take into consideration ice covers, nor does HEC-18 provide guidelines on how to design a pier to withstand the added scour from ice covers. The ice cover parameters in which data is severely lacking or non-existent pertains to ice cover roughness, fixed versus floating ice covers, and different levels of flow pressurization beneath fixed ice covers. These are amongst the most influential ice cover parameters that can affect scour.

The aim of this thesis is to contribute to the areas mentioned above. Specifically, by introducing an improved bridge pier scour countermeasure that outperforms existing countermeasures, as well as generating more bridge pier scour data under an ice cover that can ultimately assist in future bridge pier design.

Chapter 3. Collar Prototype No. 1 (CPN1) and the Hybrid Design Approach

3.1 Hybrid Modelling for Design of a Novel Bridge Pier Collar for Reducing Scour

Preprint of a modified version of an article printed in the Journal of Hydraulic Engineering © 2021 American Society of Civil Engineers (ASCE). DOI: 10.1061/(ASCE)HY.1943-7900.0001875.

3.1.1 Introduction and Objectives

The most recent reports have shown that many bridges are scour-critical, which can jeopardize the integrity of such bridges. Meanwhile, current scour countermeasures prove to only be moderately effective. Therefore, in order to improve public safety, countermeasures need to be improved further. Hence, the main objectives of this study are:

1) To design an improved scour countermeasure, configured in the shape of a complex three-dimensional collar, which contains the horseshoe vortex and protects against the increased velocity along the sides of the pier.
2) Utilize a hybrid design approach, which uses computational fluid dynamics (CFD) software as a tool to expedite the design process and experimental tests to yield realistic scour data, to achieve a refined design.
3) To perform an experimental comparison between a pier equipped with an FPC, the new collar, and a pier without any scour prevention methods.

3.1.2 Numerical Model Description

The open-source CFD software OpenFOAM (v1706), which employs the Finite Volume Method (FVM), was used to perform the numerical simulations (ESI Group, 2019). The solver used within OpenFOAM is *pimpleFoam*, as it is a transient solver designed for incompressible and single-phase flows, operating in pressure implicit split-operator (PISO) mode. The PISO algorithm splits the coupling between pressure (p) and velocity (u) and solves through the predictor-corrector approach (Issa, 1986). To ensure the most accurate results, while being as computationally efficient as possible, an adjustable time step feature is used such that a Courant number of 0.8 is always maintained.

For this study, Delayed Detached Eddy Simulations (DDES) are performed, which use the Large Eddy Simulation (LES) theory in the separated regions, and the Reynolds Averaged Navier Stokes (RANS) theory in the attached boundary regions, therefore saving computational time without jeopardizing accuracy (Strelets, 2001). Specifically, the k-omega Shear Stress

Transport ($k-\omega\ SST$) DDES turbulence model is used, which employs the Smagorinsky LES model in the freestream regions and the two-equation $k-\omega\ SST$ RANS model in the boundary regions (Gritskevich et al., 2012). This RANS model is beneficial, especially for domains with flow separation or adverse pressure gradients, as it incorporates the *k*-omega ($k-\omega$) model near the walls but transitions into the *k*-epsilon ($k-\varepsilon$) model towards the edge of the boundary region (Gritskevich et al., 2012; Menter, 1992; Menter et al., 2003; Spalart et al., 1997; Speziale, 1991). Additional information regarding turbulence model selection can be found in Appendix D. The initial values used for k and ω are 0.001734 $\frac{m^2}{s^2}$ and 0.8447 $\frac{1}{s}$, respectively, defined by Wilcox (2006). The governing equations for the $k-\omega\ SST$ DDES model are presented and further discussed by Gritskevich et al. (2012).

The numerical domain uses a single-phase fluid moving within a rectangular flume measuring 10m in length, 0.85m in width, and 0.15m in height. At 8.5m downstream from the inlet, a cylindrical pier with a diameter (D) of 0.09m is introduced using *snappyHexMesh*, OpenFOAM's own mesh generator. The focus area of the study is around the pier, and to ensure an acceptable resolution, two levels of refinement are used. This is shown in Fig. 3-1, where each level of refinement possesses a smaller cell size. The corresponding average dimensionless wall distance (y+) for the unrefined region is approximately 69. For the level one and two refinement regions, the average y+ is approximately 34 and 19, respectively. The cell sizes are 0.008m, 0.004m, and 0.002m for the unrefined region, level one refinement region, and level two refinement region, respectively. The entire domain totals approximately 5,500,000 cells.

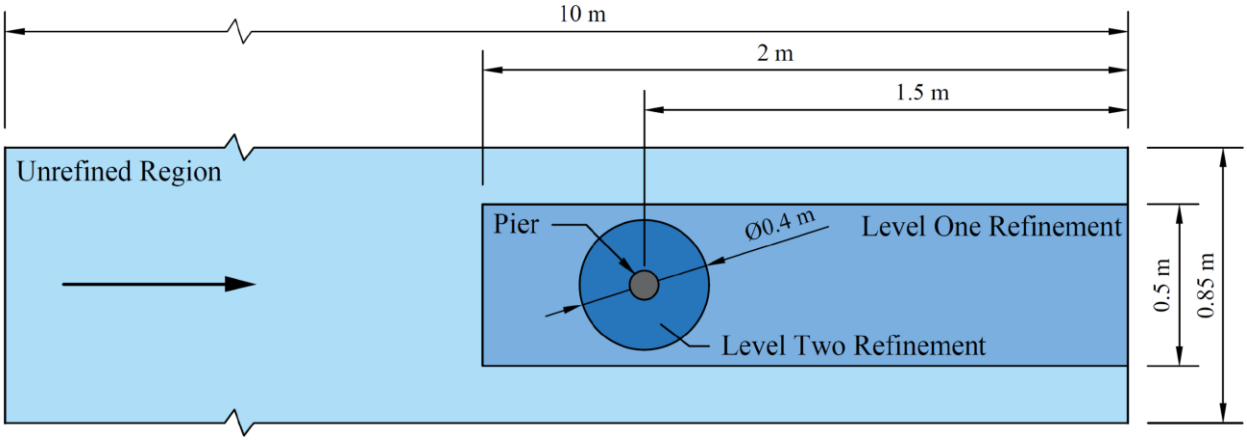

Fig. 3-1. Numerical domain with refinement regions.

The cell sizes, especially within the refinement regions, were chosen based on a mesh sensitivity analysis. The latter was performed by running the model with progressively smaller cell sizes until the mesh size no longer induced significant changes in the velocity, which was recorded at various locations within the computational domain. Fig. 3-2 shows the time-averaged velocity values for five different mesh sizes recorded in the level two refinement region, immediately upstream of the pier: its exact location is at X = -0.075m, Y = 0.000m, and Z = 0.015m. Mesh independence was achieved once a minimum cell size of 0.0025m was employed.

For the purpose of this study, a cell size of 0.002m was used in this region as it yielded a more desirable y+.

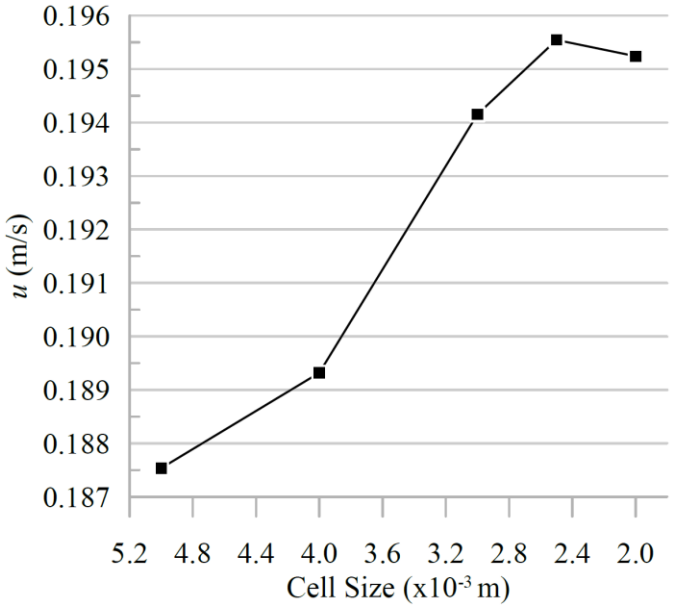

Fig. 3-2. Grid sensitivity analysis for velocity measured upstream of the pier in the level two refinement region.

The boundary conditions consist of a slip condition on the vertical sidewalls and a symmetry condition on the top surface, both for the purpose of reducing the influence of the walls. The pier and bottom of the flume use the no-slip boundary condition such that the velocity is fixed to zero at the surface. Furthermore, such surfaces possessing the no-slip condition (pier and bottom of flume) utilize wall functions for the turbulent viscosity (ν_t), ω, and k fields. Both the ν_t and ω fields use the log-law, while the k field uses a zero-gradient condition. To incorporate the roughness of the bed, the rough wall function constant (E'), found within the log-law equation for the ν_T field (Eq. 1), is modified using Eq. 2 (Knopp et al., 2009; Parente et al., 2011; Richards & Hoxey, 1993):

$$\nu_T = \nu \cdot \left(\frac{y^+ \kappa}{\log(E' y^+)} - 1 \right) \tag{1}$$

$$E' = \frac{E}{1 + C_s \frac{u_* k_s}{\nu}} \tag{2}$$

where (ν) is the kinematic viscosity, (κ) is the von Karman constant, (u_*) is the friction velocity, (E) is the model constant set to 9.8 (ESI Group, 2019), and (k_s) is the user defined sand-grain roughness height set to 0.001m so that it replicates the sand used in the experimental tests. A sensitivity analysis was performed to ensure that the specified k_s value accurately matched experimental conditions. Lastly, (C_s) is the user defined roughness constant, which is a measure of roughness type, set to 0.33 (Bates et al., 2005; Blocken et al., 2007).

To complement the LES based turbulence model, a turbulent inlet condition is used with an inlet velocity (u_{in}) set to 0.335m/s for all tests, yielding clear-water conditions. This inlet velocity was chosen so that the fully developed flow conditions match that of the experimental tests in the center of the flow. In order for the numerical velocity profile to fully develop prior to reaching the pier, and therefore match experimental conditions, the pier is placed a distance of 8.5m downstream from the inlet in the numerical model. This distance was determined from a sensitivity analysis, as it was found that the velocity profile requires approximately 8.5m to develop. Meanwhile, at the outlet, the inlet-outlet boundary condition is used which applies a zero gradient when the flux is outwards but a fixed value for reverse flows (ESI Group, 2019).

3.1.3 Experimental Setup

The experimental data were needed to provide for calibration of the numerical model and to further evaluate the performance of the collars. Experimental tests were conducted in the Civil Engineering Hydraulics Laboratory at the University of Ottawa, Canada. The tests were performed in a rectangular flume measuring 30m long, by 1.5m wide, by 0.5m deep. A cylindrical pier (D = 0.09m) made of acrylic, was bolted to the floor in the center of the flume at a location where the flow was fully developed. The pier diameter with regards to the flume width (blockage ratio) was verified so that the walls would not influence the results. The depth-averaged flow velocity (u_{avg}) was set to 0.34m/s and the flow depth (y) was maintained at 0.15m using a downstream weir. The Froude number (Fr) was calculated to be 0.28 while the Reynolds number (Re) was 3 x 10^4. These flow conditions were maintained for all tests.

Two different experimental setups were used: one with a solid bed while the other used a sand bed. For the solid bed, the bottom of the flume was made of concrete and sieved 0.001m sand was affixed (using paint) to its surface to generate a uniform roughness. The purpose of having a fixed bed with a specified roughness was to perform preliminary velocity tests to allow calibration of the numerical model, since the numerical model uses only a fixed bed.

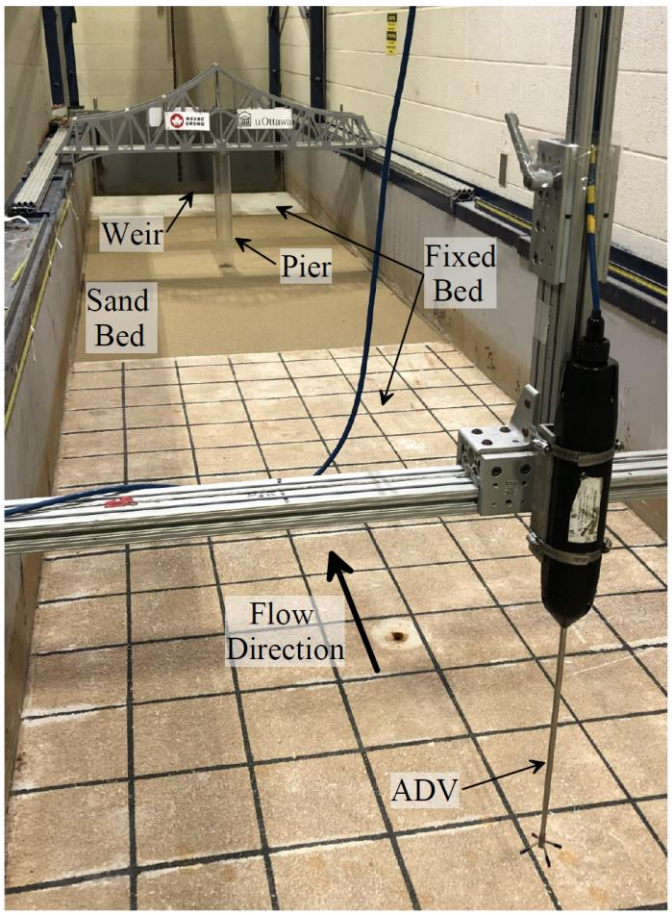

Fig. 3-3. Experimental setup for the sand bed test.

The sand bed shown in Fig. 3-3 was installed 1m from the downstream outlet and was 3m long, by 1.5m wide, by 0.2m deep. The sand was silica sand possessing a median grain size diameter (d_{50}) of 0.001m. This sediment size was used because of the desire to remain in the clear-water regime, as $\frac{u_{avg}}{u_{cr}} = 0.8$, where u_{cr} is the depth-averaged critical velocity required for bed material motion.

To determine the corresponding prototype scale d_{50}, the Shields diagram was used. First, the model scale conditions for the given u_{avg} and d_{50} were calculated and plotted on the Shields diagram. The distance of the plotted data point below the Shields curve was recorded. Then, using the same 1:30 Froude scale employed to model the other experimental parameters, the model scale u_{avg} was scaled up, which represents 1.87m/s in prototype scale. With this information, the prototype scale critical condition was calculated, and then the prototype scale d_{50} was determined. This was accomplished by plotting the data point the same distance below the Shields curve as that for the model scale. The corresponding prototype scale d_{50} was 0.0154m, which resembles a gravel bed river. One can notice that the sediment did not scale with the same 1:30 scale as the other laboratory components – this is because the sediment used in the

laboratory is small, so it does not lie on the horizontal portion of the Shields curve. Additional information regarding scaling can be found in Appendix C.

To measure velocity, an Acoustic Doppler Velocimeter (ADV) was used. The data were collected at each point for two minutes using a sampling frequency of 100Hz. A de-spiking filter was applied to the ADV data and then the data was time-averaged prior to being used (Jamieson et al., 2010).

The experimental tests were run for a duration of six hours because 95% of the equilibrium scour depth was achieved at this point. Two extended trial runs (8 and 12 hours long) were performed for confirmation and the scour depth reached after six hours, compared to that of the extended runs, was 97% and 95%, respectively. The resulting bathymetry was measured using a Leica ScanStation P50 Terrestrial Laser Scanner (TLS), which has an accuracy of +/- 0.0015m in all directions. A physical model of the new collar and FPC were constructed to test their performance in the presence of a sand bed. The new collar was manufactured from a piece of stock aluminum and machined using a Computer Numerical Controlled (CNC) HAAS Super Mini Mill 2. Whereas, the FPC was simply cut from a flat sheet of aluminum possessing a thickness of 0.003m. The outer diameter of both collars was identical measuring 0.3m. After manufacturing, post process finishing was required for both collars in order to achieve a smooth surface.

3.1.4 Model Validation

The experimental flow field data were collected by taking three vertical velocity profiles, 0.72m upstream, 0.14m upstream, and 0.75m downstream of the pier, using an ADV. These velocity profiles were used for calibration purposes of the numerical model. A plot comparing the numerical and experimental velocity profiles in these three locations was presented by Valela et al. (2018) and can be found in Appendix A.

In addition, approximately 100 experimental velocity measurements in the horizontal plane, 0.07m above the bed, were collected using an ADV for numerical model validation purposes. Fig. 3-4 shows a comparison of the velocity contour maps in the horizontal plane from both the experimental tests and the numerical model, under the flow conditions mentioned earlier ($Fr \approx 0.28$ and $Re \approx 3 \times 10^4$). Both the numerical and experimental results are time-averaged and plotted using Kriging interpolation with an anisotropy of 1.5 in the streamwise direction.

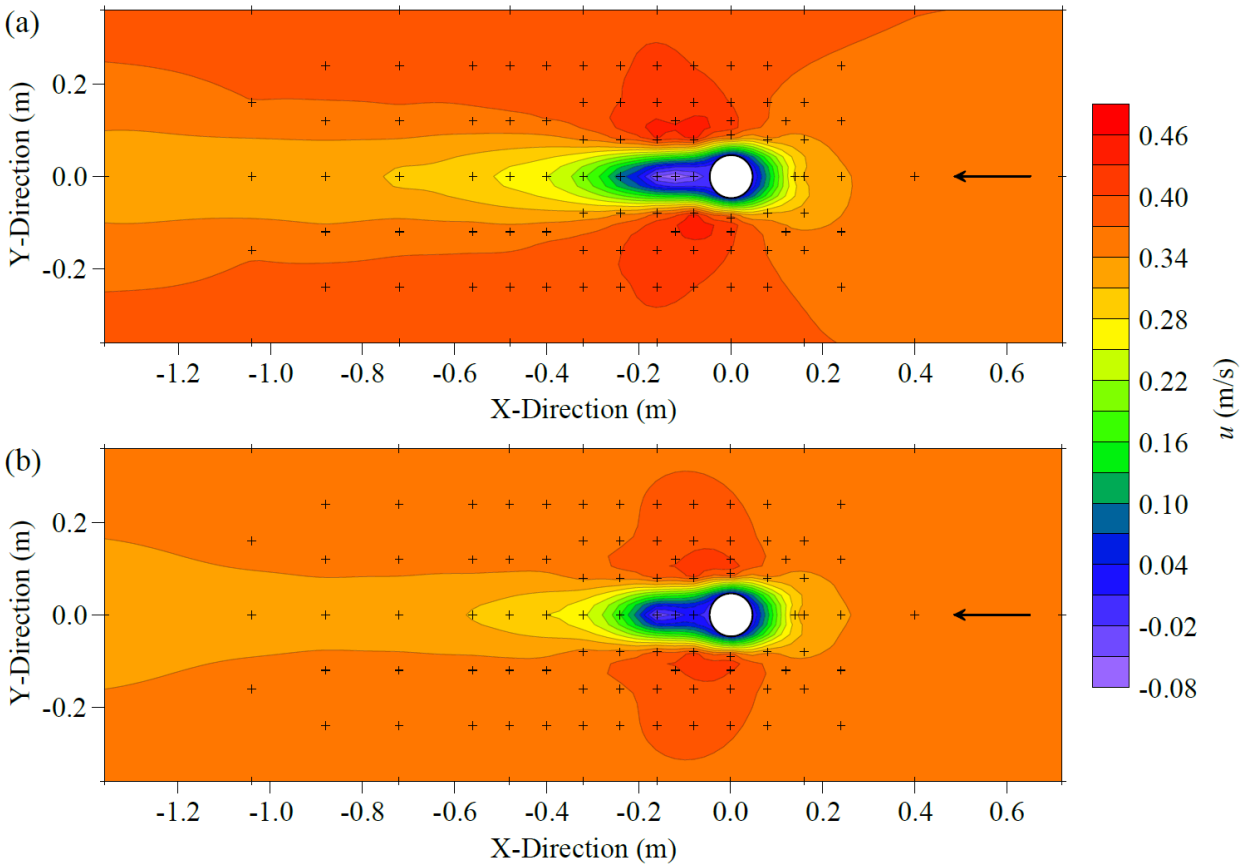

Fig. 3-4. Comparison of the streamwise direction velocity components around the pier at 7cm above the bed: (a) experimental data, and (b) numerical results.

It can be seen that the velocity field generated by the numerical model closely matches that recorded in the laboratory tests. The Root Mean Square Error (RMSE) and Mean Absolute Error (MAE) are 0.0255m/s (7.16%) and 0.0207m/s (5.82%), respectively, which are space-averaged over the whole domain. The stagnation zone on the upstream face of the pier, as well as the increased velocity along the sides of the pier, are both consistent between the numerical and experimental results. However, some differences between the measured and computed velocity fields exist. The first difference pertains to the velocity of the passing flow outside the wake of the pier, such that the experimental data indicate a large region of higher velocity when compared to that from the numerical model. The second difference pertains to the length of the velocity recovery zone downstream of the pier, where the numerical model displays a shorter velocity recovery compared to the experimental results. Despite these differences, and for the purpose of this study, which focuses on the flow immediately in front and beside the pier, the results achieved from the numerical model are considered acceptable.

3.1.5 Collar Design

3.1.5.1 Initial Collar Design

The intent is to improve on the existing FPC, which is shown in Fig. 3-5, by reducing scouring and undermining, therefore making it a more favourable scour solution.

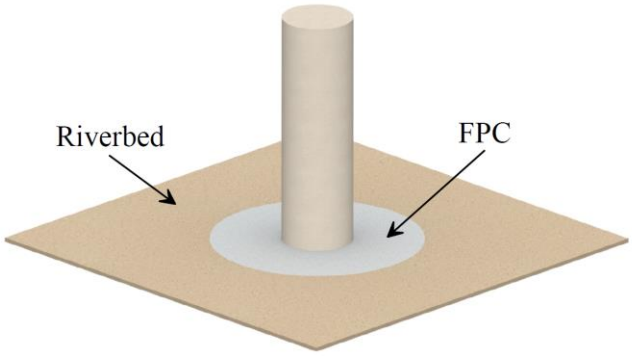

Fig. 3-5. Pier with FPC.

The method proposed to improve the existing FPC pertains to addressing the horseshoe vortex differently, as it is the largest scour contributor; existing collar designs simply protect the riverbed around the pier in a similar fashion to bed armouring. The new collar presented in this study contains, for the first time, the horseshoe vortex. By having a 3D collar shape, which allows the horseshoe vortex to circulate within, it allows a quasi-natural flow path of the water but controls and directs the horseshoe vortex such that the latter erodes the riverbed less. This is shown in Fig. 3-6, which is an illustration of the first iteration of the new collar design.

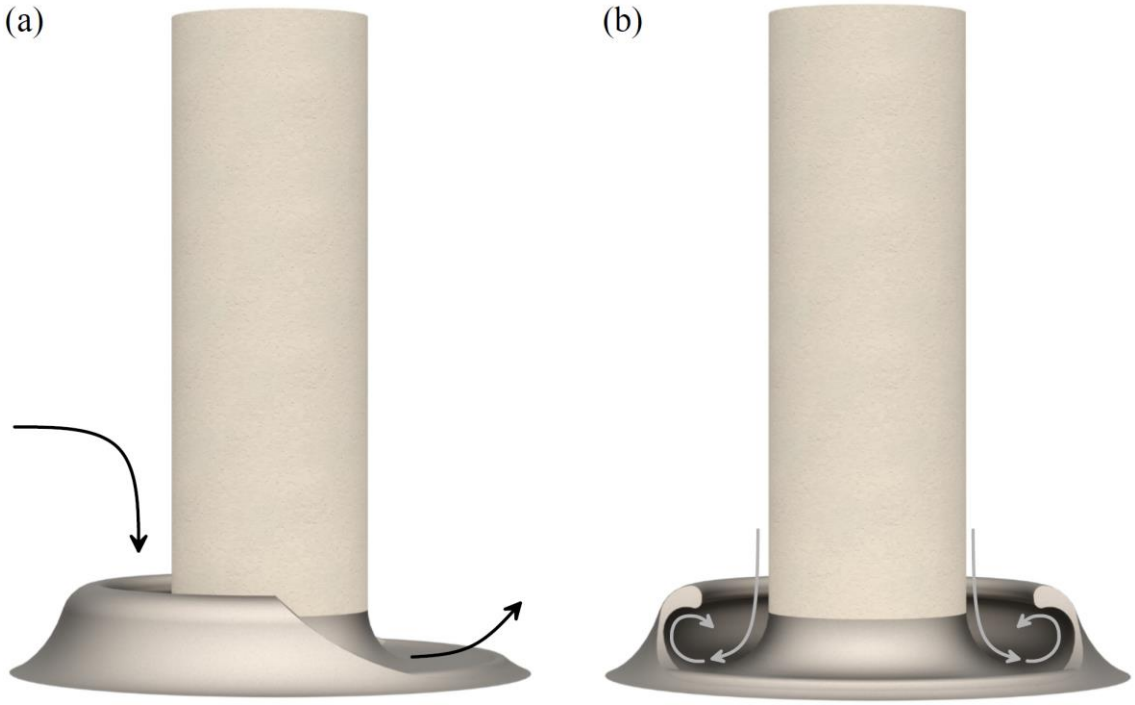

Fig. 3-6. Initial collar design mounted around the pier and the general flow path: (a) side view, and (b) rear view.

Instead of the flow circulating on top of the riverbed, it circulates inside of the rounded interior collar cavity. This circulation forms the horseshoe vortex, which propagates around the front of the pier as it normally would but is housed within the collar cavity until it reaches the sides of the pier. At this point, the cavity containing the vortex ends and the circulating flow within is directed upwards, off the rear of the collar, where it is then transported downstream, away from the critical region around the pier.

The collar is designed to rest on the bed because according to Chiew (1992) and Chen et al. (2018), the most scour reduction occurs when the collar is placed at or below the initial bed height. Furthermore, installing the collar below the initial bed height would result in a larger excavation and greater disturbance to the surrounding environment, so for those reasons the collar was fixed at the initial bed height.

Some features of the original FPC were integrated into the new design. Specifically, the circular perimeter, the large outer diameter used to protect the riverbed around the pier, and the ability for installation without harming the pier's structural integrity. However, the new collar differs in that it addresses directly the horseshoe vortex, such that the 3-D structure resting on the riverbed has the capacity to contain the vortex. In doing so, the horseshoe vortex cannot exit off the sides of the collar or interfere with the passing flow, which ultimately can assist in reducing scour. The flow exiting out the rear of the collar is also safely guided downstream, away from the riverbed, to help reduce the scouring commonly experienced immediately behind the collar. Furthermore, just as with the FPC, the erosional forces that are generated by the accelerated passing flow are shielded from reaching the riverbed in the near vicinity of the pier because of the collar's large outer diameter.

3.1.5.2 Design Progression

The process of designing this erosion countermeasure system required numerous design iterations. If physical models were to be constructed and tested experimentally for each design change, the process would have taken a significant amount of time, used a large quantity of laboratory resources, and been very costly. Alternatively, the authors employed an iterative two-stage approach, where, first, the numerical model was used as a tool to aid in the design evolution. Then, once a satisfactory design was achieved using the CFD tool, a physical replica was constructed and tested experimentally. By combining both CFD and experimental methods, the intention was to expedite the design process, decrease experimental resource consumption, and reduce costs. Further information pertaining to the hybrid design approach can be found in Appendix B.

The parameters used to measure the collar's performance while using the CFD tool were the velocity field around the pier and collar and the corresponding shear stress imposed on the bed, which are shown in Fig. 3-7. The velocity vectors are shown on a streamwise cross-section

along the centerline focusing on the upstream half of the collar and the shear stress is presented in a 3-D view looking downstream from the upper right corner of the flume. These two parameters were chosen because together they can be used to predict the scour that would occur around the pier and collar.

Assessing the performance of Design #1 in Fig. 3-7, it can be seen from the velocity map that the main horseshoe vortex is contained, as intended, within the collar. However, an undesirable secondary horseshoe vortex forms immediately upstream of the collar. This secondary vortex formed because of the collar's steep outer slope, which does not allow for a streamlined redirection of the passing flow over the top and into the collar. Based on the formation of the secondary vortex and the corresponding shear stress it imposes on the bed, large amounts of scour would likely occur. Therefore, alterations to the initial collar design were deemed necessary and led to the iterative numerical optimization process.

The goal of the numerical optimization was to reduce the shear stress on the bed around the pier and collar by weakening or eliminating the severity of the secondary horseshoe vortex, while obstructing the passing flow as little as possible. Fig. 3-7 presents the design evolution showing the progression from Design #1, which is the initial shape introduced previously in Fig. 3-6, to Design #4, which is the most improved shape.

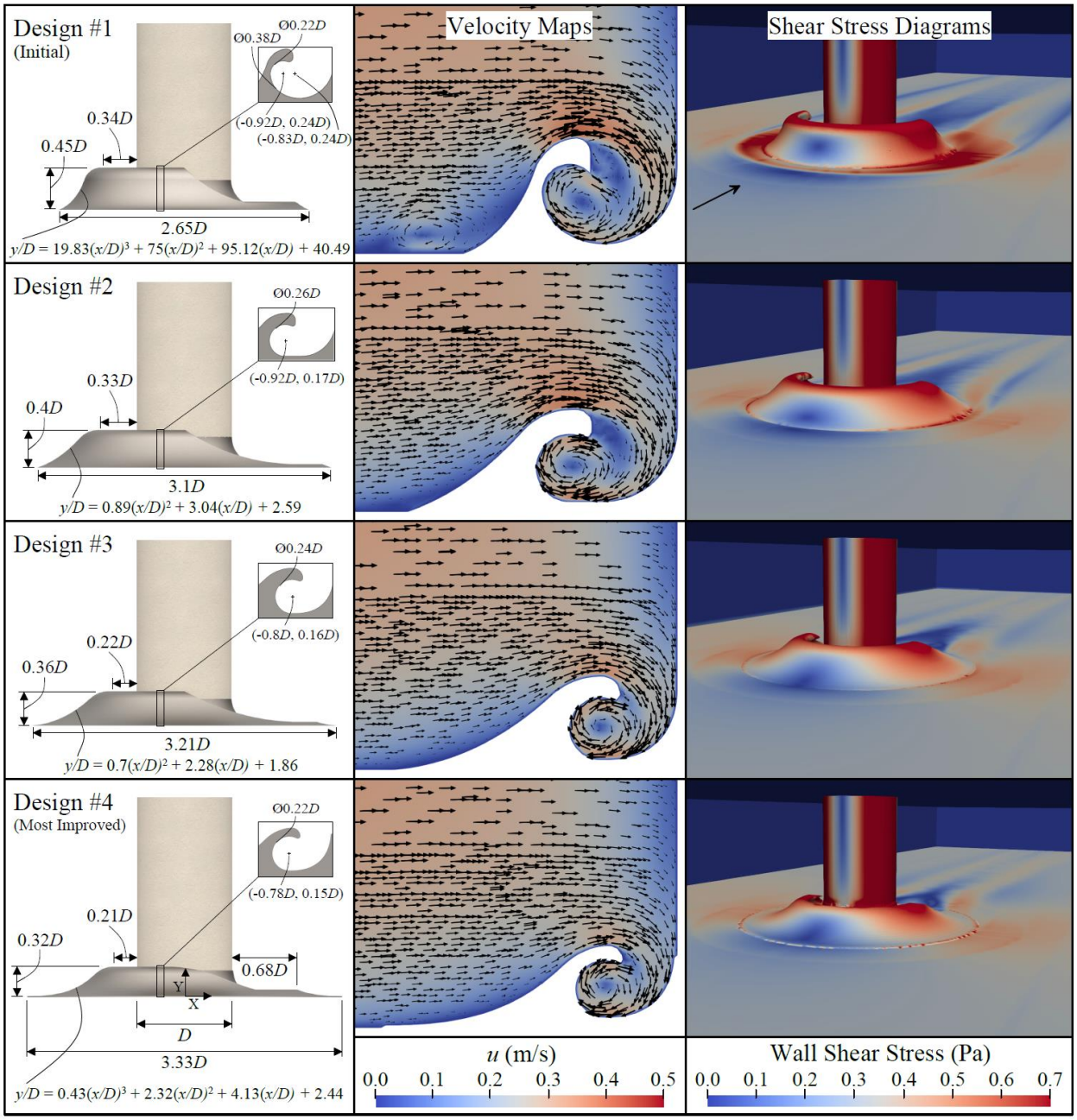

Fig. 3-7. Collar design evolution displaying the velocity magnitude maps and bed shear stress diagrams associated with each design.

As the collar designs progressed from Design #1 to Design #3, the secondary horseshoe vortex was eliminated by increasing the overall diameter and reducing the height of the collar. This created a more streamlined collar shape. In addition, the collar cavity was reduced in size decreasing its material volume and impact on the passing flow.

The objective of Design #4 was to reduce the quantity of accelerated flow that was forced around and off the sides of the collar so that there would be a reduction in shear stress on the bed. This objective was accomplished by increasing the curvature of the outer face of the collar

which consequently caused the collar cavity to be narrower and the edges to be flatter. As a result, more passing flow remained on top of the flat edges rather than being pushed off the sides of the collar, thus allowing the flow to travel a shorter distance around the collar. Therefore, a reduction in acceleration and a corresponding decrease in shear stress was observed along the sides of the collar.

Meanwhile, a flow deflector, termed as a spoiler, was re-added to the rear of the collar to direct the fast-moving horseshoe vortex up and away from the riverbed as it exits the collar cavity. The spoiler was eliminated after Design #1 in order to simplify the iteration process. However, the spoiler was later found to be beneficial. As a result, a portion of the rapidly moving flow from the horseshoe vortex is directed upwards instead of travelling along the bed. Therefore, Design #4 is the most improved collar design, as the primary horseshoe vortex is contained, the secondary horseshoe vortex is eliminated, a large quantity of accelerated flow departing off the sides of the collar is reduced, and a portion of the exiting horseshoe vortex is directed away from the bed. The changes made to the four evolving designs are summarized in Fig. 3-8. For the remainder of the paper, Design #4 is referred to as Collar Prototype No. 1 (CPN1). At this point, experimental testing was required to provide more insight as further changes, not presented in this paper, showed to have minimal performance improvements in the numerical model.

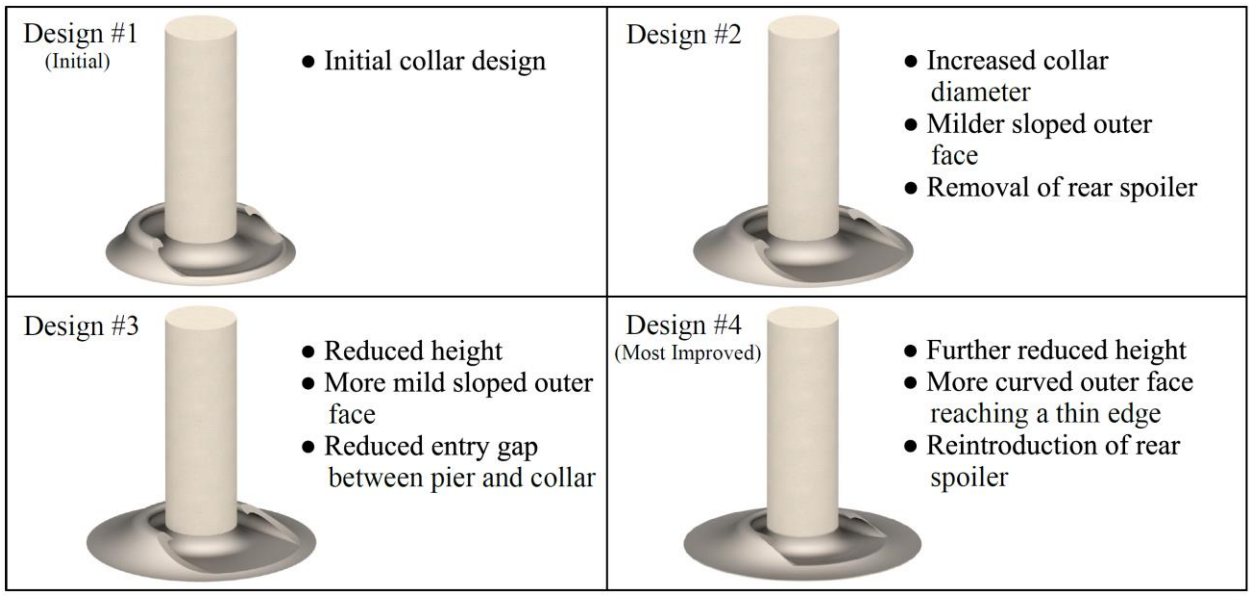

Fig. 3-8. Summary of design changes to each sequential collar.

3.1.6 Results

3.1.6.1 Numerical Results

To understand the function and benefits of CPN1, this section presents various numerical results which compare the operation of a pier with and without CPN1. The results shown in this section are time-averaged, over 15s, which allows for a better comparison between the cases without and with the collar. The first comparison, shown in Fig. 3-9, illustrates flow streamlines

looking downstream from in front of the pier. The streamlines remain horizontal and evenly spaced until reaching the front of the pier. When CPN1 is not present, the streamlines become redirected downwards where they begin to circulate on top of the riverbed, while progressing around the sides of the pier. This process was described earlier as the standard scour-causing horseshoe vortex. The horseshoe vortex is characterized by a high concentration of circulating streamlines that separate from the pier and extend out past the sides of the pier. The remainder of the streamlines, which move far enough away from the pier to avoid participating in the horseshoe vortex, experience an increase in velocity in order to travel the further distance required to bypass the pier. This leads to another scour-causing source, such that the increase in velocity induces greater shear stress on the bed. Therefore, regardless of the route taken by the flow around the pier, scour is unavoidable.

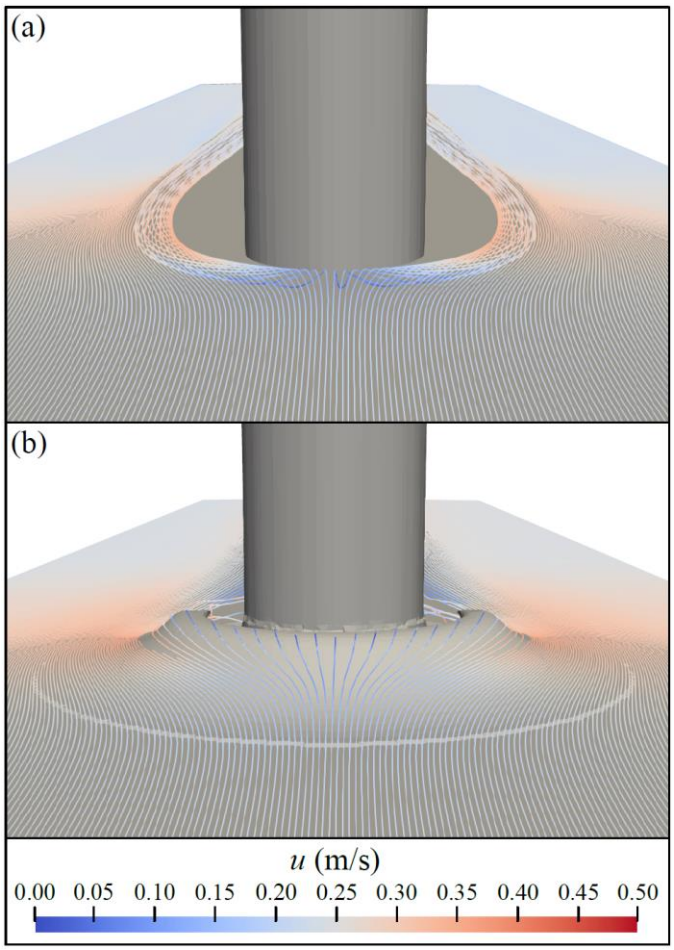

Fig. 3-9. Comparison of the front view velocity magnitude streamlines initiated 0.02m above the bed: (a) pier with no scour countermeasure, and (b) pier with CPN1 installed.

When CPN1 is present, the streamlines develop in the same fashion, but upon reaching the pier, they enter the collar cavity rather than forming the natural horseshoe vortex on top of the riverbed. Once they enter the collar cavity, they circulate within, similar to how they would in the natural horseshoe vortex, then exit out the rear without contacting the riverbed in front of

or beside the pier. Meanwhile, the streamlines that do not enter the collar cavity but are close to the riverbed, become redirected around the sides of the collar cavity and continue as normal. The collar cavity generates greater flow diversion compared to when the collar is not present, but the flat edges of the collar allow for a portion of the accelerated passing flow to travel on top of it. This helps to shield some of the shear stress that would otherwise contact the riverbed beside the pier. However, despite allowing the passing flow to travel on the collar's edges, a region of increased velocity still occurs on the riverbed towards the rear of the collar.

Fig. 3-10 presents the side view of the pier in conjunction with flow streamlines. The pier in Fig. 3-10(a), as well as the pier and CPN1 in Fig. 3-10(b), are shown with 50% transparency. For the pier without any countermeasure, the streamlines near the bed immediately in front of the pier can be seen forming the horseshoe vortex as they circulate outwards while progressing around the pier. With CPN1 installed, the flow enters the collar cavity and follows the curved confining walls, which encourages the horseshoe vortex behaviour. The streamlines are then guided around the pier within the cavity where they circulate a number of times prior to exiting. Downstream of the pier, the flow behaviour changes when CP1 is installed such that the streamlines shift from a random pattern to a large scale circular pattern, which is discussed in more detail later in this section.

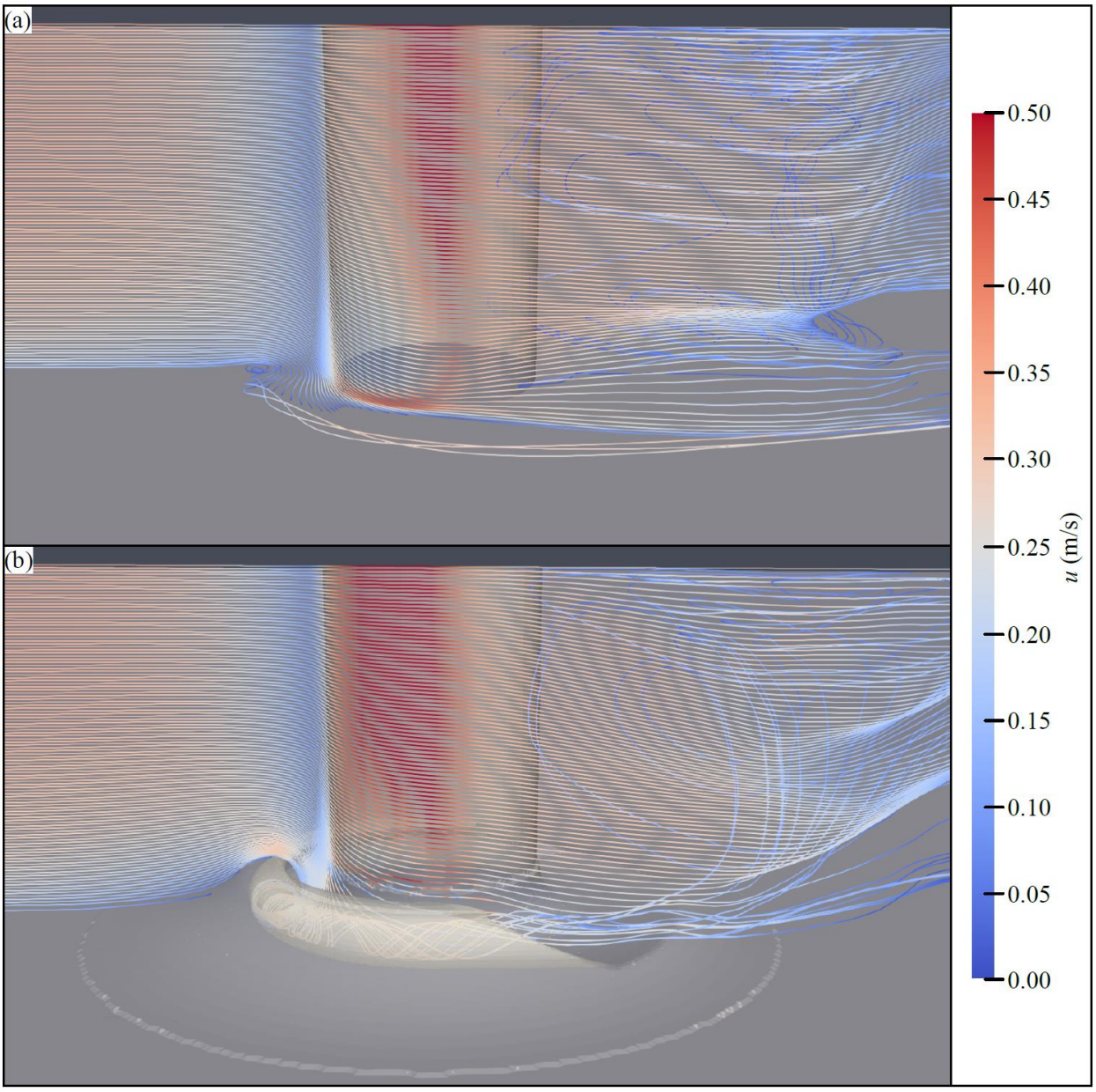

Fig. 3-10. Side view velocity magnitude streamline comparison showing the structures with 50% transparency: (a) pier with no scour countermeasure, and (b) pier with CPN1 installed.

To further investigate the flow pattern in the vicinity of the pier, Fig. 3-11 presents a slice in the streamwise direction along the centerline, illustrating a velocity map for a pier without and with CPN1. In Fig. 3-11(a), which displays the pier without any countermeasure, the size and shape of the horseshoe vortex cross section is shown. The vortex shape is elongated in the streamwise direction but shallow in the vertical direction, illustrating that it resides in the low velocity region against the bed.

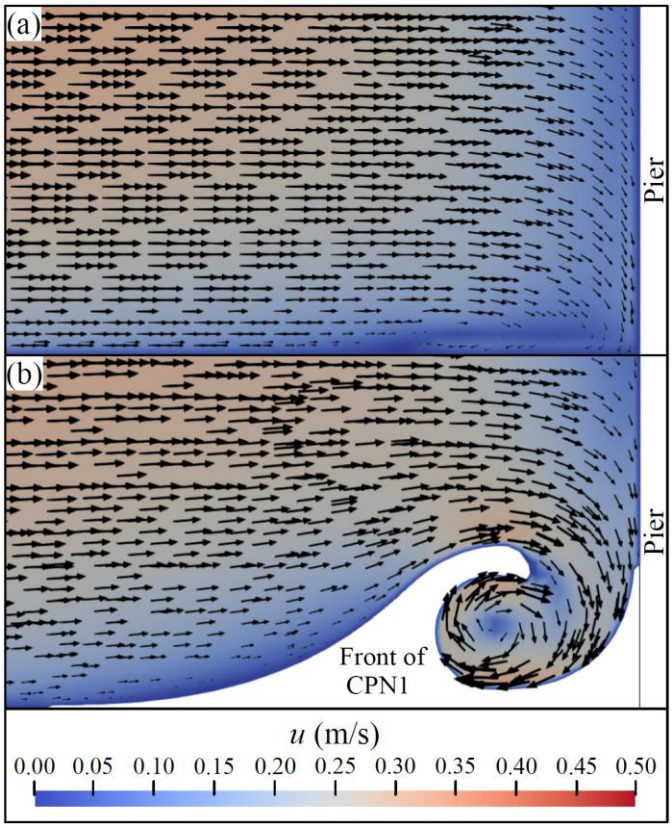

Fig. 3-11. Comparison of streamwise-vertical slice of velocity upstream of pier: (a) pier with no scour countermeasure, and (b) pier with CPN1 installed.

Upon installing CPN1, as shown in Fig. 3-11(b), the flow pattern below the mid-depth and upstream of the pier changes substantially. The approaching flow that is drawn down towards the riverbed, instead of reaching the riverbed at a 90^{o} angle as per the case with no collar, it is guided along the curved inner face as it enters the collar. Once the flow enters the collar, it follows the inner face for a complete revolution where it then meets the new incoming flow entering the collar. The constant entering flow helps the recirculating flow within the collar to be pushed through the cavity to the rear of the collar.

The presence of the top cantilevered surface of the collar, confines the approaching streamlines, thus causing an increase in velocity of the flow entering the cavity. This increased velocity extends over the top edge and into the collar. In doing so, the vortex maintains a high velocity inside of the collar cavity.

Downstream of the pier, regardless of whether CPN1 is installed or not, the flow pattern is turbulent, exhibiting small and large scale eddies. When CPN1 is not installed, as shown in Fig. 3-12(a), the flow velocity is minimal immediately downstream of the pier for the majority of the flow depth. However, there are two regions showing a mild increase in velocity: one located near the bed and the other located near the surface, of which the flow direction in both regions is

orientated upstream. This is the result of the flow separation created by the pier such that the flow is recirculating behind the pier.

When CPN1 is installed, as shown in Fig. 3-12(b), the flow exhibits a higher velocity downstream of the pier and that is due to the contained horseshoe vortex exiting the collar cavity. Once the horseshoe vortex leaves the containment of the collar and reaches the rear spoiler, a large portion is directed upwards to the surface. Once the upward flow reaches the surface, it turns upstream towards the pier, creating a large circulation extending from the top of the collar to the water surface.

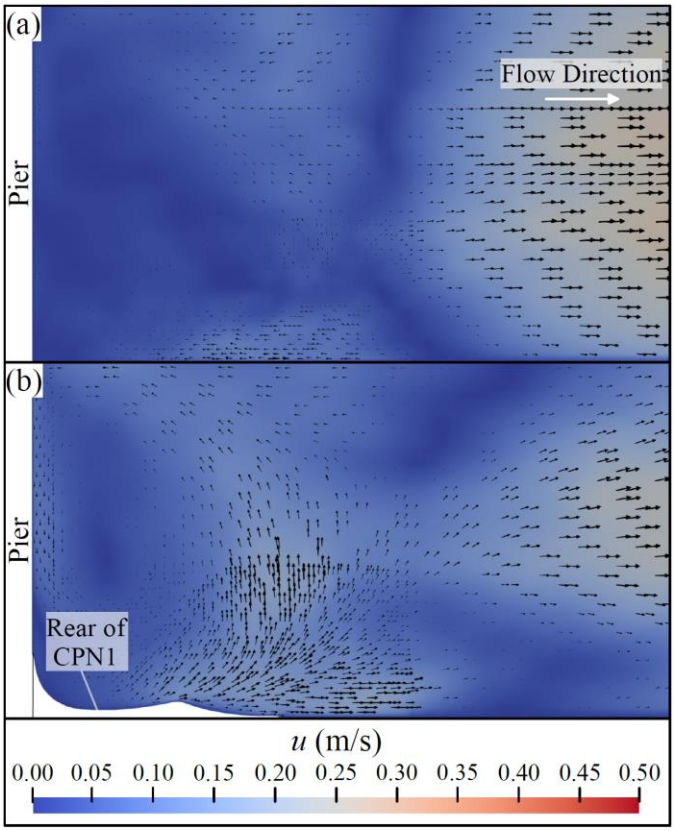

Fig. 3-12. Comparison of streamwise-vertical slice of velocity downstream of pier: (a) pier with no scour countermeasure, and (b) pier with CPN1 installed.

To better illustrate the scour potential and its location, the bed shear stress, which is used as a scour indicator, is presented in Fig. 3-13. When CPN1 is not installed, the maximum bed shear stress occurs immediately adjacent to the pier, extending in the downstream direction. The magnitude of the shear stress on either side of the pier is extremely high when compared to the surrounding region, which would result in large localized scour holes. This is caused by a combination of the horseshoe vortex and the accelerated flow passing the sides of the pier. However, directly in front of the pier, the bed shear stress is nearly zero because of the stagnation zone that occurs from the flow contacting the pier.

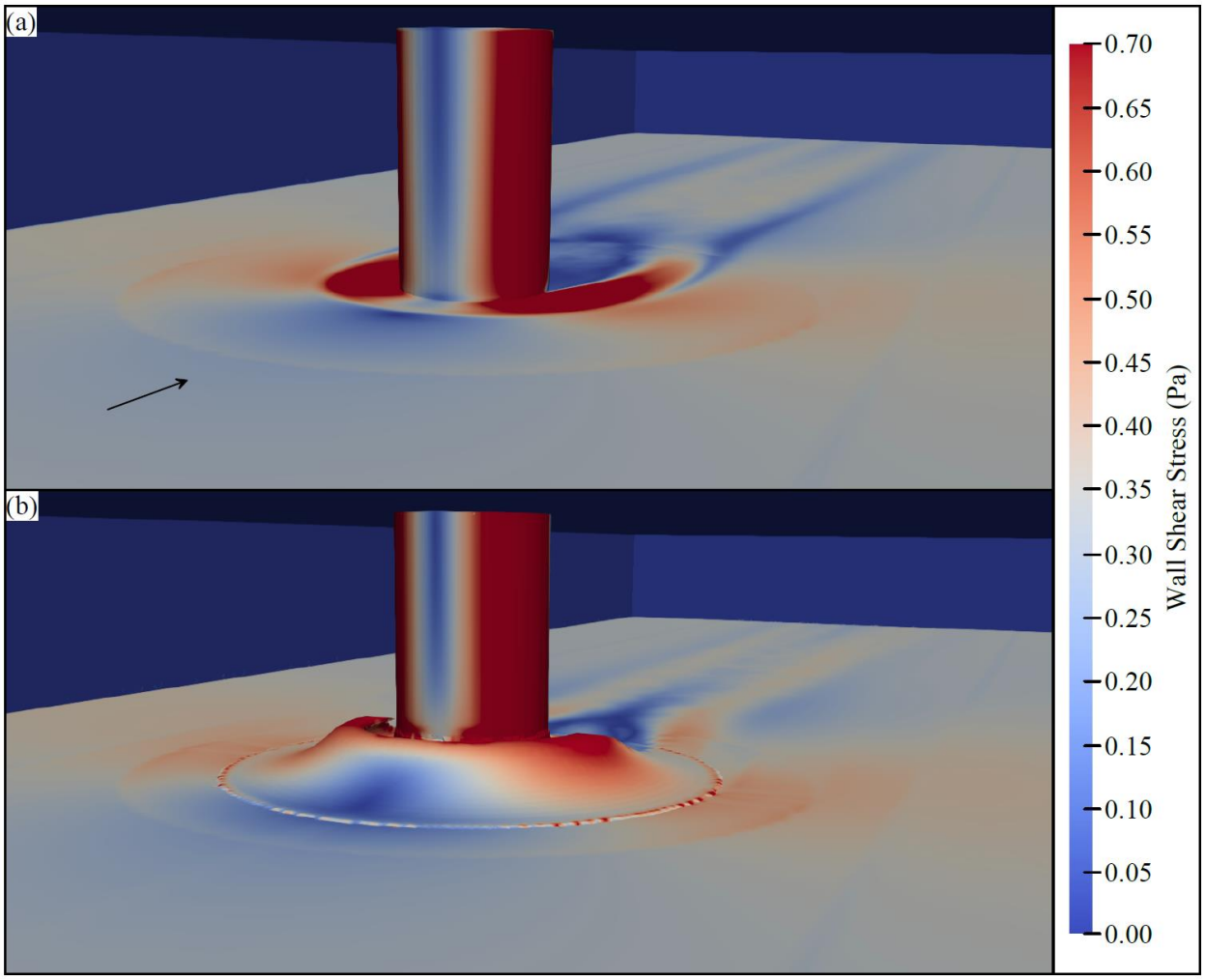

Fig. 3-13. Comparison of the wall shear stress: (a) pier with no scour countermeasure, and (b) pier with CPN1 installed.

Upon the addition of CPN1, the regions of extremely high shear stress around the pier no longer occur on the riverbed; instead they occur within or on top of the collar. However, some areas of slightly increased shear stress still remain around the collar. Since the shear stress that normally is induced on the riverbed, particularly upstream and along the sides of the pier, has been reduced, this indicates that the quantity of scour should also be reduced.

3.1.6.2 Experimental Results

As the second stage in the hybrid design process, which is to further test the effectiveness of the numerically improved design, a series of experimental tests, possessing a sand bed, were performed. The intention was to use the results from the experimental tests to evaluate CPN1's performance and if required, provide insight for design improvements, which would lead to repeating the hybrid design cycle. This paper presents one complete iteration through the hybrid design cycle.

Three different scour tests were performed: 1) consisting of a pier without any scour countermeasure, 2) consisting of a pier with an FPC, and 3) consisting of a pier with CPN1. For all three tests, flow conditions were kept constant and the same experimental protocol was used. Specifically, the sand bed was first levelled and then the tests were run for a duration of six hours. Finally, the resulting bathymetry was measured upon dewatering the flume. The corresponding bathymetry measurements are presented in Fig. 3-14. The tests were repeated three times, achieving a standard deviation of 0.0017m pertaining to the maximum scour depth (d_s).

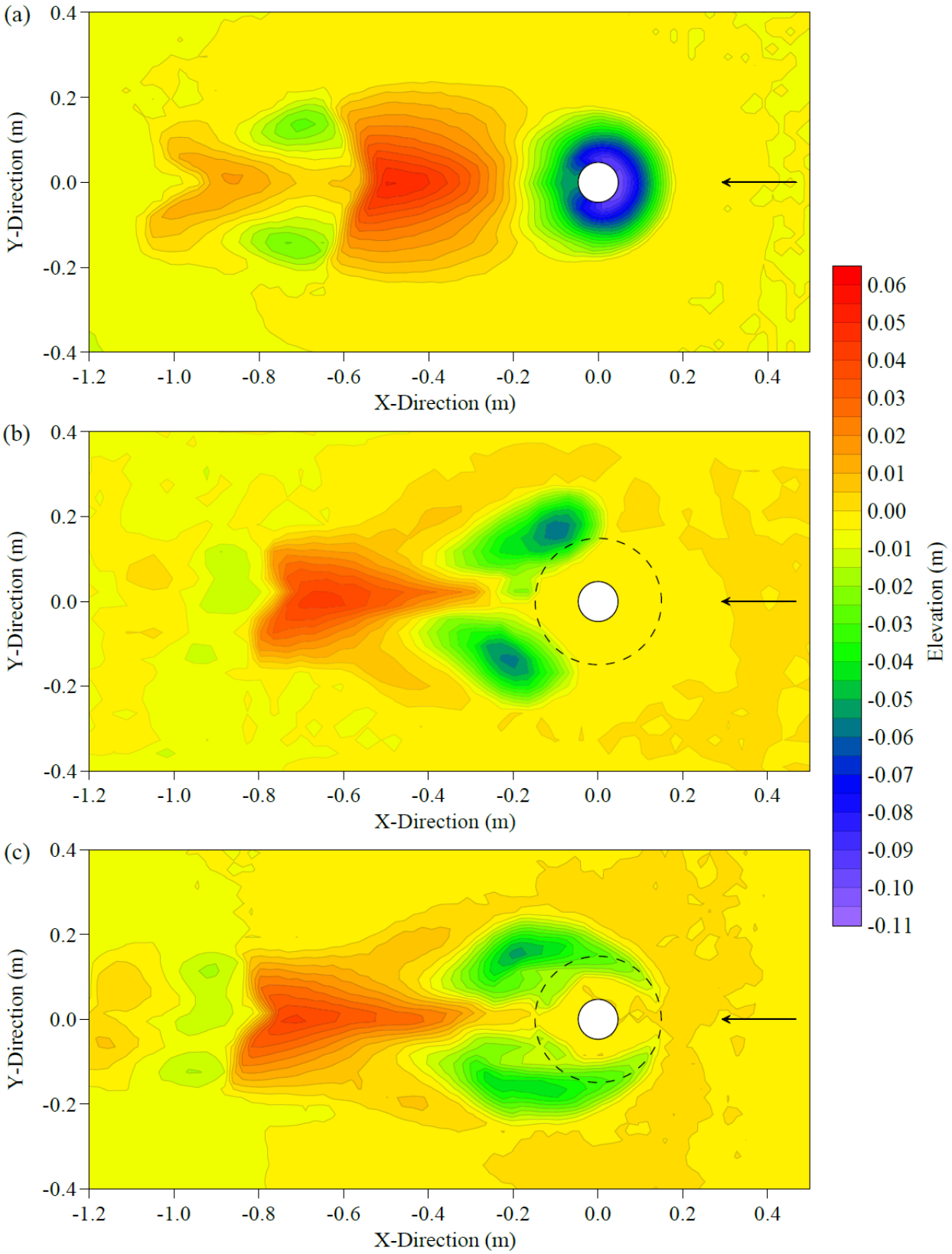

Fig. 3-14. Pier scour comparison: (a) pier with no scour countermeasure, (b) pier with FPC, and (c) pier with CPN1 (dotted line indicates the plan edge of the collars).

Fig. 3-14(a) displays the resulting bathymetry around a pier without any scour countermeasure. Most of the scour was experienced within a close proximity to the pier, with d_s measuring 0.100m, occurring immediately in front of the pier. The scour hole uniformly reduced in depth with increasing distance away from the pier, until it reached the original non-scoured bed elevation, which was observed approximately 1.6D away from the pier's edge in the upstream and cross-stream direction. This scour pattern is problematic because the deepest location is adjacent to the pier, which is directly above the pier's foundation.

A significant change in scour pattern was seen when the FPC was installed, as shown in Fig. 3-14(b). Rather than one deep scour hole forming on the upstream face of the pier, two significantly smaller scour holes formed on either side of the collar, downstream from the pier. The average d_s of the two holes was 0.06m, implying a 40% d_s reduction when compared to a pier without any scour countermeasure. Similar scour tests were performed by Chiew (1992), where it can be interpolated from the published results that an FPC of the same diameter reduces d_s by approximately 35%. Therefore, the results obtained in this test match closely to that of previous literature.

When CPN1 was installed, as shown in Fig. 3-14(c), some similarities in the scour pattern to that of the FPC were present. Specifically, two separate scour holes formed on either side of the collar, downstream from the pier. The difference is that the average d_s of the two scour holes for CPN1 was 0.049m, which is a d_s reduction of 51% when compared to a pier without any scour countermeasure. This implies an 11% greater d_s reduction over the FPC.

In addition to reducing the magnitude of scour, both the FPC and CPN1 produce a scour pattern that is more desirable from a scour protection point of view, because the location of d_s is pushed further away (1.5-2D from the pier's edge) to a less impactful location. Therefore, both collars protect the bed in the near vicinity of the pier, typically above where the foundation is located. It is also worth noting that since the quantity of scour around the pier is reduced by the presence of either collar, the height of sediment accumulation downstream is also reduced, because the quantity of deposition is directly related to the quantity of scour.

The location of d_s for CPN1 was similar to that of the FPC but the extent of the scour regions for CPN1 reached much further upstream toward the leading edge of the collar. The scour holes that formed on either side of both collars lead to both experiencing some degree of undermining. CPN1 had 0.000682935m^3 of undermining beneath its side edges, whereas the FPC had only 0.000267399m^3 of undermining along its downstream edge. Therefore, CPN1 experienced 2.55 times more undermining than that of the FPC.

3.1.7 Discussion

This paper presents a new scour countermeasure, in the shape of a 3-D collar, designed to be an improvement over the FPC. The collar is novel in that it reduces scour through containing the horseshoe vortex, while protecting the bed around the pier from the accelerated passing flow.

CPN1 did in fact reduce scour around bridge piers but was also found to experience greater undermining when compared to that of the FPC.

CPN1 was designed to contain the horseshoe vortex for the purpose of stopping the vortex from exiting off the sides of the collar, so that ultimately scouring and undermining can be reduced. The horseshoe vortex was successfully contained and the maximum scour depth was reduced, but, because of the increased pier width at the base of the pier from the 3-D collar, a greater quantity of flow was obstructed. This caused more flow to travel around the collar and experience an increase in velocity. CPN1 was not able to shield all of the bed around the pier such that a portion of the accelerated passing flow exited off the sides of the collar. As a result, greater undermining occurred along the sides of the pier when compared to the FPC. Undermining also occurred at the downstream end of CPN1 on either side of the pier, but to a lesser degree than the sides. This is because of the horseshoe vortex exiting out of the rear of the collar, which induced a region of high velocity along the bed immediately downstream of the collar. The combination of the increased flow exiting off the sides of the collar and the horseshoe vortex exiting out the rear of the collar, caused scour to propagate further underneath the edges of CPN1. In order for CPN1 to be a technically compelling solution, the collar undermining must be addressed. To do so, further iterations through the hybrid design cycle are required using data provided by experimental tests as insight for further design improvements.

The design process used to generate the new prototype was hybrid in nature since it utilized both CFD and experimental methods. Based on the results presented, the capabilities of the numerical model are deemed satisfactory, especially for the purpose of aiding in prototype design prior to experimental testing. The shear stress pattern calculated numerically in Fig. 3-13 matches very closely to the scour that occurred experimentally in Fig. 3-14. Specifically, the spatial distribution of the increased shear stress beside and behind the collar, caused by the accelerated bypassing flow and exiting horseshoe vortex, respectively, is nearly identical in relative magnitude and location to the scour that occurred in the laboratory setting. Therefore, despite the numerical model not having sediment transport capabilities, the calculated shear stress is an accurate indicator of the resulting scour. Furthermore, the numerical model provided detailed flow field information that would otherwise be difficult or impossible to achieve with only experimental testing. By using CFD as the first stage in this iterative design process, the laboratory and prototyping costs, in addition to time, were greatly reduced.

CFD models should not replace experimental modelling in its entirety, as the numerical results have some limitations in accuracy (overprediction of bed shear stress which is discussed below) and scope (lack of sediment transport capabilities in this particular case). However, when numerical models are paired with experimental testing, the limitations of the numerical model are diminished, and a well-rounded hybrid design process emerges.

The velocity plots presented in Fig. 3-4, which compare the X-direction velocities from the numerical model to that of the experimental tests, demonstrated some differences. The larger

experimental velocities outside the wake may be due to the location of the measurements with regards to depth. This is because all the measurements were taken in a horizontal plane, at 0.07m above the bed. At this specific elevation, the experimental freestream velocity was slightly larger than that obtained with the numerical model. This was not the case throughout the entire depth, as the numerical model was mass conservative.

When developing the mesh for the numerical model, in order to achieve the most accurate results, yet reasonable computational costs, refinement regions and wall functions were used. A sensitivity analysis was performed with the specified wall functions and it was found that the wall shear stress was not impacted by the y+ until it dropped below a value of 25. Once the y+ dropped below 25, the wall shear stress started to increase as the y+ approached zero. As a result, the average y+ value of 19 within the level two refinement region yielded an increase in shear stress of approximately 7.8%. This difference in shear stress, which can be observed slightly in Fig. 3-13, is considered acceptable. That is because all collar designs were tested using the same numerical model and mesh parameters, and the numerical results were only used as a tool to help improve the design, prior to constructing an experimental model. In addition, the difference in shear stress is conservative so it would not harm the safety of the design.

There are a number of limitations to the research presented within this paper. The *first limitation* is that the tests were performed with the flow approaching directly head-on with no skew angle. The collar was designed with a rounded front with the intent to accommodate a wide range of approaching flow angles. However, this function is not demonstrated in the current study. Regardless, an FPC can accommodate all approaching flow angles due to its non-directional shape, whereas CPN1 is limited to only a sector of flow angles approaching from upstream. The *second limitation* is that the design was tested under only one flow condition (within the clear-water regime) consisting of a constant y, u_{avg}, and d_{50}, which does not fully verify the robustness of the collar design. The *third limitation* is that the collar was designed and tested for circular piers only. Therefore, further research needs be done to demonstrate the collar's performance under different conditions and to adapt its shape to become applicable for different shaped piers. The *fourth limitation* is that CPN1, and its predecessor the FPC, are rigid in nature. A countermeasure such as riprap, which is flexible, has an advantage as it can adjust to changes in the bed, whereas rigid countermeasures cannot. The *fifth limitation* is that debris or sediment accumulation within the collar was not tested. A potential concern is that the collar cavity could become obstructed, which could impact the performance of the collar. The *sixth limitation* is that the shape of the rear spoiler of CPN1 was not fully optimized. Its shape could be improved to better direct the exiting flow while also helping to replenish the sediment downstream of the collar.

3.1.8 Conclusions

This study introduces a new scour countermeasure, in the shape of a three-dimensional collar, to be an improvement over existing FPCs. The collar works by containing and guiding the horseshoe vortex so that it does not contact the bed near the pier, while also partially shielding

the bed from the increased velocity along the sides of the pier, as these are the largest contributing factors in pier scour. CPN1 was found to be effective at reducing the scour depth such that a 51% reduction was achieved over a pier without any countermeasure and an 11% reduction over an FPC. However, greater undermining was experienced around the perimeter of CPN1 which indicates that further design revisions are required. Currently, CPN1 is not yet a preferred scour countermeasure for bridge designers, but upon addressing the undermining issue, it could be an attractive solution given its scour reducing capabilities.

The design was reached through a hybrid approach that incorporated both CFD modelling and experimental testing. First, a CFD model was used such that collar designs were tested and adjusted iteratively, based on the flow behaviour and shear stress induced on the bed, until an improved shape was achieved. Then, experimental tests were conducted to provide velocity and erosion data. The velocity field and shear stress data obtained from the numerical model was found to match the experimental results closely, implying that the numerical model is a sufficient tool to aid in prototype design. However, determining the quantity of undermining that would occur from only the numerical model was challenging. For that reason, the numerical model should be paired with experimental testing in such situations.

Chapter 4. Collar Prototype No. 2 (CPN2) and 3 (CPN3)

4.1 A Novel Collar Design to Mitigate Bridge Pier Scour (CPN2)

Preprint of a modified version of a conference proceeding printed in the 38th IAHR World Congress © 2019 International Association for Hydro-Environment Engineering and Research (IAHR). DOI: 10.3850/38WC092019-0671.

4.1.1 Introduction and Objectives

Collar Prototype No. 1 (CPN1) was previously introduced as an improved bridge pier scour collar, but was found to be in need of further revisions in order to be an effective countermeasure (Valela, Nistor, et al., 2021). The primary goal of this paper is to address the issues pertaining to CPN1, through introducing Collar Prototype No. 2 (CPN2). Thus, the objectives are to:

1) Reduce the quantity of flow undermining around the front and sides of the pier while still containing, at the same time, the horseshoe vortex.
2) Utilize both numerical and experimental methods to evaluate the performance of the new design changes
3) Demonstrate an alternative method of prototype manufacturing to reduce costs and save time.

4.1.2 Numerical Model

The governing equations for the given study, of water flow around a bridge pier, are the Navier-Stokes equations for 3-D, one-phase, incompressible fluids. These equations include the continuity equation Eq. 3 and the momentum equation Eq. 4, which are presented below.

$$\frac{\partial u_i}{\partial x_i} = 0 \tag{3}$$

$$\frac{\partial u_i}{\partial t} + \frac{\partial u_i u_j}{\partial x_j} = -\frac{1}{\rho}\frac{\partial p}{\partial x_i} + \nu\left(\frac{\partial^2 u_i}{\partial {x^2}_j}\right) \tag{4}$$

where, p is pressure, ρ is fluid density, ν is kinematic viscosity, x_i is the Cartesian position vector with respect to the reference frame (x_1, x_2, x_3), and u_i are the fluid velocity components with respect to the Cartesian coordinates (u_1, u_2, u_3) (Maza et al., 2015).

In order to solve the aforementioned Navier-Stokes equations, the OpenFOAM Computational Fluid Dynamics (CFD) toolbox is used which employs the finite volume approach. The solver utilized within OpenFOAM is pimpleFoam, which a transient solver intended for incompressible, single-phase flows. For this application, the solver operates in Pressure Implicit Split-Operator (PISO) mode which solves through the pressure corrector approach, as a Courant number of 0.8 is maintained (Issa, 1986). To capture the large quantity of turbulence present around the pier and collar, the Delayed Detached Eddy Simulation (DDES) model is used because it incorporates both the Large Eddy Simulation (LES) and the Reynolds Averaged Navier-Stokes (RANS) theories to achieve an accurate, yet computationally efficient solution (Gritskevich et al., 2012; Menter, 1992; Spalart et al., 1997). Specifically, RANS is used near the wall through the k-omega SST turbulence model, while LES is used outside of the boundary region through the Smagorinsky subgrid model. The benefit of using this approach is that the accuracy of the LES model is utilized for the freestream, while the near wall qualities of the RANS model is used to capture the flow separation and adverse pressure gradients in the boundary layers (Gritskevich et al., 2012; Menter, 1992; Spalart et al., 1997). Therefore, a hybrid turbulence model is achieved which OpenFOAM refers to as kOmegaSSTDDES.

The domain used for the numerical simulations is 10m long, 0.85m wide, and 0.15m deep. A pier measuring 0.09m in diameter (*D*) and equal height of the flume, is situated 8.5m downstream from the inlet and is created using OpenFOAM's snappyHexMesh. To save computational time, two refinement regions are used encompassing the pier and collar, each with a reduction in cell size. The first refinement region is a large rectangle, measuring from the center of the pier, 0.5m upstream, 0.25m across the flume in both directions, and 1.5m downstream which coincides with the flume outlet. The second refinement region is cylindrical in shape measuring 0.2m in diameter and 0.06m in height. The corresponding y+ values for the unrefined region, first level of refinement, and second level of refinement are 69, 34, and 19, respectively. A mesh sensitivity analysis was performed, and grid independence was achieved in the focus region around the pier, and, therefore, approximately 5,500,000 cells were employed to mesh this domain.

The boundary conditions include a slip condition on the side walls and a symmetry condition along the top surface, so that the effects of the walls are minimized. Meanwhile, the pier, collar, and bed use a no-slip condition, as a realistic interaction between these components and the passing flow is desired. To save computational time and incorporate a surface roughness on the regions with a no-slip condition, wall functions are utilized. Wall functions, available within the OpenFOAM platform, are implemented for this case in three areas consisting of the turbulent viscosity, turbulent kinetic energy, and specific turbulent dissipation rate fields, with the surface roughness being incorporated in the turbulent viscosity wall function. The surface

roughness of the pier and collar are set to zero, re-enacting a smooth condition, whereas the bed roughness is set to 0.001m. This roughness was chosen to replicate the sediment used in the laboratory, and, through a sensitivity analysis, they were found to match well. The OpenFOAM specific wall functions used are the nutkWallFunction and nutkRoughWallFunction for the turbulent viscosity field, the kqRWallFunction for the turbulent kinetic energy field, and the omegaWallFunction for the specific turbulent dissipation rate field.

To improve the accuracy of the numerical results, a turbulent inlet condition is used, where the inlet velocity (u_{in}) is set to 0.335m/s which was determined from calibration with the experimental data discussed below. It was found that the velocity profiles within the laboratory tests were fully developed prior to reaching the pier, therefore it is important that the velocity profiles of the numerical model behave in the same manner. In order to achieve fully developed velocity profiles numerically before reaching the pier, the pier must be placed 8.5m downstream of the flume inlet. The corresponding numerical and experimental velocity profiles and velocity map comparisons can be found in Valela et al. (2018) and Valela, Nistor, et al. (2021), respectively.

4.1.3 Experimental Setup

Experimental tests were conducted in a 30m long, by 1.5m wide, by 0.5m deep flume at the University of Ottawa's Civil Engineering Hydraulics Laboratory in Ottawa, Canada. The flume was equipped with a 3m long by 0.2m deep sand section which possessed silica sand with a median grain size (d_{50}) of 0.001m. In the center of the sand section, a cylindrical acrylic tube (D = 0.09m) was fixed to the bottom of the flume, through a bolted connection, to represent the model of a bridge pier. A geometric scaling ratio of 1:30 was used for the experimental tests, as it yielded realistic prototype scale dimensions. The flow depth (y) was maintained at 0.15m by means of a downstream gate at the end of the flume, and the depth-averaged flow velocity (u_{avg}) was set to 0.34m/s using the inlet valve. These flow conditions yielded a Reynolds number (Re) of approximately 30,000 which reside in the clear-water regime just prior to initiating bed motion. Tests were run for a duration of six hours because, by this point, 95% of the equilibrium scour depth was reached. Bathymetry measurements were recorded, after the water was drained from the flume using a laser altimeter, which was mounted onto a specially designed mechanized gantry. The gantry was computer controlled to move the attached altimeter in both the X- and Y-directions, therefore improving data accuracy and reducing data collection time. Velocity measurements were recorded in vertical profiles and horizontal planes using an Acoustic Doppler Velocimeter (ADV), for the purpose of calibrating the numerical model.

4.1.4 Methodology

4.1.4.1 Design Novelty

To improve on the scour reduction of CPN1, the high velocity flow exiting off the sides of the collar had to be addressed. The flow will experience an unavoidable increase in velocity around the sides of the pier because it must travel a longer distance in order to bypass the pier. Therefore, reducing the velocity of the passing flow is an option to solve the scour problem, but

it is rather difficult to execute solely. Instead, if the increased velocity can remain on top of the collar's flat edges until it reaches the rear of the collar, then the scouring along the sides of the pier can be overcome in a simpler fashion. By having the flow travel the entire length of the collar and not exit off early, several expected benefits arise. First, the increased velocity of the flow will naturally decrease because after the pier, the streamlines expand back to normal, and the flow returns to the mean velocity. This will help minimize scour downstream. Then, by allowing the flow to remain attached to the collar for longer, instead of detaching earlier on, the amount of turbulence generated will be reduced, leading to a more uniform transition into the mean flow and less interference with the passing flow (Milne-Thomson, 1973). Lastly, by having the flow exiting downstream in the same direction as the mean flow, if any scour does occur it will be far enough away from the collar that it is not a concern. Therefore, changing the flow path, such that the passing flow remains on top of the collar for a longer period of time, has the potential to reduce the scouring that CPN1 experienced along its side and front edges.

Implementing this change was achieved by streamlining the shape of CPN1. Specifically, the front of the collar cavity was moved further upstream to create a sharper leading edge, and the sides were brought in closer to the pier to create a narrower cavity section. Previously, the collar cavity was perfectly circular which caused the approaching flow to separate early on and be redirected outwards at a large angle, leading to the scour along the collar's side edges. Whereas now, the changes to the cavity assist in dividing the approaching flow and delaying the point of separation such that flow is not directed as far out the sides of the collar. Then, the rear of the collar cavity was extended from beside the pier, to the downstream edge of the collar. This changed the plan view shape of the collar cavity from elliptical into that of a tear-drop, which further streamlined the collar. By doing so, the curvature of the downstream portion of the collar cavity is reduced such that the passing flow will stay attached to the collar for longer, therefore prolonging the point of separation even further. Having the collar cavity extend further rearward also assists in guiding the horseshoe vortex, such that the two legs of the horseshoe vortex are joined together behind the pier and then finally released at the most downstream edge of the collar. The combination of the tear-drop shaped cavity and smooth exit of the horseshoe vortex help to reduce turbulence around the collar and interference with the passing flow. This newly adapted collar is referred to as Collar Prototype No. 2 (CPN2) and is shown in Fig. 4-1.

Fig. 4-1. Flow path through Collar Prototype No. 2 (CPN2).

4.1.4.2 Model Fabrication

The CPN1 model, which was the first model created for experimental testing, was machined out of solid aluminum using a HAAS Super Mini Mill 2. Due to the complexity of the design, the inner core was machined as one piece and the outer region was machined as a second piece. The two were then fused together in a seamless fashion to create a uniform object. The process of manufacturing 3-D objects using a milling machine inevitably leaves behind thin grooves on the part's surface which requires post manufacturing finishing. To finish such surfaces, a series of sanding steps were completed beginning with a coarse sand paper, progressing to a fine sand paper, and ending with a rubbing compound polish to achieve a smooth surface. The end result of the whole process was excellent, and the model served its purpose very well. However, the combination of the aluminum stock, the cost associated with the machining equipment, and the large quantity of skilled labor, made this model manufacturing process costly, resource-intensive, and time-consuming.

When numerous models need to be created in a prototyping process, a faster and less expensive route is required. This paper used a different approach to create CPN2, which utilized a MakerBot Replicator 2 (3-D printer) and Polylactic Acid (PLA) plastic. The 3-D printer heated the PLA plastic and then melted it into the specified shape. Due to the size limitations of the specific 3-D printer used, the collar was divided into five pieces and printed separately, as shown in Fig. 4-2(a). The pieces were then glued together and fastened to a thin steel plate for the purpose of adding rigidity to the object. 3-D printing also leaves behind small grooves on the

surface of the pieces, in a similar fashion to machining, therefore requiring post manufacturing finishing. The exact same process that was used for finishing the aluminum surface was also used for the plastic, so that the roughness of the surfaces would be identical and not effect the scour results. The completed CPN2 model can be seen in Fig. 4-2(b). Upon testing CPN2 in the laboratory setting, it was found to function, from a material and manufacturing point of view, as well as CPN1. The benefit to the manufacturing approach used for CPN2 is that the PLA plastic is significantly less expensive than aluminum, skilled labour is not required to operate the 3-D printer as it is user-friendly, and the entire process can be done in a fraction of the time machining would take. Therefore, utilizing a 3-D printer and PLA plastic for model manufacturing is an excellent option and highly recommended by the authors for these circumstances.

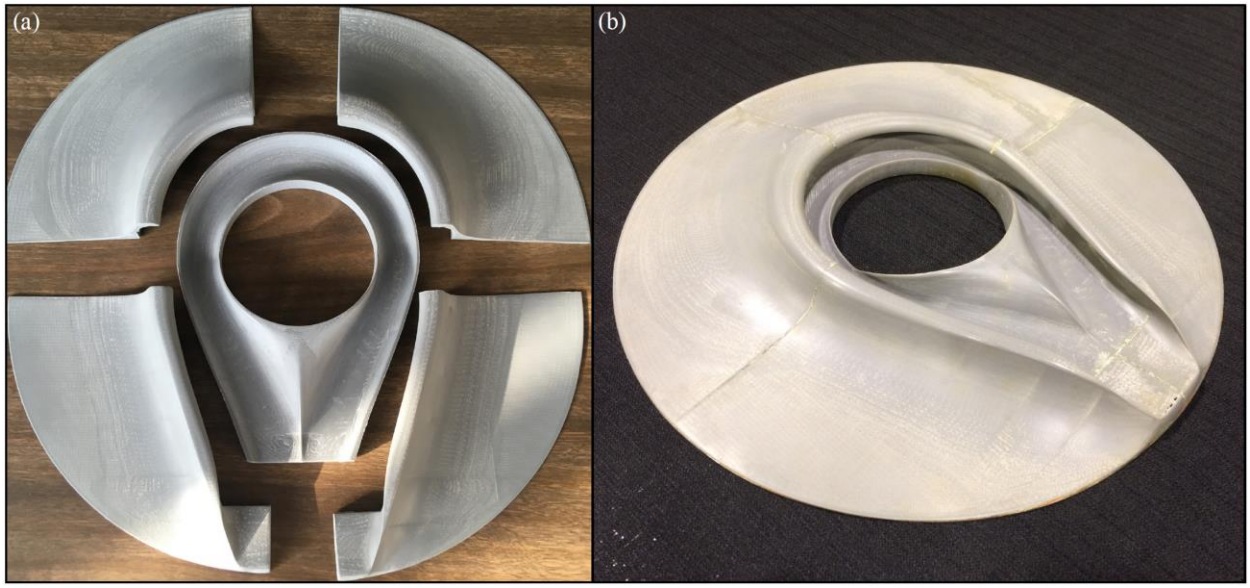

Fig. 4-2. (a) Disassembled PLA pieces which form CPN2, and (b) the complete CPN2 model.

4.1.5 Results

4.1.5.1 Numerical Results

CPN2 was tested numerically, using the model presented earlier, to evaluate its performance. The images presented within this section are time-averaged for the purpose of better illustrating the results. Fig. 4-3(a) presents the flow behaviour around a pier and CPN2, through means of a set of vertically sourced streamlines coloured with respect to the velocity (u) magnitude. The streamlines can be seen approaching the upstream face of the pier in a horizontal and uniform fashion until they are near the pier. Once the pier is within a close proximity, the flow velocity decreases and the streamlines begin to angle downwards. The streamlines that are closer to the bed enter the collar cavity where they form into the horseshoe vortex. The horseshoe vortex circulates a number of times within the collar cavity as it progresses around the front and sides of the pier, prior to exiting out the rear of the collar. As the horseshoe vortex exits the collar, the flow is angled upwards at a slight angle which develops into the large, full-depth

circulation, that reaches the water surface and travels down the backside of the pier. Meanwhile, the remaining streamlines that are further from the bed and do not enter the collar cavity, experience an increase in velocity as they bypass the pier. Once the streamlines pass the sides of the pier, their velocity slows, and some turbulence is experienced prior to blending with the mean flow. This increase in velocity, followed by a decrease, is consistent with the theory discussed earlier.

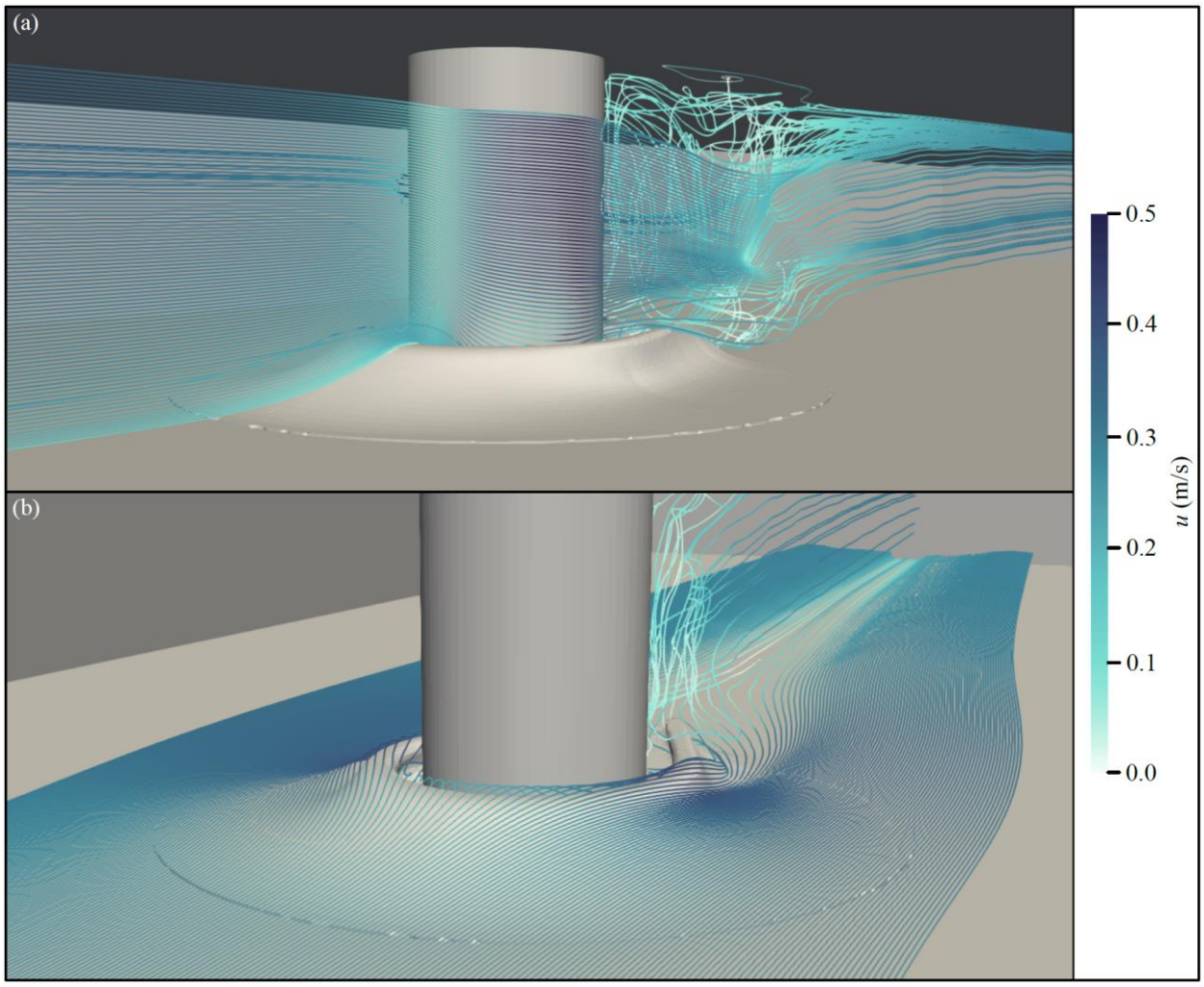

Fig. 4-3. Flow streamlines around a pier and CPN2: (a) vertically sourced streamlines, and (b) horizontally sourced streamlines.

Fig. 4-3(b) focuses on the flow behaviour around the tear-drop shaped cavity portion of the collar, through a set of horizontally sourced streamlines coloured with respect to the velocity magnitude. The streamlines approaching the collar head-on propel over the front of the collar cavity section and into the cavity, where they form into the horseshoe vortex, as mentioned earlier. Whereas, the streamlines that are not approaching the collar directly head-on, are redirected around the sides of the collar cavity and experience an increase in velocity until they bypass the pier. However, the point of separation between the collar and the flow does not occur

until past the midpoint of the pier, which can be attributed to the streamlined shape of the cavity. As a result, it can be seen that the streamlines, which possess an increased velocity, do not propel off the sides of the collar's edges, rather they continue to the rear of the collar in a more concentrated fashion with some streamlines following the cavity surface closely. Therefore, the quantity of turbulence generated from the passing flow around the front, sides, and rear of the collar is minimal, but it is worth noting that the passing flow does not return fully to the mean velocity until further downstream, beyond the end of the collar.

To better understand the impact which CPN2 has on scour, the shear stress exerted on the pier, collar, and bed, by the passing flow, is examined. The numerical model used for this study is not equipped with sediment transport capabilities; however the shear stress on the bed can be used as an indicator of scour potential. It can be seen in Fig. 4-4, that the front face of the pier and collar exhibits low shear stress: this is because of the stagnation region which is induced by the approaching flow colliding with the pier and collar. The shear stress then increases towards the sides of the pier and collar: this is due to the increase in velocity as the flow accelerates away from stagnation region. The largest shear stress occurs in the collar cavity and directly beside the pier on the collar. Therefore, the collar protects the riverbed from the largest shear stress, induced by the horseshoe vortex and the increased velocity occurring along the sides of the pier.

However, the most valuable information provided by Fig. 4-4 is the shear stress that is exerted on the bed, such that two regions of increased shear stress are present. The first is on either side of the collar, slightly downstream of the pier, and that is caused by any remaining flow exiting off the sides of the collar or accelerated flow travelling around the perimeter of the collar. This increase in shear stress is relatively moderate, as a majority of the flow remains on top of the collar for longer, however minor scour depths may result. Meanwhile, the second location immediately downstream of the collar, where the horseshoe vortex and separated passing flows exit the collar, a relatively large increase in shear stress is experienced. This increase in shear stress is large enough that it could lead to the generation of considerable scour. It is worth noting that there are two of these high shear stress regions downstream of the collar in a close proximity to each another, one on either side of where the horseshoe vortex exits the collar, with a region of almost zero shear stress in between.

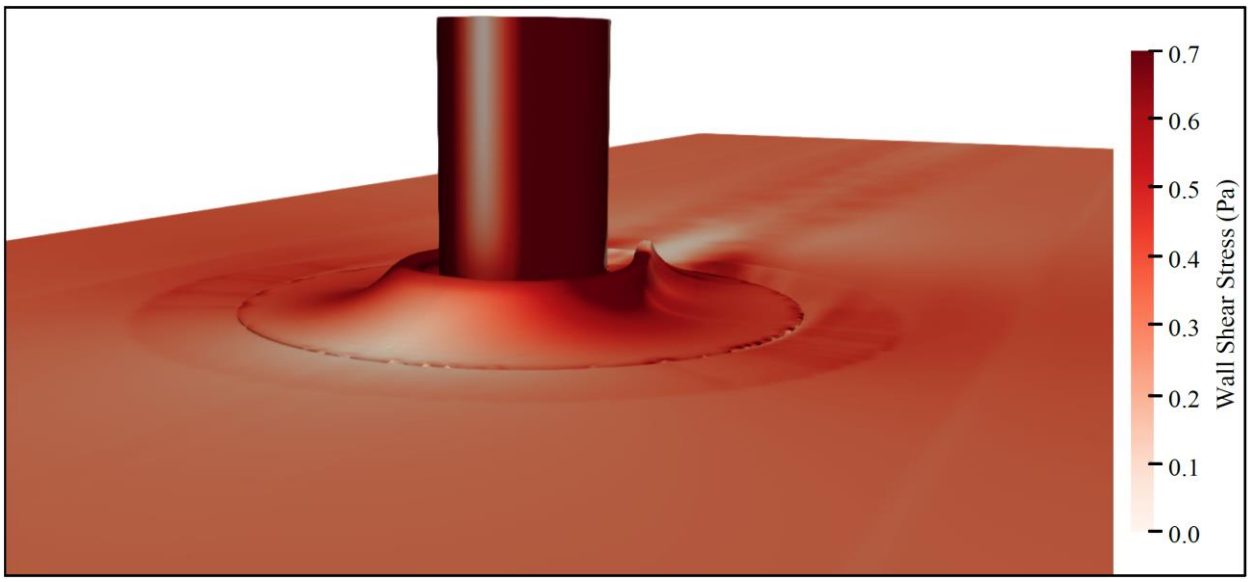

Fig. 4-4. Shear stress exerted by the passing flow on the pier, collar, and bed.

4.1.5.2 Experimental Results

In order to fully evaluate CPN2's performance, experimental tests were performed. The results shown in Fig. 4-5 represent the difference in scour between when CPN2 is present versus when no countermeasure is installed. It can be seen that, by adding CPN2, significantly less scour occurred around the pier, such that for a radius of 0.06m around the perimeter of the pier, the riverbed remained completely unchanged. Furthermore, the entire bed, from the mid point of the pier to the upstream extent of the study, did not experience any scour.

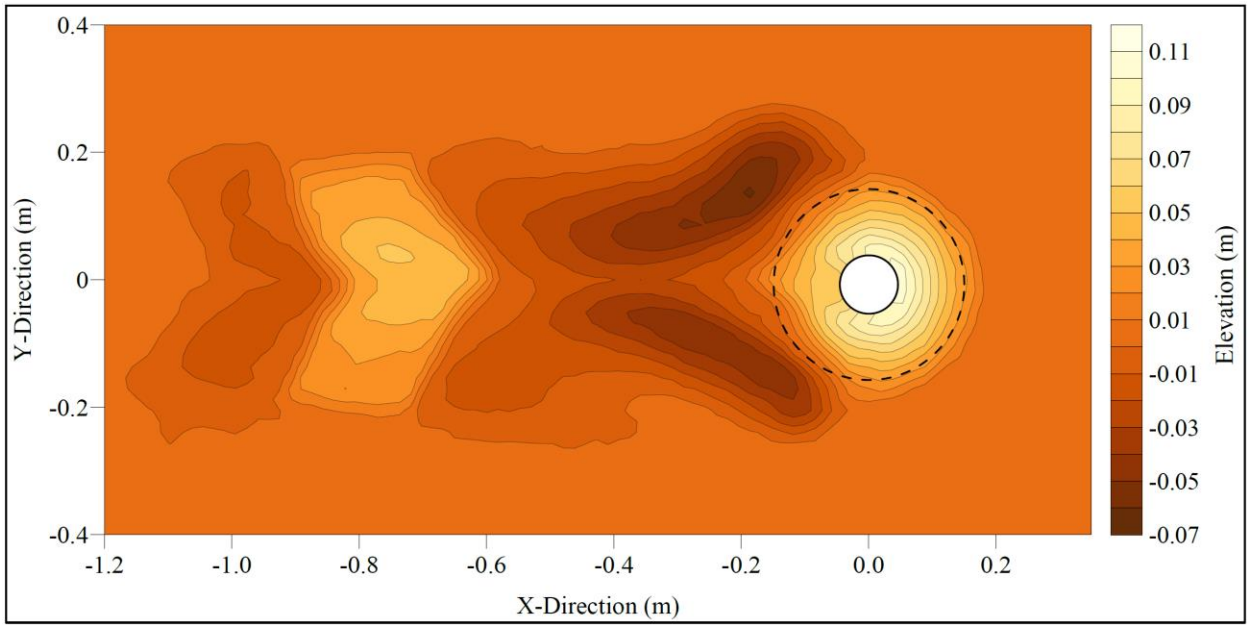

Fig. 4-5. Scour difference between using CPN2 and a pier without any scour countermeasure.

Meanwhile, that is not the case for the region downstream of the pier. Scour began behind the collar on both sides and progressed upstream until it reached the rear of the collar.

Upon reaching the collar, which is outlined by the dashed line, a small degree of undermining occurred. The maximum scour depth (d_s) experienced with CPN2 was 0.064m, which implies a reduction of 36% compared to when no countermeasure is present (Valela, Nistor, et al., 2021). Due to the scour location being behind the collar, the dislodged sediment was transported a shorter distance and resulted in an even higher localized deposition pile, seen 0.75m downstream from the pier. Fig. 4-5 demonstrates that scour is no longer an issue along the sides or upstream of the collar but is now an issue downstream. The location of d_s normally does not occur in this location when no countermeasure is present. Rather, this is something that is caused specifically by CPN2 and the influence it has on the passing flow.

4.1.6 Discussion

CPN2 was introduced as an improvement of CPN1, for the purpose of achieving greater scour reduction. CPN2 works along the same premise as CPN1 such that the horseshoe vortex is contained and the riverbed surrounding the pier is protected. When no scour countermeasure is present, the horseshoe vortex occurs around the base of the pier directly on top of the riverbed, but when either version of the collar is present, the horseshoe vortex is contained within the collar cavity and does not contact the riverbed. Therefore, containing the horseshoe vortex has been successfully executed using both versions of the collar.

CPN1 has some areas which could be improved because scour occurs along its side and front edges. To overcome this issue, CPN2 was designed with a more streamlined shape so that the passing flow would not separate as early on and be directed off the sides of the collar, but rather remain attached for longer. By doing so, scour beside and upstream of the collar was completely avoided and the design changes can be deemed a success in addressing the identified issues pertaining to CPN1. Specifically, the flow did not separate and exit off the sides of the collar prematurely, rather a majority remained on top of the collars flat edges and exited at the rear, as per the design intention.

However, more scour occurred downstream of the collar which led to undesirable undermining of the rear of the collar. As a result, the d_s achieved by CPN2 was 15% deeper than when using CPN1 (Valela, Nistor, et al., 2021). The d_s location of the two collars was however different: CPN1 led to scour along the sides and front of the collar, whereas CPN2 experienced scour at the rear of the collar. The distance between the maximum scour holes to the pier for both collars was approximately the same. The authors concluded that, overall, CPN2 does not reduce scour more than CPN1, nor does it relocate scour to a better location, ultimately making it a less desirable countermeasure.

The reason such a large scour hole developed is because of how the streamlined shape redirected the passing flow along the sides of the collar cavity. Previously, the flow separated early on and dispersed into the mean flow over a large area, whereas now the flow stays attached for longer and is more concentrated as it exits the rear of the collar. As the concentrated flow travels off the rear of the collar, it still exhibits a slightly increased velocity which leads to the

scour seen immediately downstream of the collar. The intention of streamlining the collar was to reduce scour, which was successfully executed upstream; however greater scour resulted downstream. This suggests that not only is the horseshoe vortex an important factor in causing scour, but also the increased velocity along the sides of the pier. To achieve a countermeasure design that substantially reduces scour, both the horseshoe vortex and the accelerated passing flow need to be addressed.

Although the scour reduction of CPN2 may not be significant, there is still the potential for it to outperform other countermeasures, contingent upon further revisions. The reason for that is because the problem of the side and upstream scouring has been addressed. Therefore, if the same front of CPN2 is kept but its rear is changed such that the exiting flow has a decreased velocity and is more dispersed, then scour may be substantially reduced.

Numerical results, consisting of flow streamlines and wall shear stress, were utilized as an indication of the collars' performance and their associated scour. The wall shear stress data revealed two bed locations on either side of the pier with increased shear stress, which as mentioned before, could lead to scouring. The largest shear stress of the two locations was observed to occur immediately downstream of the collar. Based on the magnitude of the shear stress, it was predicted that considerable scour depths could result. This was in fact confirmed through experimental testing, such that this area of high shear stress lied within the scour hole near the deepest location. The scour hole shape is slightly different than the area of increased shear stress and that is likely due to the contribution of the moderate increase in shear stress experienced in the second location beside the collar, or the falling of surrounding sediment into the scour hole. Regardless, the shear stress calculated through the numerical model is in agreement with the experimental scour patterns observed, confirming that the numerically obtained shear stress is a relatively accurate indication of scour.

Another comment worth noting is that the scour holes and deposition piles are not exactly symmetric. A possible explanation for this behaviour is that the collar was not positioned perfectly parallel to the flow; rather it exhibited a very small skew angle. As a result, the flow exiting the collar cavity and bypassing the sides was influenced by this skew angle and, therefore, led to nonsymmetric scour patterns. In the future, this issue could be addressed by aligning the collar exactly parallel to the flow or the design of the cavity could be altered in such a way that it is more accommodating to slight skew angles.

4.1.7 Conclusions

The purpose of developing CPN2 was to eliminate the scouring that occurred along the sides and front of CPN1. This was successfully achieved, such that no scour occurred from the mid point of the pier to the upstream extent of the study, when CPN2 was present. Therefore, the main objective of the study was accomplished. However, by streamlining the shape of the collar, greater scour resulted downstream. The depth of scour was so great that it surpassed that of CPN1 by 15%. Despite solving the scour problem upstream, a worse condition occurred

downstream, implying that this design is not preferred as it currently stands. However, there is potential for it to outperform the previous collar in terms of scour depth, since the upstream scour is eliminated, by incorporating the front of CPN2 and a redesigned rear. Constructing the physical model of CPN2 was done differently than that of CPN1, because three-dimensional printers and PLA plastic were used rather than metal machining practises. This approach proved to be significantly better and the preferred method of model manufacturing, due to the substantial cost and time savings associated with it. Lastly, to test the performance of the collar with regards to scour, numerical and experimental methods were used, and it was confirmed that the numerical results were an accurate indication of the resulting scour.

4.2 Improved Bridge Pier Collar for Reducing Scour (CPN3)

Preprint of a modified version of an article printed in the International Journal of Sediment Research © 2021 Elsevier B.V.. DOI:10.1016/j.ijsrc.2021.04.004.

4.2.1 Introduction and Objectives

In an attempt to improve on Collar Prototype No. 1 (CPN1), Valela et al. (2019) designed Collar Prototype No. 2 (CPN2), both of which are shown in Fig. 4-6. The intention of CPN2 was to reduce undermining, and more specifically, the quantity of bypassing flow being directed off the sides of the collar. This was achieved by creating a narrower, more streamlined collar cavity, which delayed the point of flow separation and allowed more of the bypassing flow to remain on top of the collar's flat edges until the rear of the collar. However, CPN2 was found to reduce the maximum scour depth (d_s) by only 36%, implying 4% less than the Flat Plate Collar (FPC) and 15% less than CPN1 (Valela et al., 2019; Valela, Nistor, et al., 2021). Nonetheless, the quantity of undermining was reduced, and scour did not occur upstream of the pier. Instead, the scour shifted to behind the collar and this was due to a high concentration of shear stress, from the bypassing flow and horseshoe vortex, exiting together at the rear of the collar. Despite attempting to streamline the shape, a device that increases the width of the pier causes more flow interruption, leading therefore to greater flow diversion and acceleration (Valela et al., 2019). This suggests a collar that contains the horseshoe vortex inside of a cavity residing above the bed is not the best approach. Rather, if the horseshoe vortex were guided below the bed, minimizing obstruction of the bypassing flow, then this could be a better performing design.

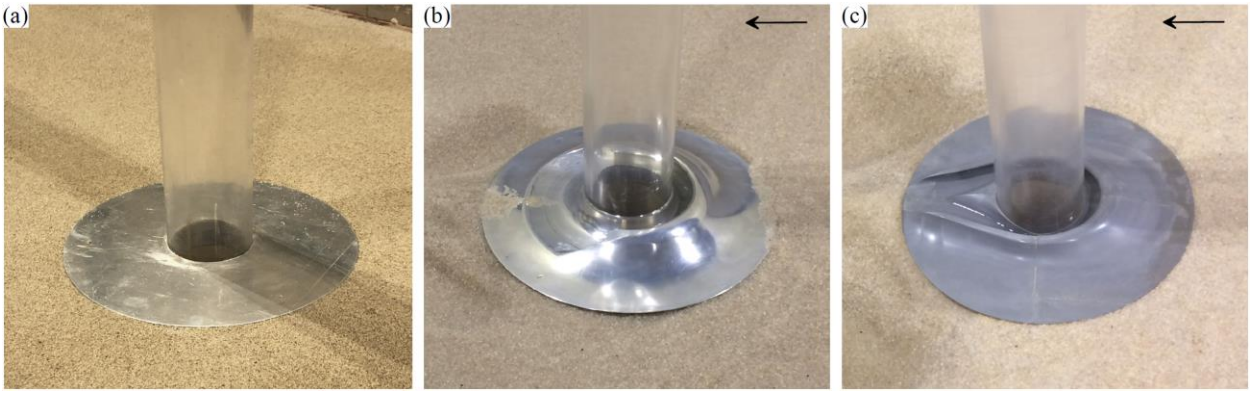

Fig. 4-6. Previous collar designs: (a) FPC, (b) CPN1, and (c) CPN2.

This paper presents a bridge pier collar comparison while introducing an improved collar design, Collar Prototype No. 3 (CPN3), which guides the horseshoe vortex below the bed in a way that lessens the interruption of the bypassing flow. The objectives of this study are to:

1) Introduce an improved bridge pier collar, CPN3, for the purpose of reducing scouring and collar undermining more than previous collar designs.
2) Demonstrate the function of CPN3 through the use of a numerical model.

3) Evaluate the performance of CPN3 and an FPC under a wide array of clear-water experimental conditions.
4) Perform a comparison of bridge pier collars, consisting of CPN3, CPN2, CPN1 and an FPC.

4.2.2 Numerical Model

The numerical simulations were performed using the open-source Computational Fluid Dynamics (CFD) toolbox, OpenFOAM v1706, which employs the Finite Volume Method (FVM) (ESI Group, 2019). OpenFOAM's *pimpleFoam* solver is utilized, and for the purpose of this study, operates in the Pressure Implicit Split-Operator (PISO) mode as the Courant number is set to 0.8. The turbulence model used is of the Delayed Detached Eddy Simulation (DDES) type, specifically ($\kappa - \omega\ SST$) DDES, which uses a Reynolds Averaged Navier Stokes (RANS) model near the walls and a Large Eddy Simulation (LES) model in the rest of the flow domain.

The numerical domain is 10m long, by 0.85m wide, by 0.15m deep, comprised entirely of a single-phase fluid. A cylindrical pier with a diameter (D) of 0.09m, is located 1.5m upstream from the outlet. To ensure a balance between computational efficiency and numerical accuracy, a mesh containing three different cell sizes is used. A majority of the domain consists of cells measuring 0.008m in all directions. The focus region around the pier consists of two levels of refinement, one rectangular and one circular, with cell sizes measuring 0.004m and 0.002m, respectively, in all directions. A total of approximately 5.5 million cells were used to mesh the entire domain and a mesh sensitivity analysis was performed to ensure grid independence was reached. Fig. 4-7 displays the mesh, at the downstream end of the flume, highlighting the cell refinement near the pier.

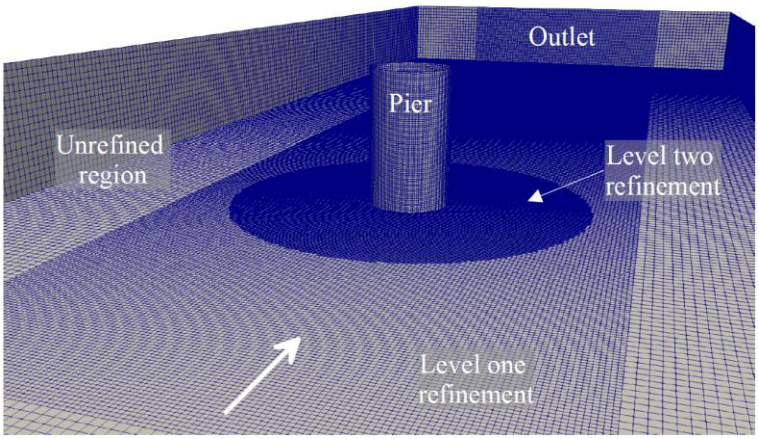

Fig. 4-7. Numerical model mesh for the pier without any erosion countermeasure.

The boundary conditions utilize a slip condition on the side walls, a symmetry condition on the top surface, and a no-slip condition on the bed and pier. The bed and pier also employ wall functions to reduce the number of cells required against such surfaces. To match the experimental conditions, the pier possesses a smooth surface while the bed possesses a roughness (k_s) of 0.001m, which is defined within the wall functions. The inlet velocity (u_{in}) used for all

tests is 0.335m/s and is incorporated through a turbulent inlet condition. Lastly, the outlet contains an inlet-outlet boundary condition.

Calibration of the numerical model consisted of collecting vertical experimental velocity profiles from laboratory tests conducted by the authors for comparison purposes. For more details on the data collection, refer to Section 4.2.3.2. Then, different turbulence models, wall functions, inlet velocities, bed roughness heights, and pier locations were tested individually in the numerical model until the velocity profiles from the numerical model matched closely to that of the experimental model. Once the numerical model was calibrated, validation was completed by collecting approximately 100 velocity measurements in the horizontal plane, at 0.07m above the bed, from both the experimental and numerical models. The velocity fields from both were then compared. Further information pertaining to the details, calibration, or validation of the numerical model, can be found in Valela, Nistor, et al. (2021), where the model has been previously introduced.

4.2.3 Experimental Setup

4.2.3.1 Experimental Facility

The experimental research reported in this study was conducted in the Civil Engineering Hydraulics Laboratory at the University of Ottawa, Canada. The flume, which the tests were performed within, measures 30m long, by 1.5m wide and 0.5m deep. A sand section measuring 3.16m in length and spanning the full width of the flume was installed within the flume, for the purpose of obtaining scour results. To contain the sand, concrete false floors were installed upstream and downstream of the sand section, as shown in Fig. 4-8, with lengths of 4.16m and 1.25m, respectively. The surface of the false floors was finished with a 0.001m roughness. This was accomplished by adhering (using paint) 0.001m sand to the surface of the concrete. At the leading face of the upstream false floor, a 2.25m long ramp, made of gravel, was used to smoothly transition the flow onto the false floors and sand section. An acrylic cylinder (D = 0.09m) was bolted to the floor of the flume, in the center of the sand section, to replicate a bridge pier. The ratio of D to the flume width (blockage ratio) was verified to ensure that the location of the walls would not influence the results. Two flow straighteners were utilized towards the inlet to reduce the inherent turbulence prior to reaching the focus region.

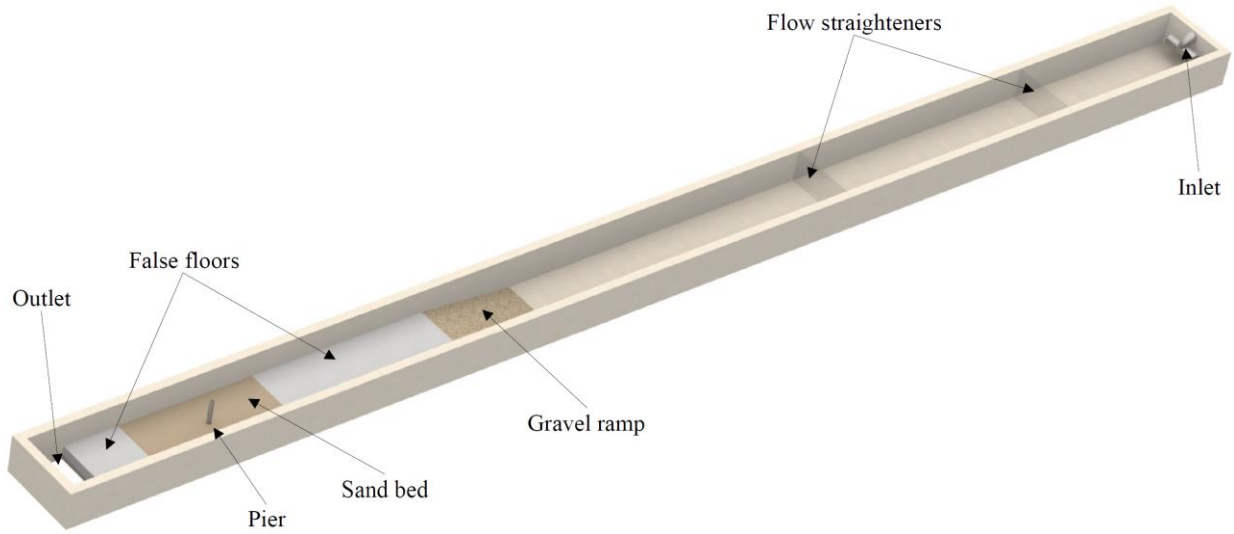

Fig. 4-8. University of Ottawa's experimental flume and setup.

The data collected to calibrate and validate the numerical model required a slightly different experimental setup than that discussed above. This is because the numerical model does not possess sediment transport capabilities and employs a rigid bed. Therefore, for comparison, the experimental flume needed a rigid bed, thus the pier was temporarily relocated upstream, to on top of the false floor, for the duration of the calibration and validation tests.

4.2.3.2 Instrumentation and Prototypes

The velocity measurements were obtained using a Vectrino Acoustic Doppler Velocimeter (ADV). The data were collected at each location using a sampling frequency of 100Hz for a duration of two minutes. The collected data were de-spiked and filtered (Jamieson et al., 2010), and time-averaged over the two minute sampling period.

After each test was completed, the water was drained from the flume. To capture the resulting bathymetry, a Leica ScanStation P50 Terrestrial Laser Scanner (TLS), with an accuracy of +/- 0.0015m in all directions, was used. The TLS was setup outside of the four corners of the sand bed and a scan was completed from each location. By performing a scan from all four corners, the entirety of the scour holes could be captured. The four scans were then joined together to create a 3-D representation of the resulting bathymetry. This process was repeated for each test.

A model of CPN3 and an FPC were constructed so they could be tested experimentally. Both collars possessed the same outer diameter of 3.3D on the bed surface. CPN3 was made of Polylactic Acid (PLA) plastic using an Ultimaker 2+ 3-D printer equipped with a 0.0008m diameter nozzle. Due to the physical print volume limitations of the Ultimaker 2+, CPN3 was printed in quarters and then glued together. To add more rigidity, a thin aluminum disc, the diameter of the outside of CPN3, was glued to the bottom of the printed pieces. The FPC, on the other hand, has a simpler design and thus was constructed out of aluminum. An aluminum sheet, 0.003m thick, was cut to the required shape using a band saw. Then, an aluminum ring with an

inside diameter equal to D, an outside diameter equal to D + 0.01m, and a height of 0.02m, was fastened to the bottom of the FPC, in the center extending the hole for the pier. This was done to add stability, so the collar remained perpendicular to the pier during testing. Since the ring was small and located on the bottom side of the collar, it did not impede on the tests in any way. After completion, both collars were sanded to a smooth finish, such they possessed the same roughness.

4.2.3.3 Experimental Protocol

The experimental study examined two different countermeasures, an FPC and CPN3, as well as the benchmark case of a pier without any erosion protection countermeasure. For all trials, the bed was levelled initially, and the countermeasures were installed in the same way, with the top surface flush with the initial bed height. The countermeasures and benchmark case were tested with two different bed sediments, which had median grain diameters (d_{50}) of 0.0007m and 0.001m. Flow conditions for testing with each sediment were selected with the assistance of the Shield's curve to ensure appropriate mobility in the clear-water scour regime. For the d_{50} = 0.0007m sand tests, the depth-averaged velocity (u_{avg}) was maintained at 0.25m/s and the flow depth (y) was maintained at 0.15m. On the other hand, for the 0.001m d_{50} sand cases, three different u_{avg} conditions (0.3m/s, 0.34m/s, and 0.38m/s) and three different y conditions (0.1m, 0.2m, and 0.3m) were tested. To determine the length of time to run the tests, a trial test was carried out for 12 hours (not shown herein) and it was found that at 6 hours, 95% of the equilibrium scour depth had been reached. Therefore, all tests were run for a duration of 6 hours. The naming convention, conditions, shear velocity (u_*), and Froude number (Fr) for each experimental test are shown in Table 4-1. Note that u_* was calculated using the log-law with the velocity measured 0.005 m above the bed and a k_s value of 0.001 m.

Table 4-1. Experimental parameters.

Test	Countermeasure	d_{50} (m)	y (m)	u_{avg} (m/s)	u_* (m/s)	Fr
A1	None	0.0007	0.15	0.25	0.015	0.21
A2	FPC	0.0007	0.15	0.25	0.015	0.21
A3	CPN3	0.0007	0.15	0.25	0.015	0.21
B1	None	0.0010	0.15	0.30	0.016	0.25
B2	FPC	0.0010	0.15	0.30	0.016	0.25
B3	CPN3	0.0010	0.15	0.30	0.016	0.25
C1	None	0.0010	0.15	0.34	0.018	0.28
C2	FPC	0.0010	0.15	0.34	0.018	0.28
C3	CPN3	0.0010	0.15	0.34	0.018	0.28
D1	None	0.0010	0.15	0.38	0.020	0.31
D2	FPC	0.0010	0.15	0.38	0.020	0.31
D3	CPN3	0.0010	0.15	0.38	0.020	0.31
E1	None	0.0010	0.20	0.34	0.017	0.24
E2	FPC	0.0010	0.20	0.34	0.017	0.24
E3	CPN3	0.0010	0.20	0.34	0.017	0.24
F1	None	0.0010	0.10	0.34	0.021	0.34
F2	FPC	0.0010	0.10	0.34	0.021	0.34
F3	CPN3	0.0010	0.10	0.34	0.021	0.34

4.2.4 Collar Prototype No. 3 (CPN3)

CPN1 and CPN2 were designed to contain and guide the horseshoe vortex inside of a 3-D cavity. Both of these designs proved to reduce the scour depth; however, the collar cavity was always above the sediment bed, which caused greater flow interruption. As a result, a larger proportion of accelerated flow was redirected causing scouring and undermining along the edges of these collars. This study presents the CPN3 design, which is an improved bridge pier collar that aims to reduce undermining and overall scour that was experienced with CPN1, CPN2, and the FPC. The premise behind CPN3 is that the horseshoe vortex is still contained in a cavity, but below the sediment bed surface. Through the latter, the pier maintains its original width and the horseshoe vortex is guided in a controlled manner.

CPN3 was designed in such a way to replicate an existing pier scour hole. The cross-sectional shape of a developed scour hole, obtained from Kirkil et al. (2005), was used as a basis to create the cavity profile, as shown in Fig. 4-9. A simpler way of viewing this new collar is that it acts as a solidified scour hole. Rather than attempting to weaken the horseshoe vortex, which has proven to be challenging, the horseshoe vortex remains uninterrupted and follows its quasi-natural flow path in this replicated equilibrium scour hole. By creating a solidified scour shape, it prohibits the horseshoe vortex and more importantly the scour hole, from growing or changing in shape.

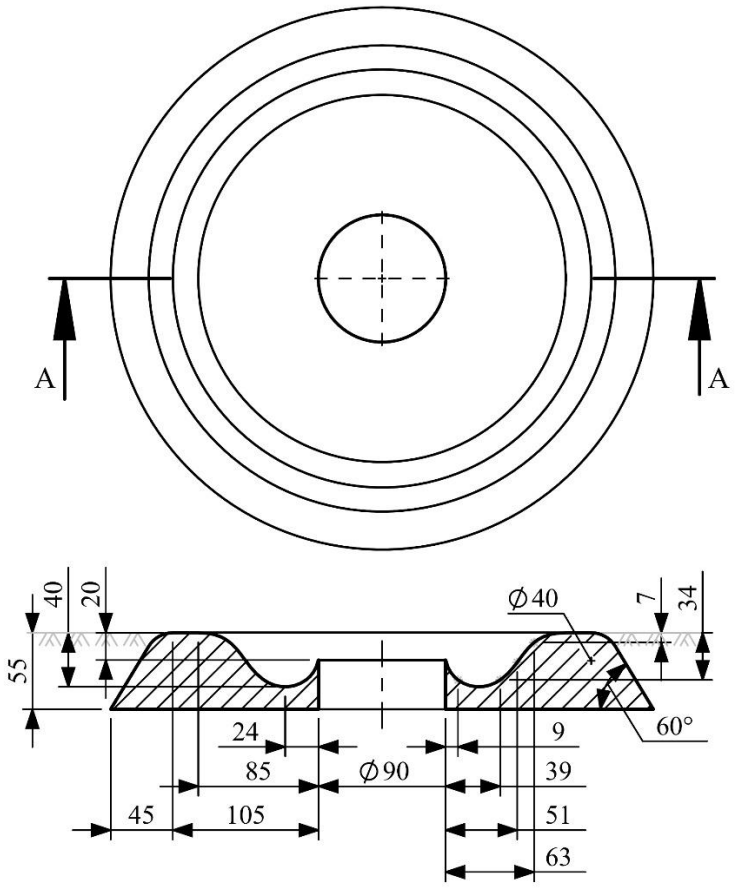

Fig. 4-9. Plan and cross-section sketches of CPN3 (all dimensions in mm).

Installing CPN3 consists of first excavating a circular region around the pier to allow for the collar to be embedded into the sediment bed. Once the excavation is complete, the collar is either slid down the pier (laboratory installation) or assembled around the base of the pier within the excavation (prototype scale field installation). It must be ensured that the collar is level in all directions and that the top surface is flush with the surrounding bed. Then, sand can be filled around the perimeter of the collar to make a seamless transition between the sand bed and the collar, as shown in Fig. 4-10. By designing the collar with a symmetric shape, it can be installed facing any direction and can accommodate multidirectional flows, which was not feasible with the previously designed CPN1 and CPN2. Furthermore, as a precautionary measure, the sides of CPN3 were built with an outward slope. This was done to help reduce scour if it were to occur around the perimeter of the collar because Bozkus and Yildiz (2004) found a sloped face of a protruding structure can reduce scour.

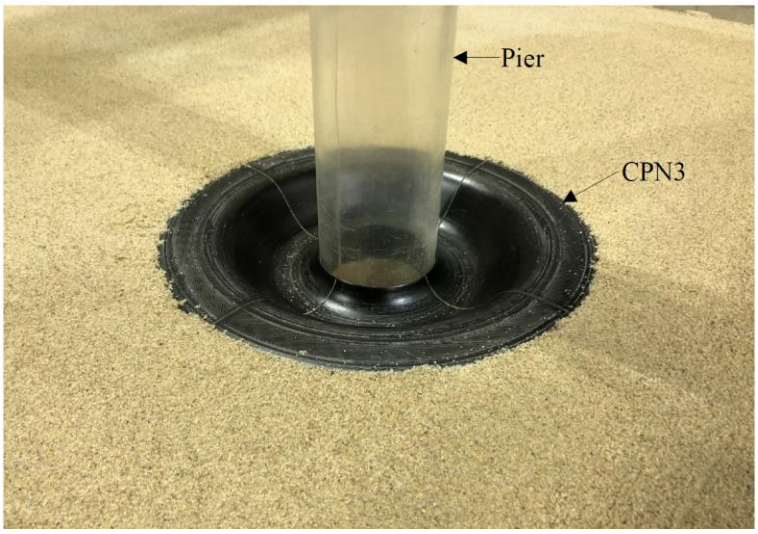

Fig. 4-10. CPN3 installed flush with the surrounding bed.

4.2.5 Results

4.2.5.1 Numerical

One of the purposes of the numerical model was to demonstrate the flow velocity (u) around a circular pier equipped with CPN3. Fig. 4-11 illustrates the side view of a pier and CPN3 with time-averaged velocity stream tracers. Upstream of the pier, the flow is similar to that when CPN3 is not installed, which is shown in Valela, Nistor, et al. (2021), except directly in front of the pier, near the bed. The horseshoe vortex, which is small in diameter and occurs on top of the bed when CPN3 is not installed, now is much larger and occurs within the cavity below the bed. The downward flow fills the entire cavity and circulates primarily within it, causing only a small redirection of the passing flow directly over top. The horseshoe vortex continues to circulate within the cavity, gradually reducing in velocity as it progresses around the pier. At the rear of the pier, the flow within the cavity stops circulating and a small portion exits straight downstream over the rear of the collar while the rest is angled up towards the water surface. By doing so, there is a large reduction in the quantity of high velocity flow travelling across the surface of the bed downstream of the pier. Through the application of CPN3, the high velocities otherwise experienced at the base of the pier, in the horseshoe vortex, or along the bed surface downstream of the pier, are reduced or contained within the collar.

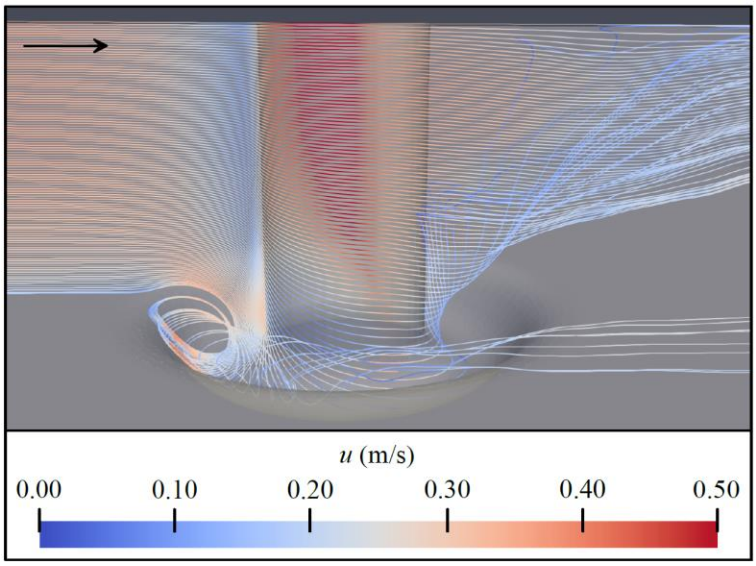

Fig. 4-11. Time-averaged velocity magnitude stream tracers showing CPN3 with 50% transparency.

To evaluate the influence CPN3 has on scour, the time-averaged bed shear stress around a pier with CPN3 needs to be investigated. When CPN3 is not installed, there is a primary region, directly adjacent to the pier, possessing an extremely high shear stress (approximately 0.7Pa), as shown in Valela, Nistor, et al. (2021). This primary region occurs on either side of the pier and extends downstream. Outside of the primary region there is a secondary region (possessing a shear stress of approximately 0.55Pa), which extends further out from the pier. The secondary region possesses a reduced shear stress when compared to the primary region, but an increased shear stress when compared to the unaffected region. Both primary and secondary regions could result in scour.

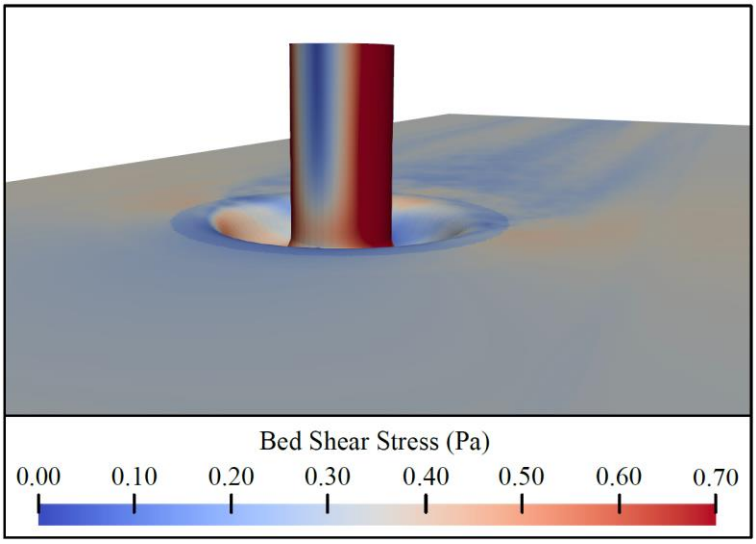

Fig. 4-12. Time-averaged bed shear stress with CPN3 installed.

In the presence of CPN3, shown in Fig. 4-12, the primary and secondary regions of increased shear stress are greatly reduced in size and magnitude. The primary region occurs only within the collar and does not contact the bed. Meanwhile, the secondary region still experiences an increase in shear stress when compared to the unaffected region, which could result in some scour, but it is much less than when CPN3 is not installed. Downstream of the pier, CPN3 causes the wake to be dispersed over a larger area, causing a more uniform distribution of shear stress on the bed. However, a region along the rear edge of the collar shows a mild increase in shear stress which could also lead to localized scour.

4.2.5.2 Experimental

The numerical model provides detailed information about the flow field that is difficult or impossible to obtain from experimental testing, but in order to accurately determine the resulting scour depth and pattern, experimental testing was required. Therefore, the FPC, CPN3, and the benchmark case (pier without any scour countermeasure), were tested experimentally with different values of d_{50}, u_{avg}, and y. The experimental tests were organized into series (A-F) based on the flow conditions, as outlined in Table 4-1. Series A consisted of a different d_{50}, series B, C, and D consisted of the same y but varying u_{avg}, and series E, C, and F consisted of the same u_{avg} but varying y. A velocity profile for each series was collected using an ADV at depth intervals of 0.005m and presented in Fig. 4-13 in semi-log scale. A down-looking ADV head was used, with a sampling volume located approximately 0.05m away from the probe tip; thus, the top portion of each velocity profile could not be measured. u_* was calculated 1m upstream of the pier for the series C experimental flow condition and the numerical model flow condition, and they were within 0.00042 m/s, resulting in a difference of 2.37%.

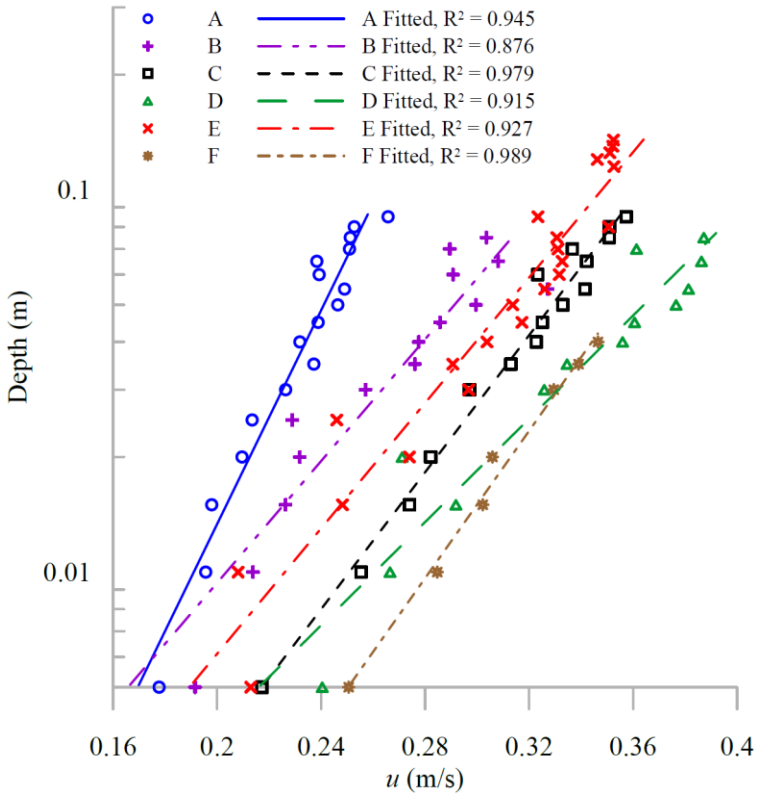

Fig. 4-13. Velocity profiles collected 1.0m upstream of the pier for each experimental condition.

After the completion of each test, a bed scan was performed of the resulting scour in the vicinity of the pier. From the 3-D scans, contour plots were generated and presented in Fig. 4-14. Within Fig. 4-14, the first column from the left pertains to the benchmark case of a pier without any scour countermeasure, the second column pertains to the FPC, and the third column pertains to CPN3. The dotted lines around the pier in column two and three represents the perimeter, on the bed surface, of the corresponding collar used in that test. For column three, the depression shown around the pier (inside the dotted line) for each test is the surface profile of the collar, not the sand bed. CPN3 was not removed before performing the scan, but the FPC was. Each row in Fig. 4-14 pertains to a test series and they are grouped based on the test parameters: d_{50}, u_{avg}, and y. Series C is repeated within the figure to better show the effects of each parameter.

For the single flow condition tested in series A, the scour patterns for all three tests are different than the other series due to the smaller size of the sediment used. Specifically, more fluctuations in the bed surface can be seen as there are approximately three scour holes, decreasing in depth, extending off each downstream corner of the pier. These three scour holes occurred regardless if a collar was installed or not. The presence of a collar does however accentuate these scour holes. On the other hand, with larger bed sediment, at most, only one scour hole formed off each downstream corner of the pier and a smoother bed surface with fewer fluctuations was observed.

When either the FPC or CPN3 was used in Series A, it can be observed that the location of d_s moved away from next to the pier. For both collars, instead of one large scour hole occurring in front of the pier, two smaller scour holes occurred downstream of the collar, on either side of the pier, where the flow exits the collar. Neither collar experienced undermining, but CPN3 did yield a reduction in d_s and scour volume (V_s) when compared to the FPC.

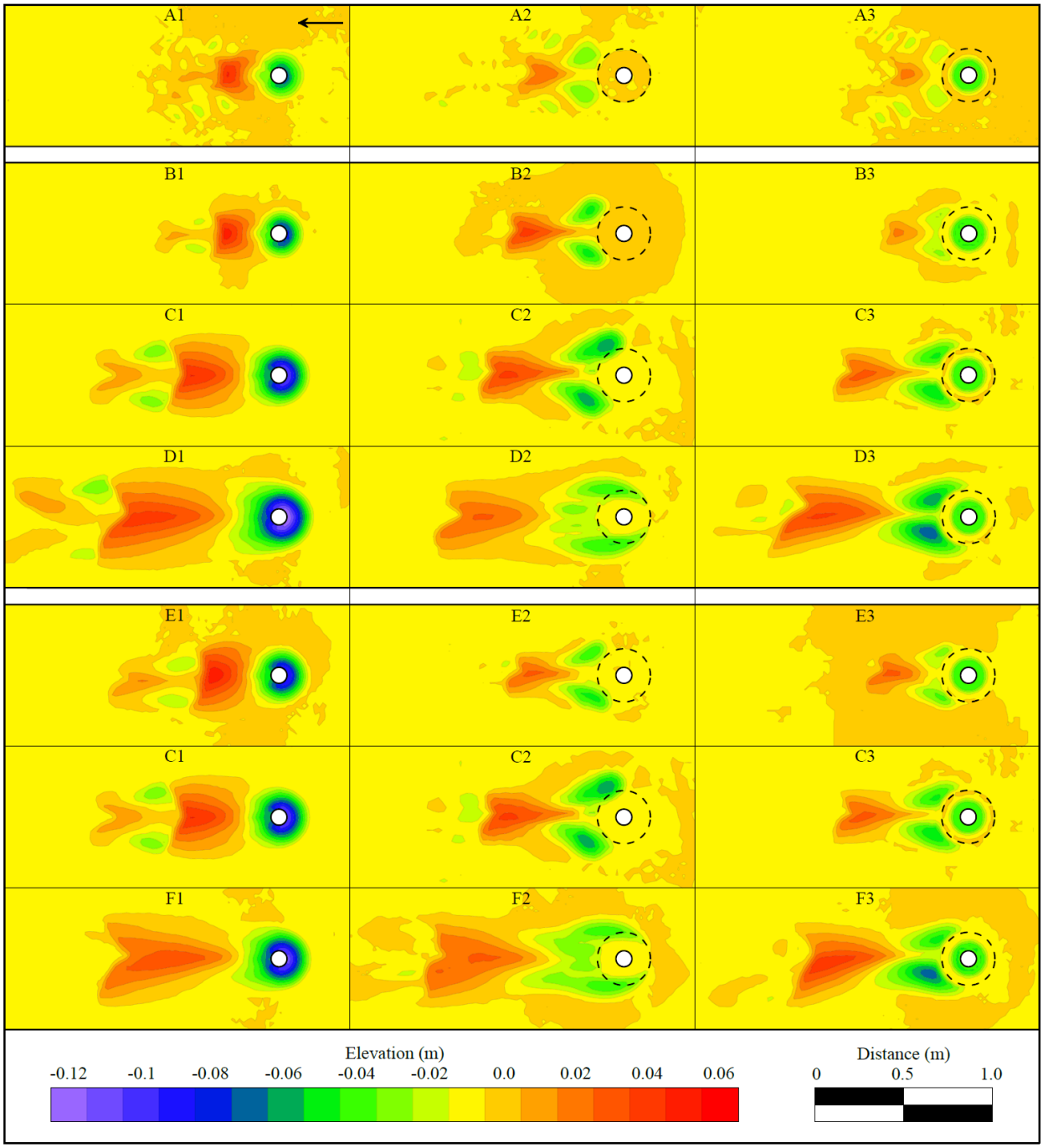

Fig. 4-14. Scour plot comparison segmented into alternate sediment size (A), increasing u_{avg} (B-C-D), and decreasing y (E-C-F). Column one, two, and three correspond to no countermeasure,

the FPC, and CPN3, respectively (dotted line indicates the perimeter of the collars at the bed surface). Note: C1 and C2 reprinted with permission from ASCE (Valela, Nistor, et al., 2021).

Series B, C, and D studied the effect of changing u_{avg} between 0.3m/s, 0.34m/s, and 0.38m/s, respectively. For the benchmark case and CPN3, as u_{avg} increased, so did d_s. However, this did not occur for the FPC. The FPC reached the greatest d_s at 0.34m/s (test C2), then d_s decreased when u_{avg} = 0.38m/s (test D2). What can be noticed in the scour pattern of test D2 is that undermining occurred beneath the left and right side of the collar. Instead of the scour reaching deeper, it penetrated under the collar covering a larger area. For series B and C, the FPC reduced the depth and region of scour, and CPN3 reduced the depth and region of scour even more. For series D, both collars reduced scour more than the benchmark case, but because of the undermining the FPC experienced, it had a shallower scour depth than that measured when using CPN3.

The scour results for a decrease in y (0.2m, 0.15m, and 0.1m corresponding to series E, C, and F, respectively) were similar to that observed for tests with an increase in u_{avg} (series B, C, and D). As y decreased, for the benchmark case and CPN3, d_s increased. The FPC experienced undermining at the shallowest y (test F2) resulting in the greatest d_s occurring for y = 0.15m (test C2). CPN3 achieved the most significant scour reduction, when compared to the FPC, except for when the FPC experienced undermining. Therefore, a reduction in y or an increase in u_{avg} both have a similar effect on scour.

Both collars, the FPC and CPN3, eliminated scour directly in front of the pier and for the entire region upstream of the pier, except for FPC when undermining occurred. However, scour occurred downstream of the pier for both collars, with two main scour holes, one on either side of the pier, regardless of d_{50}, y, or u_{avg}. When undermining did occur for the FPC, the scour hole first formed downstream of the collar and then progressed upstream along the outer perimeter of the collar.

Using the 3-D scans, d_s and V_s were calculated for each test (Table 4-2). When two quasi-symmetrical scour holes were present, d_s was calculated as the average of the two scour holes. The greatest scour reduction occurred for CPN3 when d_{50} = 0.0007m. A 69.7% d_s reduction and a 75.7% V_s reduction were achieved, which is 15.2% and 39.5% greater, respectively, than that of the FPC. CPN3's lowest d_s reduction was 46.6% and 46.7% which occurred for the highest u_{avg} and lowest y tests, respectively. Meanwhile, CPN3's lowest V_s reduction was 30.8% which occurred for the lowest y test.

Table 4-2. Summary of scour results for each test. Note: C1 and C2 data reprinted with permission from ASCE (Valela, Nistor, et al., 2021).

Test	d_s (m)	V_s (m^3 x 10^{-3})	d_s reduction (%)	V_s reduction (%)
A1	0.066	1.552576	-	-
A2	0.030	0.991272	54.5	36.2
A3	0.020	0.376541	69.7	75.7
B1	0.073	1.713928	-	-
B2	0.046	1.400149	37.0	18.3
B3	0.023	0.473903	68.5	72.3
C1	0.100	3.933098	-	-
C2	0.060	3.494451	40.0	11.2
C3	0.047	2.049618	53.0	47.9
D1	0.118	6.592580	-	-
D2	0.040	3.636713	66.1	44.8
D3	0.063	4.259840	46.6	35.4
E1	0.090	2.883586	-	-
E2	0.042	1.611134	53.3	44.1
E3	0.032	0.740573	64.4	74.3
F1	0.105	4.890834	-	-
F2	0.038	4.159936	63.8	14.9
F3	0.056	3.383495	46.7	30.8

The data presented in Table 4-2, in terms of the percentage of scour reduction when compared to the benchmark case, is plotted in Fig. 4-15 as a function of Fr. Series A was not included in the plot as the alternate sediment size does not enable a useful comparison as a function of Fr. What can be seen in Fig. 4-15(a and b) is that CPN3 achieved more scour reduction than FPC, when undermining did not occur. Furthermore, the reduction in d_s and V_s follow a similar trend for both collars such that the quantity of scour reduction decreased as Fr increased. However, the difference in scour reduction between the collars is greater in terms of V_s than d_s.

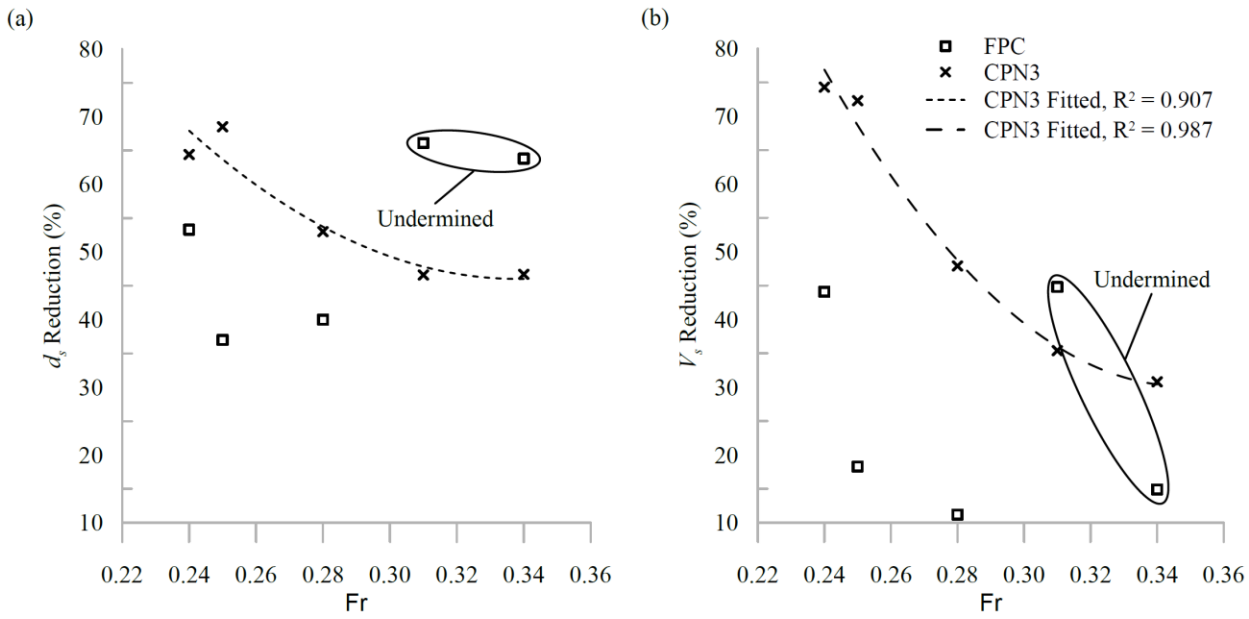

Fig. 4-15. Scour reduction as a function of Fr with respect to: (a) d_s, and (b) V_s.

When undermining did occur for the FPC, d_s greatly reduced, to levels equal to that of CPN3 at lower Fr values. However, this behaviour was not observed for the reduction of V_s. When Fr = 0.31, the FPC yielded 9.4% more V_s reduction than CPN3, but when Fr = 0.34, the FPC yielded 15.9% less V_s reduction than CPN3. Despite the FPC achieving greater d_s reduction while experiencing undermining, V_s reduction for these two Fr values had a lower average than that of CPN3. Furthermore, the test performed at Fr = 0.31 was the only test which the FPC produced more V_s reduction than CPN3. Thus, for almost all cases, CPN3 resulted in greater V_s reduction compared to the FPC.

In Fig. 4-15(a and b), the scour reduction for CPN3 decreases asymptotically as Fr increases. Specifically, when Fr = 0.34, d_s reduction for CPN3 yields a minimum of 46.7%, and V_s reduction for CPN3 yields a minimum of 30.8%. The trendlines for CPN3 regarding d_s and V_s reduction are presented as Eqs. 5 and 6, respectively.

$$d_s \text{ reduction} = 2268\text{Fr}^2 - 1534\text{Fr} + 305, \quad \text{if } \text{Fr} \leq 0.34 \tag{5}$$

$$V_s \text{ reduction} = 3981\text{Fr}^2 - 2774\text{Fr} + 513, \tag{6}$$

Based on Eqs. 5 and 6, V_s reduction displays a larger variation for the given range of Fr values than d_s reduction. Therefore, V_s grows at a higher rate than d_s. Trendlines were not created for the FPC due to the high degree of variability in scour reduction induced by collar undermining.

4.2.6 Discussion

The experimental results achieved in this study for scour around a circular pier, with and without an FPC, are consistent with those reported by other authors. For the pier without any

countermeasure, the resulting d_s achieved in test D1 was 0.118 m, given Fr = 0.31. This result matches closely, through some interpolation, the scour prediction equations of Jain and Fischer ($d_s \approx 0.125$ m for Fr = 0.3), and Laursen ($d_s \approx 0.127$ m for Fr = 0.3), as presented in the Hydraulic Engineering Circular (HEC) No. 18 technical report (Arneson et al., 2012). Furthermore, the HEC-18 scour equation overpredicts d_s by approximately 21% ($d_s \approx 0.143$ m for Fr = 0.3), which is expected as it is a conservative engineering design equation (Arneson et al., 2012). In terms of the FPC, Kumar et al. (1999) found that for FPC's that have a diameter of 2.5*D*, there was significantly less scour in front of the pier than on the sides and rear. As the collar diameter increased towards 4.0*D*, they found no scour occurred at all on the front and sides of the pier, only the rear (Kumar et al., 1999). The FPC tested within this study had a diameter of 3.3*D*, approximately halfway between 2.5*D* and 4.0*D*, and no scour occurred in front of the pier, while some occurred along the sides, and a large amount occurred at the rear. When interpolating between the 2.5*D* and the 4.0*D* results of Kumar et al. (1999), the behaviour seen with the 3.3*D* collar in this study matches well.

CPN3 was introduced as an improved collar design with the intention of reducing overall scouring and collar undermining. Under all conditions tested, CPN3 proved to reduce d_s and V_s by a minimum of 46.6% and 30.8%, respectively. The collar effectiveness improved as u_{avg} decreased or y increased. The C series tests exhibited flow conditions that are identical with those used with CPN1 and CPN2 in previous studies. When comparing the d_s results of the three collars, CPN3 yielded an increased reduction of 2% over CPN1 and 17% over CPN2. In addition, CPN3 did not experience undermining whereas both CPN1 and CPN2 did. Therefore, CPN3 reduced scour more and eliminated collar undermining, when compared to its predecessor designs. Furthermore, a distinct advantage of CPN3, as compared to CPN1 and CPN2, is its symmetrical shape that can accommodate multidirectional flows.

When comparing CPN3 to the FPC, CPN3 yielded greater reduction in terms d_s and V_s, except when the FPC experienced undermining. By omitting the V_s measurement collected at Fr = 0.31, CPN3 produced a greater reduction in V_s for all cases, even when the FPC experienced undermining and yielded reduced d_s values. When the FPC experienced undermining, the scour region increasingly displaced material from beneath the collar into the downstream scour hole. By doing so, d_s decreased, but V_s remained high. Reducing d_s is ultimately the objective; however removing sediment from beneath the collar is not recommended as it brings scour closer to the pier. Therefore, for the given test conditions, CPN3 is a better scour countermeasure than the FPC as it is more effective at reducing scour and is not prone to undermining.

The flow condition used for the numerical model is the same as that employed in the C series experimental tests. According to the bed shear stress determined by the numerical model in Fig. 4-12, scour would likely occur downstream from the pier on either side of the collar, and, potentially, directly behind the collar. The scour plot for test C3, presented in Fig. 4-14, indicates scour did occur downstream from the pier on either side of the collar. The scour holes extended from the collar in the downstream direction, while wrapping around the rear of the collar towards

one another. The scour holes wrapped around the rear of the collar because of the influence of the mild increase in shear stress behind the collar. Therefore, the numerical model enabled an accurate evaluation of potential scour locations.

A number of the scour plots presented in Fig. 4-14, for the FPC and CPN3, specifically, show non-symmetrical scour depths or patterns downstream of the collar. A possible reason for this is because of the flume itself. The side walls of the flume are not perfectly vertical and parallel to each other, which is believed to have caused slight nonuniformities in the flow. Flow nonuniformity is not noticeable with just the pier because there is only one scour hole. However, when a collar is installed and there are two scour holes which can be directly compared to one another, the flow nonuniformity becomes noticeable. To compensate for the difference in scour depth between the two holes, d_s was calculated as the average depth of both.

Other authors, such as Zarrati et al. (2006), studied the effect of FPC's on pier scour; however they indicated equilibrium did not occur until much later in time. Specifically, they found equilibrium to occur after 70 hours whereas in this paper it was found to occur after only 6 hours. Two differences between the studies exist which may explain this discrepancy. The first is that in the paper of Zarrati et al. (2006), they measured scour depth on the upstream face of the pier, whereas for this study, scour depth was measured at its deepest location, which for the collar tests happened to occur downstream of the pier. It is agreed that when collars are present, scour begins downstream and potentially progresses upstream, if the conditions promote such behaviour. This implies that the scour hole downstream of the pier may have reached equilibrium much sooner than that in front of the pier. The second reason is that the diameter of the collars tested in the studies were not the same, as it was 3.3*D* in this study versus 3.0*D* in the study of Zarrati et al. (2006). Larger diameter collars have proven to reduce or eliminate the scour that occurs upstream according to Kumar et al. (1999), implying that for this study greater scour depths are likely not expected upstream of the pier.

In addition to the differences in the studies mentioned above, the longest test, which was the trial to determine the length of time to run the experiments, was carried out for 12 hours. Prior to reaching the 12 hour mark, equilibrium had been achieved. If substantial scour were to occur beyond 12 hours of experimental testing, using the Froude scaling method with a geometric length scaling ratio of 1:30, this would equate to more than 66 hours at prototype scale. Scour at bridge piers occurs primarily during peak flow events, which according to Lu et al. (2008) often subsides in less than 66 hours. Therefore, the authors believe 6 hours is an adequate experimental time duration to produce meaningful comparisons of the performance of various scour countermeasures.

Installing CPN3 can be accomplished at either the time of pier construction or at a later date in terms of a retrofit. The method of installation will depend when CPN3 is installed with respect to the pier construction. Installing any countermeasure device on an existing bridge can be challenging. To assist with installation, one approach is to first construct CPN3 off-site, in

sections, at an equipped facility. Then, the sections, which are to be built in smaller sizes, can be transported to the pier location and assembled around the base of the pier more easily. By constructing CPN3 in such a manner, some of the challenges typically faced when installing similar countermeasures can be overcome.

The data presented in this study is bounded by several limitations. The first one is that, despite different flow conditions being tested, all tests were conducted in the clear-water regime. To fully test the capabilities of CPN3 and to increase the applicable range of Eqs. 5 and 6, live-bed testing is warranted. Specifically, live-bed conditions possessing bedforms and changing bed elevations need to be tested because collars that are fixed to the pier can be susceptible to undermining or misalignment with the bed, under such conditions. The second limitation is that only one flow condition was tested for the d_{50} = 0.0007m sediment. Having more flow conditions would provide a better comparison to that of the d_{50} = 0.001m sediment. The third limitation is that CPN3 was designed and tested for only circular piers. The collar design has the potential to accommodate different shaped piers, but this was not evaluated in the present study. The last limitation is that the numerical model possessed a flat rigid bed (which could be viewed as an equilibrium clear-water bed condition) and did not have sediment transport capabilities. As a result, the available data that can be obtained from such model, in comparison to a model that is equipped with sediment transport capabilities, is reduced.

4.2.7 Conclusions

This study introduced an improved collar for bridge pier scour reduction referred to as CPN3. CPN3 evolved from previous collar designs as the horseshoe vortex is guided inside of a 3-D cavity below the bed surface, in a way that reduces interference with the passing flow, as opposed to on top of the bed surface. CPN3 was demonstrated, through numerical and experimental testing, to be an effective countermeasure to reduce the maximum scour which occurred downstream of the pier. At a minimum, CPN3 reduced the scour depth and volume by 46.6% and 30.8%, respectively. As Fr reduced (increase in depth or decrease in velocity), CPN3's scour reduction grew, and with a smaller bed sediment size, a maximum reduction of 69.7% and 75.7% was achieved in terms of scour depth and volume, respectively. When compared to other collars, CPN3 reduced the scour depth by 2% over CPN1, 17% over CPN2, and 13% over the FPC, at a given flow condition.

Under the range of conditions tested, CPN3 was found to reduce the scour depth and volume more than the FPC, except when the FPC became undermined. When the FPC experienced undermining, the scour volume remained high while scour depth reduced, as the material from beneath the collar filled the downstream scour holes. This resulted in the scour migrating closer to the pier despite a reduction in scour depth. Overall, the FPC produced less scour reduction at lower Fr values while experiencing undermining at higher Fr values, therefore making it a less desirable countermeasure. In conclusion, CPN3 proved to be a better, more predictable overall scour countermeasure, which could be a beneficial alternative to those currently used.

Chapter 5. Riprap Collar Prototype No. 3 (RCPN3)

5.1 Novel Riprap Structure for Improved Bridge Pier Scour Protection

Preprint of a modified version of a manuscript under review at the Journal of Hydraulic Engineering © 2021 American Society of Civil Engineers (ASCE).

5.1.1 Introduction and Objectives

The lessons learned from CPN1 and CPN2 were combined and led to the creation of CPN3 (Valela, Rennie, et al., 2021). Specifically, the raised collar cavity employed on CPN1 and CPN2 induced greater flow separation around the pier. Instead, a cavity was still incorporated into the design to guide the horseshoe vortex, but it was positioned below the bed as to not obstruct the flow. In addition, the design (for circular piers) was symmetric about both the X- and Y- axis allowing it to accommodate all approaching flow angles. CPN3 was able to eliminate undermining altogether and reduce the scour depth, when compared to a pier without any countermeasure, by an additional 2% over CPN1 and 13% over the FPC (Valela, Rennie, et al., 2021). Therefore, CPN3 was the most successful out of the series of rigid collars, but the overall quantity of scour reduction was not substantial.

In an attempt to create a better countermeasure that reduces scour further, this paper combines the benefits of both riprap and CPN3 into a new countermeasure design. The countermeasure, referred to as RCPN3, consists of placing riprap stones in a strategic way to resemble the shape of CPN3. The objectives of this study are to:

1) Present an advanced riprap placement design, RCPN3, used to improve bridge pier scour protection.
2) Test RCPN3 under both clear-water and transition-flow conditions.
3) Compare the performance of RCPN3 to that of existing riprap designs, as well as the FPC, and CPN3.

5.1.2 Experimental Setup

5.1.2.1 Clear-Water Regime

The clear-water tests were performed in the Civil Engineering Hydraulics Laboratory at the University of Ottawa, Canada. The flume that was used, shown in Fig. 5-1, measured 30m in length, 1.5m in width, and 0.5m in depth. A sand section was located 1.25m from the flume outlet and measured 3.16m in length. Concrete false floors were installed on the upstream and downstream ends of the sand section to hold the sand in place and to generate uniform flow across the sand section. A gravel ramp, 2.25m in length, preceded the upstream false floor, which measured 4.16m in length, to smoothly transition the flow onto the false floor and sand section. The sand section contained sand possessing a median grain size diameter (d_{50}) of 0.001m, and

the same sand was adhered to the surface of the false floors using paint to achieve the same roughness as the sand section. A cylindrical tube, possessing a diameter (*D*) of 0.09m and made of acrylic, was positioned in the center of the sand section and bolted to the floor of the flume to replicate an idealised bridge pier. *D* was chosen so that the blockage ratio (width of the pier with respect to the width of the flume) would not greatly influence the passing flow. For further details pertaining to the clear-water flume, refer to Valela, Nistor, et al. (2021).

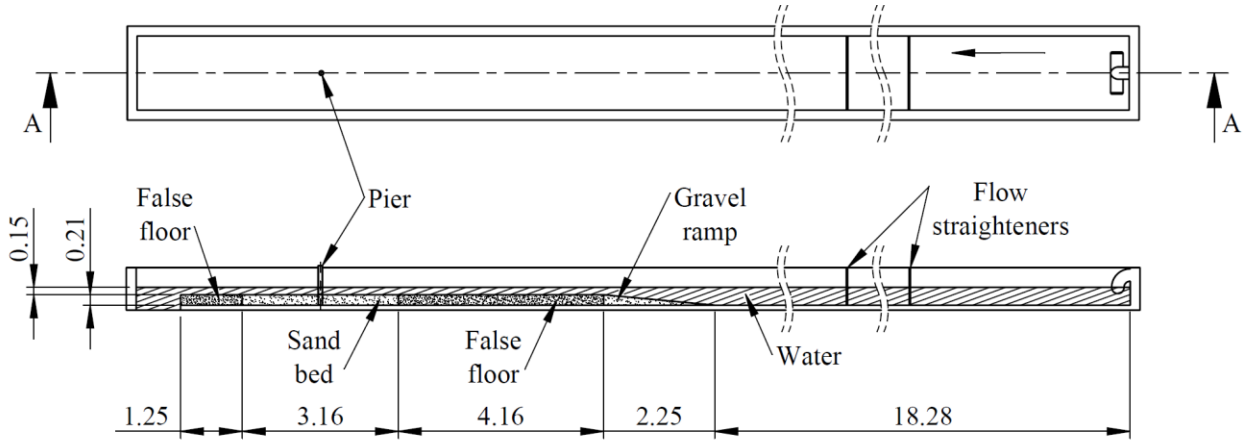

Fig. 5-1. Plan and cross-section view of the clear-water experimental flume at the University of Ottawa, Canada (all dimensions are in m).

The flow depth (*y*) was set to 0.15m using a downstream gate. The depth-averaged flow velocity (u_{avg}) for the clear-water flow was set to 0.34m/s using the inlet valve, which resulted in $\frac{u_{avg}}{u_{cr}}$ equalling 0.8, where u_{cr} is the depth-averaged critical velocity required for bed motion. All tests in the clear-water regime possessed the same flow conditions yielding a Froude number (Fr) of 0.28 and a Reynolds number (Re) of 3×10^4. Each test was run for a duration of six hours, as extended trial tests were performed and 95% of the equilibrium clear-water scour depth was achieved by the six-hour mark (Valela, Nistor, et al., 2021).

The velocity was recorded using a Vectrino Acoustic Doppler Velocimeter (ADV) equipped with a down-looking head. Data were collected at each location for two minutes, and then were subject to a de-spiking filter and time-averaging (Jamieson et al., 2010). Vertical velocity profiles and a horizontal velocity field for the given flow conditions can be found in Valela et al. (2018) and Valela, Nistor, et al. (2021), respectively.

After each test was complete, the resulting bathymetry was recorded using a Leica ScanStation P50 Terrestrial Laser Scanner (TLS). The accuracy of the TLS is +/-0.0015m in all directions. In order to capture the entire scour region, various scans were performed from different locations around the sand bed. Then, the scans were combined to create a three-dimensional model of the scour region. To avoid inaccuracies in the TLS data caused by materials possessing translucent properties, a light dusting of sodium bicarbonate was sieved onto the sand, and the pier was covered, prior to scanning.

5.1.2.2 Transition-Flow Regime

The transition-flow experiments were performed in the Fluid Mechanics Laboratory at the University of Auckland, New Zealand. The flume, shown in Fig. 5-2, measured 43m in length, 1.5m in width, and 1.1m in depth. The walls were made of glass, and the entire bed consisted of sand measuring a depth of 0.6m, possessing a d_{50} of 0.00085m. The sand used in the transition-flow experiments was 0.00015m (15%) smaller in diameter than that used in the clear-water experiments, but when applying the Shields diagram and a Froude scale of 1:30, both scale up to resemble a gravel bed river (Valela, Nistor, et al., 2021). The flume was equipped with a sediment recirculation pump which allowed for conditions above the threshold of bed motion to be achieved. The same model bridge pier used in the clear-water tests (cylindrical acrylic tube with D = 0.09m) was also used in the transition-flow tests and was bolted to the floor of the flume.

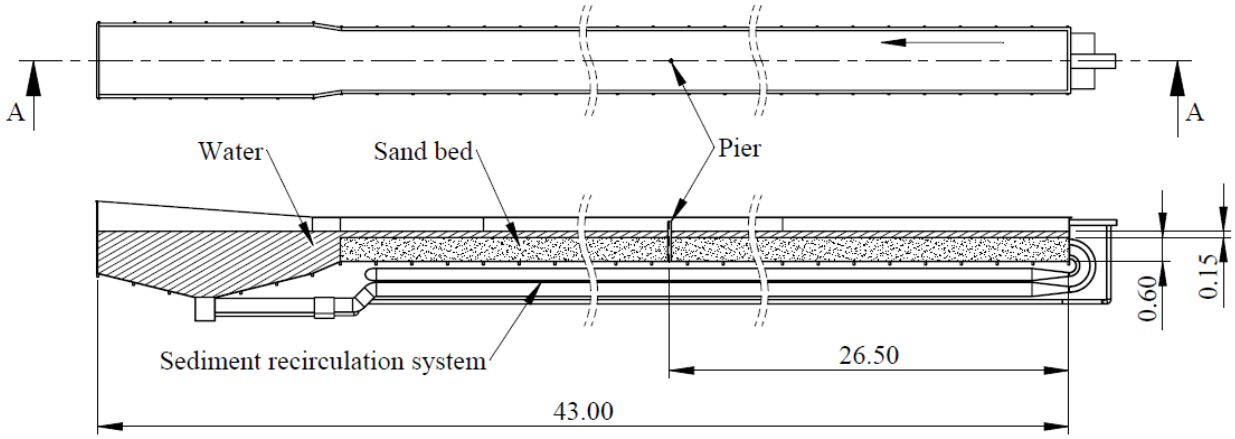

Fig. 5-2. Plan and cross-section view of the transition-flow experimental flume at the University of Auckland, New Zealand.

The flume was set to a horizontal position (no tilt angle) and y was set to 0.15m, both to match that of the clear-water tests. Since the transition-flow flume is a closed system, the flow depth was achieved by simply filling the flume to the desired level rather than using gates. u_{avg} was set to 0.45m/s, using a combination of the variable speed sediment and water pump, which resulted in $\frac{u_{avg}}{u_{cr}}$ equalling 1.15. Therefore, the flow conditions were slightly above the threshold of bed motion. All of the transition-flow tests possessed the same flow conditions such that Fr = 0.37 and $\mathrm{Re} = 4 \times 10^4$. Each test was run for a duration of six hours which, at the specified flow rate, was enough time to allow the flow regime to transition from clear-water to live-bed, and the bedforms to equilibrate. A total of two dunes passed the test section upon reaching live-bed conditions, but the tests were not run long enough in the live-bed regime to obtain meaningful live-bed results.

When $\frac{u_{avg}}{u_{cr}}$ is greater than unity, measurements of the final bathymetry are less valuable than the changing bathymetry during the test, therefore the TLS was not employed for the transition-flow tests. Instead, a SeaTek Ultrasonic Ranging System (URS) was utilized to capture

the bed changes throughout the duration of each test. The URS was comprised of 31 depth transducers possessing a vertical accuracy of +/- 0.0004m. The depth transducers were installed on a rigid mount which was attached to a trolley, as shown in Fig. 5-3. The purpose of this mounting system was to secure the depth transducers during a test, but still allow them to be moved between tests.

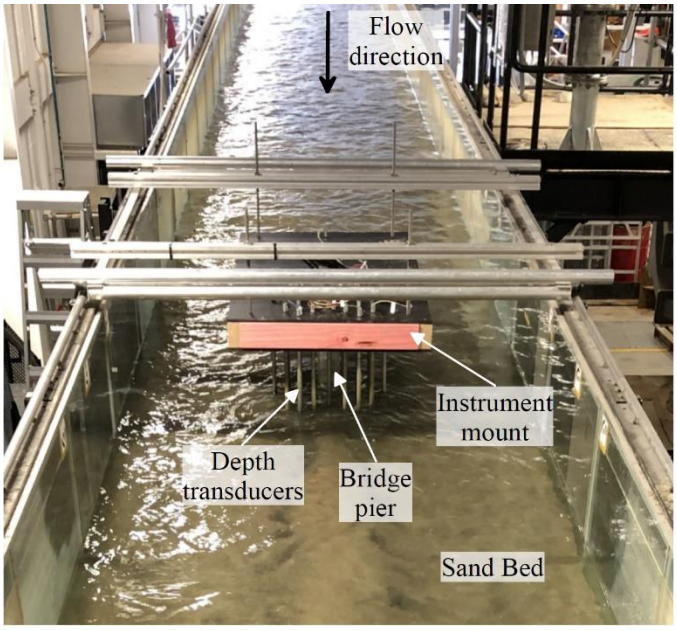

Fig. 5-3. Depth transducers installed above the transition-flow experimental flume.

The elevation of the depth transducers was critical such that they needed to remain submerged in the flow despite any water surface irregularities, while interrupting the passing flow as little as possible. Therefore, they protruded into the passing flow between approximately 0.005-0.01m, depending on their location. The spatial positioning of the depth transducers was chosen based on the results achieved from the clear-water tests of (Valela, Rennie, et al., 2021), so that the spatial variation of the scour around the pier would be captured. The depth transducer positioning with respect to the pier and countermeasures is shown in Fig. 5-4.

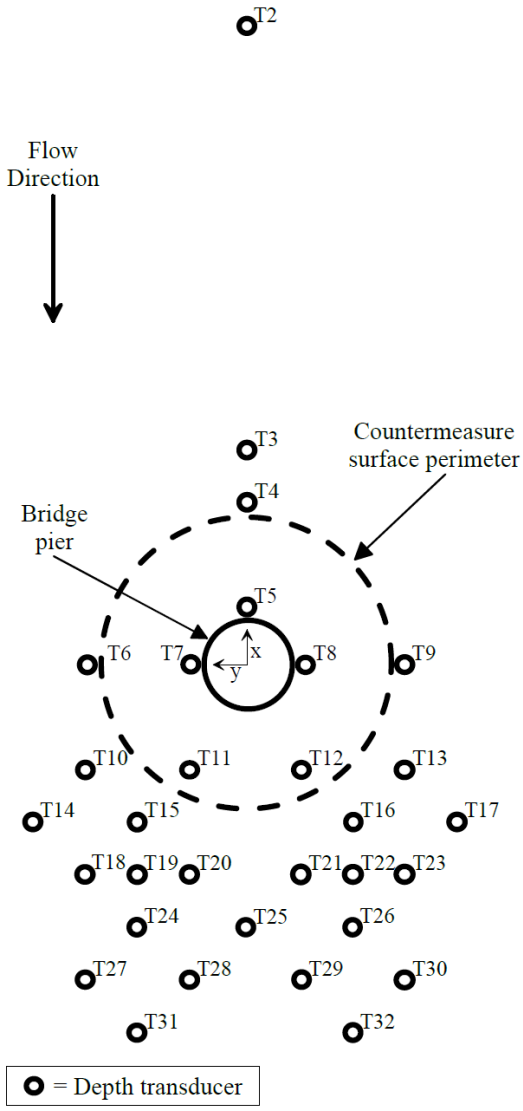

Fig. 5-4. Depth transducer layout with reference to the pier and countermeasure.

The depth transducers were positioned symmetrically about the X-axis with a focus around the pier, countermeasures, and downstream wake. The 31 depth transducers were labelled between T2-T32, with T1 omitted from the study. The exact location of the 31 depth transducers is listed in Table 5-1.

Table 5-1. Depth transducer locations.

Depth Transducer	X - Position (m)	Y - Position (m)	Depth Transducer	X - Position (m)	Y - Position (m)
T2	0.75	0.00	T18	-0.20	0.16
T3	0.21	0.00	T19	-0.20	0.11
T4	0.16	0.00	T20	-0.20	0.06
T5	0.06	0.00	T21	-0.20	-0.06
T6	0.00	0.16	T22	-0.20	-0.11
T7	0.00	0.06	T23	-0.20	-0.16
T8	0.00	-0.06	T24	-0.25	0.11
T9	0.00	-0.16	T25	-0.25	0.00
T10	-0.10	0.16	T26	-0.25	-0.11
T11	-0.10	0.06	T27	-0.30	0.16
T12	-0.10	-0.06	T28	-0.30	0.06
T13	-0.10	-0.16	T29	-0.30	-0.06
T14	-0.15	0.21	T30	-0.30	-0.16
T15	-0.15	0.11	T31	-0.35	0.11
T16	-0.15	-0.11	T32	-0.35	-0.11
T17	-0.15	-0.21			

The sampling rate of the URS was set to 0.2Hz. Prior to beginning each test, measurements of the initial flattened bed were recorded. After the measurements throughout the duration of each test were collected, the initial bed height was subtracted from each measurement, and the data were filtered. The resulting data were used to identify scour as a function of time at each location, and at specific points in time, data from each depth transducer were used to generate scour plots.

5.1.2.3 Protocol

This study focuses on comparing different riprap countermeasures to a pier without any scour countermeasure. The countermeasures included in this paper are: 1) none, 2) Flat Riprap (FR), 3) Mounded Riprap (MR), and 4) the new design (RCPN3). Each countermeasure had the same outer diameter, embedment depth, and riprap d_{50}. The riprap used was angular in shape and possessed a d_{50} of 0.0095m and 0.014m for the clear-water and transition-flow tests, respectively. A total of six experiments were completed, four in the clear-water regime and two in the transition-flow regime. Prior to each test, regardless of the flow condition, the bed was completely leveled. Then, the flow was slowly initiated until reaching the desired flow rate, as to not induce premature scour. Once the desired flow rate was reached, the time clock began. Within the clear-water and transition-flow tests, the test conditions, as well as the countermeasure dimensions, were kept constant, leaving the shape of the riprap installation to be the only independent variable. The naming convention and the corresponding experimental conditions are summarized in Table 5-2.

Table 5-2. Experimental trials.

Test	Countermeasure	Riprap d_{50} (m x 10^{-3})	Bed d_{50} (m x 10^{-3})	y (m)	u_{avg} (m/s)	u_{avg}/u_{cr}
CW0	None	9.5	1.00	0.15	0.34	0.80
CW1	FR	9.5	1.00	0.15	0.34	0.80
CW2	MR	9.5	1.00	0.15	0.34	0.80
CW3[a]	RCPN3	9.5	1.00	0.15	0.34	0.80
TF1	FR	14.0	0.85	0.15	0.45	1.15
TF3	RCPN3	14.0	0.85	0.15	0.45	1.15

[a]Test was repeated.

5.1.3 Scour Countermeasure Designs

5.1.3.1 Flat Riprap (FR)

Riprap can be installed in different ways and previous researchers found that the most reliable method was to install the riprap in a level cover that is at or below the bed elevation (Froehlich, 2013). For this study, the FR countermeasure was installed flush with the bed and possessed an embedment depth of 0.055m, as shown in Fig. 5-5(a and b). The diameter of the riprap cover exposed to the passing flow was 0.3m and grew to 0.39m at the bottom of the embedment. The reason for the outer slope on the embedded riprap was to match that of CPN3 and to help reduce scour if it were to occur around the perimeter of the riprap cover. All three riprap scour countermeasures presented in this paper possessed the same outer slope.

Installing the FR countermeasure consisted of first excavating a hole centered around the pier, 0.055m deep by 0.39m in diameter. Then, a metal ring, 0.055m in depth by 0.3m in diameter, was centered around the pier with the top of the ring positioned flush with the initial bed elevation. The ring acted as a mould and was filled to the top with riprap. The ring was then slowly removed, and additional stones were added around the perimeter of the riprap cover to create the outer slope. Lastly, bed material was added around the outside of the riprap to fill any voids and to create a smooth transition. The volume of riprap used to construct the FR countermeasure was 0.004955m^3.

5.1.3.2 Mounded Riprap (MR)

Another method of riprap installation is to mound the riprap above the bed and against the pier, instead of installing it level and flush with the bed (Lagasse et al., 2009). MR is frequently chosen due to ease of installation, lower cost, and inspection purposes (Froehlich, 2013; Lagasse et al., 2009). This countermeasure was constructed in the laboratory by first installing the FR countermeasure. Then, additional riprap was added around the pier creating a constant slope between the edge of the riprap cover and a height of 0.05m above the bed at the pier, as shown in Fig. 5-5(c and d). The volume of riprap used to construct the MR countermeasure was 0.006296m^3.

5.1.3.3 Riprap Collar Prototype No. 3 (RCPN3)

Riprap has proven to be an effective means of reducing scour around the base of bridge piers, but the authors believe that its performance could be improved further if the riprap stones were installed in a more strategic way. Rather than installing the stones in a flat or mounded fashion, this paper introduces a new installation method that follows the shape of CPN3. CPN3 was successful at moderately reducing scour but was limited by its rigid shape and smooth surface. By combining the shape of CPN3 with the flexibility, and roughness of riprap, an improved countermeasure, referred to as RCPN3, could result. Constructing RCPN3 was done by first installing the FR countermeasure. Then, stones were removed from around the pier to create a depression, as shown in Fig. 5-5(e and f). To ensure the correct shape was achieved, a cross-sectional template of CPN3 was cut out and used to check the profile. The volume of riprap used to construct the RCPN3 countermeasure was 0.004074m^3.

(a)

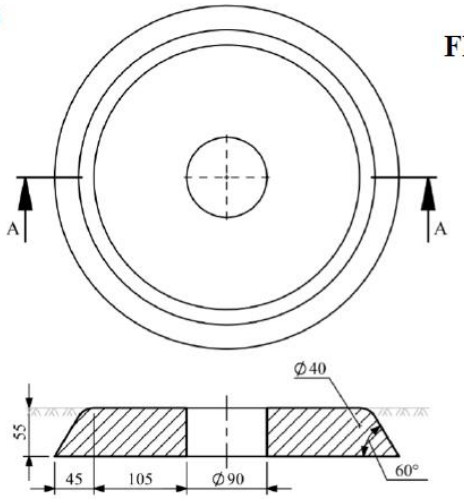
FR
A
A
Ø40
55
45
105
Ø90
60°

(b)

(c)

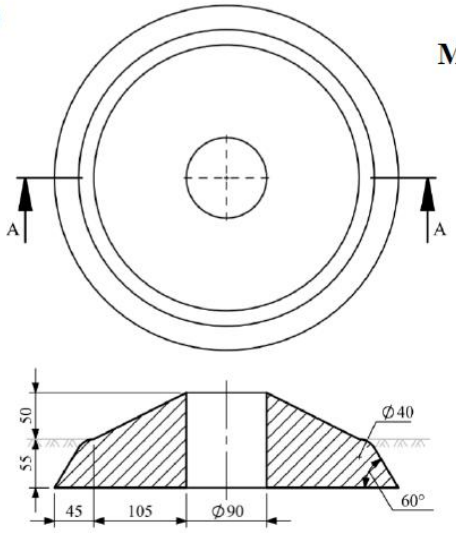
MR
A
A
50
55
Ø40
60°
45
105
Ø90

(d)

(e)

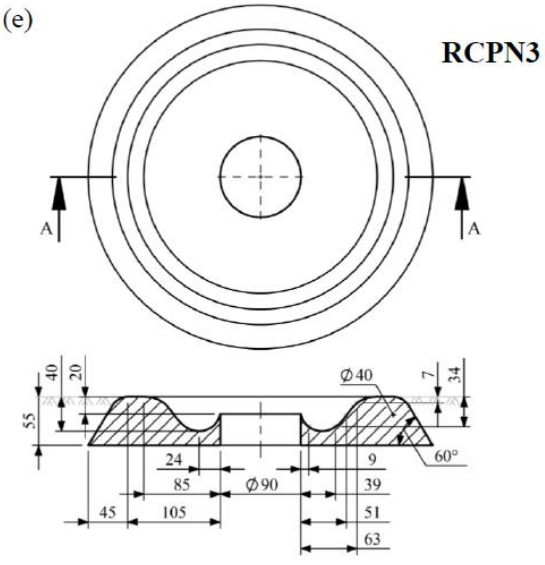
RCPN3
A
A
40
20
55
Ø40
7
34
60°
24
85
Ø90
9
39
45
105
51
63

(f)

Fig. 5-5. Annotated drawings and photographs of the scour countermeasures tested (dimensions are in mm) Note: Fig. 5-5(e) reprinted from (Valela, Rennie, et al., 2021).

5.1.4 Results

5.1.4.1 Clear-Water Regime

For the clear-water tests, no countermeasure, FR, MR, and RCPN3 were tested. Upon the completion of each test, three-dimensional scans of the bed were performed which allowed for the generation of scour contour plots. Fig. 5-6 displays the resulting bed elevations from the four tests. Test CW0, which contained no countermeasure and is displayed in Fig. 5-6(a), experienced a large quantity of scour immediately upstream and along the sides of the pier. This is the most vulnerable area for scour to occur as it is directly above the pier's foundation. Due to the large quantity of scour around the pier, a deposition pile was generated downstream of the pier, followed by two smaller scour holes immediately downstream of the deposition pile.

For the tests containing a countermeasure, the dotted line depicts the perimeter of the riprap on the surface of the bed. Test CW1, which consisted of the FR countermeasure and is displayed in Fig. 5-6(b), experienced a drastic reduction in scour. For the most part, scour did not occur where the riprap was present, except for a minor reduction in elevation at the side of the pier along the outer downstream perimeter of the riprap. However, two symmetrical scour holes formed downstream of the pier, immediately following the riprap. These scour holes were likely formed from the accelerated separated flow, that was present on either side of the pier, travelling off of the riprap and onto the unarmoured bed material, generating sufficient bed stresses to erode the sediment at these locations. A deposition pile formed downstream of the scour holes and was smaller in size than that of test CW0.

Test CW2, which possessed the MR countermeasure and is displayed in Fig. 5-6(c), experienced a large quantity of scour that extended the entire length of the sand bed, unlike any of the other tests. No scour occurred on the riprap, but along the sides and rear of the riprap, two extensive scour holes occurred. The mounding of the riprap adjacent to the pier is believed to have induced greater flow separation and acceleration along the sides of the pier which caused the increased scour downstream. In comparison to test CW1, the scour holes experienced in CW2 were much deeper and extended further upstream around the perimeter of the riprap. A large deposition pile was created downstream of the primary scour holes in test CW2, which created three additional smaller scour holes behind, followed by two more deposition piles.

Lastly, test CW3 which contained the RCPN3 countermeasure and is presented in Fig. 5-6(d), experienced a very small amount of scour. Where the riprap countermeasure was present, no scour occurred on the riprap except for a minor reduction in riprap elevation along the countermeasure's downstream perimeter. Unlike the other countermeasures, immediately downstream of the riprap only one scour hole formed which was directly in line with the pier, rather than two offset scour holes. The scour hole that formed was small in size, and as a result, only generated a small deposition pile. The shape of the RCPN3 countermeasure partially

accounts for the reduced scour, as the presence of the cavity in the countermeasure helps to guide the horseshoe vortex and passing flow around the pier and direct it away from the bed, therefore reducing bed shear stress and consequently scour (Valela, Rennie, et al., 2021). However, the reason for the remainder of the scour reduction is explained in the Discussion section.

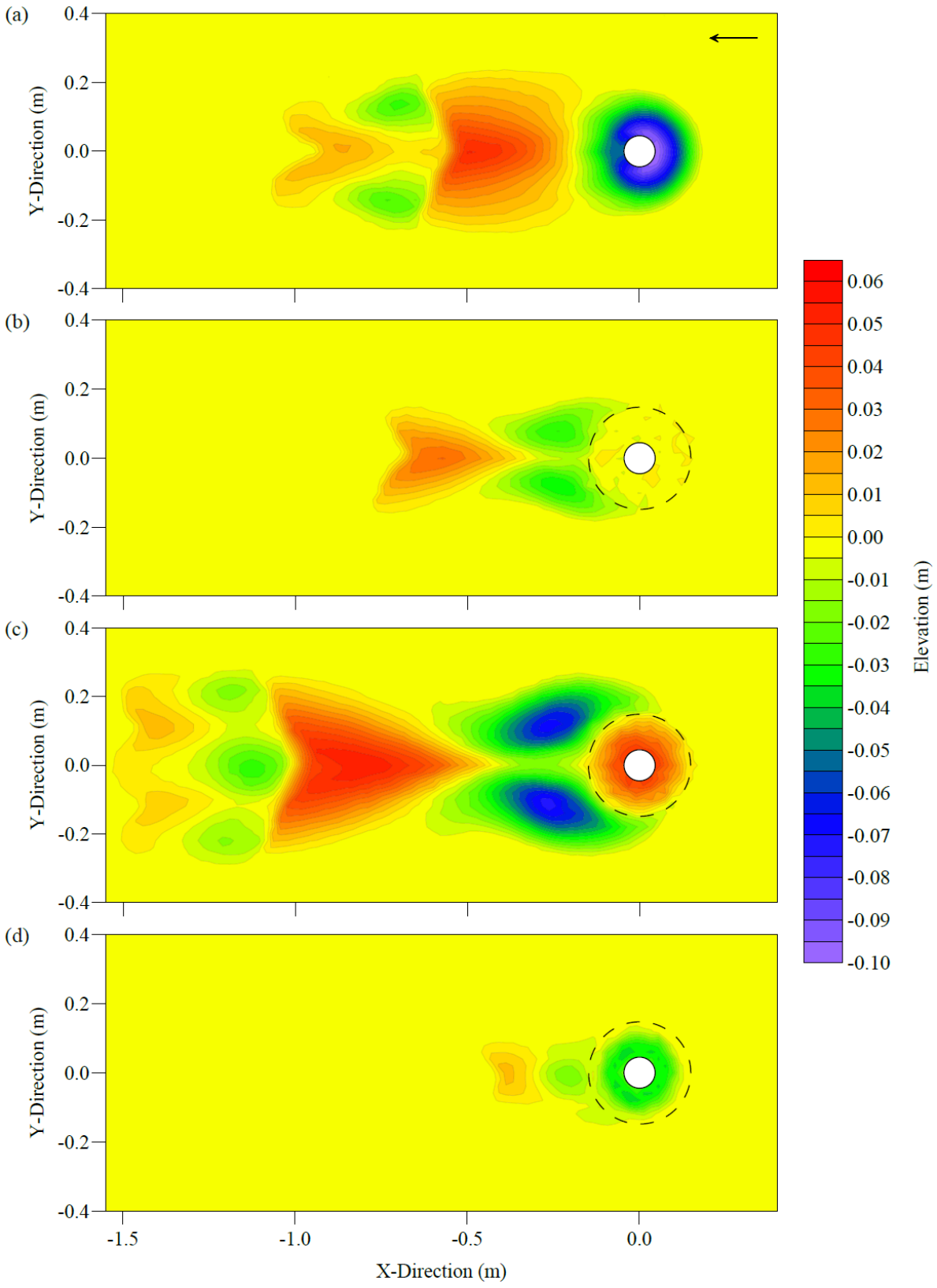
(a)
(b)
(c)
(d)
Y-Direction (m)
0.4
0.2
0.0
-0.2
-0.4
-1.5
-1.0
-0.5
0.0
X-Direction (m)
0.06
0.05
0.04
0.03
0.02
0.01
0.00
-0.01
-0.02
-0.03
-0.04
-0.05
-0.06
-0.07
-0.08
-0.09
-0.10
Elevation (m)

Fig. 5-6. Clear-water scour plot comparison: (a) CW0, (b) CW1, (c), CW2, and (d) CW3 (dotted line indicates the plan perimeter of the riprap at the bed surface) Note: Fig. 5-6(a) reprinted with permission from ASCE (Valela, Nistor, et al., 2021).

Table 5-3 presents the scour that occurred in the four clear-water tests in terms of maximum depth (d_s), and volume (V_s). When two quasi-symmetrical scour holes were present, d_s was calculated as the average of the two scour holes. The scour reduction percentages are in respect to test CW0, which experienced a d_s of 0.1m (Valela, Nistor, et al., 2021). The largest d_s of the four tests occurred for test CW0, and the smallest occurred for test CW3, resulting in an 81% d_s reduction for test CW3. Test CW3 was repeated for reliability purposes and the same d_s of 0.019m was achieved. Meanwhile, test CW1 and CW2 achieved a 67% and 30% d_s reduction, respectively. In terms of scour volume (V_s), the largest occurred for test CW2 yielding a 64.6% scour increase over test CW0. The smallest V_s occurred for test CW3 yielding a 92.3% V_s reduction, while test CW1 yielded a 60% V_s reduction.

Table 5-3. Summary of clear-water scour results. Note: test CW0 data reprinted with permission from ASCE (Valela, Nistor, et al., 2021).

Test	d_s (m)	V_s (m^3 x 10^{-3})	d_s reduction (%)	V_s reduction (%)
CW0	0.100	3.933098	-	-
CW1	0.033	1.572044	67.0	60.0
CW2	0.070	6.474634	30.0	-64.6
CW3	0.019	0.303906	81.0	92.3

In addition to performing three-dimensional scans, photographs were taken of the riprap countermeasure and the surrounding bed after each test, as shown in Fig. 5-7. The purpose of the photographs was to compare the quantity of riprap movement and overall countermeasure deterioration after a set duration of clear-water testing. The red highlighted regions indicate individual or groups of stones that appeared to have moved during the test. For test CW1, displayed in Fig. 5-7(a), two stones were dislodged and transported downstream a relatively long distance to beside the deposition pile. Furthermore, several stones along the downstream edge of the riprap cover slid down into the scour hole. Besides these areas of riprap movement, the FR countermeasure resisted the flow well.

Test CW2, displayed in Fig. 5-7(b), experienced the greatest quantity of riprap stone displacement. The furthest stone was located downstream towards the end of the sand bed, after the deposition pile. For the downstream half of the riprap cover, all of the perimeter stones experienced movement with a large number of them migrating into the scour hole.

Lastly, test CW3, displayed in Fig. 5-7(c), experienced the least amount of stone displacement. No stones were ejected from the riprap cover, the only movement that occurred was minor with a small number of stones travelling outwards along the downstream edge.

Therefore, in terms of original shape retention, the RCPN3 countermeasure performed the best, followed by the FR countermeasure, and lastly the MR countermeasure.

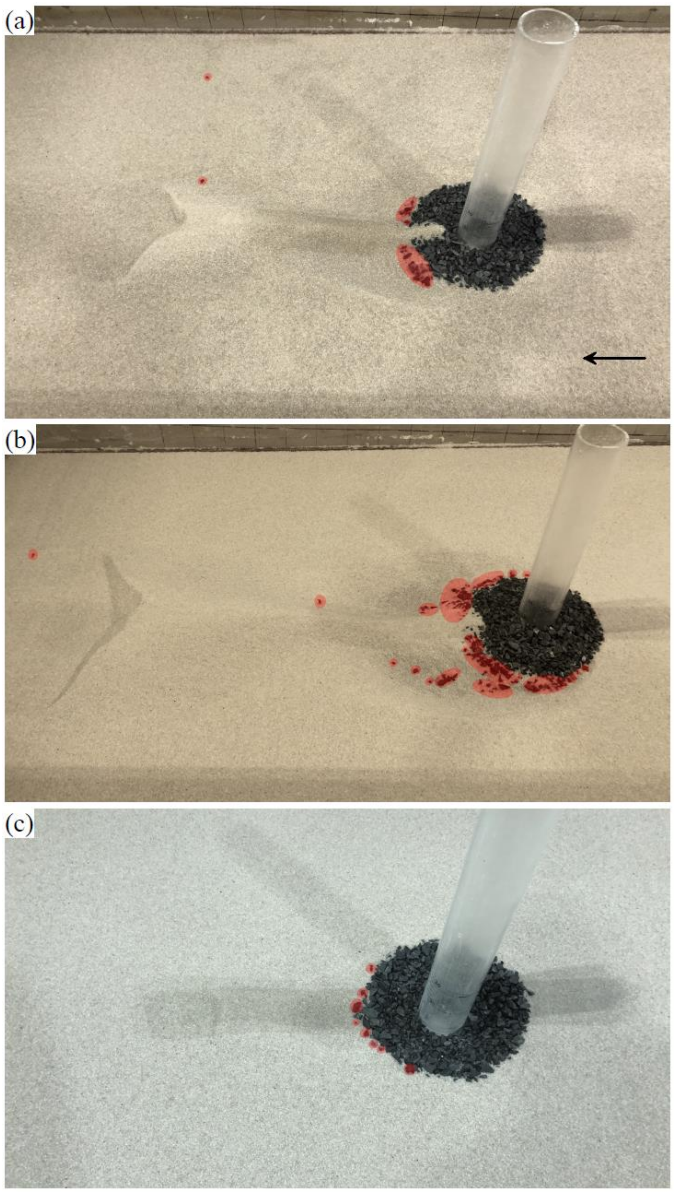

Fig. 5-7. Stone displacement comparison after completion of each clear-water test: (a) CW1, (b) CW2, and (c) CW3. Note: for test CW1 and CW2, sand observed immediately downstream of pier was deposited on top of riprap.

5.1.4.2 Transition-Flow Regime

Two tests were performed in the transition-flow study, one with the FR countermeasure (TW1), and one with the RCPN3 countermeasure (TW3). An additional test was performed without any countermeasure, but there was an error in the data collection, so it is not presented in this paper. For the given flow conditions, it took approximately four hours for the dune field to equilibrate, leaving approximately two hours of fully developed dune passage. Prior to the dune field fully developing, a series of smaller dunes passed the focus region which can be seen by the

upstream depth transducer data in Fig. 5-8(a and b). However, the volume of sediment carried by these smaller dunes was much lower than that of the fully developed dunes which resulted in reduced periodic scour hole replenishment, as seen by the downstream depth transducers in Fig. 5-8(c and d). While the flow velocity was increased above the critical entrainment threshold throughout the run, prior to reaching the fully developed state the incoming sediment supply at the pier was limited, hence achieving a transition-flow condition.

Despite collecting bed elevation measurements at 31 locations, only the data from three locations (T2, T27, and T30) are included in the time series comparison shown in Fig. 5-8. This is because for both countermeasures tested, d_s occurred downstream of the riprap cover, below depth transducer T27. To compare the symmetry in the scour results, data from both T27 and T30 are presented. In addition to temporal bed elevation measurements pertaining to the location of d_s, measurements upstream of the pier are also useful in understanding the dune field, thus the data from the most upstream transducer (T2) are included.

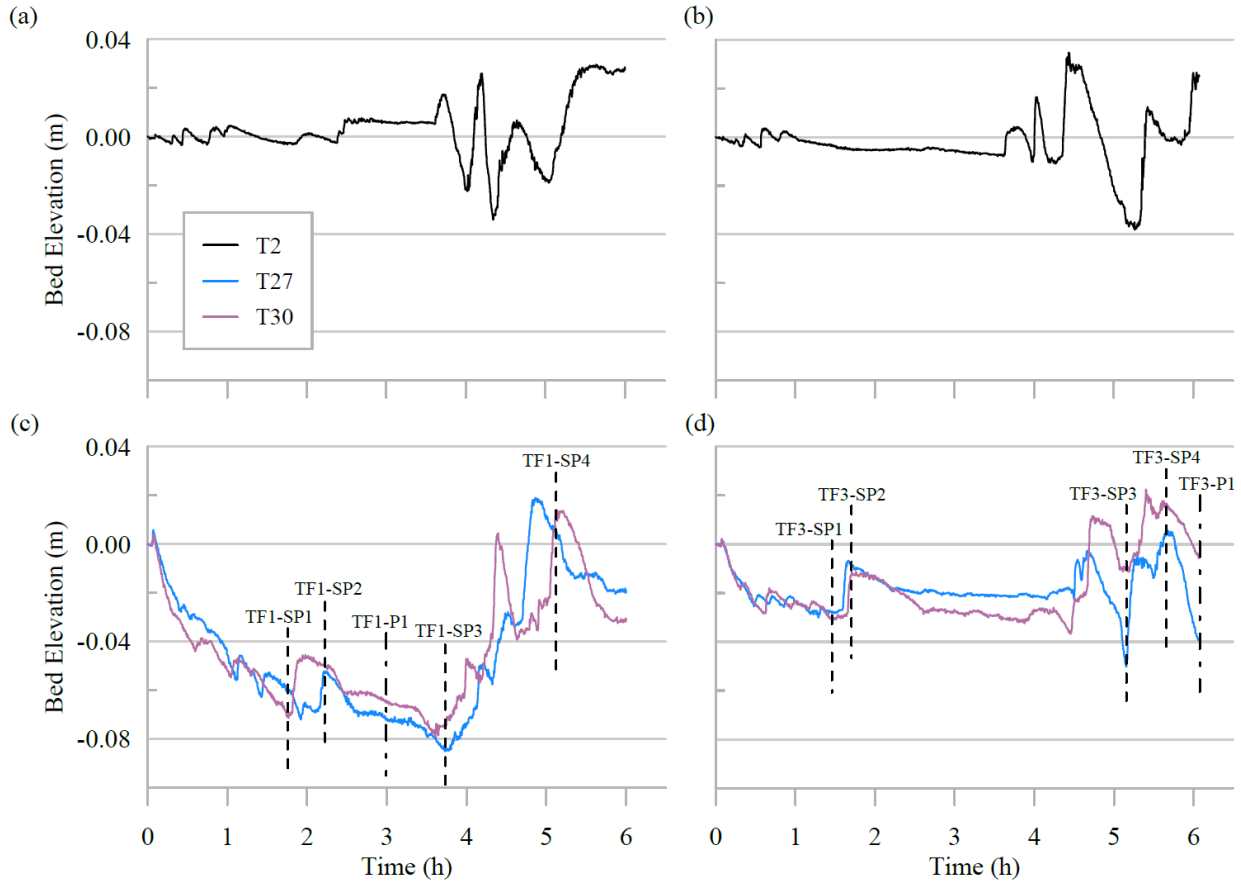

Fig. 5-8. Bed elevation at three different depth transducer locations as a function of time: (a and c) TF1, and (b and d) TF3. The vertical dotted lines correspond to the points in time when Scour Plots (SP) and Photographs (P) were generated.

The temporal bed elevation results for test TF1, displayed in Fig. 5-8(c), showed a decrease in bed elevation until the 3.73h mark, at which time the bed reached a minimum depth

(d_s = 0.082m). Prior to this point, the bed elevation had small to medium size oscillations caused by passing bedforms, but the general trend was decreasing. After 3.73h, the bed elevation increased and underwent large oscillations, reaching above the initial bed height, which was caused by the onset of the fully developed dunes.

For test TF3, displayed in Fig. 5-8(d), the temporal data results showed a decrease in bed elevation only until the 1.8h mark. After 1.8h, the bed elevation remained relatively constant until 4.6h; except for a brief increase in bed elevation caused by the passing of a medium size bedform, which was similar in size to that experienced in test TF1 at the 1.8h mark. Upon reaching the 4.6h mark, large oscillations in the bed elevation began to occur due to the passing of the fully developed dunes. The minimum bed elevation occurred in the trough of a passing dune, such that d_s = 0.044m at the 5.15h mark.

In Fig. 5-8(c and d), a series of vertical dotted lines intersect the plot at specific instants in time. These instants correspond to points of interest, based on the location of the passing bedforms and the quantity of scour, when either a Scour Plot (SP) or Photograph (P) was generated. To create scour plots throughout an ongoing test without stopping the flow of water, data from the depth transducers at the specified instants in time were used rather than the TLS. The limitations of using the depth transducers instead of the TLS is that the spatial resolution is much lower, and the data are limited to the locations of the depth transducers.

Fig. 5-9 displays the scour plots generated during test TF1 and TF3. The scour shown is the difference in bed elevation experienced from the initial condition before the test begin to the specified instant in time. For both tests, SP1 and SP3 correspond to notable troughs or low points in the bed elevation and SP2 and SP4 correspond to notable crests or high points in the bed elevation. For test TF1, the scour experienced in SP1, SP2, and SP3 was deep and the scour pattern was similar to that of CW1, where two symmetrical scour holes were generated immediately downstream of the riprap cover. In SP2, the scour depth reduced due to the passing bedform, but was still relatively large.

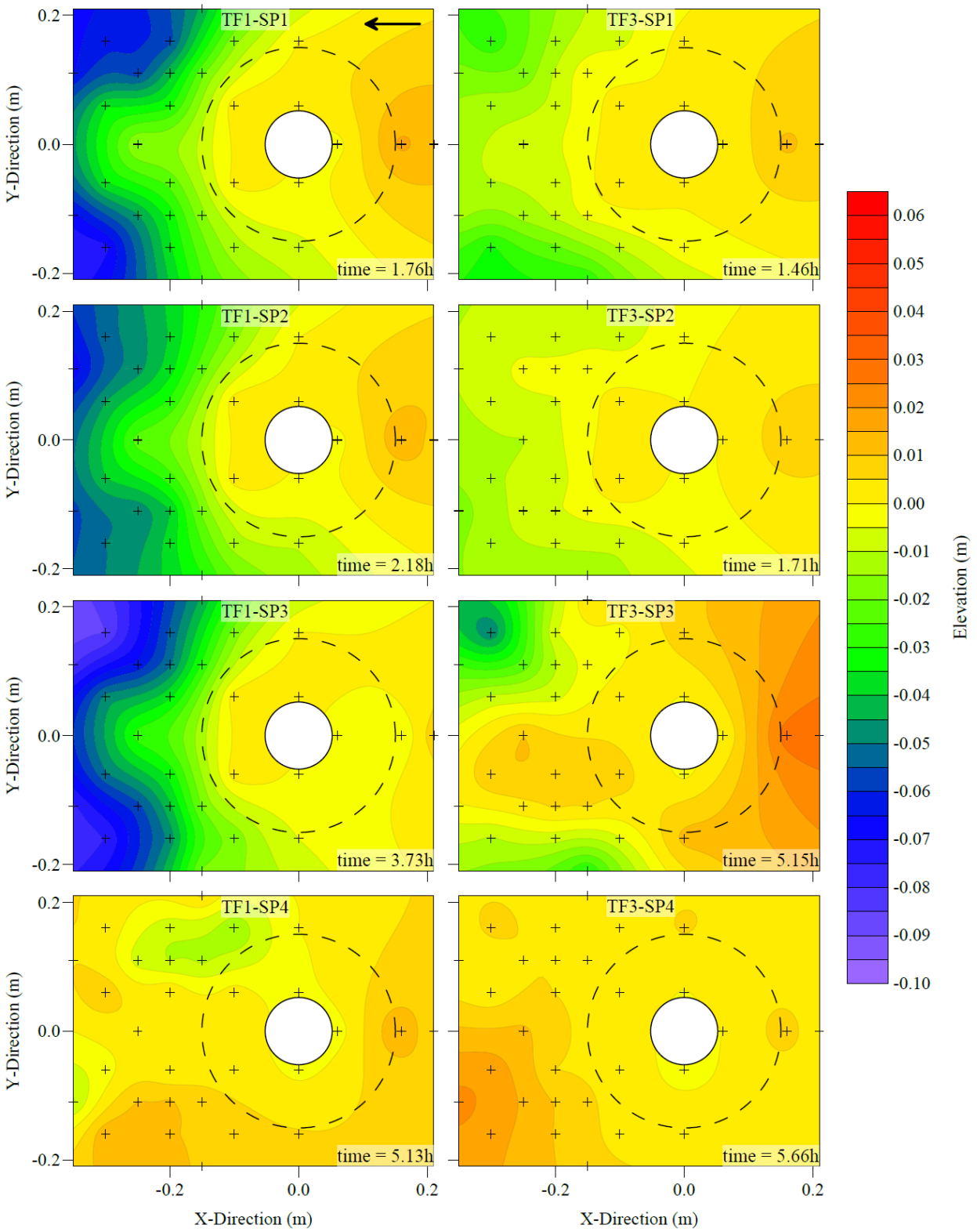

Fig. 5-9. Scour plots generated from TF1 and TF3 at the times specified in Fig. 5-8 (dotted line indicates the plan perimeter of the riprap at the bed surface).

For test TF3, SP1 and SP3 experienced noticeable scour, however the depth for each was significantly less than that of TF1. Furthermore, the scour was localized to smaller areas, as opposed to the larger region experienced in TF1, resulting in less scour volume. The scour that occurred formed a different pattern than that observed in test CW3, as two scour holes on either side of the pier developed instead of one directly in line with the pier. In SP2, the passing of the medium size dune filled the existing two scour holes almost to the point of the initial bed elevation. Meanwhile, for both TF1 and TF3, when the large dune crest passed (SP4), the scour holes became completely filled and the bed surpassed the initial elevation.

During both the TF1 and TF3 tests, a photograph was taken at the point in time when the riprap countermeasure appeared to be the most deteriorated. The time in which the photographs were taken is defined in Fig. 5-8. Fig. 5-10 presents the photographs, and in a similar manner to Fig. 5-7, the red highlighted regions are stones or groups of stones that appeared to have moved during testing. Test TF1 experienced most stone movement prior to the onset of the fully developed dunes. Stones were displaced from the sides and rear of the riprap cover and transported into the downstream scour hole. Meanwhile, test TF3 experienced minimal deterioration during the first five hours of testing and only started to encounter stone movement after the passing of the first large dune. At this point, some stones along the sides of the cover slid into the adjacent scour hole but were not transported downstream.

Fig. 5-10. Stone displacement photographs from TF1 and TF3 collected at the times specified in Fig. 5-8.

It is worth noting that for both countermeasures, the majority of stones that experienced movement were located along the outer perimeter of the riprap cover and not near the pier. Furthermore, regardless of which countermeasure was being tested, once the large dunes passed the focus region, the displaced stones became buried in the sediment.

5.1.5 Discussion

The purpose of this research was to test and compare the performance of different riprap pier scour countermeasures. In clear-water flow conditions, the RCPN3 countermeasure yielded the least scour in terms of both depth and volume, improving on the FR countermeasure by 14% and 32.3%, respectively. In addition, the quantity of stone displacement was the least for

RCPN3, as no stones were transported away from the riprap cover. Therefore, RCPN3 outperformed the other countermeasures in all aspects within the clear-water flow regime.

Meanwhile, the MR countermeasure performed the poorest in clear-water flow conditions by only mildly reducing d_s and considerably increasing V_s, while experiencing the most shape deterioration of all the countermeasures. The undesirable performance of the MR countermeasure is in agreement with the findings of past studies in the literature (Froehlich, 2013).

For the transition-flow conditions, only the RCPN3 and FR countermeasures were tested, and the reliability of the results is limited because repeated tests were not performed. However, from the data collected, RCPN3 achieved a d_s value that was 0.038m less than that of FR, which is a 46.3% reduction. Unlike with RCPN3, the scour depth in the presence of FR steadily increased until the arrival of the fully developed dune field. When the RCPN3 countermeasure was installed, the equilibrium scour depth was reached rapidly and remained relatively constant until the fully developed dunes arrived. In terms of countermeasure deterioration, RCPN3 experienced stone movement, but only after the passing of the large dunes. However, none of these stones appeared to have been transported downstream. Meanwhile, the FR countermeasure experienced greater stone movement, which occurred prior to the arrival of the large dunes, with numerous stones being transported downstream and away from the riprap cover. From the limited data available, RCPN3 appeared to outperform FR, regarding both scour and shape deterioration, during the transition period when the bed had not yet equilibrated.

The countermeasures tested in this study each contain different volumes of riprap, despite possessing the same outer diameter and embedment depth. The volume of riprap for the FR, MR, and RCPN3 countermeasures was 0.004955m^3, 0.006296m^3, and 0.004074m^3, respectively. By using RCPN3, a riprap volume reduction of 18% is achieved, but when using MR, there is a riprap volume increase of 27%, when compared to FR. It is understood that the installation of RCPN3 could be more time consuming compared to FR, however the material cost savings could help compensate for the additional installation costs.

CPN3, which is rigid by design, achieved a d_s reduction of 53% and a V_s reduction of 47.9%, under the same clear-water flow conditions used in this study (Valela, Rennie, et al., 2021). Instead, by using riprap and forming it into the shape of CPN3, d_s reduction improved by an additional 28% and V_s reduction improved by 44.4%. The improvements in scour reduction are believed to be attributed mainly to two countermeasure characteristics: flexibility and surface roughness, depending on the flow conditions. Since RCPN3 is made of riprap, it is flexible and can adapt to changes in the bed, avoiding the concern of undermining associated with rigid designs. In terms of surface roughness, RCPN3 possesses a surface that is significantly rougher (and more porous) than that of CPN3. By possessing such a surface, the flow behaviour and more specifically the boundary layer over and immediately around the countermeasure changes, achieving a reduction in bed shear stress in such regions.

To further investigate the improvements experienced by switching from a smooth rigid countermeasure material to riprap, a Flat Plate Collar (FPC) can be compared to FR under clear-water conditions, as they both possess the same shape and differ only primarily in material. According to (Valela, Rennie, et al., 2021), FPC was found to reduce d_s by 40% and V_s by 11.2%, for the same clear-water flow conditions used in this study. Therefore, FR outperformed an FPC by improving d_s reduction by 27% and V_s reduction by 48.8%; granted, undermining of the FPC did not occur. The improvements in d_s and V_s reduction from CPN3 to RCPN3, and from an FPC to FR, are very similar, within 1% and 4.4%, respectively. Therefore, when switching from a smooth rigid countermeasure material to riprap, a predictable trend, regardless of the countermeasure shape, is present.

A number of limitations can be associated to the research presented in this paper. The *first limitation* is that only clear-water and transition-flow studies were executed. To fully evaluate the performance of the new countermeasure, it should be tested under live-bed conditions. The *second limitation* is that only circular piers were investigated. Further research needs to be performed to include other pier shapes. The *third limitation* is that a partially filled cavity, resulting from excess bed material or debris deposition, was not tested under clear-water conditions. However, it is assumed that a fully filled cavity will behave as a standard FR countermeasure, which has proven in this study to still provide adequate scour protection. The *fourth limitation* is that only one type of riprap was tested for each flow condition. The quantity of scour reduction could potentially be improved or hindered, depending on the riprap properties, such as d_{50} and angularity. Additional testing is warranted to determine the impact such parameters have on scour.

RCPN3 was designed and tested for bridge piers under steady flow conditions only. However, the use of RCPN3 could be expanded given its flexible shape, large scour reducing capabilities, and ability to accommodate all approaching flow angles. One such example could be offshore applications, contingent upon further research in the presence of wave action.

5.1.6 Conclusions

This study tested conventional MR and FR countermeasures, in addition to the new RCPN3 countermeasure. When compared to a pier without any countermeasure, MR was demonstrated to reduce the scour depth by only a small amount, and actually generated a larger volume of scour. In addition, MR also experienced considerable deterioration, overall making it an undesirable countermeasure.

Both FR and RCPN3 successfully reduced scour in both clear-water and transition-flow conditions, however RCPN3 outperformed the FR countermeasure. Specifically, RCPN3 reduced scour more and experienced less shape deterioration, than that of the FR countermeasure. Furthermore, RCPN3 required 18% less riprap material than the FR countermeasure. Therefore, RCPN3 is the most desirable countermeasure of those tested as it greatly reduces scour,

maintains its original shape best, requires less riprap, can accommodate all approach flow angles, and is flexible.

By switching from the smooth rigid material of CPN3, to the rough flexible riprap material of RCPN3, the depth and volume of scour reduced. This reduction in scour was mirrored through the comparison of an FPC and FR, as both possess the same shape, but FR is made of riprap. FR yielded greater scour reduction, with an increase over the FPC that was nearly identical to that experienced advancing from CPN3 to RCPN3. This trend indicates that the benefits of using riprap are consistent regardless of the countermeasure shape. Riprap countermeasures are also able to follow bed motions under live-bed conditions, although more research is necessary to quantify RCPN3 performance under these conditions. In conclusion, this study confirms the excellent scour reducing characteristics of riprap, which has made it so popular and advantageous as a countermeasure material.

Chapter 6. Ice Cover

6.1 Bridge Pier Scour Under Ice Cover

Preprint of a modified version of an article printed in Water © 2021 MDPI. DOI:https://doi.org/10.3390/w13040536. Additional data, which was not included in this paper, that pertains to the performance of CPN3 under an ice cover, can be found in Appendix E.

6.1.1 Introduction and Objectives

Various researchers have identified ice covers as a parameter that requires further research; e.g., Ettema et al. (2011) ranked ice covers at a medium-level priority in terms of bridge pier scour research needs. Wu et al. (2016) performed a bridge pier scour study in the presence of a floating ice cover, which examined the effect of different pier diameters and water depths on scour depth and scour width. The limitations of this study were that pressurized ice covers and different ice cover roughnesses were not considered. Ackermann et al. (2002) studied bridge pier scour with a floating ice cover possessing either a smooth or a rough surface. Various velocities under both live-bed and clear-water conditions were tested. The limitations of this research were that pressurized conditions were not tested and only the maximum scour depth was recorded. Lastly, Hains and Zabilansky (2004) performed a thorough study of bridge pier scour under a floating and pressurized ice cover. The limitations of this study were that live-bed conditions were reached in a number of clear-water tests making the final scour data for these points unusable, and the flow rate (Q) was changed for each test rather than being kept constant.

It is understood that ice covers influence the hydrodynamics of the flow passing beneath, which can in turn increase bed erosion. However, the full extent of the impacts an ice cover has on bridge pier scour are not known. Therefore, the intent of this study is to expand the existing knowledge base pertaining to bridge pier scour in the presence of an ice cover. In addition to maintaining a constant flow rate and remaining in the clear-water regime amongst all tests, the objectives are to:

1) Examine the differences in scour for floating versus fixed ice covers.
2) Investigate the effect of different levels of ice cover submergence (flow pressurization) on scour.
3) Evaluate the influence both smooth and rough ice covers have on scour.

6.1.2 Experimental Setup

6.1.2.1 Flume

The research presented in this study was completed in the University of Ottawa's Civil Engineering Hydraulics Laboratory in Ottawa, Canada. The flume utilized for the research measured 30m long, by 1.5m wide, by 0.5m deep. A sand section, extending the width of the flume and measuring 3.16m in length and 0.2m in depth, was installed near the outlet. To contain

the sand, concrete false floors, the same height as the sand, were installed upstream and downstream of the sand section. The downstream false floor measured 1.25m in length and ended at the outlet. The upstream false floor measured 4.16m in length and included an additional gradual gravel slope, 2.25m in length, extending upstream from the leading face to smoothly transition the passing flow onto the false floor. An acrylic cylindrical bridge pier, 0.09m in diameter (D), was positioned in the center of the sand section and bolted to a large steel plate situated beneath the sand. The width of the pier with respect to the width of the flume was checked to ensure flow blockage would not occur. The sediment used in the sand section was uniformly graded silica sand with a median grain size diameter (d_{50}) of 0.001m. This sand size was selected based on a Shield's curve analysis. To maintain a constant bed roughness before and after the sand section, the same sand was adhered to the surface of both concrete false floors. Lastly, to reduce turbulence, two flow straighteners were installed near the inlet. An illustration of the flume can be seen in Valela, Nistor, et al. (2021).

6.1.2.2 Ice Cover Construction

One of this paper's objectives was to study scour under a fixed ice cover that induced pressurized flow conditions. To generate pressurized flow conditions, the ice cover was partially submerged. In order to ensure rigidity of the ice cover, it was constructed of dimensional lumber with a plywood bottom surface. The ice cover spanned the entire width of the flume and measured 7.5m in length, therefore covering the sand section and a majority of the false floors (Fig. 6-1). By making the ice cover this length, the ends were far enough away from the pier that the flow entering the front and exiting the rear of the ice cover did not influence the scour around the bridge pier. In addition, a fully developed flow profile was achieved prior to reaching the pier. To help guide the flow under the ice cover and avoid flow over top, two 30^o sloped sections were attached to either end of the ice cover.

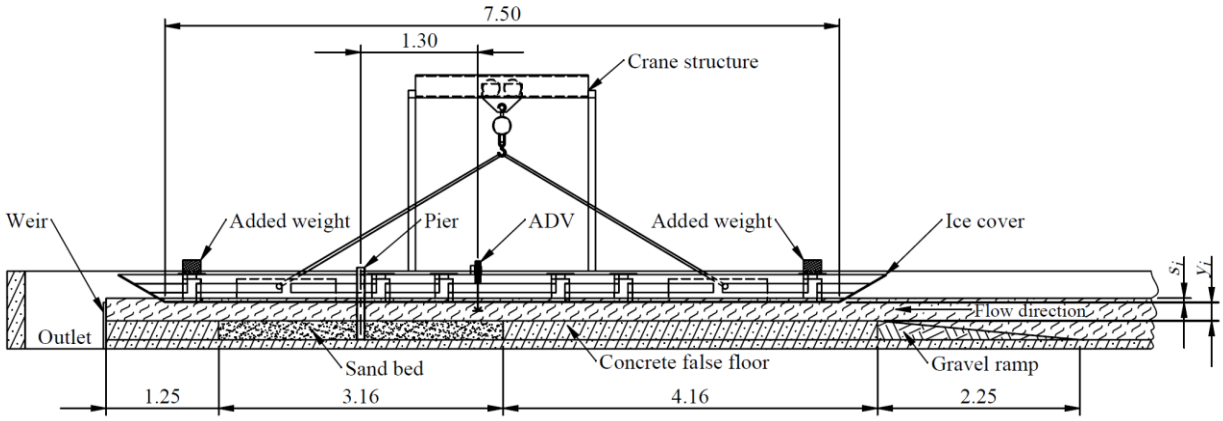

Fig. 6-1. Cross-sectional drawing of the ice cover apparatus installed in the flume (dimensions in m). y_i is the flow depth under the ice and s_i is the ice cover submergence.

A hole, the diameter of the pier, was drilled through a bottom-flush viewing window in the ice cover to allow the pier to protrude through (Fig. 6-2(b)). The hole was made so that the ice cover would fit tight around the pier, limiting the flow passage in between. Due to the overall

weight of the ice cover, it was constructed in three sections with a bolted connection between the sections. Once the ice cover was in the flume, it was bolted together and lowered into place for each test as one solid unit using a crane. Fig. 6-2(a) displays the ice cover sections bolted together and resting on the side walls of the flume in preparation for a test.

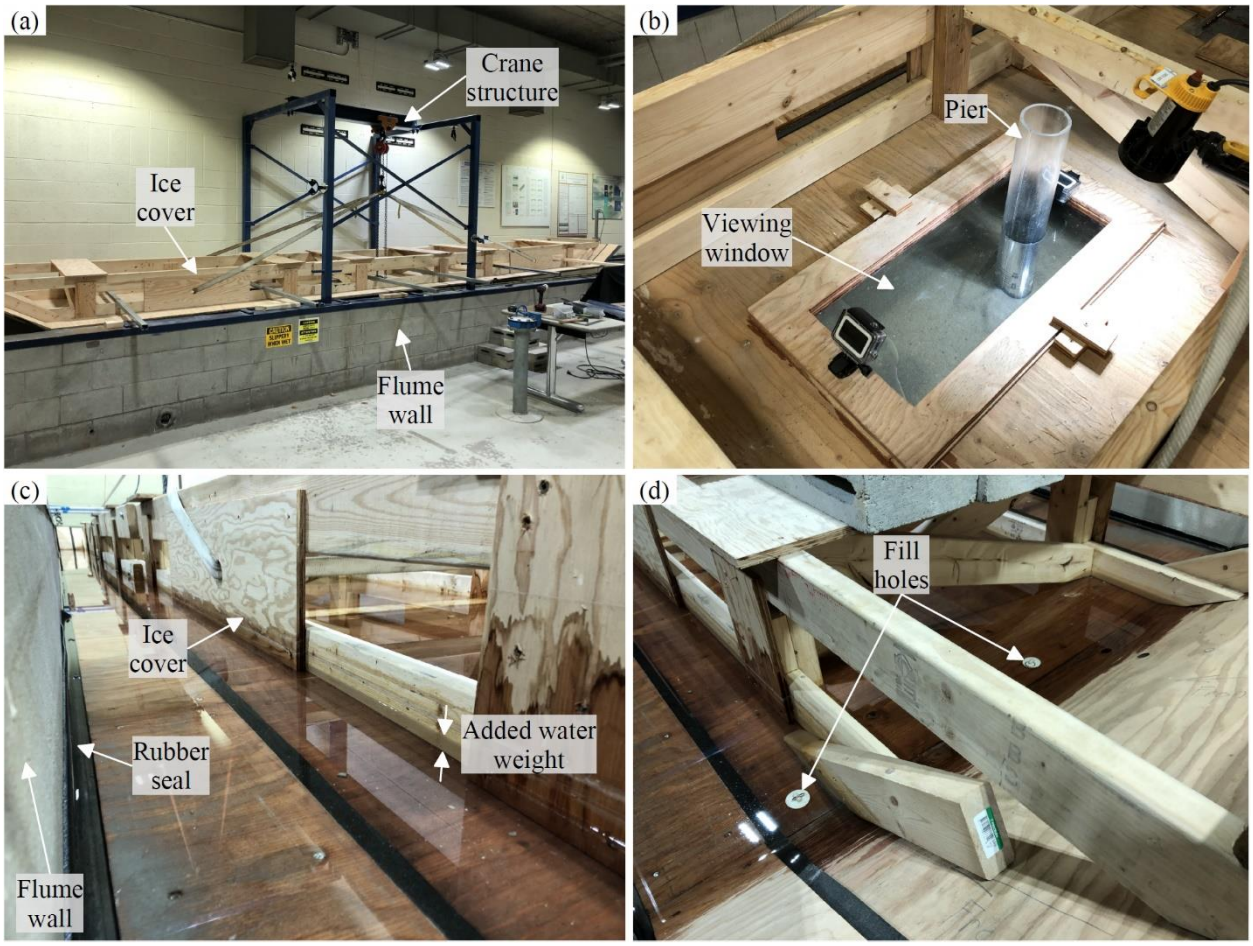

Fig. 6-2. Ice cover apparatus: (a) ice cover resting above the flume to allow for the flow conditions to be set, (b) pier protruding through the ice cover, (c) top view of the ice cover, and (d) fill holes used to allow the added water weight to enter above the ice cover.

The pressurized ice cover tests performed in this study were intended to replicate an ice cover that grows in the vertical direction, where the cross-sectional area under the ice decreases, while a constant Q is maintained. To recreate these conditions, the ice cover was submerged into the flow to different desired depths. Due to the large buoyancy forces that would otherwise be generated, water was allowed to enter the top side of the ice cover as added weight, as seen in Fig. 6-2(c). This was done using three fill holes at the front and three fill holes at the rear of the ice cover, as seen in Fig. 6-2(d). Once the water on top of the ice cover equilibrated with the water height in the flume, the fill holes were plugged for the duration of each test. Depending on s_i, additional weight was added in the form of concrete blocks to the top of the ice cover. An effort was made to reduce the transfer of water between the passing flow and the top side of the ice cover. This was done by using a rubber seal between the flume walls and the sides of the ice

cover, as shown in Fig. 6-2(c). Furthermore, between each sheet of plywood contacting the passing flow, the edges were cut on a 45^{o} degree angle and joined to eliminate the passage of water between the sheets.

6.1.2.3 Ice Cover Roughness

Another objective of this study was to compare scour under a smooth versus a rough ice cover. A smooth surface was created by first using plywood that possesses sanded faces. Then, any imperfections, joints, and screw heads were filled with a waterproof wood filler. Next, the entire surface was sanded to ensure a smooth finish, including the added wood filler. Lastly, a waterproofing product was applied to seal the surface using a paint brush. This resulted in a smooth and waterproof surface, as shown in Fig. 6-3(a), which closely resembles that of a thermally grown ice sheet.

Fig. 6-3. Bottom surface of the ice cover: (a) smooth condition, and (b) rough condition.

Once all of the tests requiring a smooth ice cover were complete, the rough surface tests were performed. To achieve the desired roughness, 0.3m by 0.3m Polyvinyl Chloride (PVC) acoustic wall panels were used to cover the existing smooth bottom of the ice cover (Fig. 6-3(b)), including the viewing window installed around the pier. The acoustic panels are waterproof, rigid, and possess the desired jagged shape which resembles the bottom of an ice jam. Each individual panel, shown in Fig. 6-4(a), has the same pattern which is symmetric about the diagonal axis. To ensure a more random configuration, the panels were staggered when installed. A topographic plot of an individual panel, Fig. 6-4(b), shows a maximum peak elevation of 0.025m. The volumetric average elevation, for a given panel, was calculated to be located at

0.005m from the base. When the ice cover was set at specific depths, the roughness's average elevation was used as the bottom of the ice cover.

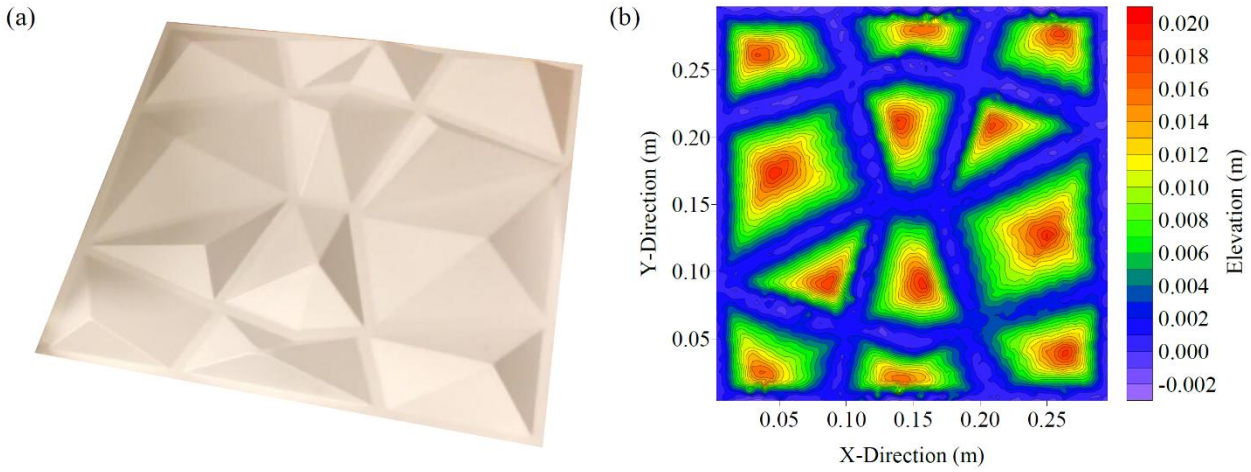

Fig. 6-4. Rough ice cover: (a) individual panel, and (b) contour plot of the surface elevation of an individual panel.

To determine the roughness of the rough ice cover, a trial test was performed with the ice cover panels positioned flat on the flume floor facing upwards, without the presence of the ice cover. The flume was filled to a depth of 0.10m, and a depth-averaged velocity (u_{avg}) of 0.37m/s was maintained. A vertical velocity profile was collected over the ice cover panels where the flow was fully developed, and using the law of the wall, the ice cover roughness was found to be k_s = 0.013m (Sirianni et al., In review). When using a scaling factor of 30, the maximum peak elevation and the roughness equate to 0.75m and 0.39m, respectively, which falls within the average range of an ice jam indicated by previous literature. Converting the k_s value to a Manning's coefficient (n) value, using the method presented by Li (2012), yields an approximate average value of 0.0189s/m$^{1/3}$.

6.1.2.4 Instrumentation

The velocity measurements were collected using a Vectrino Acoustic Doppler Velocimeter (ADV). For each ice cover condition tested, a vertical velocity profile was collected 1.3m upstream of the pier in the center of the flume. To collect the velocity measurements, a hole, the diameter of the ADV probe head, was cut in the ice cover so the probe head could protrude through. The ADV mounting setup can be seen in Fig. 6-5. A side-looking, rather than a down-looking, probe head was utilized to ensure velocity measurements close to the ice cover were captured. Individual velocity time series were collected at 0.01m intervals between the bed and the water surface or ice cover. Data were collected at each point for two minutes at a sampling frequency of 100Hz. The measured data were filtered, despiked, and time-averaged (cf., Jamieson et al., 2010).

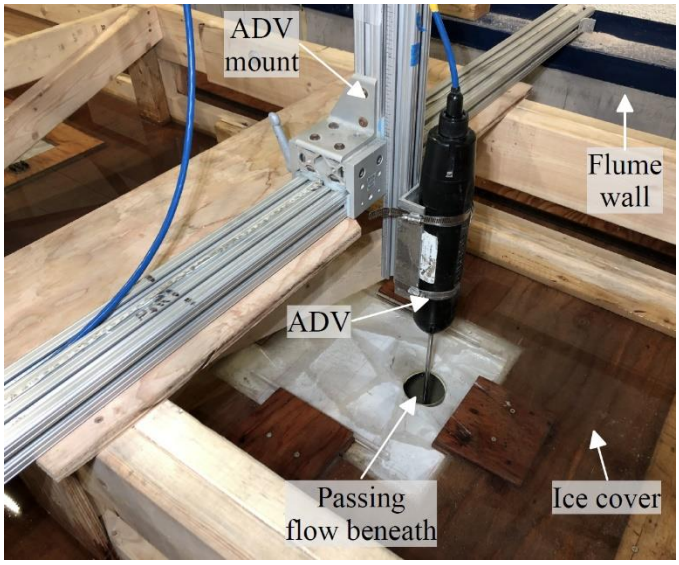

Fig. 6-5. ADV setup with side-looking head protruding through the ice cover.

After each test was complete, the resulting bathymetry was recorded using a Leica ScanStation P50 Terrestrial Laser Scanner (TLS) (Fig. 6-6). The accuracy of this device is +/- 0.0015m in all three directions. To capture the sand bed with the TLS, the ice cover needed to be partly disassembled and raised after each test. To ensure accurate elevations, a very thin dusting of sodium bicarbonate was sprinkled upon the sand bed before scanning to increase opacity. Similarly, the Perspex pier was wrapped with fabric during scanning. To capture the entire bed, the TLS was set up at three locations around the pier, where a scan was performed from each location. Joining the scans together after was aided by four targets, which were placed in clear view of all three scanning locations. Once the scans were joined together, a detailed three-dimensional model of the entire scour region was created.

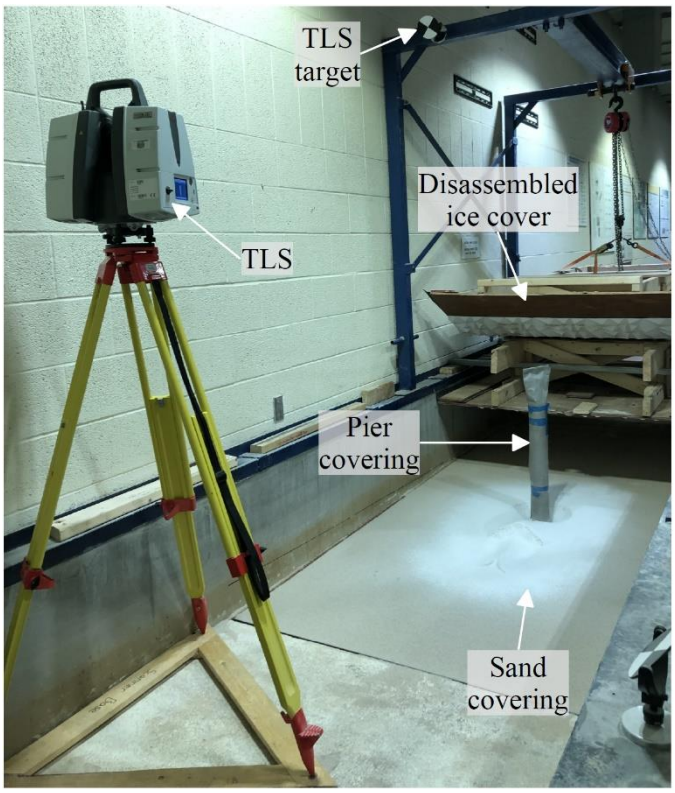

Fig. 6-6. Post-test scanning procedure.

6.1.2.5 Protocol

A total of 13 tests were completed to examine the scour behaviour beneath an ice cover, which consisted of six tests with a smooth ice cover, six tests with a rough ice cover, and one test without any ice cover as a benchmark case. For both the smooth and rough ice covers, the same conditions were tested. One of the six tests was performed with the ice cover bottom touching the water surface, replicating the floating condition, as the flow was not pressurized below the ice cover. The remaining five tests were performed with the ice cover submerged to depths (s_i), which incremented by 0.015m up to 0.075m, achieving pressurized flow conditions under the ice cover. Setting the ice cover for each test was done by, first, lowering it into position with the crane. Then, depending on the required elevation, weight was added to the ice cover, in the form of water and concrete blocks, to reach the desired y_i. The ice cover remained attached to the crane throughout the duration of each test to maintain the desired elevation. The distance between each of the four ice cover corners and the bed was verified prior to commencing each test to ensure the ice cover was set at the required elevation and level in all directions. The experimental trials and the corresponding naming convention are presented in Table 6-1.

Table 6-1. Experimental trials.

Test	s_i (m)	y_i (m)	Ice cover roughness	Water temperature (°C)	Reynolds number	Stream Froude number	Pier Froude number
Open	-	-	-	20	41237	0.163	0.055
SF	0.000 (Floating)	0.250	Smooth	20	91187	0.104	0.052
S1	0.015	0.235	Smooth	20	90329	0.112	0.056
S2	0.030	0.220	Smooth	20	99949	0.135	0.077
S3	0.045	0.205	Smooth	20	99960	0.148	0.088
S4	0.060	0.190	Smooth	20	100299	0.164	0.101
S5	0.075	0.175	Smooth	20	107527	0.196	0.134
RF	0.000 (Floating)	0.250	Rough	20	95501	0.109	0.057
R1	0.015	0.235	Rough	20	97901	0.121	0.066
R2	0.030	0.220	Rough	20	100791	0.136	0.079
R3	0.045	0.205	Rough	20	102657	0.152	0.092
R4	0.060	0.190	Rough	20	103761	0.170	0.108
R5	0.075	0.175	Rough	20	106497	0.195	0.132

This study is unique as each test was performed for the same duration (t) of 6 hours and under the same Q (0.0825m^3/s). Q was selected to be in the clear-water regime, for all ice cover conditions, determined from initial trial tests. To ensure the flow conditions were constant among all the tests, the flow was first set and verified without the ice cover. This was accomplished using a flow control valve on the pump and an outlet weir. Then, depending on the test that was being performed, the ice cover was either lowered into position at the desired elevation or left above the water surface for the duration of the test. By beginning each test in this manner, the same flow depth (y) of 0.25m and u_{avg} of 0.22m/s could be set for each test, whether or not the ice cover was being used. The time began once the ice cover was positioned at the desired elevation.

Prior to beginning each test, the ice cover was disassembled, and the bed was completely levelled. The ice cover was then reassembled and secured above the water surface. It was critical when beginning each test that the flume was slowly filled with water and that Q was gradually increased, as to avoid any initial scour.

6.1.3 Results

6.1.3.1 Velocity Data

During each of the experimental conditions tested, a vertical velocity profile was measured upstream of the pier. The velocity profiles beneath the smooth and rough ice covers are presented in Fig. 6-7(a) and Fig. 6-7(b), respectively. In addition, the velocity profile from the Open case (possessing no ice cover) is presented in both plots for comparison purposes.

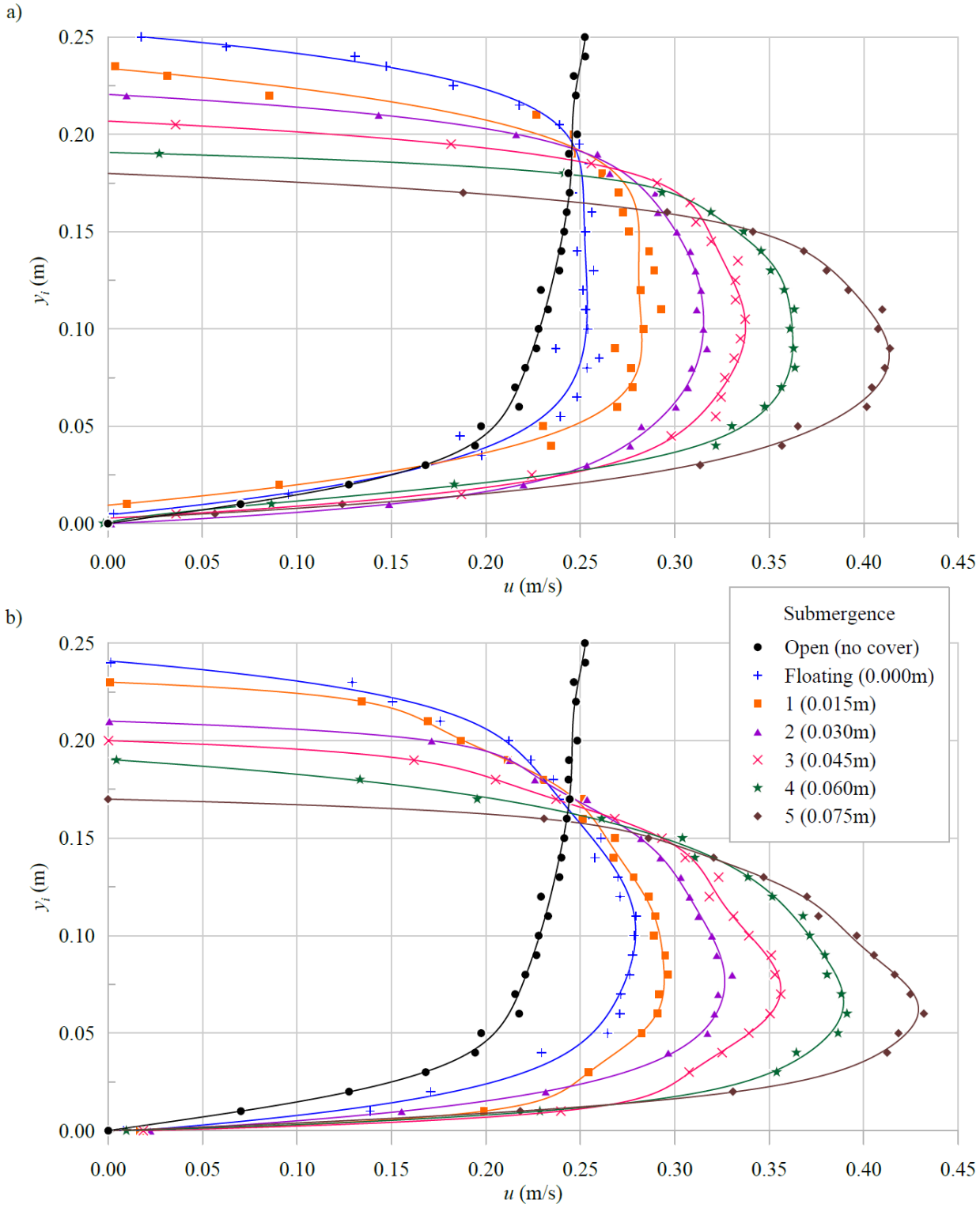

Fig. 6-7. Velocity (u) profiles for Open, Floating, and submerged conditions: (a) smooth ice cover, and (b) rough ice cover.

The Open case velocity profile behaves as expected, with the maximum velocity occurring near the surface. The velocity gradient near the bed for the Open case is mild, which induces a low quantity of shear stress on the bed. Meanwhile, when any ice cover is present, the velocity profile changes to that resembling a pipe flow. The maximum velocity is reached towards the mid-depth while the velocity at the top and bottom boundary approaches zero. As either ice cover becomes more submerged reducing the depth under the ice cover, the maximum velocity increases and the location of the maximum velocity shifts downwards to remain at approximately the mid-depth. Furthermore, despite some anomalies, a general trend shows that the velocity gradient near the bed is lower for the Open condition than most of the ice covered conditions, especially the more submerged cases. This can result in the ice covered cases inducing greater shear stress on the bed.

The roughness of the ice cover shows to have further influenced the shape of the velocity profile beneath. For the same s_i, the velocity profile under the rough ice cover possesses a greater maximum velocity and a sharper crest, when compared to the velocity profile under the smooth ice cover. In addition, the location of the maximum velocity under the rough ice cover occurs below the mid-depth, closer to the bed, whereas the location of the maximum velocity under the smooth ice cover occurs at approximately the mid-depth. This trend is consistent amongst all s_i levels. As a result, the velocity gradient near the bed is greater under the rough ice covers.

When comparing velocity profiles between the floating versus submerged (fixed) ice covers, little difference is present besides the influence of s_i. The shape of the velocity profiles for the floating cases match closely to those of s_i = 0.015m. The main dissimilarity is the lower maximum velocity for the floating cases and that corresponds to the greater cross-sectional area.

6.1.3.2 Scour Data

After each test was performed and scans of the resulting bathymetry were collected, three-dimensional models of the bed were generated. Using these models, elevation plots were created to compare the differences in scour patterns between tests. Fig. 6-8 displays the resulting scour for the Open case, where the flow travelled in the negative X-direction. In the absence of an ice cover and under the given flow conditions, the quantity of scour around the pier is minimal. A small depression can be seen wrapping around the front and sides of the pier with a corresponding mound immediately behind the pier.

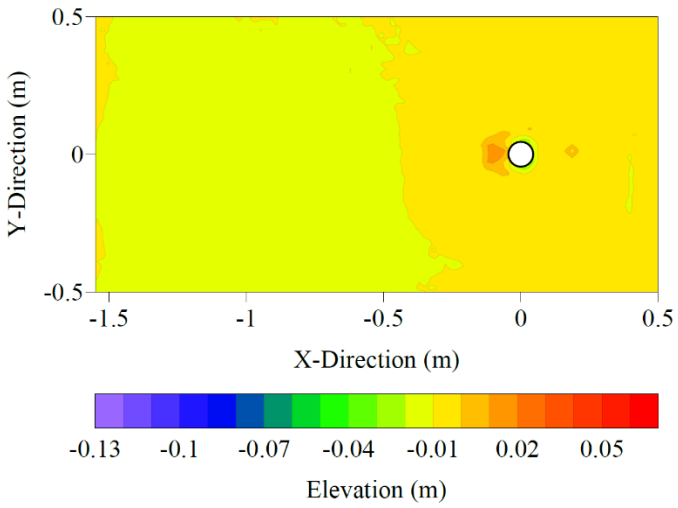

Fig. 6-8. Scour contour plot for the Open trial.

Fig. 6-9 displays the scour plots from each of the ice cover tests. The left and right column contain the smooth and rough ice cover results, respectively, while the rows contain increasing s_i levels. Regardless of the ice cover roughness or submergence, all tests possessing an ice cover yielded greater scour compared to the Open case. The floating cases (SF and RF) possess the least amount of scour, of the ice cover conditions tested, and the patterns look similar to that of the Open case. The difference is a magnified version of the Open case, where there is a deeper depression around the pier followed by a larger deposition pile behind the pier. As the ice cover becomes submerged, the quantity of scour and deposition increases steadily based on the level of s_i. The scour grows not only in depth but also proportionally in diameter. Once the deposition pile reaches approximately 0.05m in height, two small scour holes begin to form immediately downstream of the deposition pile, as seen in test S2 and R2. These scour holes grow in size as the ice cover becomes further submerged and, as a result, create a second deposition pile further downstream.

The difference in scour between the smooth and rough ice covers is minimal for the floating and mildly submerged ice cover tests. As s_i increases, the ice cover roughness has a greater influence causing there to be a larger difference in scour between the smooth and rough ice covers. However, for all test conditions, the rough ice cover yielded more scour than the smooth ice cover. Test R5 contained the greatest scour with the upstream and side depression continuing around the rear of the pier and the deposition pile extending over double the length of that in test R4 and S5. Due to the deposition pile in test R5 nearing the end of the sand section, additional scour holes were not generated downstream of the deposition pile.

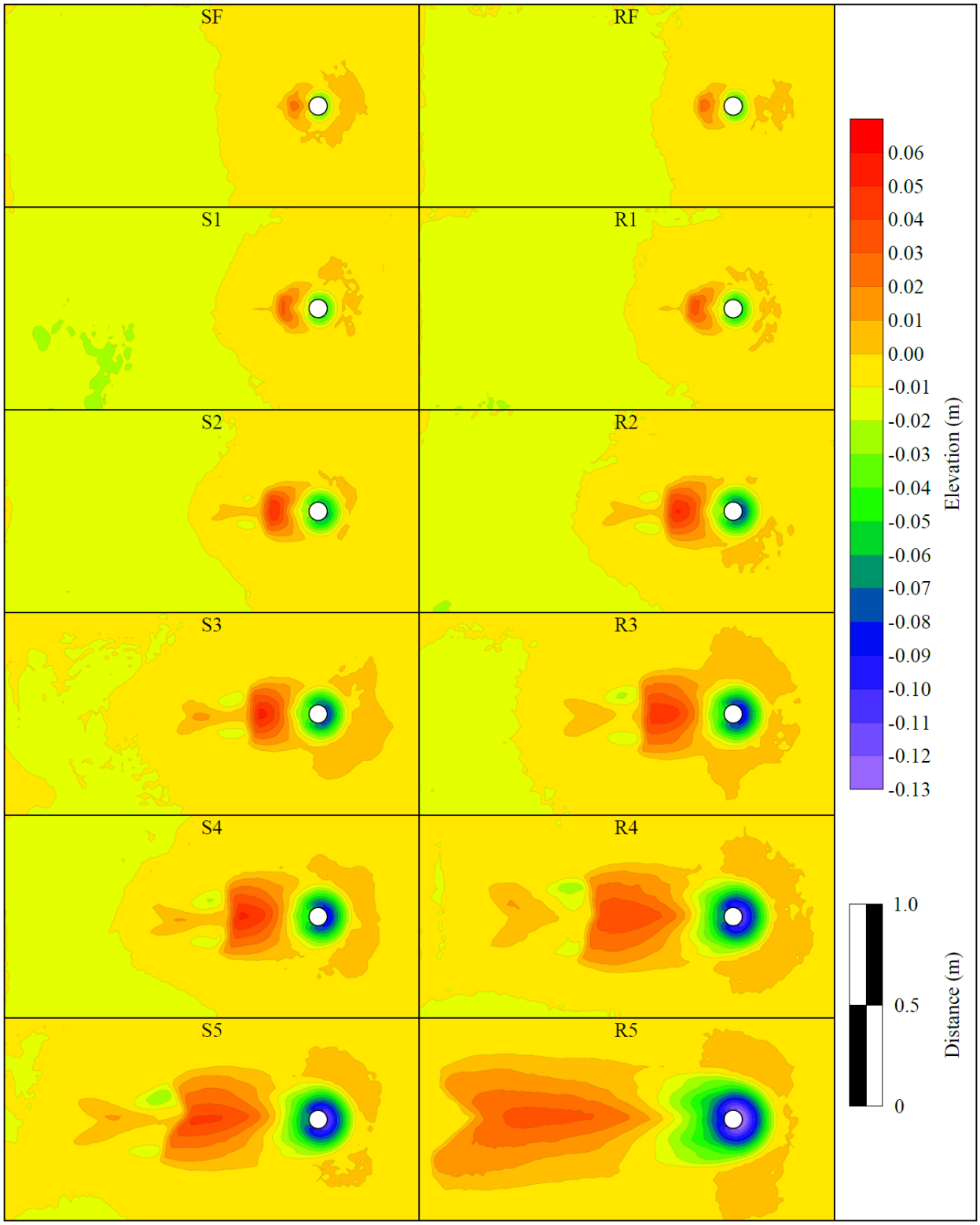

Fig. 6-9. Scour contour plot comparison for the Floating and submerged trials.

The maximum scour depth (d_s) for each test, as well as the percent increase in d_s when compared to the Open case, are presented in Table 6-2. All tests were within the clear-water

regime, as live-bed conditions were not reached even under the most submerged ice cover. The Open case experienced a d_s of only 0.025m, which increased drastically with the presence of any ice cover. The floating ice cover tests, SF and RF, yielded a 40% and 52% increase in d_s, respectively. Whereas, when the ice covers became submerged for tests S2 and R2, the increase in d_s grew to 76% and 92%, respectively. The greatest d_s was achieved for test R5, reaching a depth of 0.128m, implying a 412% increase over the Open case. The smooth and rough ice cover tests had a difference in d_s of 0.004m between tests S1 and R1 and that grew to 0.019m between tests S5 and R5.

Table 6-2. Scour depth results.

Test	d_s (m)	Increase in d_s (%)
Open	0.025	-
SF	0.035	40
S1	0.044	76
S2	0.062	148
S3	0.079	216
S4	0.090	260
S5	0.109	336
RF	0.038	52
R1	0.048	92
R2	0.074	196
R3	0.088	252
R4	0.107	328
R5	0.128	412

To better understand the difference between the effects of the smooth and rough ice cover on scour, the nondimensionalized ice cover scour depth (d_i) as a function of the nondimensionalized y_i, for both ice cover roughnesses, is plotted in Fig. 6-10(a). Note that d_i refers to the scour caused only by the ice cover, which is d_s minus the scour depth of the Open case (d_p). The purpose of plotting d_i, as opposed to d_s, was to highlight the additional scour induced by the presence of an ice cover.

Fig. 6-10(a) confirms that the difference in scour between the smooth and rough ice covers is small for the floating condition but grows as the ice cover becomes more submerged. The equations of the smooth and rough fitted lines are presented in Eq. 7 and Eq. 8, respectively.

$$\frac{d_i}{D} = -2.78\frac{y_i}{y} + 2.86 \tag{7}$$

$$\frac{d_i}{D} = -3.39\frac{y_i}{y} + 3.50 \tag{8}$$

where (y_i/y) represents the flow confinement (pressurization), such that $y_i \leq y$. Eqs. 7 and 8 were developed from y_i/y data ranging from 0.7 to 1.

The relationship between scour and flow confinement is linear for both smooth and rough ice covers. Due to a difference of 0.61 in the slopes, the data converges as y_i increases.

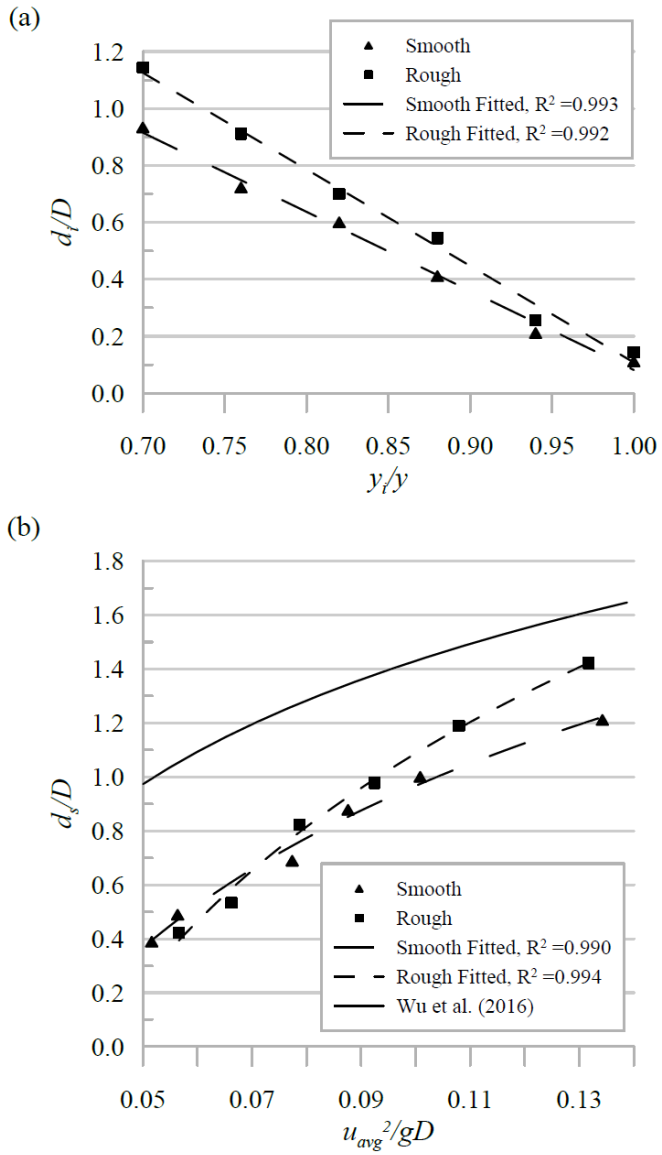

Fig. 6-10. (a) Additional scour induced by the ice cover, and (b) the relationship between nondimensionalized d_s and pier Froude number.

Another method of presenting the scour depth is as a function of the pier Froude number $\left(\frac{{u_{avg}}^2}{gD}\right)$, where g is the gravitational constant. According to Ettema, Kirkil, et al., (2006), the pier Froude number can be seen as a way of conveying the similitude in the frequency and strength of vortices shed from the rear of a pier. This parameter is often neglected when studying pier scour but has shown to be largely influential (Wu et al., 2016). Fig. 6-10(b) displays the

nondimensionalized d_s as a function of pier Froude number. Similar to Fig. 6-10(a), this plot also indicates that the rate of change for the smooth and rough ice covers is not the same. For pier Froude numbers below approximately 0.07, the rough ice cover data points drop below that of the smooth ice cover. In other words, to achieve the same quantity of scour under both ice covers, greater pier Froude number values are required in the presence of a rough ice cover. Whereas, above the pier Froude number of approximately 0.07, the rough ice cover yields greater scour for the same pier Froude number. The equations for the smooth and rough ice cover fitted lines, which are nonlinear, are shown in Eq. 9 and Eq. 10, respectively.

$$\frac{d_s}{D} = 0.87 \ln\left(\frac{{u_{avg}}^2}{gD}\right) + 2.96 \quad (9)$$

$$\frac{d_s}{D} = 1.22 \ln\left(\frac{{u_{avg}}^2}{gD}\right) + 3.89 \quad (10)$$

The pier Froude number was altered through changing u_{avg} and leaving D constant, therefore implying that d_s is proportional to u_{avg}. Eqs. 9 and 10 are valid for $D > 0$ and $0 < u_{avg} < u_{cr}$, where u_{cr} is the critical velocity required for bed material motion.

6.1.4 Discussion

In this study, a number of conditions pertaining to the presence of surface ice around bridge piers, in regard to bridge pier scour, were analysed. One objective, which proved to be challenging to correctly replicate experimentally, was a floating ice cover. In the field, a floating ice cover can both freely adjust its elevation to accommodate the changing water levels, and it can also protrude into the passing flow to some degree, depending on the characteristics of the ice. Therefore, it is possible that a floating ice cover can generate accelerated flow beneath, which could result in similar scour behaviours to that of the mildly submerged fixed ice covers. To overcome this issue, a range of s_i levels were tested from just touching the surface, to protruding into the flow 30% of the initial flow depth. Since the flow depth throughout each test remained constant and the ice cover was weighted to achieve the desired s_i, whether the ice cover was fixed in place or not would have no impact on the scour results. This implies that the submerged ice cover cases could represent a floating ice cover that protrudes into the flow.

Upon analysing the velocity and scour results with and without an ice cover, it is evident that the presence of any ice cover increases scour. Specifically, as an ice cover grows and becomes more submerged, the quantity of pier scour becomes greater. These scour results were confirmed by the general trend observed from the velocity data, which indicated an increase in the near bed velocity gradient as the ice covers became more submerged. Both a smooth and rough ice cover were tested, and this was to reach both ends of the possible roughness spectrum. It was discovered that the rough ice cover induced more scour than the smooth ice cover under all conditions. In addition, the quantity of scour also increased at a greater rate for the rough ice cover than the smooth ice cover, as y_i decreased. For these reasons, the rough ice cover should be

used from a design perspective in order to achieve a conservative design. Since many pier scour equations do not take into consideration the effects of ice covers, the results presented in Fig. 6-10(a) can be used in addition to such equations to help provide further insight.

Wu et al. (2016) presented equations that relate nondimensional scour to pier Froude number, under open channel conditions Eq. 11 and smooth ice cover conditions Eq. 12.

$$\frac{d_s}{D} = 0.67 \ln\left(\frac{{u_{avg}}^2}{gD}\right) + 2.83 \tag{11}$$

$$\frac{d_s}{D} = 0.66 \ln\left(\frac{{u_{avg}}^2}{gD}\right) + 2.95 \tag{12}$$

Eq. 12 from Wu et al. (2016) and Eq. 9 presented in this paper, both pertain to a smooth ice cover and possess a number of similarities (Fig. 6-10(b)). Specifically, the constants are almost identical, and the coefficients are relatively close given the differences in the experimental conditions. This lends credence to both Eqs. 9 and 12, and indicates that the experimental results presented in this paper are reasonable. The experimental conditions of Wu et al. (2016) varied from this study in that y = 0.108m, 0.150m, 0.210m, d_{50} = 0.00051m, and u_{avg} = 0.24m/s. It can be noted that of the different experimental conditions, d_{50} and y are not considered in Eqs. 9 and 12, only u_{avg}.

When comparing the equations pertaining to a smooth ice cover (Eqs. 9 and 12) to Eq. 10 presented in this paper, which pertains to a rough ice cover, there are notable differences. The constant and the coefficient for Eq. 10 are significantly greater than that of Eqs. 9 and 12. Wu et al. (2016) stated that the presence of a smooth ice cover, when compared to no ice cover, has only a limited influence on the pier Froude number. Meanwhile, the results presented in this study (Eqs. 9 and 10) show that the presence of a rough ice cover, in comparison to a smooth ice cover, has a substantial influence on the pier Froude number. Therefore, given the findings of this paper and that of Wu et al. (2016), the pier Froude number only becomes influenced with rough ice covers.

The work presented in this paper contains a number of limitations which warrants further research. First, bridge pier scour is a complex process which is influenced by numerous parameters, and due to the scope of the project, not all parameters could be examined to their full extent. Specifically, only one Q, y, D, and d_{50} were tested, and all the tests lied within the clear-water regime. The next limitation to this paper is that only one size of ice covering was used. The ice covering extended in the upstream and downstream direction a far distance from the pier, as to replicate an infinitely long ice cover, but perhaps shorter ice covers, such as ones localized around the pier, could have a different effect on the quantity of pier scour. Furthermore, the ice cover itself was artificial as the smooth surface consisted of treated plywood and the rough surface consisted of PVC panels. While using artificial materials improves constructability, and the chosen materials were intended to mimic natural river ice, it is possible that natural river ice

would induce different flow characteristics. Lastly, only one velocity profile was measured for each test condition and it was collected in the center of the flume upstream of the pier. Additional velocity profiles would be beneficial as it would create a more detailed flow field; however, this is difficult to achieve with an ADV in the presence of a solid ice cover.

A point worth noting is that when the ice cover was submerged, the flow depth beneath the ice cover consequently reduced. In the absence of an ice cover, the authors acknowledge that a change in flow depth could influence the scour depth. Therefore, the scour depth experienced under a submerged ice cover could be a combination of both the flow pressurization and the reduction in flow depth. Further research is required to distinguish the contribution of both factors.

6.1.5 Conclusions

Pier scour under increasing ice cover submergence was investigated. Velocity measurements collected under the ice cover for each experimental condition confirmed that the ice cover induced an upper boundary layer resulting in maximum velocity near mid-depth. Increased ice cover submergence resulted in greater maximum velocity, and an associated increase in near-bed velocity gradient. Furthermore, a rougher ice cover displaced the maximum velocity closer towards the bed, and thus near-bed velocity gradient was even greater.

After each experiment, three-dimensional scans of the bed were performed. It was found that the presence of an ice cover, regardless of the submergence level or roughness, caused an increase in scour. The bathymetry measurements confirmed that the tests with an increased velocity gradient near the bed resulted in greater scour. Specifically, as the ice cover was submerged deeper into the flow, the quantity of scour grew, and for each level of submergence, the rough ice cover generated more scour than the smooth ice cover. The most scour occurred under the rough ice cover submerged to 30% of the flow depth (the largest submergence tested), as it resulted in a 412% increase in scour depth. Therefore, solid ice covers that span the water surface around bridge piers are an influential parameter in pier scour and additional research into the topic is a necessity. Importantly, when designing a bridge pier foundation to resist the additional erosive forces induced by an ice cover, focus should be put on rough ice covers that protrude into the passing flow, as such conditions yielded the most concerning scour depths.

Chapter 7. Conclusions and Recommendations for Future Work

7.1 Conclusions

The thesis presented herein examined different aspects of bridge pier scour. The overall research was divided into two categories consisting of: developing an improved bridge pier scour countermeasure and increasing the body of knowledge pertaining to bridge pier scour in the presence of an ice cover. The following general conclusions can be drawn from this study:

- The iterative hybrid method, that utilized both numerical and experimental modelling to achieve a new countermeasure design, proved to be efficient and effective.
    - The numerical model greatly aided in the prototype design process by saving experimental time and costs, while providing otherwise unattainable flow field information.
- Collar Prototype No. 1 (CPN1), intended to be an improved pier collar design, was found to be moderately effective at reducing the scour depth. However, greater undermining was experienced around the perimeter of CPN1 than the Flat Plate Collar (FPC). This was caused by increased flow separation, indicating that CPN1 required additional design revisions.
- Collar Prototype No. 2 (CPN2) was designed to eliminate the undermining that occurred along the sides and front of CPN1. This was successfully achieved, but by streamlining the shape of the collar, large quantities of scour occurred downstream. CPN2 resulted in a low scour reduction warranting further design improvements.
- Collar Prototype No. 3 (CPN3) evolved from the previous collar designs as the horseshoe vortex was guided inside of a three-dimensional cavity below the bed surface, as opposed to on top. In addition, CPN3 possessed a radially symmetric shape that functioned independently of the flow direction. CPN3 demonstrated to be a successful collar countermeasure as it outperformed the FPC by achieving greater (overall moderate) scour reduction while eliminating undermining.
    - Developing a countermeasure that interrupts the passing flow less was found to achieve greater scour reduction while reducing undermining.
- The FPC was demonstrated to reduce the scour depth by only a low-to-moderate amount, while being prone to undermining, therefore making it a less desirable countermeasure.
    - When undermining was experienced, the volume of scour remained relatively constant as the scour depth decreased, because material from beneath the collar filled the surrounding scour holes. This resulted in the scour migrating closer to the pier.
- Mounded Riprap (MR) generated a larger volume of scour, when compared to a pier without any countermeasure, while only reducing the scour depth by a small amount. In

addition, MR also experienced sizeable shape deterioration, overall making it an inferior countermeasure.

- Flat Riprap (FR) proved to be an effective scour countermeasure by achieving moderate-to-high scour reduction while maintaining mild shape deterioration.
- Riprap Collar Prototype No. 3 (RCPN3), designed to be an overall improved scour countermeasure, outperformed the FR countermeasure by reducing scour more (in both clear-water and transition-flow conditions) and experiencing less shape deterioration. Furthermore, RCPN3 required 18% less riprap material than the FR countermeasure. Therefore, RCPN3 developed in this thesis was the best countermeasure studied.
- Switching the physical composition of a countermeasure from a smooth rigid material to rough flexible riprap material, reduced both the scour depth and volume.
- The presence of any ice cover, regardless of the submergence level or roughness, caused an increase in scour.
- The scour depth beneath an ice cover is proportional to the maximum velocity (near bed velocity gradient).
    - As the ice cover was submerged deeper into the flow, the depth of scour grew. Therefore, fixed (pressurized) ice covers generate deeper scour than floating ice covers.
    - The rough ice cover generated more scour than the smooth ice cover.
    - The deepest scour occurred under the rough ice cover submerged to the largest value tested.

The work presented in this thesis, which pertains to bridge pier scour, aimed to improve public safety and infrastructure preservation. This was accomplished by, first, developing a new countermeasure to help reduce the harmful effects of scour, and second, collecting bridge pier scour data in the presence of an ice cover to help better predict scour in cold climate regions. Through these and other contributions, the widespread and devasting problem that has challenged researchers and engineers alike for many years, is becoming better understood, allowing for bridges to last longer and ultimately be safer.

7.2 Recommendations for Future Work

The studies presented in this thesis examine bridge pier scour, by developing an improved solution to reduce scour and by investigating the influence ice covers have on scour. However, further research is necessary in order to continue developing and testing the new scour countermeasure in different conditions, and to expand the understanding of the effects an ice cover has on scour. Some areas specifically where additional work would greatly improve the body of knowledge are:

- Adapting the design of RCPN3 to accommodate different pier shapes and sizes. RCPN3 was designed in such a way that it can be easily installed on piers possessing shapes other than circular, but these shapes were never tested. Many bridges utilize piers with varying

shapes and sizes, such as elongated, so by adapting and testing RCPN3 for different piers, its applicability can be greatly increased.

- Examining the configuration of RCPN3 around bridge pier groups. When multiple piers are positioned within a close proximity, the scour behaviour can change. Therefore, additional testing should be conducted to determine the most effective configuration of RCPN3 for piers in groups as well as its performance in such situations.
- Exploring the application of RCPN3 in other locations besides steady state rivers with a constant flow direction. RCPN3 was designed to remain flexible (due to its riprap material) and accommodate all flow directions (through its symmetrical shape), implying that it could be beneficial for piers or other structures in tidal, ocean, or changing flow direction regions. The effects of wave action on the performance of RCPN3 would also need to be studied.
- Performing larger or prototype scale tests. The maximum scale utilized in this thesis was 1:30 for both numerical and experimental models. Providing results from larger scale tests would add additional design validation as well as assist in it becoming adopted in practise.
- Conducting laboratory experiments with a real ice cover as opposed to an artificial ice cover. The artificial ice used in these studies closely resembled real ice, however there were still inherent differences in the material properties and behaviours. Instead, by using real ice, a more accurate flow field can be generated, therefore yielding a more representative scour pattern.
- Expanding the test conditions used in the presence of an ice cover. The water depth, flow velocity, pier diameter, and sediment size used in this thesis remained constant. Expanding the test conditions would not only increase the knowledge base pertaining to scour under an ice cover, but it would also allow for a more encompassing scour prediction equation to be generated.
- Testing RCPN3 under the presence of an ice cover. CPN3 was tested under the harshest ice cover conditions studied in this thesis, but RCPN3 was not tested under any ice cover. Due to the promising results of RCPN3 achieved thus far, it is predicted RCPN3 could be a good scour reducing option when ice covers are present.
- Examining different ice cover configurations. The artificial ice covers that were employed in this thesis were completely horizontal with a constant depth beneath, however, ice covers in the field can possess nonuniformities in the form of a toe, heel, or ridges. These nonuniformities can cause a localized reduction in cross-sectional area beneath the ice cover which can potentially influence the resulting scour.
- Testing RCPN3 under live-bed conditions. Clear-water and transition-flow experiments were conducted, but performing live-bed experiments would generate a complete understanding of the performance of RCPN3 under all flow condition types.
- Utilizing a numerical model equipped with sediment transport capabilities would complement the experimental results, as it can provide further insight into the scour problem, with respect to both influence of ice cover and countermeasure design.

References

Abdalla, M. G. (2016). A Study on Scour for Irrigation Canals in Egypt, “Case Study: The First Reach of El-ibrahimeya Canal.” *American Journal of Engineering and Technology Management*, *1*(4), 65–77. https://doi.org/10.11648/j.ajetm.20160104.13

Ackermann, N. L., Shen, H. T., & Olsson, P. (2002). Local Scour around Circular Piers Under Ice Covers. *Ice in the Environment: Proceedings of the 16th IAHR International Symposium on Ice*, 149–155.

Agrawal, A. K., Khan, M. A., & Yi, Z. (2005). Handbook of Scour Countermeasures Designs. *New Jersey Department of Transportation (Report No. 49777-11-04)*. http://www.utrc2.org/sites/default/files/pubs/Handbook-of-Scour-Countermeasures-Designs.pdf

Ambtman, K. E. D., & Hicks, F. E. (2012). Field Estimates of Discharge Associated with Ice Jam Formation and Release Events. *Canadian Water Resources Journal*, *37*(1), 47–56. https://doi.org/10.4296/cwrj3701868

Ambtman, K. E. D., Hicks, F. E., & Steffler, P. M. (2011). Experimental Investigation of the Pressure Distribution beneath a Floating Ice Block. *Journal of Hydraulic Engineering*, *137*(4), 399–411. https://doi.org/10.1061/(ASCE)HY.1943-7900.0000315

Arneson, L. A., Zevenbergen, L. W., Lagasse, P. F., & Clopper, P. E. (2012). Evaluating Scour at Bridges - Fifth Edition. *Hydraulic Engineering Circular 18 (HEC-18)*.

AUR Inc. (2020). *Bridge Scour Prevention & Protection*. https://www.noscour.com/scaur--products.html

Bates, P. D., Lane, S. N., & Ferguson, R. I. (Eds.). (2005). *Computational Fluid Dynamics: Applications in Environmental Hydraulics*. John Wiley & Sons, Ltd.

Beltaos, S. (1983). River Ice Jams: Theory, Case Studies, and Applications. *Journal of Hydraulic Engineering*, *109*(10), 1338–1359. https://doi.org/10.1061/(ASCE)0733-9429(1983)109:10(1338)

Beltaos, S. (2001). Hydraulic Roughness of Breakup Ice Jams. *Journal of Hydraulic Engineering*, *127*(8), 650–656. https://doi.org/10.1061/(ASCE)0733-9429(2001)127:8(650)

Blocken, B., Stathopoulos, T., & Carmeliet, J. (2007). CFD Simulation of the Atmospheric Boundary Layer: Wall Function Problems. *Atmospheric Environment*, *41*(2), 238–252. https://doi.org/10.1016/j.atmosenv.2006.08.019

Bozkus, Z., & Yildiz, O. (2004). Experimental Investigation of Scouring around Inclined Bridge Piers. *Wetlands Engineering and River Restoration*, 1–12. https://doi.org/10.1061/40581(2001)122

Chang, W.-Y., Lai, J.-S., & Yen, C.-L. (2004). Evolution of Scour Depth at Circular Bridge Piers. *Journal of Hydraulic Engineering*, *130*(9), 905–913. https://doi.org/10.1061/(asce)0733-9429(2004)130:9(905)

Chen, S.-C., Tfwala, S., Wu, T.-Y., Chan, H.-C., & Chou, H.-T. (2018). A Hooked-Collar for Bridge Piers Protection: Flow Fields and Scour. *Water*, *10*(9), 1251–1263. https://doi.org/10.3390/w10091251

Chiew, Y.-M. (1992). Scour Protection at Bridge Piers. *Journal of Hydraulic Engineering*, *118*(9), 1260–1269. https://doi.org/10.1061/(ASCE)0733-9429(1992)118:9(1260)

Chiew, Y.-M. (1995). Mechanics of Riprap Failure at Bridge Piers. *Journal of Hydraulic Engineering*, *121*(9), 635–643. https://doi.org/10.1061/(ASCE)0733-9429(1995)121:9(635)

Chiew, Y.-M., & Lim, F.-H. (2000). Failure Behaviour of Riprap Layer at Bridge Piers under Live-Bed Conditions. *Journal of Hydraulic Engineering*, *126*(1), 43–55. https://doi.org/10.1061/(ASCE)0733-9429(2000)126:1(43)

Conaway, J. S. (2006). Comparison of Long-Term Streambed Scour Monitoring Data with Modeled Values at the Knik River, Alaska. *3rd International Conference on Scour and Erosion (ICSE-3)*, 145–153. https://hdl.handle.net/20.500.11970/100008

Dargahi, B. (1990). Controlling Mechanism of Local Scouring. *Journal of Hydraulic Engineering*, *116*(10), 1197–1214. https://doi.org/10.1061/(ASCE)0733-9429(1990)116:10(1197)

Das, S., Das, R., & Mazumdar, A. (2013). Circulation Characteristics of Horseshoe Vortex in Scour Region around Circular Piers. *Water Science and Engineering*, *6*(1), 59–77. https://doi.org/10.3882/j.issn.1674-2370.2013.01.005

ESI Group. (2019). *OpenFOAM® - Official Home of the Open Source Computational Fluid Dynamics (CFD) Toolbox*. https://www.openfoam.com/

Ettema, R., Constantinescu, G., & Melville, B. W. (2011). Evaluation of Bridge Scour Research: Pier Scour Processes and Predictions. *National Cooperative Highway Research Program (NCHRP Project 24-27(01))*. https://doi.org/10.17226/22886

Ettema, R., Constantinescu, G., & Melville, B. W. (2017). Flow-Field Complexity and Design Estimation of Pier-Scour Depth: Sixty Years Since Laursen and Toch. *Journal of Hydraulic Engineering*, *143*(9), 03117006. https://doi.org/10.1061/(ASCE)HY.1943-7900.0001330

Ettema, R., Kirkil, G., & Muste, M. (2006). Similitude of Large-Scale Turbulence in Experiments on Local Scour at Cylinders. *Journal of Hydraulic Engineering*, *132*(1), 33–40. https://doi.org/10.1061/(ASCE)0733-9429(2006)132

Ettema, R., Mostafa, E. A., Melville, B. W., & Yassin, A. A. (1998). Local Scour at Skewed Piers. *Journal of Hydraulic Engineering*, *124*(7), 756–759. https://doi.org/10.1061/(ASCE)0733-9429(1998)124:7(756)

Ettema, R., Nakato, T., & Muste, M. (2006). An Illustrated Guide for Monitoring and Protecting Bridge Waterways against Scour. *Iowa Highway Research Board Project TR-515*. http://www.iihr.uiowa.edu/wp-content/uploads/2013/06/TR449-Guide-for-Monitoring....pdf

Froehlich, D. C. (2013). Protecting Bridge Piers with Loose Rock Riprap. *Journal of Applied Water Engineering and Research*, *1*(1), 39–57. https://doi.org/10.1080/23249676.2013.828486

Gaudio, R., Tafarojnoruz, A., & Calomino, F. (2012). Combined Flow-Altering Countermeasures against Bridge Pier Scour. *Journal of Hydraulic Research*, *50*(1), 35–43. https://doi.org/10.1080/00221686.2011.649548

Ghaderi, A., & Abbasi, S. (2019). CFD simulation of local scouring around airfoil-shaped bridge piers with and without collar. *Sadhana*, *44*(216), 1–12. https://doi.org/10.1007/s12046-019-1196-8

Ghorbani, B., & Kells, J. A. (2008). Effect of Submerged Vanes on the Scour Occurring at a Cylindrical Pier. *Journal of Hydraulic Research*, *46*(5), 610–619. https://doi.org/10.3826/jhr.2008.3003

Gris, R. B. (2010). Sheath for Reducing Local Scour in Bridge Piers. *International Conference on Scour and Erosion 2010*, 987–996. https://doi.org/10.1061/41147(392)99

Gritskevich, M. S., Garbaruk, A. V., Schütze, J., & Menter, F. R. (2012). Development of DDES and IDDES Formulations for the k-ω Shear Stress Transport Model. *Flow, Turbulence and Combustion*, *88*, 431–449. https://doi.org/10.1007/s10494-011-9378-4

Hager, W. H., & Castro-Orgaz, O. (2017). William Froude and the Froude Number. *Journal of Hydraulic Engineering*, *143*(4), 02516005. https://doi.org/10.1061/(asce)hy.1943-7900.0001213

Hains, D. B., & Zabilansky, L. J. (2004). Laboratory Test of Scour Under Ice: Data and Preliminary Results. *US Army Corps of Engineers Research and Development Center, Cold Regions Research and Engineering Laboratory, Technical Report TR-04-9*.

Hanrahan, T. P., Dauble, D. D., & Geist, D. R. (2004). An Estimate of Chinook Salmon (Oncorhynchus Tshawytscha) Spawning Habitat and Redd Capacity Upstream of a Migration Barrier in the Upper Columbia River. *Canadian Journal of Fisheries and Aquatic Sciences*, *61*(1), 23–33. https://doi.org/10.1139/f03-140

Hong, J.-H., Chiew, Y.-M., Yeh, P.-H., & Chan, H.-C. (2017). Evolution of Local Pier-Scour Depth with Dune Migration in Subcritical Flow Conditions. *Journal of Hydraulic Engineering*, *143*(4), 04016098. https://doi.org/10.1061/(ASCE)HY.1943-7900.0001261

Hosur, S. M., Ramesha, D. K., & Basu, S. (2014). Transient Simulation of Flow Past Smooth Circular Cylinder at Very High Reynolds Number Using OpenFOAM. *Applied Mechanics and Materials*, *592–594*, 1972–1977. https://doi.org/10.4028/www.scientific.net/AMM.592-594.1972

Idil-Bektur, P., & Ettema, R. (2017). Large-Flume Observations of Scour at Bridge Abutments with Weak Compacted-Soil Embankment Approaches. *Journal of Hydraulic Engineering*, *143*(11), 06017020. https://doi.org/10.1061/(asce)hy.1943-7900.0001375

Issa, R. I. (1986). Solution of the Implicitly Discretised Fluid Flow Equations by Operator-Splitting. *Journal of Computational Physics*, *62*(1), 40–65. https://doi.org/https://doi.org/10.1016/0021-9991(86)90099-9

Jamieson, E. C., Post, G., & Rennie, C. D. (2010). Spatial Variability of Three-Dimensional Reynolds Stresses in a Developing Channel Bend. *Earth Surface Processes and Landforms*, *35*(9), 1029–1043. https://doi.org/10.1002/esp.1930

Jamieson, E. C., Rennie, C. D., & Townsend, R. D. (2013). 3D Flow and Sediment Dynamics in a Laboratory Channel Bend with and without Stream Barbs. *Journal of Hydraulic Engineering*, *139*(2), 154–166. https://doi.org/10.1061/(asce)hy.1943-7900.0000655

Jones, J. S., Kilgore, R. T., & Mistichelli, M. P. (1992). Effects of Footing Location on Bridge Pier Scour. *Journal of Hydraulic Engineering*, *118*(2), 280–290. https://doi.org/10.1061/(ASCE)0733-9429(1992)118:2(280)

Kirkil, G., Constantinescu, G., & Ettema, R. (2005). The Horseshoe Vortex System around a Circular Bridge Pier on Equilibrium Scoured Bed. *World Water and Environmental Resources Congress 2005: Impacts of Global Climate Change*, 1–12. https://doi.org/10.1061/40792(173)414

Knopp, T., Eisfeld, B., & Calvo, J. B. (2009). A New Extension for k-ω Turbulence Models to Account for Wall Roughness. *International Journal of Heat and Fluid Flow*, *30*(1), 54–65. https://doi.org/10.1016/j.ijheatfluidflow.2008.09.009

Kumar, V., Raju, K. G. R., & Vittal, N. (1999). Reduction of Local Scour around Bridge Piers Using Slots and Collars. *Journal of Hydraulic Engineering*, *125*(12), 1302–1305. https://doi.org/10.1061/(ASCE)0733-9429(1999)125:12(1302)

Lagasse, P. F., Clopper, P. E., Pagan-Ortiz, J. E., Zevenbergen, L. W., Arneson, L. A., Schall, J. D., & Girard, L. G. (2009). Bridge Scour and Stream Instability Countermeasures: Experience, Selection, and Design Guidance-Third Edition (Vols. 1 and 2). *Hydraulic Engineering Circular 23 (HEC-23)*.

Lagasse, P. F., Clopper, P. E., Zevenbergen, L. W., & Girard, L. G. (2007). Countermeasures to Protect Bridge Piers from Scour. *National Cooperative Highway Research Program (NCHRP Report 593)*. www.TRB.org

Lai, Y. G. (2018). Development and Verification of a Three-Dimensional Model for Flow Hydrodynamic and Sediment Transport Simulation. *World Environmental and Water Resources Congress 2018*, *1*, 18–30. https://doi.org/10.1061/9780784481424.003

Larsson, K., & Jog, D. (2014). Performance of Micropiles Used to Underpin Highway Bridges. *Journal of Performance of Constructed Facilities*, *28*(3), 592–607. https://doi.org/10.1061/(asce)cf.1943-5509.0000426

Lauchlan, C. S., & Melville, B. W. (2001). Riprap Protection at Bridge Piers. *Journal of Hydraulic Engineering*, *127*(5), 412–418. https://doi.org/10.1111/j.1475-4983.2008.00808.x

Li, S. S. (2012). Estimates of the Manning's Coefficient for Ice-Covered Rivers. *Proceedings of the Institution of Civil Engineers - Water Management*, *165*(9), 495–505. https://doi.org/10.1680/wama.11.00017

Lu, J.-Y., Hong, J.-H., Su, C.-C., Wang, C.-Y., & Lai, J.-S. (2008). Field Measurements and Simulation of Bridge Scour Depth Variations during Floods. *Journal of Hydraulic Engineering*, *134*(6), 810–821. https://doi.org/10.1061/(ASCE)0733-9429(2008)134:6(810)

Marris, A. W. (1964). A Review on Vortex Streets, Periodic Wakes, and Induced Vibration Phenomena. *Journal of Basic Engineering*, *86*(2), 185–193. https://doi.org/10.1115/1.3653027

Marshall, J., Hill, C., Perelman, L., & Adcroft, A. (1997). Hydrostatic, Quasi-Hydrostatic, and Nonhydrostatic Ocean Modeling. *Journal of Geophysical Research*, *102*(C3), 5733–5752.

Mashahir, M. B., Zarrati, A. R., & Mokallaf, E. (2010). Application of Riprap and Collar to Prevent Scouring around Rectangular Bridge Piers. *Journal of Hydraulic Engineering*, *136*(3), 183–187. https://doi.org/10.1061/(ASCE)HY.1943-7900.0000145

Maza, M., Lara, J. L., & Losada, I. J. (2015). Tsunami Wave Interaction with Mangrove Forests: A 3-D Numerical Approach. *Coastal Engineering*, *98*, 33–54. https://doi.org/10.1016/j.coastaleng.2015.01.002

Melville, B. W. (2008). The Physics of Local Scour at Bridge Piers. *Proceedings of the 4th International Conference on Scour and Erosion*, 28–40. https://hdl.handle.net/20.500.11970/100095

Melville, B. W., & Hadfield, A. C. (1999). Use of Sacrificial Piles as Pier Scour Countermeasures. *Journal of Hydraulic Engineering*, *125*(11), 1221–1224. https://doi.org/10.1061/(ASCE)0733-9429(1999)125:11(1221)

Melville, B. W., Parola, A. C., & Coleman, S. E. (2008). Chapter 11: Bridge-Scour Prevention and Countermeasures. In *Sedimentation Engineering* (pp. 543–577). https://doi.org/10.1061/9780784408148.ch11

Melville, B. W., van Ballegooy, R., & van Ballegooy, S. (2006). Flow-Induced Failure of Cable-Tied Blocks. *Journal of Hydraulic Engineering*, *132*(3), 324–327. https://doi.org/10.1061/(ASCE)0733-9429(2006)132

Menter, F. R. (1992). Improved Two-Equation κ-ω Turbulence Models for Aerodynamic Flows. *National Aeronautics and Space Administration (NASA TM-103975)*.

Menter, F. R., Kuntz, M., & Langtry, R. (2003). Ten Years of Industrial Experience with the SST Turbulence Model. *Turbulence, Heat and Mass Transfer 4*, 625–632.

Milne-Thomson, L. M. (1973). *Theoretical Aerodynamics (4th Edition)*. Dover Publications.

Parente, A., Gorlé, C., van Beeck, J., & Benocci, C. (2011). A Comprehensive Modelling Approach for the Neutral Atmospheric Boundary Layer: Consistent Inflow Conditions, Wall Function and Turbulence Model. *Boundary-Layer Meteorology*, *140*, 411–428. https://doi.org/10.1007/s10546-011-9621-5

Parker, G., Toro-Escobar, C., & Voigt, R. L. J. (1998). Countermeasures to Protect Bridge Piers from Scour. *National Cooperative Highway Research Program (NCHRP 24-7)*. http://hdl.handle.net/11299/108221

Parsapour-Moghaddam, P., & Rennie, C. D. (2017). Hydrostatic versus Nonhydrostatic Hydrodynamic Modelling of Secondary Flow in a Tortuously Meandering River: Application of Delft3D. *River Research and Applications*, *33*(9), 1400–1410. https://doi.org/10.1002/rra.3214

Ramos, P., Pêgo, J. P., & Maia, R. (2014). Numerical Simulation of the Flow around a Pier Using OpenFOAM. *3rd IAHR Europe Congress*, 1–12.

Raudkivi, A. J. (1986). Functional Trends of Scour at Bridge Piers. *Journal of Hydraulic Engineering*, *112*(1), 1–13. https://doi.org/10.1061/(ASCE)0733-9429(1986)112:1(1)

Raudkivi, A. J., & Ettema, R. (1983). Clear-Water Scour at Cylindrical Piers. *Journal of Hydraulic Engineering*, *109*(3), 338–350. https://doi.org/10.1061/(ASCE)0733-9429(1983)109:3(338)

Richards, P. J., & Hoxey, R. P. (1993). Appropriate Boundary Conditions for Computational Wind Engineering Models using the k-ϵ Turbulence Model. *Journal of Wind Engineering and Industrial Aerodynamics*, *46–47*, 145–153. https://doi.org/10.1016/0167-6105(93)90124-7

Saha, R. K., Zhang, C., & Ray, M. B. (2015). Similitude in an Open-Channel UV Wastewater Disinfection Reactor. *Journal of Environmental Engineering*, *141*(3), 04014065. https://doi.org/10.1061/(asce)ee.1943-7870.0000902

Sarker, A. (1998). Flow Measurement around Scoured Bridge Piers using Acoustic-Doppler Velocimeter (ADV). *Flow Measurement and Instrumentation*, *9*(4), 217–227. https://doi.org/10.1016/S0955-5986(98)00028-4

Schwimmer, R. (2019). *Teaching Sedimentary Geology in the 21st Century: Calculation of Stream Discharge Required to Move Bed Material*. Teach the Earth. https://serc.carleton.edu/NAGTWorkshops/sedimentary/activities/14100.html

Shen, H. T., & Wang, D. S. (1995). Under Cover Transport and Accumulation of Frazil Granules. *Journal of Hydraulic Engineering*, *121*(2), 184–195. https://doi.org/10.1061/(ASCE)0733-9429(1995)121:2(184)

Sheppard, D. M., Jones, J. S., Odeh, M., & Glasser, T. (2000). Local Sediment Scour Model Tests for the Woodrow Wilson Bridge Piers. *Joint Conference on Water Resource Engineering and Water Resources Planning and Management 2000*, 1–9. https://doi.org/10.1061/40517(2000)132

Shim, J., Duan, J., & Jo, H. (2016). Simulating Sediment Transport around a Bridge Pier Using Open FOAM Software. *World Environmental and Water Resources Congress 2016*, 362–369. https://doi.org/10.1061/9780784479872.037

Simpson, R. L. (2013). Full-Scale Prototype Testing and Manufacturing and Installation Plans for New Scour- Vortex-Prevention scAUR TM and VorGAUR TM Products for a Representative Scour-critical Bridge. *NCHRP- IDEA Project 162 Final Report Prepared for the Transportation Research Board*. https://nebula.wsimg.com/3edffcb27cebffbca3f4114d7cbf21ad?AccessKeyId=DE796BC2996E25316182&disposition=0&alloworigin=1

Sirianni, D. A. B., Valela, C., Rennie, C. D., Nistor, I., & Almansour, H. (n.d.). Effects of Developing Ice Covers on Local Bridge Pier Scour. *Journal of Hydraulic Research*. [In review].

Spalart, P. R., Jou, W.-H., Strelets, M., & Allmaras, S. R. (1997). Comments on the Feasibility of LES for Wings, and on a Hybrid RANS/LES Approach. *Advances in DNS/LES: Proceedings of the First AFOSR International Conference on DNS/LES*, 137–147.

Speziale, C. G. (1991). Analytical Methods for the Development of Reynolds-Stress Closures in Turbulence. *Annual Review of Fluid Mechanics*, *23*, 107–157. https://doi.org/https://doi.org/10.1146/annurev.fl.23.010191.000543

Stevens, M. A., Gasser, M. M., & Saad, M. B. A. M. (1991). Wake Vortex Scour at Bridge Piers. *Journal of Hydraulic Engineering*, *117*(7), 891–904. https://doi.org/10.1061/(ASCE)0733-9429(1991)117:7(891)

Strelets, M. (2001). Detached Eddy Simulation of Massively Separated Flows. *39th Aerospace Sciences Meeting and Exhibit 2001*, 1–18. https://doi.org/10.2514/6.2001-879

Sui, J., Wang, D., & Karney, B. W. (2000). Suspended Sediment Concentration and Deformation of Riverbed in a Frazil Jammed Reach. *Canadian Journal of Civil Engineering*, *27*(6), 1120–1129. https://doi.org/https://doi.org/10.1139/l00-038

Sui, J., Wang, J., He, Y., & Krol, F. (2010). Velocity Profiles and Incipient Motion of Frazil Particles under Ice Cover. *International Journal of Sediment Research*, *25*(1), 39–51. https://doi.org/10.1016/S1001-6279(10)60026-1

Tabarestani, M. K., & Zarrati, A. R. (2013). Design of Stable Riprap around Aligned and Skewed Rectangular Bridge Piers. *Journal of Hydraulic Engineering*, *139*(8), 911–916. https://doi.org/10.1061/(ASCE)HY.1943-7900.0000731

Tafarojnoruz, A., & Lauria, A. (2020). Large Eddy Simulation of the Turbulent Flow Field around a Submerged Pile within a Scour Hole under Current Condition. *Coastal Engineering Journal*, *62*(4), 489–503. https://doi.org/10.1080/21664250.2020.1807453

Valela, C., Nistor, I., & Rennie, C. D. (2018). Reduction of Bridge Pier Scour Through the use of a Novel Collar Design. *6th International Disaster Mitigation Specialty Conference 2018; Canadian Society for Civil Engineering*, 235–244.

Valela, C., Nistor, I., Rennie, C. D., Lara, J. L., & Maza, M. (2021). Hybrid Modelling for Design of a Novel Bridge Pier Collar for Reducing Scour. *Journal of Hydraulic Engineering*, *147*(5), 04021012. https://doi.org/10.1061/(ASCE)HY.1943-7900.0001875

Valela, C., Rennie, C. D., & Nistor, I. (2021). Improved Bridge Pier Collar for Reducing Scour. *International Journal of Sediment Research*. https://doi.org/10.1016/j.ijsrc.2021.04.004

Valela, C., Rennie, C. D., & Nistor, I. (2019). A Novel Collar Design to Mitigate Bridge Pier Scour. *38th IAHR World Congress*, 4391–4400. https://doi.org/10.3850/38WC092019-0671

Valela, C., Sirianni, D. A. B., Nistor, I., Rennie, C. D., & Almansour, H. (2021). Bridge Pier Scour under Ice Cover. *Water*, *13*(536), 1–17. https://doi.org/10.3390/w13040536

Vijayasree, B. A., Eldho, T. I., Mazumder, B. S., & Ahmad, N. (2019). Influence of Bridge Pier Shape on Flow Field and Scour Geometry. *International Journal of River Basin Management*, *17*(1), 109–129. https://doi.org/10.1080/15715124.2017.1394315

Vittal, N., Kothyari, U. C., & Haghighat, M. (1994). Clear-Water Scour around Bridge Pier Group. *Journal of Hydraulic Engineering*, *120*(11), 1309–1318. https://doi.org/10.1061/(ASCE)0733-9429(1994)120:11(1309)

Wilcox, D. C. (2006). *Turbulence Modelling for CFD (Third Edition)*. DCW Industries.

Wu, P., Balachandar, R., & Sui, J. (2016). Local Scour around Bridge Piers under Ice-Covered Conditions. *Journal of Hydraulic Engineering*, *142*(1), 04015038. https://doi.org/10.1061/(ASCE)HY.1943-7900.0001063

Wuebben, J. L. (1988). A Preliminary Study of Scour under an Ice Jam. *Proceedings of the 5th Workshop on Hydraulics of River Ice / Ice Jams*, 177–192.

Yoon, T. H., & Kim, D.-H. (2001). Bridge Pier Scour Protection by Sack Gabions. *World Water and Environmental Resources Congress*. https://doi.org/10.1061/40569(2001)256

Zabilansky, L. J. (2002). Ice Cover Effects on Bed Scour: Case Studies. *11th International Conference on Cold Regions Engineering*, 795–803. https://doi.org/10.1061/40621(254)68

Zabilansky, L. J., Hains, D. B., & Remus, J. I. (2006). Increased Bed Erosion Due to Ice. *13th International Conference on Cold Regions Engineering*, 1–12. https://doi.org/10.1061/40836(210)16

Zare, S. G. A., Moore, S. A., Rennie, C. D., Seidou, O., Ahmari, H., & Malenchak, J. (2016). Boundary Shear Stress in an Ice-Covered River during Breakup. *Journal of Hydraulic Engineering*, *142*(4), 04015065. https://doi.org/10.1061/(ASCE)HY.1943-7900.0001081

Zarrati, A. R., Gholami, H., & Mashahir, M. B. (2004). Application of Collar to Control Scouring around Rectangular Bridge Piers. *Journal of Hydraulic Research*, *42*(1), 97–103. https://doi.org/10.1080/00221686.2004.9641188

Zarrati, A. R., Nazariha, M., & Mashahir, M. B. (2006). Reduction of Local Scour in the Vicinity of Bridge Pier Groups Using Collars and Riprap. *Journal of Hydraulic Engineering*, *132*(2), 154–162. https://doi.org/10.1061/(ASCE)0733-9429(2006)132

Appendix A. First Introduction of Collar Prototype No. 1 (CPN1)

Reduction of Bridge Pier Scour Through the Use of a Novel Collar Design

Preprint of a modified version of a conference proceeding printed in the 6th International Disaster Mitigation Specialty Conference © 2018 Canadian Society for Civil Engineering (CSCE).

Introduction and Objectives

There is not one ideal method that is low cost, maintenance-free, and easy to installation while guaranteeing protection under extreme flow conditions, which, as a result, is what motivated the research presented in this paper. There are three main objectives of this paper and they are to:

1) Introduce a new, state-of-the-art scour countermeasure for cylindrical piers which takes the shape of a collar,
2) Explain the workings of the new collar and its ability to overcome the problems associated with existing scour countermeasures, and
3) Perform a numerical modelling flow comparison between a pier with and without the new collar.

Methodology

Numerical Model

The design of the new pier scour countermeasure was guided intensively by the use of a numerical model. The modelling software chosen was the open-source computational fluid dynamics (CFD) software, OpenFOAM v1706, which was used to illustrate the flow behaviour in a channel in the presence of a bridge pier. The solver used within OpenFOAM was *pimpleFoam* operating in *piso* mode which is a transient solver applicable for turbulent, incompressible flows (Hosur et al., 2014). In order to replicate the experimental flow conditions best, the k-omega-SST Delayed Detached Eddy Simulation (DDES) turbulence model was utilized. Detached Eddy Simulation (DES) models switch between Reynolds-Averaged Navier-Stokes (RANS) and Large Eddy Simulation (LES) turbulence models based on the grid size and turbulent length scale for the purpose of reducing the computational cost that is normally associated with LES models. DDES turbulence models improve on the DES models by addressing the issue where the turbulence models switch by shielding the RANS model from the DES model (Gritskevich et al., 2012).

The model domain consisted of a rectangular flume 10m in length, 0.85m in width, and 0.15m in depth, filled entirely with water. A cylindrical pier, possessing a diameter (D) of 0.09m and a height of 0.15m tall, was generated used *snappyHexMesh* and situated 1.5m from the outlet. An 8.5m approach was used because, based on a sensitivity analysis, it was found that the flow becomes fully developed after approximately 8m. A flume width of 0.85m was used because when the walls are situated that far apart, they do not interfere with the wake generated by the pier.

In order to achieve the most accurate results while maintaining a reasonable computational cost, two refinement regions were used. First, a level one rectangular refinement, yielding a cell size of 0.004m, was used at the downstream end of the flume stretching 2m upstream by 0.5m across by 0.15m high, therefore encompassing the pier and downstream wake. Then, a level two cylindrical refinement, yielding a cell size of 0.002m, was used around the pier, 0.2m in diameter by 0.06m high, to ensure a high resolution result in the focus area at the base of the pier. In total, this complete mesh yielded a cell count of approximately 5.5 million cells and an average y+ value of 25 at the base of the pier. This mesh was chosen because a sensitivity analysis was performed consisting of six different meshes each possessing an equally finer mesh and the velocities at specified locations, for this chosen level of refinement, no longer changed in the focus region and remained constant for finer meshes.

The inlet velocity condition used was *turbulentInlet*, as it consists of an inlet velocity (u_{in}) which was set to 0.335m/s but also includes a turbulent fluctuation which was set to ten percent of the inflow velocity. The pier and the bottom of the flume were given a *noSlip* condition, while the walls were given a *slip* condition to ensure the walls had as little impact on the passing flow as possible. The top of the flume, which was filled to the surface with water, utilized a *symmetryPlane* to reduce the influence of the top boundary on the flow behaviour especially around the pier. Wall functions were used for the pier and bottom of the flume specifically employing the nutkWallFunction and the nutkRoughWallFunction, respectively. The rough wall function was used only for the bottom of the flume because it allows for the bed roughness to be specified, which in this case was 0.001m. To ensure the most efficient computational time, *adjustTimeStep* was turned on such that it adjusted the time step to maintain a maximum Courant number of 0.8. In order to calibrate and further validate the results obtained from the numerical model, preliminary experimental tests were performed in a laboratory setting.

Experimental Setup

The experimental tests were conducted within a straight rectangular flume possessing a length of 30m, a width of 1.5m, and a depth of 0.5m, located in the University of Ottawa's Civil Engineering Hydraulics Laboratory. The focus area was a 4m long section located 3m from the downstream end of the flume. This section possessed a rigid concrete floor surfaced with sieved silica sand possessing a median grain size diameter (d_{50}) of 0.001m, which was affixed to the concrete surface in a uniform layer. The purpose of using a fixed floor was to replicate the conditions within the numerical model since OpenFOAM is not equipped with sediment

modelling capabilities. In the center of the 4m long focus area of the flume, a cylindrical acrylic pier with a diameter (D) of 0.09m was installed to the floor vertically. The tests were run under constant flow conditions where the flow depth (y) was set to 0.15m and the depth-averaged flow velocity (u_{avg}) was maintained at 0.34m/s at a height of 0.07m above the bottom. To measure the velocity, an acoustic Doppler velocimeter (ADV) was used. The values used for both experimental and numerical tests were based off of a 1:30 Froude scale.

Model Validation

In order to validate the numerical model, velocity profiles of the flow were taken in the laboratory flume using the ADV at three locations: 0.72m upstream of the pier where the flow is fully developed yet undisturbed by the pier, 0.14m upstream of the pier at the beginning of the stagnation region, and 0.75m downstream of the pier in the turbulent wake. The velocity profiles consist of a series of point measurements taken 0.05m apart in the vertical direction. A comparison between the velocity profiles obtained numerically and experimentally at the three locations can be seen in Fig. A-1. At all three locations the numerical model matched the experimental results respectively well indicating a high level of trust in the numerical results. The downstream location possesses error bars, representing the standard deviation, that are substantially larger than the other two locations due to the turbulence induced by the bridge pier.

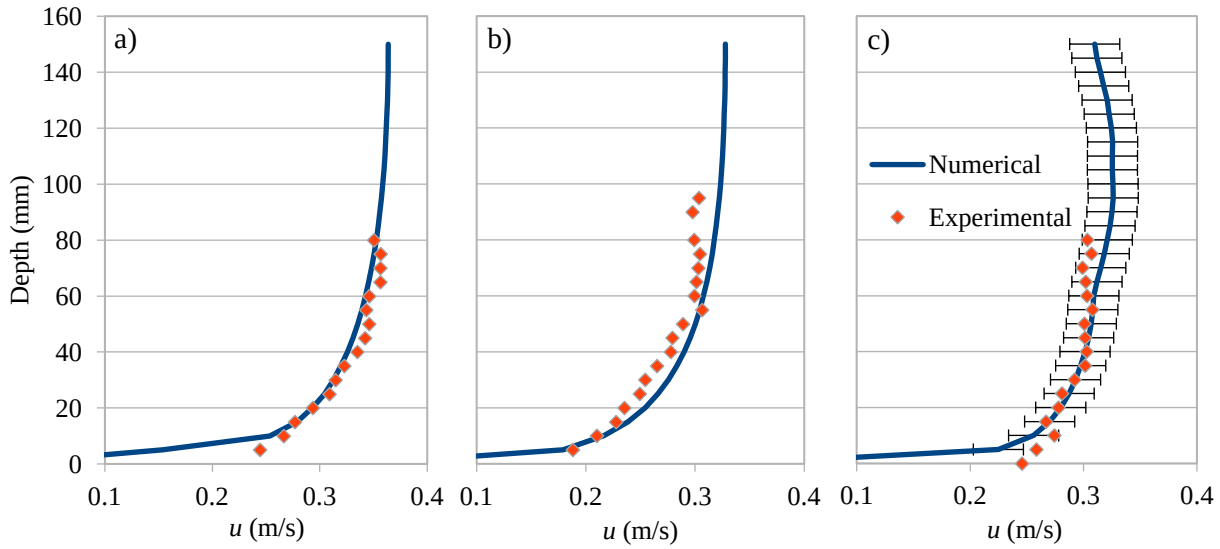

Fig. A-1. Velocity (u) profile comparison: (a) 0.72m upstream of pier, (b) 0.14m upstream of pier, and (c) 0.75m downstream of pier.

Scour Countermeasure Design

It is known that the largest contributor to pier scour is the horseshoe vortex, and then to a lesser degree, the wake vortices (Stevens et al., 1991). Therefore, if the goal is to reduce scour, then the horseshoe vortex must be addressed. The approach taken with this new countermeasure was to harness the horseshoe vortex rather than trying to interrupt or impede its very powerful forces. In doing so, the objective was to disallow the horseshoe vortex from contacting the

riverbed by containing it within a structure. This structure was formed into the shape of a circular collar which mounts around the pier and rests on the riverbed. The only similarity between this design and existing pier scour prevention collars is that both revolve around the pier, otherwise the differences are significant. Specifically, as the flow approaches the upstream face of the pier and is drawn downwards to the riverbed, this new collar design allows the flow of water to enter into a rounded cavity within the collar where it can circulate forming the common horseshoe vortex and propagate around the upstream face of the pier as it naturally would. This occurs within the collar cavity until it passes the sides of the pier, then the circulating flow is directed out of the rear of the collar and the energy is dissipated downstream. This can be seen in Fig. A-2 as the new collar design, more formally known as Collar Prototype No. 1 (CPN1), is presented. The main concern is to protect the immediate vicinity around the base of the pier especially on the upstream side and transfer the turbulent flow downstream away from the pier where it cannot harm the stability of the pier foundation.

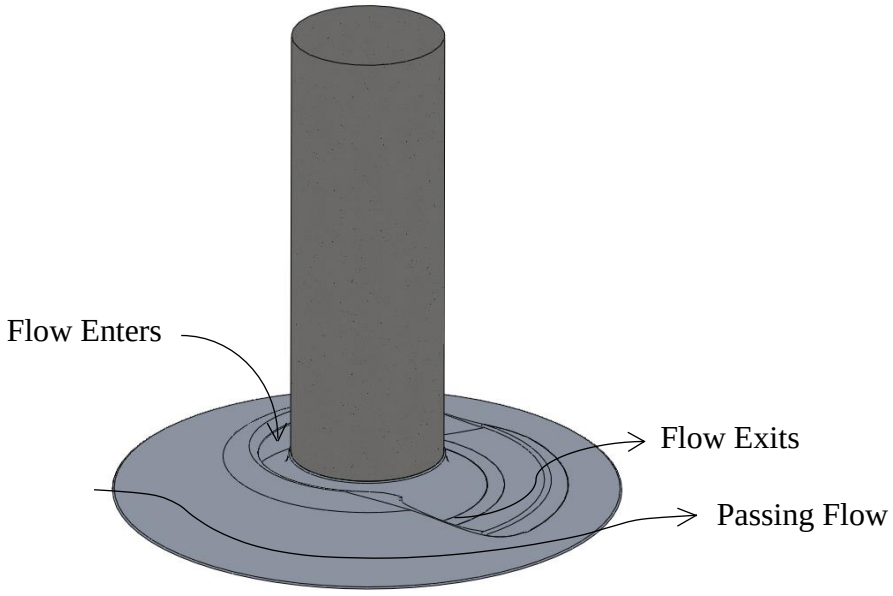

Fig. A-2. New countermeasure design (CPN1).

The remainder of the flow that does not enter into the collar cavity passes over the outer surface. The outer surface was designed in such a way that it slopes down to the riverbed, then curves outwards reaching a thin edge in an asymptotic fashion. This thin flat edge was incorporated to allow the passing flow to step smoothly onto and off of the collar generating as little turbulence as possible, therefore reducing the chances of scour occurring beneath the collar. In addition, the outer diameter of the collar was designed to be 3.3*D* because the optimal size for reducing scour is approximately 3*D* but in order to accommodate the inner cavity while maintaining the correct outer shape, a slightly larger diameter was required (Kumar et al., 1999). Therefore, any residual turbulence generated by the presence of the pier or raised collar region will not be able to contact the riverbed in the critical region around the pier because it is shielded

by the large diameter collar. Lastly, the gradual change in slope was then utilized to gently transition the flow that does not enter the collar cavity to bypass over the collar and around the pier with the goal of minimizing any additional vortices that may form as a result of the collar's presence.

Results

The numerical model was utilized throughout the design process as a tool to guide the changes made necessary to achieve a successful design. Specifically, stream tracers were used, as one of the main goals was to entirely contain the horseshoe vortex while using the smallest cavity possible for the purpose of reducing the influence on the passing flow. This took a series of trial and error iterations of analysing the stream tracers to obtain the correct diameter of the inner cavity and the correct outer slope. The shape was deemed successful and the design iterations were seized when the entire horseshoe vortex occurred inside the collar cavity and the redirected flow that did not enter the cavity remained on top of the collar's edge for the entire upstream half of the collar. Initial designs possessed a slope that was too steep which caused the flow that did not enter the cavity to be separated forming a secondary vortex immediately upstream of the collar on top of the riverbed. As a result, this would induce greater amounts of scour counteracting the purpose of the collar.

In Fig. A-3, a time-averaged comparison is presented showing the flow behaviour around a standard cylindrical pier and the same pier with CPN1. Fig. A-3(a), which shows the pier without the collar, illustrates the standard flow behaviour where the flow separates in the presence of the pier causing a majority to be redirected around the sides of the pier but also a large portion to be drawn down to the riverbed. In the stagnation region immediately upstream of the pier, almost all of the streamlines approaching the pier are drawn downwards to some degree in the z-direction; however, only the streamlines in approximately the bottom one-third of the water depth are drawn all the way down to the riverbed. This portion of the flow that does reach the riverbed, redirects itself into a circular path, propagating around the upstream face of the pier forming the famous horseshoe vortex. Meanwhile, the remainder of the flow that does not become drawn all the way down to the riverbed redirects itself around the sides of pier but increases in velocity while doing so. The combination of the horseshoe vortex and the increased velocity around the sides of the pier, especially at the base, is what causes the sediment in that region to be dislodged and transported downstream.

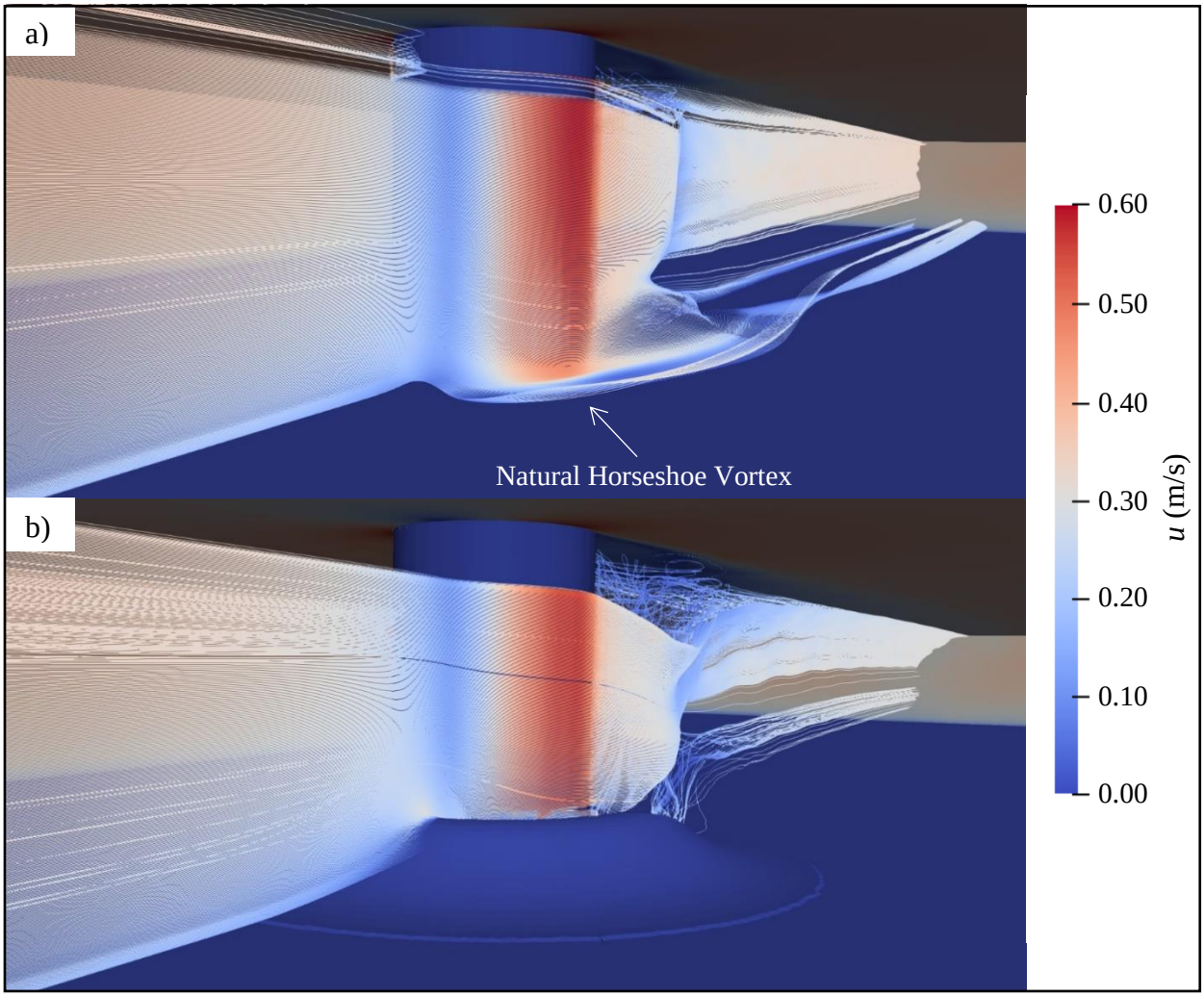

Fig. A-3. Upstream flow behaviour comparison: (a) without any scour countermeasure, and (b) with CPN1.

Fig. A-3(b) shows the flow behaviour as a result of adding the new collar. The streamlines approach the pier and separate in the same manner as when the collar is not present but any of the streamlines that are drawn down to the riverbed enter directly into the collar cavity, circulate within, and then exit out the rear without being interrupted. Due to the collar presence, both scour causing mechanisms, seen when the collar is not installed, are addressed. Firstly, the entire horseshoe vortex no longer contacts the riverbed because it occurs inside of the collar cavity. While secondly, the high velocity flow along the sides of the pier also can no longer induce higher shear stress on the riverbed as the collar protects the entire critical region around the pier. In addition, since the critical region is protected, wake vortices that are naturally generated and shed off of the sides and rear of the pier are not able to scour around the base as it is protected by the collar.

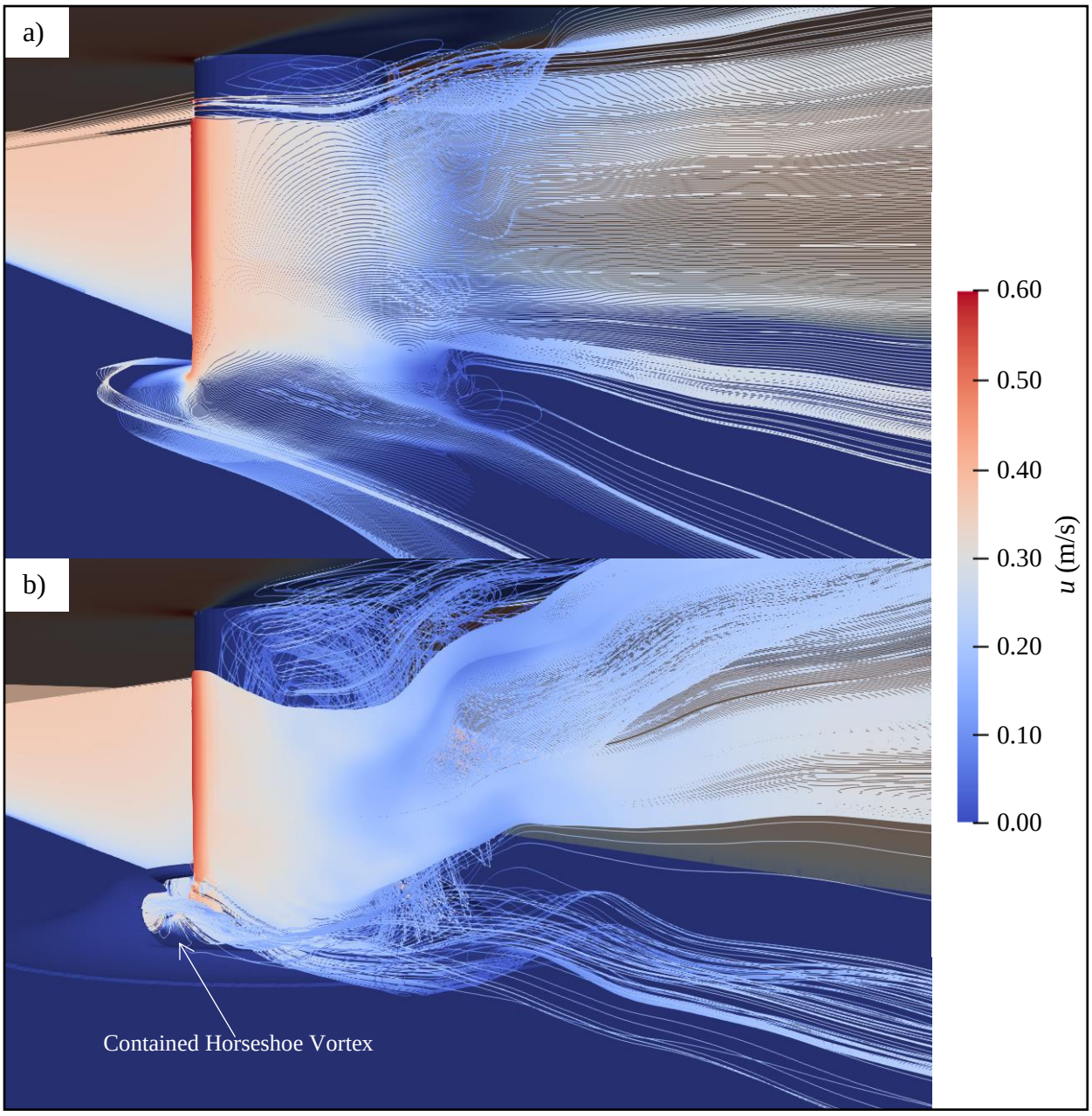

Fig. A-4. Downstream flow behaviour comparison: (a) without any scour countermeasure, and (b) with CPN1.

Fig. A-4 is another comparison at a different angle, looking upstream, of the time-averaged flow behaviour around a pier with and without the collar. When the collar is not present, as seen in Fig. A-4(a), the horseshoe vortex extends further out from the pier and naturally contacts a large area of riverbed. However, when the collar is installed, the vortex is contained in a more compact manner close to the pier, allowing the remaining flow that is passing by to smoothly traverse over the collar and around the sides of the pier. The benefit to such collar over other countermeasures is that the location and size of the horseshoe vortex is stationary and known despite varying flow conditions because it is confined to the predetermined

shape of the collar. Fig. A-4(b) confirms that the horseshoe vortex does actually occur inside the collar cavity because the stream tracers demonstrate the circulating motion within. Once the vortex passes the sides of the pier, it exits out the rear of the collar in an upward direction off of a spoiler. This helps lessen the contact between the exiting vortex and the riverbed, even though there is little harm in small amounts of scour occurring downstream of the pier outside of the critical region.

Discussion

CPN1 overcomes the installation issue faced with many other countermeasures because it can be constructed offsite in a specific facility. In doing so, the quality of the final product and the accuracy of the shape will be significantly better because there is access to more equipment in a weather controlled environment. To further simplify the installation, the collar will be constructed in pieces at the offsite location and transported to the pier site in smaller manageable sections. Upon arriving to the pier site, these sections will be bolted together around the pier and rested directly on the riverbed. It is crucial that when the collar is installed there is as small of a gap between the collar and pier as possible because the downward flow upstream of the pier will otherwise pass through the gap and erode underneath. This method of construction and installation is minimally intrusive as the pier does not need to be altered and no excavation of the existing riverbed is required, which ultimately results in less of an impact on the surrounding environment.

Another positive aspect of CPN1 is the lack of maintenance required. Once the collar is installed on the pier, for the remainder of the collar's life there is no foreseeable maintenance that is needed since increased flow will not harm the collar. If a large quantity of sediment is transported from upstream and enters into the collar cavity, due to the high velocity that occurs within the horseshoe vortex, the sediment will be washed out and sent downstream. Any stones or debris that are too large to be flushed out will be blocked from entering through the use of a screen affixed to the top of the cavity opening.

To further confirm the versatility and robustness of the design, experimental tests are underway in the laboratory. Numerous other existing scour countermeasures, in addition to CPN1, are being examined for comparison purposes under varying flow conditions.

The research presented in this paper possesses some limitations which are mainly attributed to the fact that the collar design is still in its infancy stage. The first limitation is that the collar was made for cylindrical piers only. The intention was to validate the design concept on cylindrical piers due to simplicity, then following validation, adapt it for different shaped piers such as square, rectangular, and elongated. Once the shape has been adapted, a solution will then be available for bridge piers of every shape. The second limitation is that the collar was designed for unidirectional flow only, while it is understood that some locations where piers are present experience tides or flows that change direction. The goal is to eventually adjust the design in such a way to accommodate flood and ebb tides but the current focus is on perfecting

unidirectional flow. The third limitation is that the physical construction and material of the actual full-size collar has yet to be determined as a thorough investigation into these areas still needs to be performed. The final limitation is that the collar was tested under only one flow velocity and that is due to the high computational cost associated with numerical modelling. However, upon achieving satisfactory results from the experimental tests for this collar design, additional velocities will be investigated to fully evaluate the collar's capabilities.

Conclusion

Bridge pier scour has been an issue for many years and a significant amount of time and money has been invested into researching the topic. Many countermeasures have been designed; however, there is not one solution that is ideal. The introduction of a new state-of-the-art three-dimensional collar looks to overcome issues existing in the previous scour countermeasures by being easy to install, minimally intrusive, maintenance free, and low cost. The newly proposed design, works by containing the horseshoe vortex that occurs on the upstream face and sides of the pier within a collar structure that prevents it from contacting the riverbed. As a result, the erosive forces associated with the horseshoe vortex occur within the inner collar cavity and scour is avoided. Therefore, this novel design has the potential to change the way bridge pier scour is currently being addressed and will significantly improve the safety of bridges.

Appendix B. Countermeasure Design and Validation Methodology

Achieving a new countermeasure that proved to be greatly effective at reducing scour required a lengthy iterative design process. Such procedure is outlined in Fig. B-1.

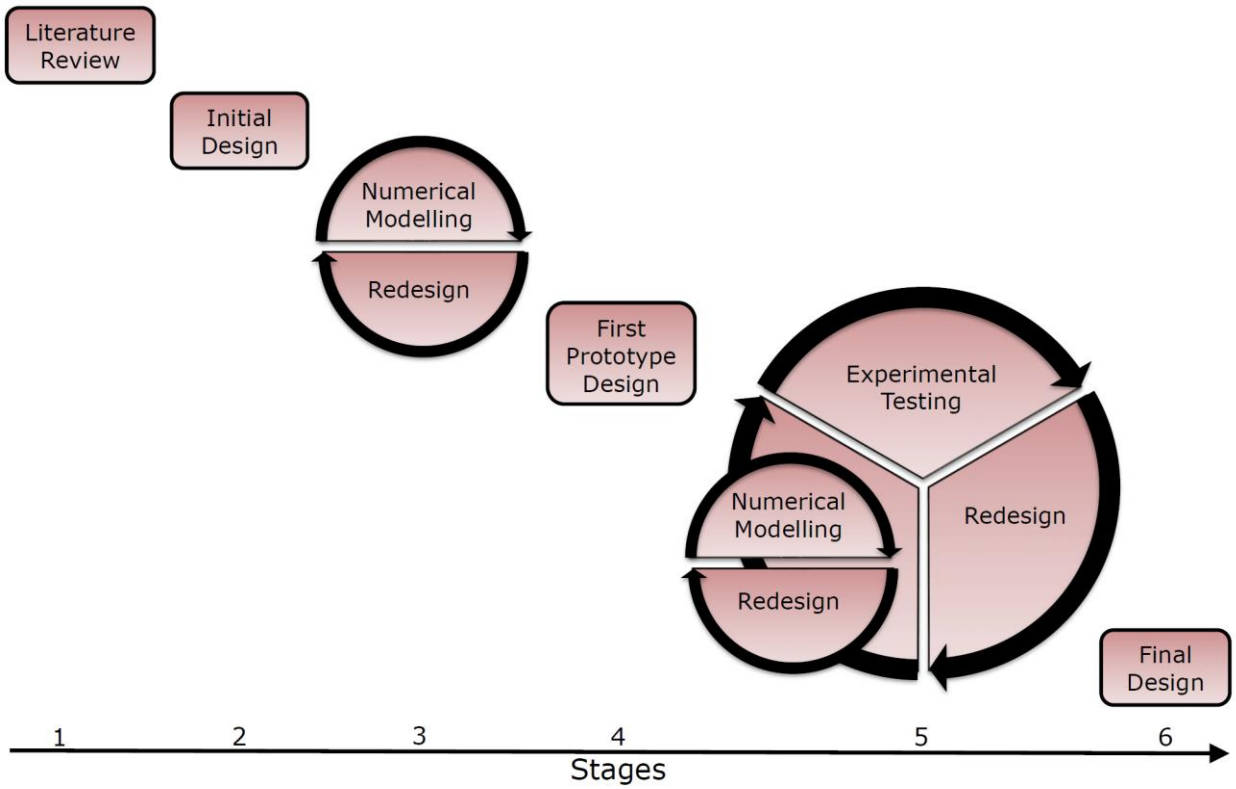

Fig. B-1. Countermeasure design procedure.

Stage 1 began with an in-depth literature review (Chapter 2), which investigated the advantages and disadvantages of each of the common bridge pier scour countermeasures. Upon better understanding the factors that constitute a successful countermeasure, an initial design was created (stage 2). The initial design was not tested or validated at this point, as it was simply a draft. Stage 3 then consisted of computer simulations, using the numerical model discussed earlier, to begin evaluating the performance of the new design. The simulations provided flow field and bed shear stress estimates around the pier and countermeasure, allowing for the scour in the region to be predicted. After a number of redesigns and improvements, a countermeasure shape was reached which reduced shear stress on the bed and was therefore believed to reduce scour. The first prototype was constructed of this design for the purpose of experimental testing (stage 4).

The results of the experimental tests provided valuable information into the required design changes, which was otherwise unattainable from the numerical model. Stage 5 consisted of numerous iterations through the cycle of redesigning, numerical modelling, and experimental testing. The countermeasure designs presented in this thesis only consist of a limited number of the total designs created. Traditional countermeasures were also tested and compared, as they acted as the minimum threshold for when to seize iterations in stage 5. Once a design was reached that outperformed existing countermeasures and was optimized as much as reasonably possible, it was deemed the final design (stage 6).

Appendix C. Model Scaling

Determining the size and scaling of the experimental and numerical tests was done based on three main components: pier diameter (*D*), flow depth (*y*), and pier spacing. The goal was to select a model scale *D* such that it was relatively large but did not block the passing flow as to induce a backwater effect. If *D* is smaller than 10% of the flume width, then the effects of contraction will not occur, and a backwater will be avoided (Raudkivi & Ettema, 1983; Sarker, 1998). The chosen model scale *D* for all experimental and numerical tests in this thesis was 0.09m, as it blocks the passing flow by only 6% and was an easily obtainable size (Chang et al., 2004; Kumar et al., 1999).

The scour that occurs around a pier is influenced by *y*, in conjunction with *D* (as well as other parameters), but such combination can be categorized based on the ratio of *y/D* (Arneson et al., 2012; Ettema et al., 2011). When this ratio is less than 1.4, the pier is classified as being wide or transitional and a change in *y* will greatly affect the quantity of scour. Whereas, when this ratio is larger than 1.4, the pier is classified as being narrow and an increase in *y* will have only a minor impact on the quantity of scour (Ettema et al., 2011). Therefore, $y = 0.15$m was used for a majority of tests as a ratio of 1.6 was obtained, given $D = 0.09$m. The purpose of this was to ensure that any fluctuations in *y*, amongst different countermeasure tests, would have as minimal affect on scour as possible.

The chosen geometric scaling ratio was 1:30 as it was found to yield the most suitable prototype scale dimensions, as seen in Table C-1(Idil-Bektur & Ettema, 2017; Sheppard et al., 2000). Using such scaling ratio, the prototype scale *D*, *y*, and pier spacing was 2.7m, 4.5m, and 21m, respectively. Had a larger scaling ratio been used (1:20 for example), then the prototype scale pier spacing would have been smaller which is less realistic. Whereas, if a smaller scaling ratio was used (1:40 for example), then the prototype scale *D* would have been larger which is also unrealistic. Given the characteristics of the flume and the concepts that were being studied, the chosen dimensions and scaling ratio were the most practical.

Table C-1. Summary of geometric scaling components.

Geometric Scaling (1:30)		
	Model Scale (m)	Prototype Scale (m)
Pier diameter (*D*)	0.09	2.7
Flow depth (*y*)	0.15	4.5
Pier spacing	0.7	21

In order to scale the other components within this study, such as velocity and time, the Froude number modelling approach was used. The corresponding scaling factor for velocity and time was 5.5, as calculated below in Eq. 13.

$$\lambda_u = \lambda_t = \sqrt{\lambda_L} \tag{13}$$
$$= \sqrt{30}$$
$$\approx 1:5.5$$

Where λ_L is the geometric scaling ratio, λ_u is the velocity scaling ratio, and λ_t is the temporal scaling ratio (Saha et al., 2015).

When the depth-averaged flow velocity (u_{avg}) of 0.34m/s is scaled up from model scale to prototype scale, it yields a u_{avg} of approximately 2m/s (1.87m/s). This prototype scale u_{avg} is common within rivers, such that to put it into perspective, Chinook salmon typically spawn within flows possessing a u_{avg} of 0.25-2.25m/s (Hanrahan et al., 2004).

To ensure that the same Froude number was maintained for the flow conditions at model and prototype scale, the Froude numbers for each are calculated below using Eq. 14.

$$\mathrm{Fr} = \frac{u_{avg}}{\sqrt{gy}} \tag{14}$$

Prototype:

$$\mathrm{Fr} = \frac{1.87}{\sqrt{9.81*4.5}}$$

$$\mathrm{Fr} = 0.28$$

Model:

$$\mathrm{Fr} = \frac{0.34}{\sqrt{9.81*0.15}}$$

$$\mathrm{Fr} = 0.28$$

Where g is the gravitational acceleration constant (Hager & Castro-Orgaz, 2017).

The sand used for the laboratory experiments performed at the University of Ottawa (majority of experiments presented in this thesis) was silica sand with a median particle diameter (d_{50}) of 0.001m (Chang et al., 2004; Mashahir et al., 2010; Vittal et al., 1994). This d_{50} was chosen because of its lack of cohesiveness, ease of access, and realistic prototype scale size (Vittal et al., 1994). The corresponding prototype scale d_{50} is approximately 0.0154m and that value was calculated using the Shields curve, which can be seen in Fig. C-1. First, the Shields stress and the boundary Reynolds number were determined for the model scale sediment, for both the critical and laboratory condition. The difference between these two conditions in terms of Shields stress was measured and recorded, as such distance of the laboratory condition below the critical condition is important when scaling up to prototype scale. Then, assuming the prototype scale sediment lies on the horizontal portion of the Shields curve, the Shields stress was determined, corresponding to the critical condition. Lastly, using both, the Shields stress at the critical condition, and the measured distance between the laboratory and critical condition for the model scale sediment, the prototype scale d_{50} was calculated.

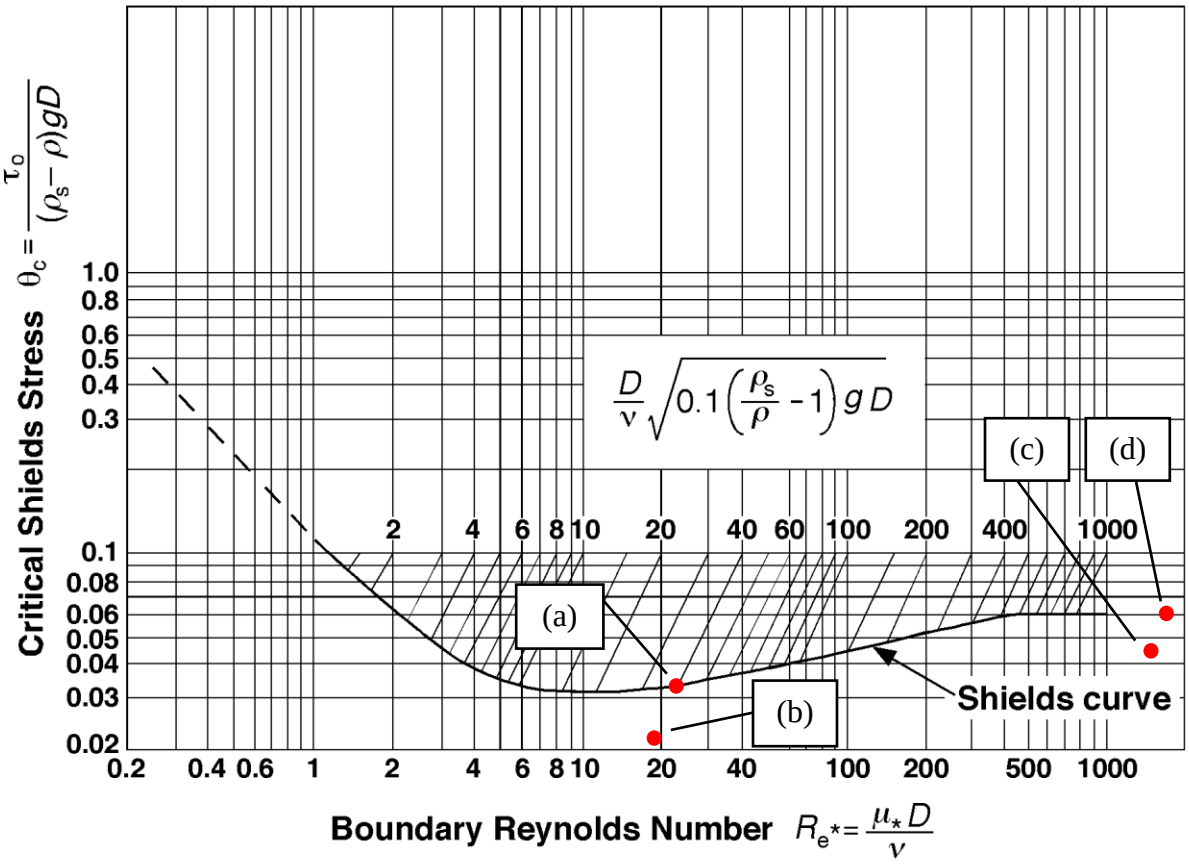

Fig. C-1. Shields curve used for sediment scaling: (a) model scale sediment critical condition, (b) model scale sediment lab condition, (c) prototype scale sediment equivalent condition, and (d) prototype scale sediment critical condition (Schwimmer, 2019).

Appendix D. Numerical Model

Single-Phase Versus Multiphase domain

The OpenFOAM solver that was employed is pimpleFoam, which is a transient solver designed for incompressible fluids. For this specific application, the solver was run in Pressure Implicit Split-Operator (PISO) mode which solves the Navier-Stokes equations through the predictor-corrector approach (Issa, 1986). The pimpleFoam solver is only applicable for single-phase flow, implying that the simulations consist of only water and not a body of air above. When there is both, a volume of water and a volume of air, this is referred to as multiphase flow. pimpleFoam was chosen specifically because it is designed for only single-phase flow (ESI Group, 2019).

The benefit to having only single-phase flow simulations is the reduced computational cost, and since the focus of this research pertains to the flow behaviour around the base of bridge piers, the air above the water surface is not largely influential. Furthermore, it was found that some of the multiphase flow solvers experienced difficulties calculating the correct velocity at the boundary between air and water, therefore making such solvers even less desirable.

It is understood that omitting the region of air above the domain could induce some inaccuracies in the flow field around the pier. The reason for this is primarily because the lack of air region above the water prohibits the generation of the bow wave on the front face of the pier. Without the bow wave, the water surface elevation directly in front of the pier does not increase, therefore reducing the downflow experienced on the front of the pier. The downflow is important in pier scour problems because it is a primary driver in the powerful horseshoe vortex (Chiew, 1992). To ensure omitting the air region did not greatly impact the numerical results, a rudimentary test was performed of a channel possessing a partial ice cover with and without a body of air above the water. Some minor differences were noticed in the flow field, but the velocity magnitudes were found to be similar. Therefore, it was decided to not include the air region above the water, as the flow field was only mildly altered, and the computational cost savings outweighed the slight improvements in the flow field accuracy. Furthermore, all countermeasures were tested using the same numerical model and domain, implying single-phase flow was adequate since it would be used only for comparative purposes.

Turbulence Model Selection

Choosing the correct turbulence model to provide the necessary near wall details as well as the wide range of eddies present around the pier, consisted of a trial-and-error procedure. After performing a series of tests, it was found that the Reynolds-Averaged Navier-Stokes (RANS) turbulence model could not accurately predict the flow circulation of the horseshoe

vortex, nor could it predict the Von Karman street downstream of the pier. Meanwhile, the Large Eddy Simulation (LES) turbulence model was also tested, and it was found to incorrectly predict the velocity profile before and after the pier. Therefore, both the RANS and LES turbulence models were not sufficient options for the simulations being performed within this thesis. Further research was then invested into turbulence models and the Detached Eddy Simulation (DES) hybrid turbulence model appeared to be more suitable as it combines the RANS features near the wall and the LES features away from the wall (Gritskevich et al., 2012; Menter et al., 2003; Strelets, 2001). Specifically, the kOmegaSSTDDES turbulence model was tested and found to successfully predict the horseshoe vortex, the Von Karman street, and the velocity profiles. For those reasons, kOmegaSSTDDES was the chosen turbulence model for this study.

Sensitivity Analysis

A grid sensitivity analysis was performed to verify that the results were grid independent. This was achieved by running the numerical model with progressively smaller grid sizes until the time-averaged velocity, measured in specified locations inside of both the level one and two refinement regions, was no longer changing.

To ensure the accuracy of the results was adequate with respect to the time steps, a Courant number of 0.8 was maintained. This was achieved using an adjustable time step, but to confirm that the time steps were sufficient, a time step sensitivity analysis should have been performed.

When setting the user defined numerical model boundary conditions, it is important to verify that they produce results similar to that measured experimentally. Specifically, the roughness of the sand used in the comparative experimental tests was 0.001m, thus a sensitivity analysis was performed to determine the most accurate numerical model k_s value. This can be seen in Fig. D-1, where velocity profiles were collected for different k_s values and they were compared to the experimental velocity profile. It was concluded that k_s = 0.001m generated a velocity profile that best matched the experimental velocity profile.

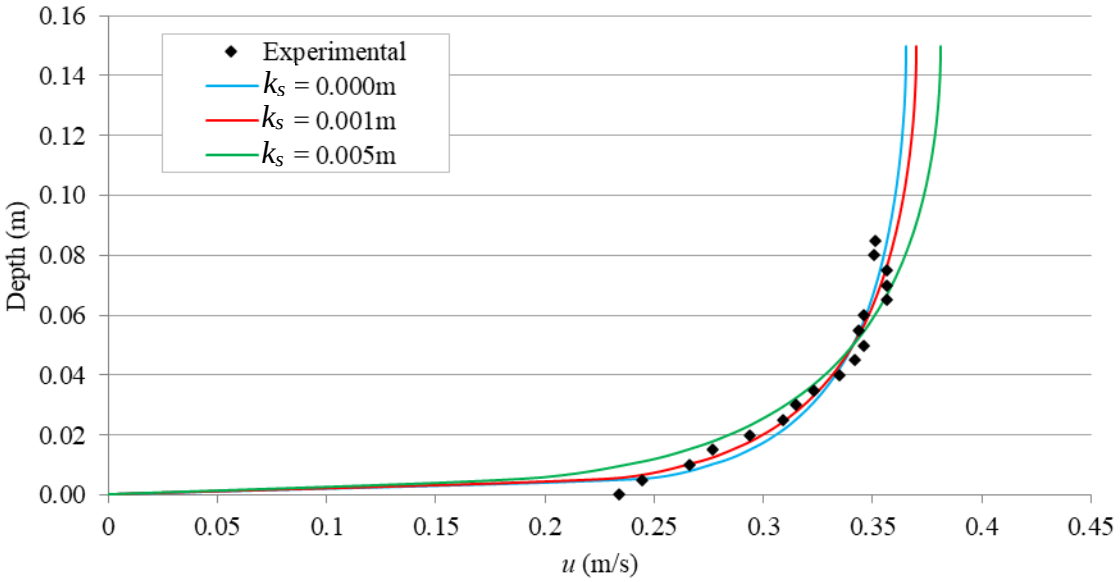

Fig. D-1. Velocity (u) profile sensitivity analysis for different numerical model k_s values.

Additional Information

The numerical results presented in this thesis were time-averaged for the purpose of better illustrating the hydrodynamic results. Time-averaging was achieved by collecting 30 equally spaced measurements (taken at 0.5s intervals for a total of 15s) after the numerical model had reached a quasi-converged solution. This was done for both the velocity and bed shear stress data.

The initial values used for k and ω were calculated using Eqs. 15 and 16, respectively, presented by ESI Group (2019) for isotropic turbulence:

$$k = \frac{3}{2}\left(Iu_{avg}\right)^2 \tag{15}$$

$$\omega = \frac{k^{0.5}}{C_\mu^{0.25} L} \tag{16}$$

Where I is the turbulence intensity, C_μ is a constant equal to 0.09, and L is a reference length scale (ESI Group, 2019; Wilcox, 2006).

Lastly, Eqs. 1 and 2 are the typical equations used to incorporate the bed roughness in wall functions but are not the exact formulas used in OpenFOAM.

Appendix E. CPN3 in the Presence of an Ice Cover

An additional experimental test was performed, which contributes to this thesis, but was not included in any journal paper or conference proceeding. The test consists of Collar Prototype No. 3 (CPN3) installed in the presence of an ice cover. The chosen ice cover condition was that of test R5 specified in Chapter 6, which is a rough ice cover submerged to 0.075m. This ice cover condition was found to yield the greatest scour. Fig. E-1 displays a comparison of the scour experienced under such ice cover without any countermeasure (Fig. E-1(a)) and with CPN3 installed (Fig. E-1(b)). Fig. E-1(a) was presented as test R5 in Fig. 6-9 from Valela, Sirianni, et al. (2021).

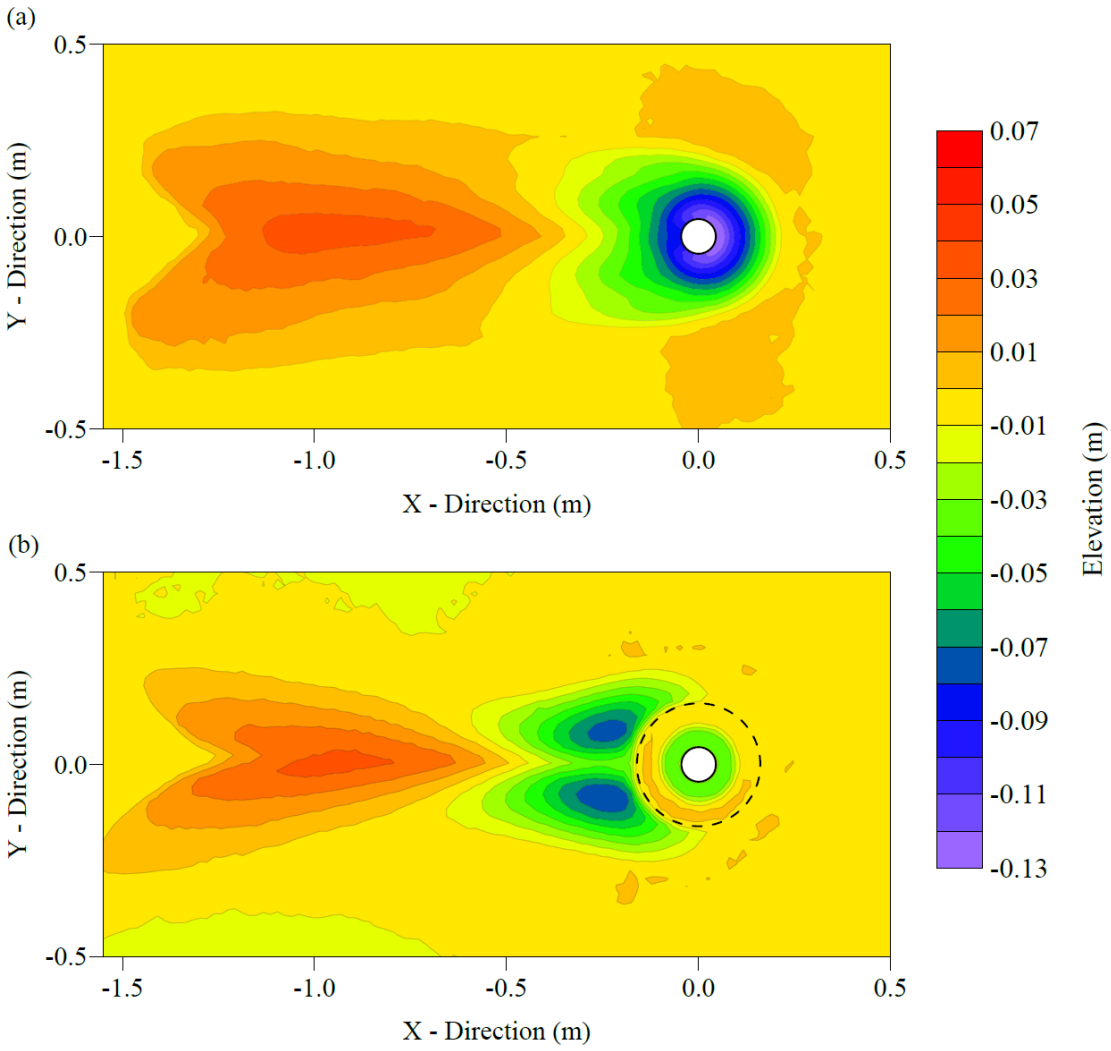

Fig. E-1. Scour comparison under rough ice cover submerged to 0.075m containing: (a) no scour countermeasure (presented as test R5 in Fig. 6-9 from Valela, Sirianni, et al. (2021)), and (b) CPN3 (dotted line indicates the perimeter of the collar at the bed surface).

The scour pattern experienced in Fig. E-1(b) is similar to that of some of the tests presented in Fig. 4-14 which possessed a large Froude number. The presence of CPN3 caused two large scour holes to form immediately downstream of the pier, however no collar undermining was experienced. The scour depth (d_s) achieved without any countermeasure was 0.128m and with CPN3 installed was 0.079m. Therefore, a d_s reduction of 38.3% was achieved using CPN3.

The most successful countermeasure design, Riprap Collar Prototype No. 3 (RCPN3), was still in its design stages during the time of the ice cover tests. For that reason, it was not tested under an ice cover, but in the future would make for a valuable study.